Ribosome Assembly, Proteolysis and Pathogenesis in Human Mitochondria

Christie L Waddington

Wellcome Trust Centre for Mitochondrial Research
Institute for Neuroscience
Newcastle University

Thesis submitted to Newcastle University in candidature for the degree of Doctor of Philosophy

September 2017

ABSTRACT

The human mitochondrial genome is approximately 16.6kbp and encodes 22 tRNAs, 2 rRNAs and 13 polypeptides. These polypeptides are synthesised by the mitoribosome, composed of a large (39S) and small (28S) subunit. Although recently published cryo-EM structures of the human, porcine and yeast mitoribosomes have identified a number of significant differences including new components with uncharacterised functions.

One such component was mS38 (AURKAIP1) as a part of the mt-SSU of the mitoribosome. This was consistent with previous work in my host laboratory using a siRNA screen of candidate mitochondrial proteins, which identified AURKAIP1 as having a role in mitochondrial gene expression. I continued this work and confirmed levels of AURKAIP1 are tightly controlled within the cell. Overexpression of both AURKAIP1 and AURKAIP1-FLAG caused disruption to the mitoribosome and mitochondrial translation, and depletion of AURKAIP1 impaired cell growth and resulted in cell death. Although the exact function of AURKAIP1 is still elusive, AURKAIP1 may have a role as an RNA chaperone. When overexpressed, AURKAIP1 was cleaved by the mitochondrial matrix protease LONP1, from a 25kDa to a 15kDa species by two cleavage events, although this could not be determined in the endogenous species.

This work led to the characterisation of LONP1 variants that were believed to be pathogenic. Whole exome sequencing identified two novel mutations (p.Tyr565His; p.Glu733Lys) in LONP1 in a paediatric patient with a severe mitochondrial disease. By cloning and sequencing LONP1 from patient samples, I showed compound heterozygosity in the patient for 2 independent mutations, confirming the disorder to be autosomal recessive. Skeletal muscle showed severe defects in OXPHOS complexes I, III and IV, reduced mtDNA copy number and a decrease in the steady state levels of TFAM. Steady state levels of LONP1 remained unaffected. The p.Tyr565His mutation is localised to a highly conserved aromatic-hydrophobic (Ar-ϕ) motif present in hexameric ATP-dependent proteases and i*n vitro* assays indicated a retained ability to hydrolyse ATP but a loss of proteolytic activity. This suggests that the mutation is likely to prevent the substrate from reaching the proteolytic site.

ACKNOWLEDGEMENTS

First and foremost, I would like to give my uttermost thanks to my supervisors Prof. Rob Taylor, Prof. Zofia Chrzanowska-Lightowlers and Prof. Robert Lightowlers for the giving me the opportunity to pursue this PhD project. Their continued support and guidance has allowed me to develop both personally and professionally and for that I will always be grateful.

Secondly, I would also like to thank Professor Maria Falkenberg and her colleagues at Gothenburg University for welcoming me into their lab and sharing their expertise. I am eternally grateful to Dr Jeremy Brown for being a great mentor over the last 7 years, having played such a key part in my scientific and personal development.

I would like to thank everyone in the MRG and NHS Highly Specialised Mitochondrial Diagnostic Service who have given me technical and emotional support throughout my PhD. My project has been a collaborative effort and I have been very fortunate to work with a group of people who have been willing to give up their time and expertise when I have needed. I am truly going to miss working in such a great environment. Thanks also go to lab members past and present: Kyle, Monika, Ewen, Nicole, Rawaa, Marysia, Francesco, Yasmin and particularly to my office girls Fei and Agata, whose friendship and advice over the last 4 years have been indispensable.

I would like to thank Saltwell Harriers, especially the lads, who have welcomed me into the club and have provided great respite over the course of my studies. I look forward to running with you for many years to come as Lady W.

I would like to thank my family and friends who have supported me over the years, particularly to my father Ian Waddington who sadly passed away in December 2016. He allowed me to pursue my love of sport, my love of learning and was always there to offer advice. And finally, I would like to thank Dr Robert Panting, who supported me throughout this journey.

AUTHOR'S DECLARATION

This thesis is submitted for the degree of Doctor of Philosophy at Newcastle University. The research was conducted at the Wellcome Trust Centre for Mitochondrial Research, Institute of Neuroscience, under the supervision of Professor Robert N. Lightowlers, Professor Zofia M.A. Chrzanowska-Lightowlers and Professor Robert W. Taylor. All research is my own unless stated otherwise.

I certify that none of the material offered in this thesis has been previously submitted by me for a degree of any other qualification at this, or any other, university.

TABLE OF CONTENTS

LIST OF FIGURES

LIST OF TABLES

ABBREVIATIONS AND SYMBOLS

ψ_m	membrane potential
A	adenine
aa	amino acids
AAA	ATPases associated with diverse cellular activities
ADP	adenosine diphosphate
AFG3L2	AFG3-like AAA ATPase 2
ARHSP	autosomal recessive hereditary spastic paraplegia
Ala-RS	alanyl-tRNA synthetase
APAF-1	apoptotic protease activating factor 1
APS	ammonium peroxidisulphate
A-site	aminoacyl-tRNA site
AspN	flavastacin, an endoproteinase.
ATP	adenosine-5'-triphosphate
AUR1/AURKAIP1	aurora-A kinase interacting protein 1 (mS38)
β-ME	β-mercaptoethanol
bp	base pairsincucyte
BN-PAGE	blue native polyacrylamide gel electrophoresis
BSA	bovine serum albumin
C	cytosine
CARD11	caspase recruitment domain family member 11
c-HPP	chromosome-centric Human Protein Project
CLIP	cross-linking and immunoprecipitation
CLPP	caseinolytic mitochondrial matrix peptidase proteolytic subunit
CLPX	caseinolytic mitochondrial matrix peptidase chaperone subunit
CODAS	cerebral, ocular, dental, auricular, skeletal
cpm	counts per minute
cryo-EM	cryo-electron microscopy
C_t	threshold cycle
C-terminal	carboxyl terminal
CTP	cytidine-5'-triphosphate
Cu	copper
D-loop	displacement loop
DAP3	death associated protein 3
DEPC	diethyl pyrocarbonate
ddH_2O	deionised sterile water
DHFR	dihydrofolate reductase
dH_2O	distilled sterile water
DMEM	Dulbecco's minimum essential medium
DMSO	dimethyl sulphoxide
DNA	deoxyribonucleic acid
DNase	deoxyribonuclease
dN-TOP	doublet N-terminal orientated proteomics

dNTP	deoxynucleotide triphosphate
DRP1	dynamin-related protein
ds	double-stranded
DSP	dithiobis syccinimidyl propionate
DTT	dithiolthreitol
e^-	electron
E. coli	*Escherichia coli* (Gram negative bacterium)
EDTA	ethylene diamine tetra-acetic acid
eEF1/1α	eukaryotic elongation factor 1/1α
EGTA	ethylene glycol tetra-acetic acid
EMEM	minimal essential media with Earle's salts
EMSA	electrophoretic mobility shift assay
ERAL1	Era-like 12S mitochondrial rRNA chaperone 1
eRF1/3	eukaryotic release factor 1/3
E-site	exit site
EtBr	ethidium bromide
EtOH	ethanol
FAD	flavin adenine dinucleotide
FCS	foetal calf serum
Fe-S	iron-sulphur
FIS1	mitochondrial fission 1 protein
fMet	formyl-methionine
FMN	flavin mononucleotide
FRT	Flip recombinase target
g	relative centrifugal force
G	guanine
GDP	guanosine-5'-diphosphate
GRSF1	G-rich sequence factor 1
GTP	guanosine-5'-triphosphate
H^+	hydrogen ion/proton
HCl	hydrochloric acid
HEK293T	human embryonic kidney 293 Flip-In™/TREx™ cells
HeLa	Henrietta Lacks cervical cancer cell line
His	histidine
hr(s)	hour(s)
H. sapiens	*Homo sapiens* (human)
HSP1/2	heavy strand promoter 1/2
HTRA2	high temperature requirement peptidase A2
IBM	inner boundary membrane
iAAA	intermembrane ATPases associated with diverse cellular activities
ICT1	immature colon carcinoma transcript 1
IgG	immunoglobulin G
IMM	inner mitochondrial membrane
IMS	intermembrane space
IP	immunoprecipitation

IPTG	isopropyl-β-D-thiogalactoside
ISC	iron-sulphur cluster
kb	kilobases
KCl	potassium chloride
K_d	dissociation constant
kDa	kilo Dalton
LC-MS	liquid chromatography mass spectrometry
LONP1	Lon peptidase 1
LSP	light strand promoter
M	molar
µ	micro
µCi	microCurie
mAAA	matrix ATPases associated with diverse cellular activities
MDa	mega Dalton
$MgCl_2$	magnesium chloride
MgOAc	magnesium acetate
µl	microlitre
µM	micromolar
mA	milliampères
Met	methionine
MFF	mitochondrial fission factor
MFN1/2	mitofusin-1/2
min(s)	minute(s)
mM	millimolar
MOPS	4-morpholine-propanesulphonic acid
mRNA	messenger ribonucleic acid
MRPP1/2/3	mitochondrial ribonuclease P protein 1/2/3
mtDNA	mitochondrial DNA
mtEF-G1/G2	mitochondrial elongation factor G1/G2
mtEF-Ts	mitochondrial elongation factor thermostable
mtEF-Tu	mitochondrial elongation factor thermo-unstable
MTG1	mitochondrial ribosome-associated GTPase 1
MTG2	mitochondrial ribosome-associated GTPase 2
mt-HPP	mitochondrial Italian Human Project Initiative
mtIF2/3	mitochondrial initiation factor 2/3
mt-LSU	mitochondrial large subunit
mtRF1/1a/2b/2c	mitochondrial release factor 1/1a/2b/2c
mtRRF1/2	mitochondrial ribosome recycling factor 1/2
mS38	mitochondrial small subunit protein 38 (AURKAIP1).
mtSSB	mitochondrial single-stranded DNA binding protein
mt-SSU	mitochondrial small subunit
mV	millivolt
MW	molecular weight
NaCl	sodium chloride
NAD	nicotinamide adenine dinucleotide

NaOAc	sodium acetate
NaOH	sodium hydroxide
ncRNA	non-coding RNA
NEAA	non-essential amino acids
NGS	next generation sequencing
NH_4OAc	ammonium acetate
NOA1	nitric oxide associated-1
nm	nanometres
NP-40	nonidet P-40; octyl phenoxy-polyethoxy-ethanol
nt	nucleotide
N-terminal	amino-terminal
^oC	degree Celsius
OD_{600}	optical density at a wavelength of 600nm.
O_H	origin of replication, heavy strand
O_L	origin of replication, light strand
OMA1	overlapping activity with m-AAA protease 1
OMM	outer mitochondrial membrane
OPA1	optic atrophy 1
OriB	origin of replication B.
ORF(s)	open reading frame(s)
OXPHOS	oxidative phosphorylation
PABP	poly (A) binding protein
PAG	polyacrylamide gel
PBS	phosphate-buffered saline
PCR	polymerase chain reaction
P. falciparum	*Plasmodium falciparum* (protozoan parasite)
pH	potential hydrogen
^{32}P	phosphorous-32
P_i	inorganic phosphate
pmf	proton motive force
PMPCA/B	peptidase mitochondrial processing alpha/beta subunit
PMSF	phenylmethanesulphonylfluoride
POLG	DNA polymerase γ
POLRMT	DNA-directed mitochondrial RNA polymerase
PRELID1	PRELI domain-containing protein 1
pre-tRNA	precursor tRNA
P-site	peptidyl site
PTC	peptidyl transfer centre
PVDF	polyvinylidene difluoride
PVP	polyvinylpyrrolidone
Q	ubiquinone
QH_2	ubiquinol
qPCR	quantitative real-time PCR
ρ^0	Rho^0 cell line
RF1/2/3	release factor 1/2/3

RITOLS	RNA Incorporated Throughout the Outer Lagging Strand
RNA	ribonucleic acid
RNase	ribonuclease
rNTPs	ribonucleoside triphosphates
rRNA	ribosomal RNA
RT-PCR	reverse transcription PCR
S	sedimentation coefficient
^{35}S	sulphur-35
S. cerevisiae	*Saccharomyces cerevisiae* (baker's yeast)
SDS	sodium dodecyl sulphate
SDS-PAGE	sodium dodecyl sulphate polyacrylamide gel electrophoresis
sec(s)	second(s)
siNT	non-targeting siRNA
siRNA	small interfering RNA
SmpB	small protein B
ss	single-stranded
S. scrufa	*Sus scrufa* (pig)
SSPE	sodium chloride, sodium phosphate, EDTA
StAR	steroidogenic acute regulatory protein
T	thymine
TAE	Tris/acetate/EDTA
TAS	termination-associated sequence
TBE	Tris/boric acid/EDTA
TBS-T	Tris-buffered saline/0.1% Tween-20
TCA	tricarboxylic acid
TEMED	N,N,N',N-tetramethylethylenediamine
Tet	tetracycline
TFAM	mitochondrial transcription factor A
TFB2M	mitochondrial transcription factor B2
TIMM	translocase of the inner mitochondrial membrane
T_m	melting temperature
TMPP	trimethoxyphenyl phosphonium
TMRM	tetramethylrhodamine methyl ester
tmRNA	transfer messenger ribonucleic acid
TOMM	translocase of the outer mitochondrial membrane
Tris	Trishydroxyaminomethane
tRNA	transfer ribonucleic acid
Tween-20	polyoxyethelene sorbitanmonolaurate
U	units
U	uracil
UMP	uridine monophosphate
USP30	ubiquitin-specific peptidase 30
UTP	uridine-5'-triphosphate
UTR	untranslated region
UV	ultraviolet

V	volts
WES	whole exome sequencing
WGS	whole genome sequencing
YME1L1	yeast mitochondrial escape 1-like 1

CHAPTER 1: INTRODUCTION

1.1 Mitochondria: An Overview

Mitochondria are essential organelles that are present in the cytosol of all nucleated eukaryotic cells and are one of the major sources of adenosine triphosphate (ATP) production within the cell. As a reticulum, the mitochondrial mass within a human cell can vary, depending on the cell type and ATP requirement.

1.1.1 *Evolutionary Origin of Mitochondria*

All eukaryotes contain an organelle of mitochondrial origin. It had been widely-accepted that mitochondria evolved from an endosymbiotic event between the ancestral pre-eukaryote and a prokaryotic α-proteobacteria (Margulis, 1970, Gray, 1983), approximately 1.5 billion years ago, (Brocks *et al.* 1999) to generate the first eukaryote. *Rickettsia prowazekii* was found to contain a genome that is highly similar to the mitochondrial genome (Andersson *et al.* 1998), indicating that a Rickettsiales microbe could be the origin of mitochondria. More recently, opinion is not unanimous as the marine microbe SAR11 was proposed as the original α-proteobacterium (Thrash *et al.* 2011) and then contested soon after (Rodríguez-Ezpeleta and Embley, 2012). It is unclear as to whether the ancestral pre-eukaryote already contained a nucleus, or that the nucleus evolved simultaneously during the endosymbiotic event. Over time, the α-proteobacteria evolved into our modern mitochondria, including the introduction of the components of mitochondrial replication and transcription from an ancestral T-odd bacteriophage (Shutt and Gray, 2006).

Mitochondria contain their own genome, and current data suggests that the mitochondrial genome (mtDNA) is monophyletic (Gray *et al.* 1999) despite mtDNA sizes ranging from ~6kb in *Plasmodium falciparum* (Conway *et al.* 2000) to 2.9Mb in *Cucumis melo* (Ward *et al.* 1981). Since the endosymbiotic event, many of the mitochondrial genes have been transferred to the nucleus including the genes for all mitoribosomal proteins, but exceptions exist including that for the mitochondrial protein *var1* in yeast (Foury *et al.* 1998). In humans, mitochondrial genes encoding certain subunits of the respiratory chain have been retained. Their retention in the mitochondrial genome has been suggested to be due to the hydrophobic nature of these subunits, which may make it more difficult to import from the cytosol and assemble (Claros *et*

al. 1995) although genes such as *ATP9*, which encodes ATP synthase subunit 9, are highly hydrophobic and yet are located on the nuclear genome (Anderson *et al.* 1981).

There are four types of mitochondria that have currently been identified in eukaryotes: classic mitochondria, anaerobic mitochondria (Tielens *et al.* 2002), hydrogenosomes (Lindmark and Müller, 1973) and mitosomes (Tovar *et al.* 1999). Classic mitochondria are present in all aerobic eukaryotes and are one of the major sources of adenosine triphosphate (ATP) production within the cell, producing 36 moles of ATP on oxidative metabolism of 1 mole of glucose and using O_2 as the final electron acceptor during aerobic respiration (Martin, 2010). Anaerobic mitochondria are most often associated with invertebrates that have anaerobic phases of their life cycle, utilising compounds either produced endogenously e.g. fumarate or present in the local environment, such as nitrate, as their final electron acceptor (Tielens *et al.* 2002), producing 5 mol of ATP per mole of glucose (Martin, 2010).

Hydrogenosomes and mitosomes are considered as reduced mitochondria, since they have lost a number of pathways seen in classic mitochondria (reviewed in Embley and Martin, 2006). Hydrogenosomes were originally identified in parasitic unicellular eukaryotes, producing hydrogen by fermentative pyruvate oxidation (Müller *et al.* 2012) and generating 4 mol of ATP per mole of glucose (Martin, 2010). Mitosomes are highly-reduced mitochondria that were identified in *Entamoeba* (Tovar *et al.* 1999), with no direct role in ATP synthesis but are involved in iron-sulphur (Fe-S) cluster assembly (Embley and Martin, 2006).

Due to the variety in the types of mitochondria, for this body of work I will focus on classic mitochondria, present in aerobic eukaryotes.

1.1.2 *Structure of Mitochondria*

Mitochondria are cytosolic, double-membraned organelles consisting of the outer (OMM) and inner (IMM) mitochondrial membranes, separated by the intermembrane space (IMS) (Sherratt, 1991). The IMM then encloses the mitochondrial matrix and is folded into structures called cristae (Figure 1.1).

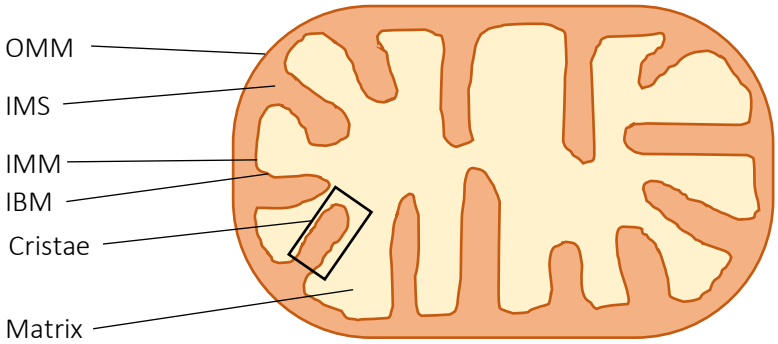

Figure 1.1 – A cross-section of the basic structure of the mitochondrion. A 2D cartoon drawing depicting the different compartments of the mitochondrial organelle. OMM = outer mitochondrial membrane, IMM = inner mitochondrial membrane, IMS = intermembrane space, IBM = inner boundary membrane.

The OMM is a simple phospholipid bilayer and unlike other membranes, the OMM is permeable to most small molecules and ions, acting as a barrier for large hydrophilic solutes (Benz, 1994). This permeability is largely due to multiple copies of the transmembrane channel protein, porin (VDAC1, voltage-dependent anion channel 1) (Benz, 1994). The IMM, however, is only permeable to O_2, CO_2 and H_2O and has a different lipid content, notably a higher percentage of cardiolipin (Osman *et al.* 2010), and a higher protein:lipid ratio of 3:1 compared to the OMM, with a ratio of 1:1 respectively (Gohil and Greenberg, 2009). The cardiolipin is thought to be important for the structure of the membrane, as well as for mitochondrial dynamics (1.1.3) (Frohman, 2015). The IMM is further subdivided into two compartments: the inner boundary membrane (IBM) and the cristae (Frey and Mannella, 2000). These two IMM compartments are contiguous, and the connection between the boundary membrane and the cristae are called crista junctions (Perkins *et al.* 1997). The cristae are predominantly tubular in structure but are known to take other forms and are described as having a dynamic structure (Hackenbrock, 1966). During apoptosis, for example, the cristae respond to pro-apoptotic signalling proteins e.g. BAX and BAK (Yamaguchi *et al.* 2008) and are inverted resulting in the release of cytochrome *c* (Scorrano *et al.* 2002). It is thought that the shape of the cristae can determine the efficiency of mitochondrial respiration by influencing the assembly and stability of membrane protein complexes, notably the respiratory chain supercomplexes (Cogliati *et al.* 2013). Briefly, narrower, longer cristae appear to increase rates of respiration compared to wider, shorter cristae (Cogliati *et al.* 2013). In addition, the more energy-demanding the cell, the more cristae that are present within the IMM. Proteins involved in oxidative phosphorylation are enriched on the cristae membrane and it has been

hypothesised that F_0F_1-ATP synthase (complex V) supercomplexes can influence the curvature of the IMM, contributing to the shape of the cristae (reviewed in Zick *et al.* 2009).

The IMM maintains the mitochondrial membrane potential (ψ), which is generated by the transport of protons across the IMM as a function of electron transfer through the respiratory chain (Mitchell, 1961). This membrane potential is maintained at 150-180mV and is used to import nuclear-encoded mitochondrial proteins into the matrix. The matrix contains the majority of mitochondrial proteins including, but not limited to, those involved in mtDNA replication, transcription and replication, the citric acid cycle and iron-sulphur cluster biogenesis. It has been suggested that the matrix contains two additional but transient sub-compartments: nucleoids and RNA granules.

Nucleoids house the mtDNA and mtDNA-associated proteins, and their primary function is to provide a separate compartment for mtDNA replication and transcription to occur. The average nucleoid in cultured mammalian cells was thought to contain 5-7 mtDNA genomes (Iborra *et al.* 2004), although more recent data suggests that more often they contain only a single mtDNA molecule (Kukat *et al.* 2011). The mtDNA within these nucleoids are packaged with the aid of various DNA-binding proteins e.g. TFAM (mitochondrial transcription factor A) (Kaufman *et al.* 2007) and mtSSB (mitochondrial single-stranded binding protein). Other proteins that have been identified in nucleoids, notably in the oocytes of *Xenopus laevis*, include proteins involved in mtDNA maintenance, replication and transcription as well as proteins with unknown mtDNA functions e.g. LONP1 (Lon protease 1) (Barat *et al.* 1985).

Closely associated with the nucleoids are RNA granules. RNA granules are ribonucleoparticles that lack a defined membrane and have been found in the nucleus and cytosol of somatic cells, neurons and germ cells (Jourdain *et al.*, 2016). Structures resembling cytosolic RNA granules were also identified in mitochondria (Iborra *et al.* 2004, Antonicka *et al.* 2013, Jourdain *et al.* 2013) and they colocalised with GRSF1 (G-rich RNA sequence binding factor 1), a mitochondrial RNA binding protein involved in RNA processing and translation (Antonicka *et al.* 2013). Further research on these mitochondrial RNA granules identified proteins involved in RNA processing, mitoribosome assembly, rRNA methylation, tRNA processing, RNA degradation and translation initiation (summarised in Jourdain *et al.* 2016),

allowing immature polycistonic RNAs to be processed and mitoribosome assembly to occur away from the translational machinery (Jourdain *et al.* 2016).

1.1.3 *Mitochondrial Dynamics*

The mitochondrial membranes are not static as mitochondria are dynamic organelles that are constantly undergoing fusion and fission. The mitochondrial network can be present in different morphological states, reflected in the name 'mitochondria' derived from the Greek 'mitos' (μίτος) and 'chondron' (χονδρόν) meaning threads and grains respectively as they continually fuse and divide.

In brief, mitochondrial fission (Figure 1.2A) is initiated by the recruitment of a cytosolic GTPase, DRP1 (dynamin-related protein) by the OMM proteins FIS1 (mitochondrial fission protein 1, Yoon *et al.* 2003) and MFF (mitochondrial fission factor, Otera *et al.* 2010). DRP1 forms constrictive spiral multimers around the mitochondria, severing the IMM and OMM via a GTP-hydrolysis-dependent mechanism (Smirnova *et al.* 2001) resulting in division.

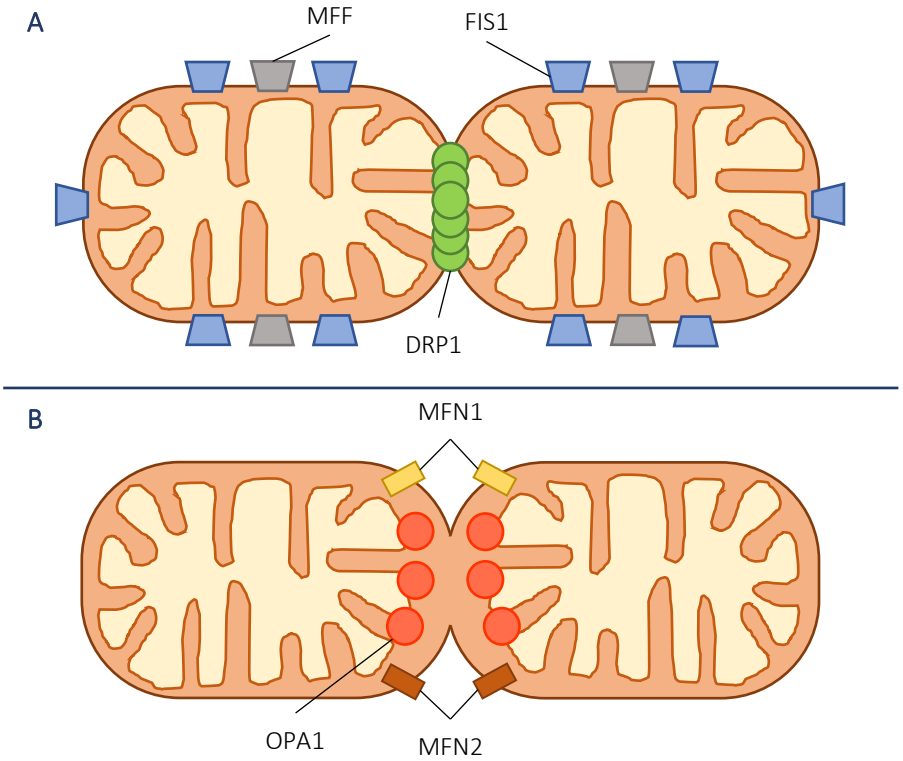

Figure 1.2 – Mitochondrial fission and fusion. A 2D cartoon drawing of the major proteins involved in both mitochondrial fission (A) and fusion (B). MFF = mitochondrial fission factor, FIS1 = mitochondrial fission 1, DRP1 = dynamin-related protein 1, MFN1 = mitofusin 1, MFN2 = mitofusin 2, OPA1 = optic atrophy 1.

Mitochondrial fusion is also regulated by dynamin family proteins, notably the GTPases MFN1 and MFN2 (mitofusin 1 and 2 respectively) for the OMM and OPA1 (optic atrophy 1) for the IMM (Figure 1.2B). Fusion can either be complete, in which two mitochondrial fully fuse or fusion can be transient, in which only soluble proteins are exchanged (Liu *et al.* 2009). Mitochondria will continually fuse and divide depending on the ATP requirements of the cell, generated by a process called oxidative phosphorylation (OXPHOS).

1.1.4 *The OXPHOS System*

In eukaryotes, mitochondria are associated with the production of ATP via OXPHOS, involving 5 multi-subunit enzymatic complexes: complexes I-IV comprising the electron transport chain or the respiratory chain, and complex V, F_0F_1-ATP synthase (Figure 1.3). In brief electrons, generated from the oxidation of NADH and FADH on complexes I and II, are transported via Fe-S clusters through ubiquinol (QH_2) and reduced cytochrome *c* on complexes III and IV. This movement of electrons allows the pumping of protons across the IMM, resulting in a proton gradient and together produces the proton motive force (pmf) that generates potential energy (ψ_m), utilised by complex V to phosphorylate ADP (adenosine diphosphate) to ATP (Mitchell, 1961).

Complex I is ~980kDa and consists of 44 subunits (Vinothkumar *et al.* 2014, Balsa *et al.* 2012): 14 conserved core subunits and 30 supernumerary subunits. Of the 14 conserved core subunits, 7 are hydrophobic and encoded by mtDNA (Anderson *et al.* 1981) and 7 are hydrophilic, and they form two distinct domains: a hydrophilic redox domain in the mitochondrial matrix and a hydrophobic antiporter-like (Na^+/H^+) domain in the IMM (Vinothkumar *et al.* 2014). NADH, generated by the tricarboxylic acid (TCA) cycle and β-oxidation of fatty acids, binds to the redox domain and is oxidised by flavin mononucleotide (FMN) (Hirst, 2013) to NAD. From this reaction, two electrons are carried by eight Fe-S clusters to bound ubiquinone (Q), which is subsequently reduced to QH_2, and the generated potential energy is used to transfer 4 protons per reaction across the IMM (Galkin *et al.* 1999).

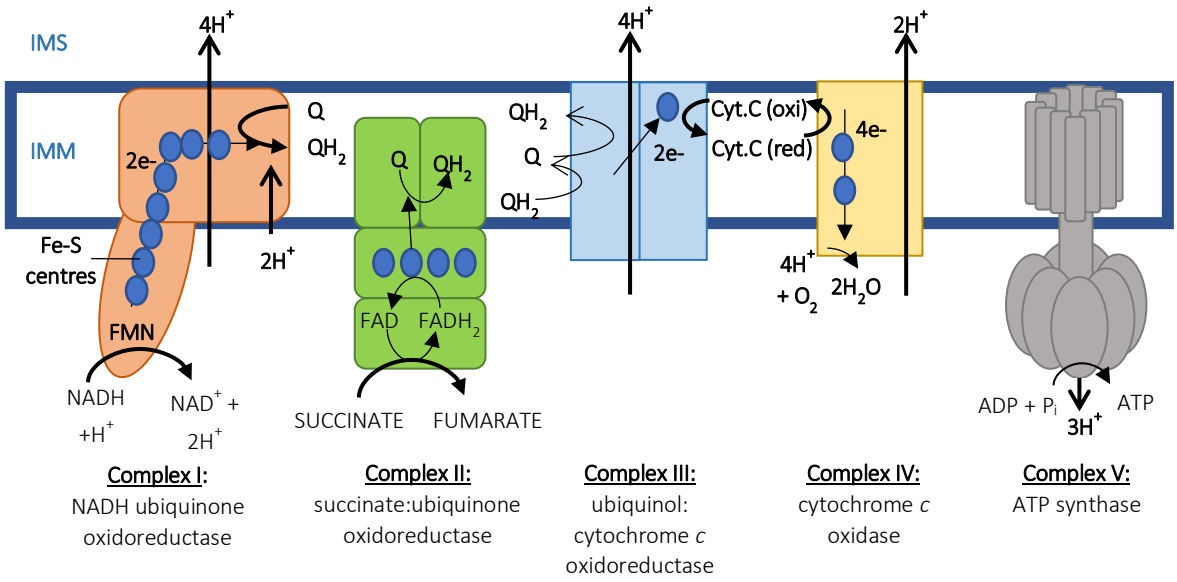

Figure 1.3 – Enzymatic complexes of oxidative phosphorylation. A 2D cartoon drawing (not to scale) of the five complexes involved in OXPHOS. Fe-S clusters = blue circles, IMS = intermembrane space, IMM = inner mitochondrial membrane, NAD = nicotinamide adenine dinucleotide, FAD = flavin adenine dinucleotide, Cyt.C = cytochrome C, oxi = oxidised, red = reduced, FMN = flavin mononucleotide, Q = ubiquinone, QH_2 = ubiquinol, e^- = electron, P_i = inorganic phosphate.

Complex II is ~124kDa, consisting of a hydrophilic head and hydrophobic membrane anchor (Sun *et al.* 2005), the subunits of which are encoded by the nuclear genome (nDNA). Complex II couples the TCA cycle with OXPHOS, in which the oxidation of succinate to fumarate is dependent on the reduction of flavin adenine dinucleotide (FAD) to $FADH_2$, resulting in the loss of 2 electrons. These electrons are carried along Fe-S clusters and a heme group to Q, which is reduced to QH_2 (Hägerhäll, 1997). Unlike the other OXPHOS complexes, complex II is the only complex not to transport protons across IMM (Rutter *et al.* 2010).

Complex III is a dimer, with each monomer ~240kDa in size and consists of 11 subunits, 1 of which is encoded by mtDNA, cytochrome *b* (Iwata *et al.* 1998). Between these 2 monomers lies the catalytic centre consisting of cytochrome *b*, cytochrome c_1 and the Rieske [2Fe-2S] protein (Robertson *et al.* 1993). By a process known as the Q cycle, via this catalytic centre, 2 electrons from QH_2 are transferred to cytochrome c_1, which is subsequently reduced, and 2 QH_2 are oxidised to 2 Q, with one rereduced to QH_2 (Trumpower, 1990). The Q cycle is coupled with the net transfer of 4 protons per cycle to the IMS (Mitchell, 1976).

Complex IV is a dimer, with each monomer consisting of 14 subunits (Balsa *et al.* 2012, Piceathly *et al.* 2013), 3 of which are encoded by mtDNA (Anderson *et al.* 1981). The two monomers are connected via a cardiolipin molecule (Tsukihara *et al.* 1996). Complex IV is the terminal electron acceptor in the chain of complexes, oxidising cytochrome *c* and transporting the electrons via Fe-S and Cu^{2+} clusters to reduce molecular O_2 forming H_2O. The movement of 2 electrons from cytochrome *c* is also coupled to the transport of 4 protons into the IMS.

Complex V consists of 2 functional domains: F_0, located in the IMM and F_1, located in the mitochondrial matrix (Capaldi *et al.* 1994). Using the electrochemical gradient of the pmf provided by complexes I, III and IV, the released energy causes rotation of subunits in F_0 in relation to F_1 in a fixed direction (Noji *et al.* 1997). The rotation of subunit γ in the F_1 domain provides the energy for synthesising ATP from ADP and inorganic phosphate (P_i) by a process known as rotary catalysis (Menz *et al.* 2001).

There are currently 2 proposed models for the OXPHOS complexes: the fluid-state model and the solid-state model. The fluid-state model states the complexes I-IV diffuse freely in the IMM, and that the electron transfer between these complexes is due to random collision events between the complexes. The solid-state model states that the OXPHOS complexes also form supercomplexes, where the interactions are stable. Supercomplexes that have so far been identified include a dimeric ATP synthase (V_2, Arnold *et al.* 1998), supercomplex I+III_2, supercomplex III_2+IV_{1-2} and supercomplex I+III_2+IV_{1-4} (Schägger and Pfeiffer, 2000). Supercomplex I+III_2+IV_{1-4} is unique in that it can carry out respiration in the presence of ubiquinone and cytochrome *c*, and has thus been termed the respirasome. The function of this respirasome is thought to assemble and activate complex I, which cannot assemble as a free holoenzyme, or on supercomplex intermediates (Moreno-Lastres *et al.* 2012).

1.1.5 *Additional Functions of Mitochondria*

Mitochondria have a range of diverse functions besides OXPHOS that are vital for the survival of the cell (Figure 1.4). The proton motive force (pmf) generates potential energy (ψ_m) in the IMM that is maintained at 150-180mV. The pmf and the ψ_m is used to import nuclear proteins across the IMM into the mitochondrial matrix (Nicholls *et al.* 2000) and utilised for the biosynthesis of both Fe-S clusters and haem, both of which are components of many nuclear and mitochondrial proteins. Pyrimidine biosynthesis however only utilises the import

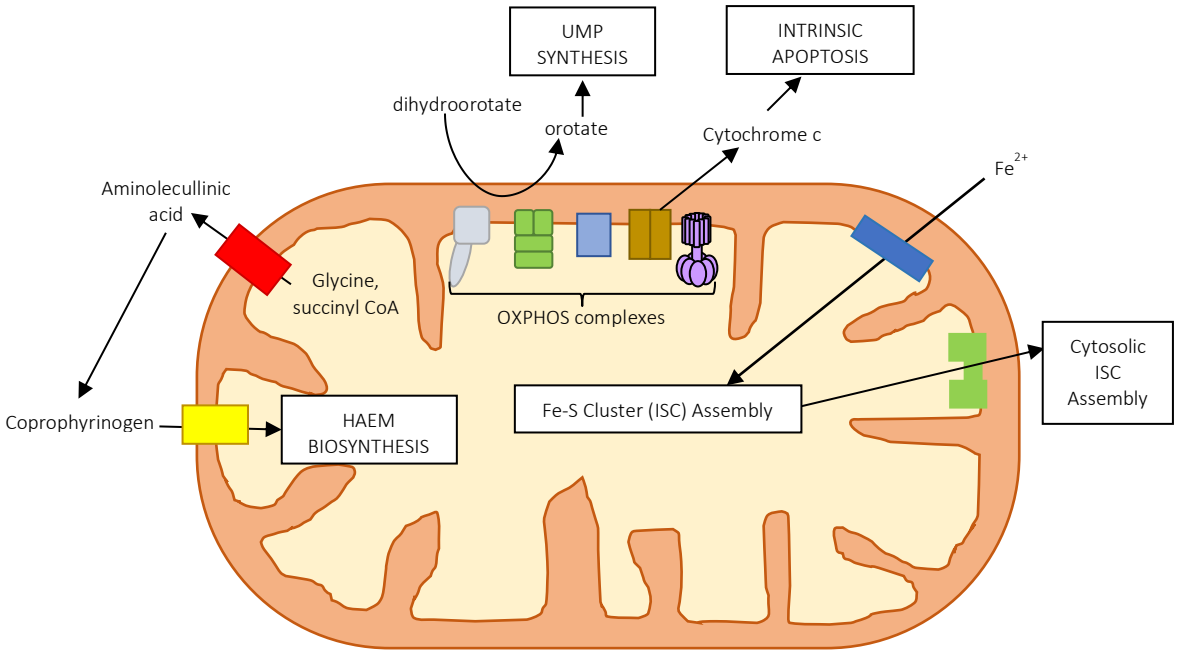

Figure 1.4 – Additional functions of mitochondria. A 2D cartoon drawing (not to scale) summarising some of the functions performed by the mitochondria. UMP = uridine monophosphate, ISC = iron-sulphur cluster.

machinery of the OMM. Dihydroorotate is imported into the IMS and converted to orotate by dihydroorotate dehydrogenase, also located in the IMS. Orotate is subsequently used in the cytosol for the synthesis of uridine monophosphate (UMP), a key molecule for pyrimidine biosynthesis (Rawls *et al.* 2000).

Mitochondria are also involved in the intrinsic pathway of apoptosis. When the cell receives stimuli to undergo apoptosis, oxidised cytochrome *c* is released from the IMS into the cytosol (Borutaite and Brown, 2007). Cytochrome *c* forms a vital component of the apoptosome, together with APAF-1 (apoptotic protease activating factor 1) and procaspase-9 (Ow *et al.* 2008). Once procaspase-9 has been recruited to the apoptosome and activated, the caspase cascade is triggered, initiating apoptosis.

Proteins used for these functions are nuclear-encoded but for 13 polypeptides that make up some of the OXPHOS complex subunits, they are encoded on the mitochondrial genome.

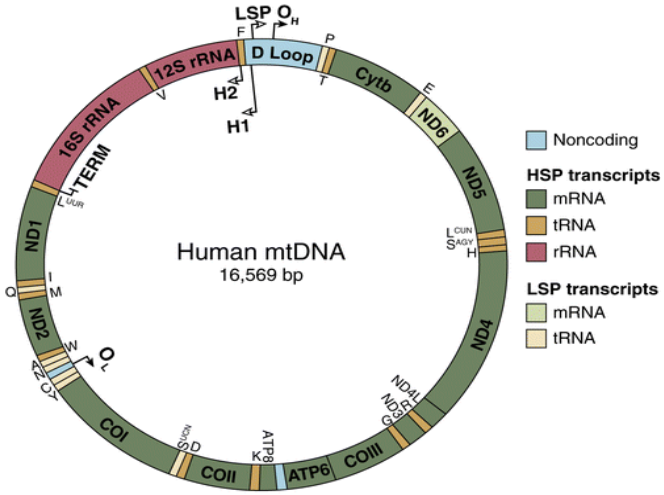

Figure 1.5 – **Human mtDNA molecule.** Image taken from Falkenberg *et al*. 2007. The 16.6kb mtDNA molecule encodes genes for 13 polypeptides, 22tRNAs and 2 rRNAs. Replication originates at O_H (origin of replication, heavy strand) and O_L (origin of replication, light strand). Transcription originates at HSP (heavy strand promoter, here H1 and H2) and LSP (light strand promoter). H1/H2 are both present in the D loop (Displacement loop).

1.2 Mitochondrial DNA

Human mitochondria contain their own genome in the form of a circular, double-stranded 16,569bp molecule that is maternally inherited (Figure 1.5). The mitochondrial network contains mitochondrial DNA (mtDNA) molecules packaged with additional proteins into structures called nucleoids (1.1.2, Bogenhagen *et al.* 2008), in a similar way to nuclear DNA (nDNA) being contained within chromatin. The mtDNA molecule encodes 37 genes (Anderson *et al.* 1981): 13 polypeptides encoding for subunits of OXPHOS complexes I, III, IV and V (Table 1.1), 22 transfer RNAs (tRNAs) and 2 ribosomal RNAs (rRNAs). These genes are encoded on two strands: the G-rich heavy strand of mtDNA contains 28/37 genes and the C-rich light strand contains the remaining 9 genes. Some studies have suggested that mtDNA could encode for more peptides (Capt *et al.* 2015) including humanin (Hashimoto *et al.* 2001) and gau (Faure *et al.* 2011) although this is yet to be confirmed.

The mtDNA molecule undergoes replication and transcription within the mitochondria, utilising machinery that is imported from the cytosol.

Table 1.1 – OXPHOS complex subunits encoded by mtDNA.

OXPHOS Complex	mtDNA	mtDNA genes	nDNA
Complex I	7 proteins	*MTND1, MTND2, MTND3, MTND4, MTND5, MTND6, MTND4L*	36 proteins
Complex II	-	-	4 proteins
Complex III	1 protein	*MTCYB*	10 proteins
Complex IV	3 proteins	*MTCOI, MTCOII, MTCOIII*	11 proteins
Complex V	2 proteins	*MTATP6, MTATP8*	14 proteins

1.2.1 *Replication*

Replication of mtDNA occurs in the nucleoids, independently of the cell cycle (Bogenhagen *et al.* 2008) and is initiated at two origins of replication that are found on the heavy strand (O_H) and the light strand (O_L) of mtDNA (Falkenberg *et al.* 2007). Replication is achieved through DNA polymerase γ (POLG), a hexameric 5'-3' DNA helicase (TWINKLE) and mitochondrial single-stranded binding protein (mtSSB). There are currently two major theories for mtDNA replication: the strand displacement model (Clayton, 1982) and RITOLS (RNA Incorporation Throughout the Outer Lagging Strand) (Reyes *et al.* 2013).

The strand-displacement model states that replication is initiated from O_H on the heavy strand and is unidirectional. Frequently, replication can terminate after 650bp at 15bp DNA elements called termination-associated sequences (TAS), producing the triple-stranded D-loop (Doda *et al.* 1981). If the replication machinery proceeds past the TAS, two thirds of the heavy strand of the mtDNA molecule is synthesised, before exposing O_L. When the L-strand becomes exposed, RNA primers for replication initiation at O_L are produced by POLRMT (Kühl *et al.* 2016), allowing for synthesis of the light strand from O_L in the opposite direction (Fusté *et al.* 2010). Once both strands are fully synthesised, the 5' and 3' ends of the strands will ligate to form a closed circle.

In the RITOLS model, replication is initiated either at O_H or OriB (origin of replication B) located within the D-loop, and proceeds unidirectionally. At the same time, nascent 200-600bp RNA strands (Yasukawa *et al.* 2006) synthesised by POLRMT (DNA-directed mitochondrial RNA polymerase) bind to the lagging strand by the 'bootlace mechanism', protecting it from degradation (Yang *et al.* 2002). As the leading strand is synthesised, O_L is exposed and synthesis of the light strand from O_L is initiated in the opposite direction (Fusté

et al. 2010). The RNA that was on the lagging strand is subsequently replaced by, or converted to, DNA (Yasukawa *et al.* 2006).

In addition to the strand-displacement and RITOLS models, there is a third that is termed the "strand-coupled model" that is thought to only occur following ethidium bromide (EtBr)-induced depletion of mtDNA. Replication is initiated on both strands at the 'initiating region' of mtDNA that contains *MTCYB, MTND5* and *MTND6*. Replication continues bidirectionally until it reaches the D-loop where it terminates (Bowmaker *et al.* 2003). However, this model is yet to be validated.

1.2.2 *Transcription*

In humans, the minimal components for transcription are mitochondrial transcription factor B2 (TFB2M), mitochondrial RNA polymerase (POLRMT) and mitochondrial transcription factor A (TFAM) (Falkenberg *et al.* 2002). There are different promoter sites for the light strand (LSP) and debatably one or two for the heavy strand (HSP or HSP1 and HSP2) (Falkenberg *et al.* 2007, Lodeiro *et al.* 2012). First, TFAM binds to specific sequences upstream of the promoter sites, causing the mtDNA to bend. POLRMT is then recruited to the promoter sites by binding TFAM and specific sequences on mtDNA, forming the pre-initation complex. The formation of this complex leads to the recruitment of TFB2M, initiating transcription. Once transcription is initiated, TFB2M dissociates. Mitochondrial transcription elongation factor (TEFM) enhances the activity of POLRMT, promoting transcription (Posse *et al.* 2015). Polycistronic mRNA transcripts covering the entire heavy strand or light strand of the mitochondrial genome are generated from HSP and LSP respectively (Montoya *et al.* 1983). An additional transcript is also generated from HSP (or HSP2) that contains the two rRNAs, *MT-RNR1* (12S rRNA) and *MT-RNR2* (16S rRNA) and two mt-tRNAs (mt-tRNA^{Val} and mt-tRNA^{Phe}).

Following transcription, the transcripts undergo processing and modifications.

1.2.3 *Post-transcriptional modifications*

The open reading frames (ORFs) of most polycistronic transcripts generated from transcription of mtDNA are flanked by precursor tRNAs (pre-tRNAs). These tRNAs are removed by a process described as the "tRNA punctuation model" (Ojala *et al.* 1981). The tRNAs are

cleaved off the transcripts at the 5' and 3' ends by the endonucleases mtRNaseP and mtRNaseZ respectively post-transcription and prior to translation.

Mitochondrial RNase P is a multimeric enzyme consisting of 3 subunits: MRPP1, MRPP2 and MRPP3 (mitochondrial ribonuclease P protein 1,2,3). Unlike other RNaseP complexes, human mitochondrial RNaseP has no RNA component (Rossmanith and Karwan, 1998). MRPP1 is involved in the methylation of mitochondrial tRNAs, MRPP3 has a catalytic role and MRPP2 has a currently unknown function. More precisely, RNaseP is a metallonuclease, using Mg^{2+} for phosphodiester hydrolysis, generating a 5'-PO_4 and 3'-OH at the 5' end of tRNAs (Hartmann *et al.* 2009) following cleavage.

RNaseZ is encoded by two genes, *ELAC1* and *ELAC2*, which encode a short form and a long form respectively. The short form localises to the cytosol and at present little is known about its physiological role (Takahashi *et al.* 2008). The long form is found in mitochondria (Zhao *et al.* 2009) and is a zinc phosphodiesterase containing a C-terminal domain with tRNA-processing endoribonuclease activity (Brzezniak *et al.* 2011). From *in vitro* studies with human mitochondria, pre-tRNAs are processed in a particular order, with mtRNaseP cleavage occurring prior to mtRNaseZ (Rossmanith, 1997).

There are 3 ORF junctions that lack mt-tRNAs but still require further processing: *MTND6*-ncRNA (non-coding RNA), *MTND5-MTCYB* and RNA14-*MTCO3*. To date, PTCD2 has been shown to be involved in the processing of *MTND5-MTCYB* (Xu *et al.* 2008) and GRSF1 for the processing of *MTND6*-ncRNA and *RNA14-MTCO3* (Antonicka *et al.* 2013). Further transcriptional modifications can also occur to the transcripts, which are further reviewed in Rorbach and Minczuk (2012).

1.3 Mitochondrial Protein Synthesis

1.3.1 *The Mitoribosome*

Mitochondrial protein synthesis occurs in the mitochondrial matrix, closely associated with the IMM (Mai *et al.* 2016, Englmeier *et al.* 2017) and is performed by the mitochondrial ribosome or mitoribosome. Similar to the cytosolic ribosome, mitoribosomes are composed of a large subunit (mt-LSU, 39S) and a small subunit (mt-SSU, 29S) that together form the

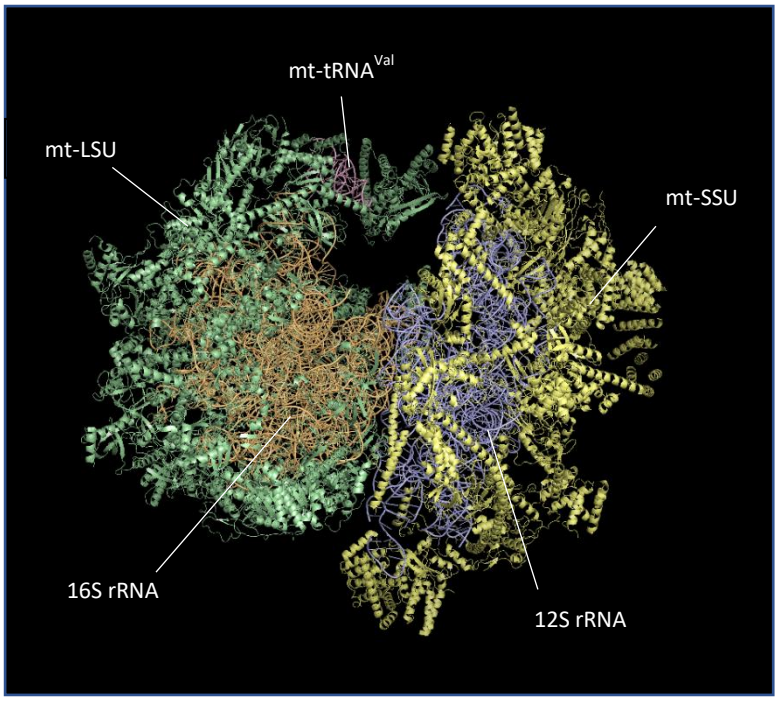

Figure 1.6 – Structure of the human mitochondrial ribosome. Complete structure of the human mitochondrial ribosome, originally published in Amunts *et al.* 2015. Structure pdb file 3J9M was imported into PyMOL and coloured. Mt-SSU = yellow, 12S rRNA = purple, mt-tRNA^{Val} = pink, mt-LSU = green, 16S rRNA = orange.

functional monosome. To date, the mammalian mitoribosome (Figure 1.6) contains 83 proteins, 37 of which are unique to mitochondria, and 3 RNA molecules: 16S rRNA in mt-LSU, 12S rRNA in mt-SSU and either mt-tRNA^{Val} (human) or mt-tRNA^{Phe} (porcine) in the mt-LSU (Amunts *et al.* 2014, Greber *et al.* 2014) rather than 5S rRNA present in the prokaryotic ribosome (Greber *et al.* 2014).

Cryo-electron microscopic (cryo-EM) structures of the complete human (Figure 1.6, Amunts *et al.* 2015), porcine (Greber *et al*. 2015) and yeast (Desai et al. 2017) mitoribosomes were recently solved to 3.5Å, 3.8Å and 3.3Å respectively. When compared to crystal structures of the prokaryotic ribosome (*E. coli,* 3.5Å, Schuwirth *et al.* 2005) and the human cytosolic ribosome (3.6Å, Khatter *et al.* 2015), differences can be seen (Table 1.2). The mammalian mitoribosome is unique in that it contains 70% protein and 30% RNA unlike its cytosolic, prokaryotic and other mitochondrial counterparts (Table 1.2). This is due to both the loss of rRNA and the addition of 36 mitochondrial-specific proteins, primarily on the periphery of the mitoribosome (Brown *et al.* 2014). Despite the greater mass, mitoribosomes have a more porous structure (Table 1.2) and like its counterparts, it still contains the aminoacyl-tRNA site

(A-site) and peptidyl-tRNA site (P site) and a recently-identified exit site (E-site) (Amunts *et al.* 2015, Greber *et al.* 2015).

Table 1.2 – Features of Ribosomes.

Feature	Human cytosolic ribosome[a]	Human mitochondrial ribosome[b]	Prokaryotic ribosome[b]
Sediment coefficient	80S	55S	70S
RNA:Protein	70%:30%	30%:70%	70%:30%
Mass	~3MDa	~3MDa	~2MDa
Large subunit	60S, 47 proteins	39S, 53 proteins	50S, 34 proteins
Small subunit	40S, 32 proteins	28S, 30 proteins	30S, 21 proteins
RNA species	28S rRNA, 5S rRNA, 5.8S rRNA, 18S rRNA.	16S rRNA, 12S rRNA, mt-tRNA^{Val}.	23S rRNA, 16S rRNA, 5S rRNA.

[a] = Anger *et al.* 2013, [b] = Mai *et al.* 2017.

1.3.2 *Mitoribosome Assembly*

Mitoribosomes contain additional proteins compared to their prokaryotic counterparts, which makes the process of mitoribosome assembly a little more complex. Assembly of the mitoribosome is regulated by several factors that coordinate the process of maturation of the rRNA with the assembly of the mitoribosomal subunits. Initial stages of mitoribosome assembly are thought to occur at mtDNA nucleoids (Bogenhagen *et al.* 2014) and RNA granules (Antonicka and Shoubridge, 2015) since both compartments were found to contain mitoribosomal proteins, assembly factors and RNA processing enzymes.

In human mitochondria, the rRNA genes are cleaved from a single polycistronic transcript that contains mt-tRNA^{Phe}, 12S rRNA, mt-tRNA^{Val} and 16S rRNA. ERAL1, an RNA-binding GTPase is thought to stabilise 12S rRNA (Dennerlein *et al.* 2010); no RNA-binding protein has been identified for 16S rRNA. Following cleavage, both the 12S rRNA and 16S rRNA are modified. The 12S rRNA is methylated at 4 bases by TFB1M (A936 and A937, Metodiev *et al.* 2009) and NSUN4 (C839 and C841/C842, Metodiev *et al.* 2014) and potentially at U429, although this has only been identified in hamster mitochondria (Baer and Dubin, 1981). Recently, RBFA has also been shown to be important for 12S rRNA maturation (Rozanska *et al.* 2017), associating with helix 44 and 45 of 12S rRNA and enhancing the methylation of A936 and A937 by TFB1M. The 16S rRNA has 2'-O'ribose methylations that are further modified by the methyltransferases MRM1, MRM2 and MRM3 (Lee and Bogenhagen, 2014) and one potential

pseudouridylation, although the enzyme responsible for this modification is yet to be identified (Ofengand and Bakin, 1997).

A number of GTPases are used in the assembly of ribonucleoproteins including cytosolic and mitochondrial ribosomes, although few have been identified in mitochondria. The GTPase NOA1 (nitric oxide associated-1, C4orf14) has been shown to be involved in assembly of the mt-SSU (He *et al.* 2012) and in binding RNA species containing G-quadruplexes *in vitro*, indicating that G-quadruplex-containing RNA may be involved in mitoribosome assembly (Al-Furoukh *et al.* 2013). Mitochondrial GTPases MTG1 and MTG2 have been shown to interact with both the IMM and the immature mt-LSU (Kotani *et al.* 2013) and MTG1 has been identified in RNA granules (Jourdain *et al.* 2016). Precise functions for these GTPases however are yet to be identified.

Other factors have also been identified including the helicases DDX28 (Tu and Barrientos, 2015) and DHX30 (Antonicka and Shoubridge, 2015), the IMM protein MPV17L2 (Dalla Rosa *et al.* 2014) and MALSU1 (Rorbach *et al.* 2012). DDX28 interacts with the mt-LSU and the 16S rRNA, with *DDX28* silencing in HEK293T cells results in the lack of mt-LSU assembly, suggesting a role in mt-LSU biogenesis (Tu and Barrientos, 2015). DHX30 is thought to be involved in all stages of monosome assembly since it interacts with the mt-LSU, mt-SSU and the assembled monosome, and silencing of *DHX30* in human fibroblast cell lines results in a substantial loss of assembled monosomes (Antonicka and Shoubridge, 2015). The IMM protein MPV17L2 is not present in Rho0 (ρ^0) cells, a 143B cell line lacking mtDNA, indicating that MPV17L2 is dependent on the presence of mtDNA and additionally, it has been shown that it interacts with the mt-LSU and the monosome (Dalla Rosa *et al.* 2014). MALSU1, also known as C7orf30, is also involved in mt-LSU assembly and through immunoprecipitation experiments, MALSU1 has been shown to specifically-interact with uL14 within the mt-LSU (Fung *et al.* 2013) although the reason for this interaction is still unknown. A recent publication describing the structures of late-stage assembly intermediates of the mt-LSU determined that MALSU1 forms a complex with L0R8F8, a LYR-motif-containing protein, and mitochondrial acyl carrier protein (mt-ACP), as additional assembly factors (Brown *et al.* 2017). It is thought that this module prevents the mt-SSU from joining with the mt-LSU, preventing early monosome assembly.

Once the monosome has assembled, protein synthesis can be initiated.

1.3.3 *Initiation*

The mitoribosome translates 9 monocistronic and 2 dicistronic transcripts (*RNA14* and *RNA7,* encoding ATP8/6and ND4L/ND4 respectively). These transcripts are unusual in that they typically lack, or have reduced, untranslated regions (UTRs) and contain no introns (Temperley *et al.* 2010a). There are 3 initiating codons in human mitochondrial transcripts: AUG, AUA and AUU (Anderson *et al.* 1981), although it is currently unknown how the mitoribosome recognises these start codons. *In vitro*, 2 initiation factors have been identified: mtIF2 (Liao and Spremulli, 1990) and mtIF3 (Koc and Spremulli, 2002). These factors are orthologous to the prokaryotic initiation factors IF1 and IF2 (mtIF2) and IF3 (mtIF3) respectively (Gaur *et al.* 2008). The mt-SSU is bound by mtIF3, preventing premature assembly of the mt-LSU with the mt-SSU. GTP-bound mtIF2 binds the mt-SSU (Gaur *et al.* 2008). The first 17 nucleotides of the mt-mRNA enter the mt-SSU and if a start codon is present in the P-site, mtIF2-GTP stimulates the binding of a formyl-methionine tRNA (fMet-tRNA) and mt-LSU associates with the mt-SSU to form the monosome (Christian and Spremulli, 2010). The GTP-bound mtIF2 is hydrolysed, mtIF2-GDP and mtIF3 dissociate from the monosome and translation is initiated (Figure 1.7). If there is no start codon present, the mt-mRNA is passed through the mt-SSU and dissociates from the complex (Christian and Spremulli, 2010).

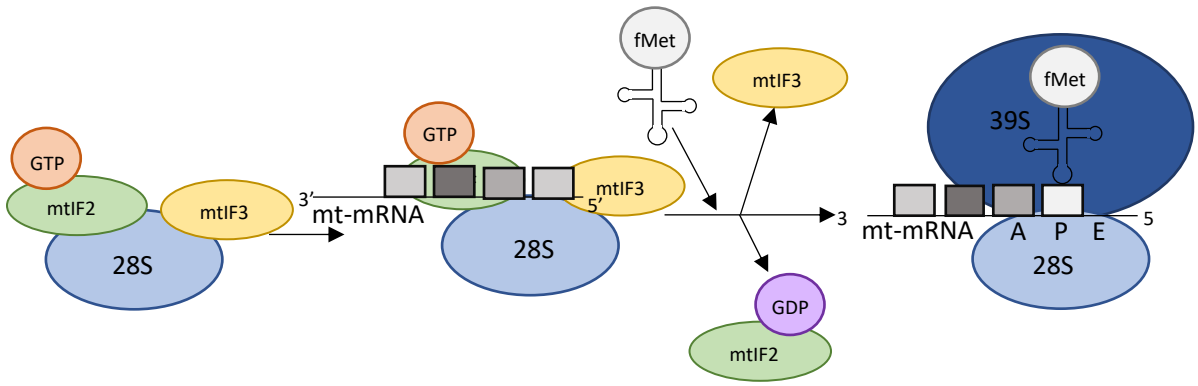

Figure 1.7 – Initiation of mitochondrial translation. A 2D cartoon image depicting the initial steps of mitochondrial translation. Process is described in detail within the text. 39S = mt-LSU, 28S = mt-SSU.

1.3.4 *Elongation*

There are three mitochondrial elongation factors (mtEFs) that are homologous to the prokaryotic EFs and are involved in elongation (Figure 1.8): mtEF-Tu (Schwartzbach and Spremulli, 1991), mtEF-Ts (Schwartzbach and Spremulli, 1991) and mtEF-G1 (Hammarsund *et al.* 2001). In order for elongation to proceed, the monosome must be assembled, the mt-mRNA must be present and fMet-tRNA must be located within the P-site. A complex of mtEF-Tu-GTP and an amino-acylated mt-tRNA enters the A-site and binds its respective cognate triplet codon. An intermediate mtEF-Tu/mtEF-Ts complex promotes the hydrolysis of GTP, triggering the release of mtEF-Tu-GDP and allowing the tRNA to enter the P-site. As the mt-tRNA is transposed to the P-site, a peptide bond is formed between the start codon and the newly-added residue (catalysed by the peptidyl transfer centre of the mt-LSU) extending the polypeptide chain. The mt-tRNA is subsequently deacylated. MtEF-G1 catalyses the

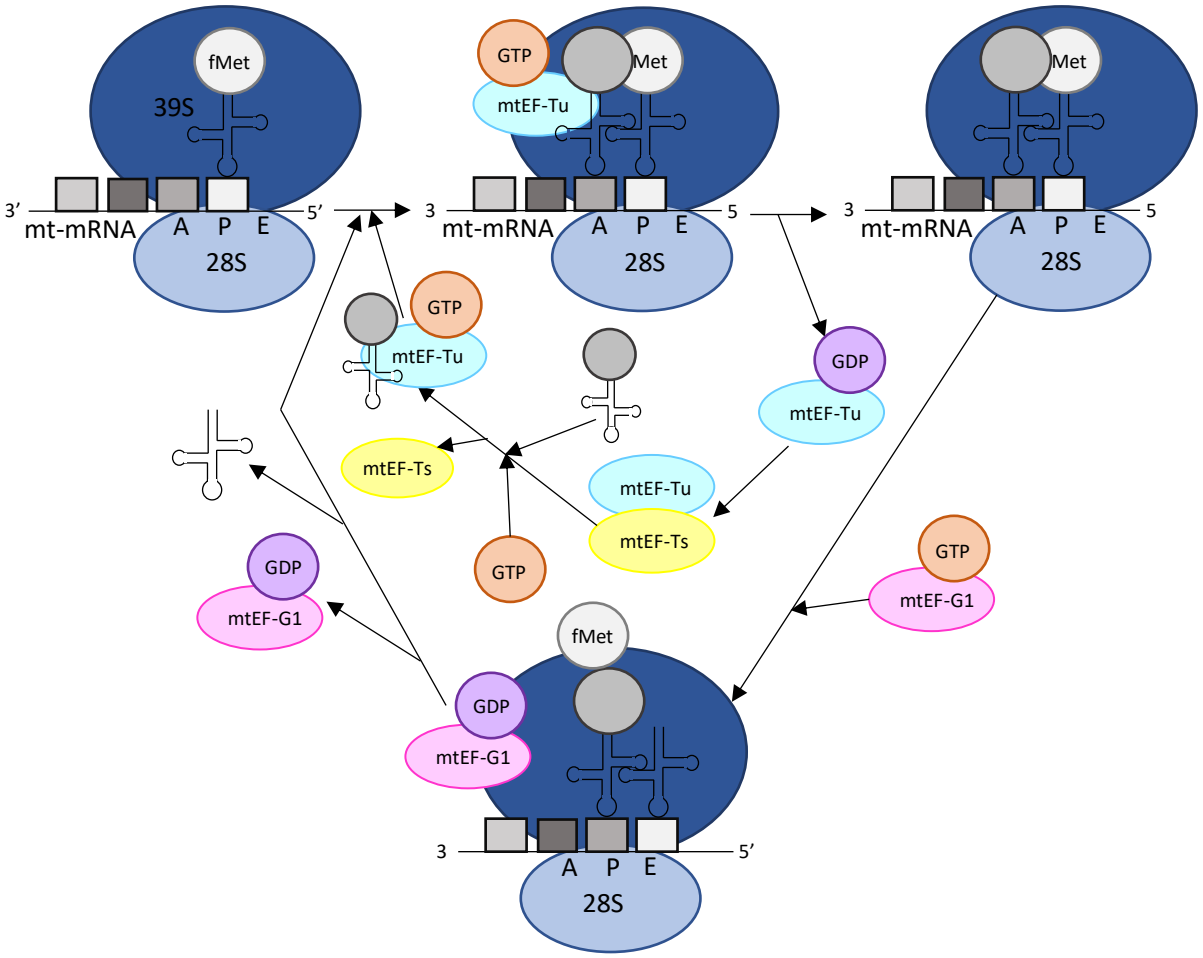

Figure 1.8 – Elongation of mitochondrial translation. A 2D cartoon image depicting the elongation steps of mitochondrial translation. Process is described in detail within the text. 39S = mt-LSU, 28S = mt-SSU.

movement of the mitoribosome, allowing the deacylated tRNA to be released and the new peptidyl-tRNA to move from the A-site to the P-site. This process continues until the mitoribosome reaches a stop codon (Christian and Spremulli, 2012).

1.3.5 *Termination*

When the stop codon enters the A-site of the mitoribosome, termination is initiated (Figure 1.9). The standard UAA/UAG stop codons are present in both nuclear and mitochondrial transcripts but UGA, present in nuclear transcripts as a stop codon, encodes for tryptophan in human mtDNA (Barrell *et al.* 1979). Additionally, AGA and AGG present at the end of *MTCO1* and *MTND6* transcripts respectively are unassigned triplet codons. Since they are unassigned, they cause a -1bp frameshift during translation (Temperley *et al.* 2010b). Both AGA and AGG codons are preceded by a 'U', placing UAG into the A-site once the frameshift has occurred. A class-1 release factor, mtRF1a, recognises the UAA/UAG stop codons (Soleimanpour-Lichaei *et al.* 2007) in the A-site via a PKT tripeptide motif and a region at the α5 helix present in its codon recognition domain. The nascent polypeptide chain is released via the mitoribosome activity in conjunction with a GGQ motif in mtRF1a that is important for hydrolysis of the ester bond between the mt-tRNA and the polypeptide chain (Temperley *et al.*, 2010). Three other class-1 release factors have been identified in human mitochondria that all contain the GGQ motifs: mtRF1 (Soleimanpour-Lichaei *et al.* 2007), ICT1 (Richter *et al.* 2010) and C12orf65 (Antonicka *et al.* 2010). Mt-RF1, unlike other class 1 release factors, does not contain a PXT motif, but contains a PEVGLS motif and to date, mt-RF1 has yet to display

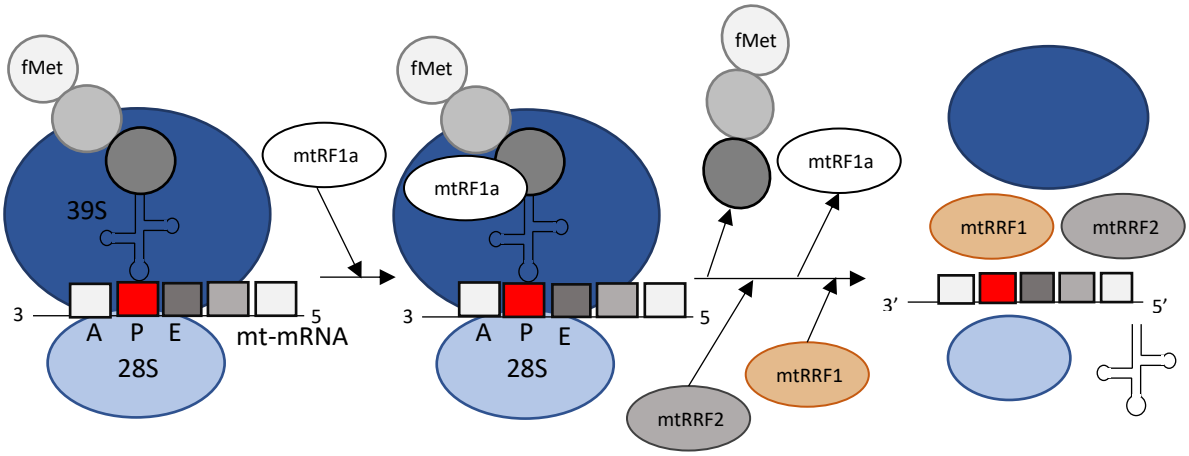

Figure 1.9 – Termination of mitochondrial translation. A 2D cartoon image depicting the elongation steps of mitochondrial translation. Process is described in detail within the text. 39S = mt-LSU, 28S = mt-SSU.

release factor activity either *in vitro* or *in vivo* (Soleimanpour-Lichaei *et al.* 2007). C12orf65 has also lost the PXT motif and to date, has not exhibited peptidyl-tRNA hydrolysis *in vitro* (Wesolowska *et al.* 2014). Finally, ICT1 is a structural component of the mt-LSU and some studies have suggested that ICT1 directly binds to the AGG and AGA stop codons directly, indicating that the -1bp frameshift would not be required (Lind *et al.* 2013). Its position in the mitoribosome precludes this so it would need to be free ICT1, however, further research is still needed to determine the functions of these identified release factors.

1.3.6 *Ribosome Recycling*

The release of mtRF1a from the mitoribosome allows mitochondrial ribosome recycling factors 1 and 2 (mtRRF1 and mtRRF2 [mt-EFG2]) to bind in the A-site. This binding facilitates the dissociation of the monosome into the mt-LSU and mt-SSU and the release of mt-mRNA and the deacylated tRNA. GTP hydrolysis appears to be necessary for the release of mtRRF1 and mtRRF2 (Tsuboi *et al.* 2009). MtIF3 then binds to the mt-SSU to prevent premature re-association of the two subunits until translation can be reinitiated (Christian and Spremulli, 2009).

1.4 Nuclear-Encoded Mitochondrial Proteins

1.4.1 *Protein Import*

MtDNA only encodes for 13 polypeptides, and thus the mitochondria must import approximately 1500 proteins encoded by nuclear DNA and synthesised in the cytosol in order to perform all of its functions. These proteins typically have an N-terminal amphipathic helical mitochondrial targeting sequence (MTS) that is recognised and imported by the TOMM (translocase of the outer mitochondrial membrane) complex on the OMM, notably TOMM20, TOMM22 and TOMM70 (Fan *et al.* 2011). From here, the protein is sorted through different sub-complexes depending on its target destination (Figure 1.10).

OMM α-helical proteins are transferred to the MIM (mitochondrial import) complex prior to insertion into the OMM; all other proteins are imported into the IMS. OMM β-barrel proteins are sorted through the SAM (sorting and assembly machinery) complex via the TIMM (translocase of the inner mitochondrial membrane) chaperone complex in the IMS, consisting of TIMM9 and TIMM10 (Wiedemann *et al.* 2004).

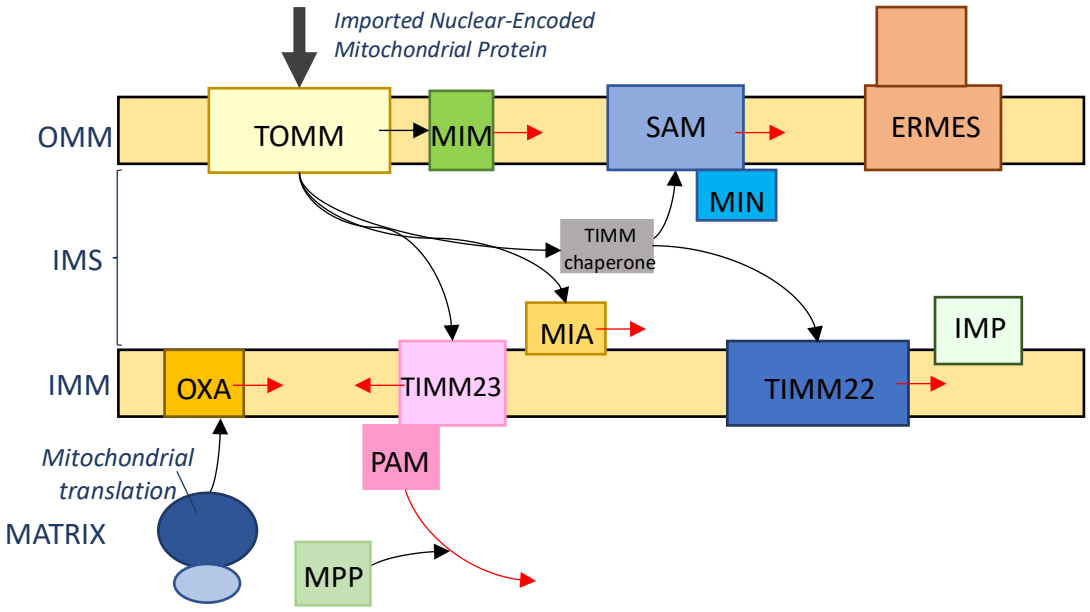

Figure 1.10 – Mitochondrial protein import mechanisms. Image is adapted from Kulawiak *et al*. 2013. A 2D cartoon (not to scale) depicting the main pathways for imported nuclear-encoded mitochondrial proteins. Black arrows = movement of imported proteins. Red arrows = final insertion of imported proteins. OMM = outer mitochondrial membrane, IMS = intermembrane space, IMM = inner mitochondrial membrane. Import mechanisms are explained within the text.

Proteins for the IMS are handled by the MIA (mitochondrial intermembrane space machinery) complex. This complex is important for both recognising the ITS (intermembrane targeting signal) present in some of these proteins and for promoting the correct folding of the proteins by introducing intramolecular disulphide bonds (Chacinska *et al.* 2004). The ITS is subsequently cleaved by the IMP (inner membrane peptidase) located in the IMM (Burri *et al.* 2005).

For proteins to pass through the IMM, the membrane potential is required for import; the TIMM22 and TIMM23 complexes are the primary complexes used to import such proteins. Furthermore, the TIMM22 complex is used for the insertion of IMM metabolite carrier proteins (Sirrenberg *et al.* 1996), which are guided through the IMS via the TIMM chaperone complex. The TIM23 complex is for the import of mitochondrial proteins with a designated N-terminal mitochondrial targeting sequence (MTS). The membrane potential of the IMM activates the TIMM23 channel (Truscott *et al.* 2001) and allows full translocation of the preproteins into the matrix together with the PAM (presequence translocase-associated motor) complex, whose energy is derived from hydrolysis of ATP (Bauer *et al.* 2000). Independently from the PAM complex, the mitochondrial processing peptidase (MPP) cleaves

off the MTS resulting in the mature protein. The primary peptidase responsible for this cleavage is the mitochondrial processing peptidase (MPP) complex that is located within the mitochondrial matrix. This complex is a heterodimer composed of peptidase mitochondrial processing alpha subunit (PMPCA), which binds and recognises the MTS, and PMPCB, which facilitates the cleavage of the MTS (Dvoráková-Holá *et al.* 2010).

1.4.2 *Identification of Nuclear-Encoded Mitochondrial Proteins*

There have been several proteomic studies to identify nuclear-encoded mitochondrial proteins using mass spectrometry. These studies have been performed in various species including mouse (Pagliarini *et al.* 2008), yeast (Reinders *et al.* 2006), plant (*A. thaliana,* Heazlewood *et al.* 2004) and protozoa (*T. thermophilus*, Smith *et al.* 2007). The coverage for each of these studies has been set at around ~85% (Meisinger *et al.* 2008), giving a total number of mitochondrial proteins in mammals of c.1500. A more recent study, the chromosome-centric Human Protein Project (c-HPP) (Marko-Varga *et al.* 2013) aimed to characterise and quantify human nuclear-encoded proteins alongside a second study, the mitochondrial Italian Human Proteome Project initiative (mt-HPP) (Urbani *et al.* 2013), investigating the structure-function relationships of the mitochondrial-encoded proteins. Using these databases, further research can be performed on these proteins to further understand mitochondria.

1.4.3 *AURKAIP1: mS38*

One of these unknown nuclear-encoded mitochondrial proteins that was identified was AURKAIP1. AURKAIP1 was first identified as a candidate mitochondrial protein in the MitoCarta study (Pagliarini *et al.* 2008) and further studies have since confirmed this finding (Szklarczyk *et al.* 2012, Koc *et al.* 2013). AURKAIP1 (mS38) is a nuclear-encoded protein, whose gene is located on chromosome 1p36.33. There are three transcript variants of human AURKAIP1 (NM_012900.2, NM_0011272291, NM_001127230), all of which encode the same 199 amino acid sequence (22.4kDa) with alternative splicing producing variation in the 5'-UTRs. Initially, AURKAIP1 was identified as an ubiquitously-expressed nuclear protein that negatively regulated Aurora-A, a mitotic serine/threonine kinase (Kiat *et al.* 2002) that regulates the assembly and maintenance of the mitotic spindle, particularly in G2 and M phases (Bischoff and Plowman, 1999) and also plays critical roles in the centrosome cycle,

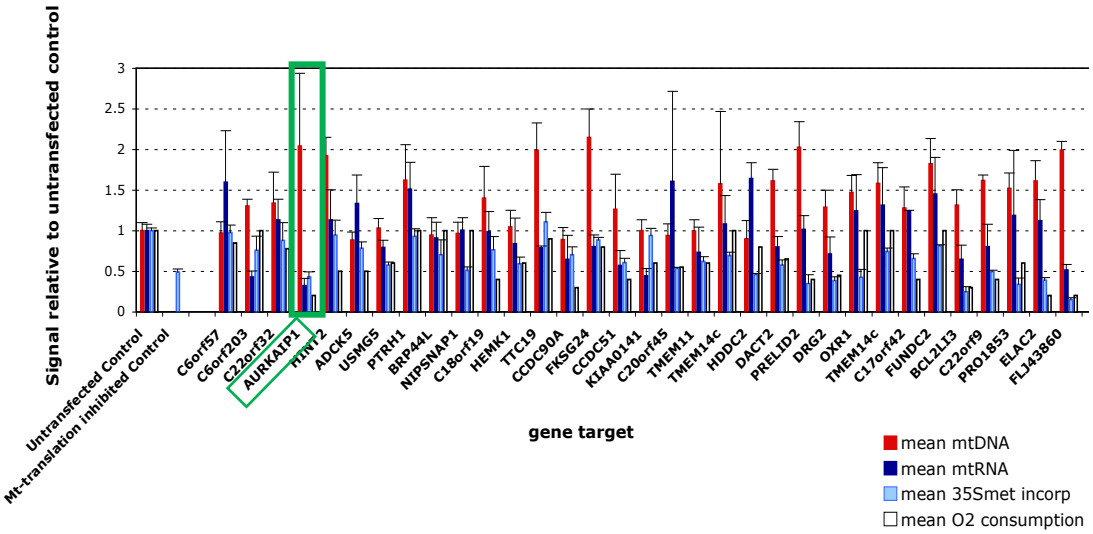

Figure 1.11 – Effects on mitochondrial translation and O_2 consumption following depletion of candidate mitochondrial proteins. HeLa cells were depleted of candidate mitochondrial proteins using siRNA. Levels of mtDNA (red), mRNA (dark blue), ^{35}S-Cys/Met incorporation (light blue) and O_2 consumption (white) were determined for each depletion. AURAIP1 is highlighted (green box).

spindle assembly and chromosome segregation (Meraldi *et al.* 2004). The same research group also determined that Antizyme1 was a binding partner of Aurora-A and that this interaction was enhanced by AURKAIP1 (Lim and Gopalan, 2007). However, another group suggested that AURKAIP1 promoted the stability, and not the degradation, of Aurora-A kinase (Katayama *et al.* 2007). Additionally, AURKAIP1 was shown to bind to glycogen synthase kinase 3-beta (GSK-3β) in the nucleus (Fumoto *et al.* 2008), which is another serine/threonine kinase that is also reported to regulate Aurora-A. Fomoto *et al.* hypothesised that phosphorylation of AURKAIP1 by GSK-3β would reduce the interaction between AURKAIP1 and Aurora-A, activating Aurora-A kinase activity (Doble and Woodgett, 2003, Fumoto *et al.* 2008) and allowing for mitotic entry.

Utilising the MitoCarta study, my host laboratory identified 224 proteins that were likely to be both mitochondrial and involved in mitochondrial gene expression. Each protein was depleted in both HeLa and ρ^0 cells using 3 different small interfering RNAs (siRNAs). AURKAIP1 was one of the proteins identified that when depleted, caused a significant growth defect in HeLa cells, but not ρ^0 cells (Figure 1.11). Since ρ^0 lack mtDNA (King and Attardi, 1989), a growth defect in HeLa cells but not ρ^0 cells suggests that the protein is involved in maintaining or transcribing mtDNA, translating mt-mRNA or involved in rRNA/tRNA modifications. During the course of my project, four studies have placed AURKAIP1 within the

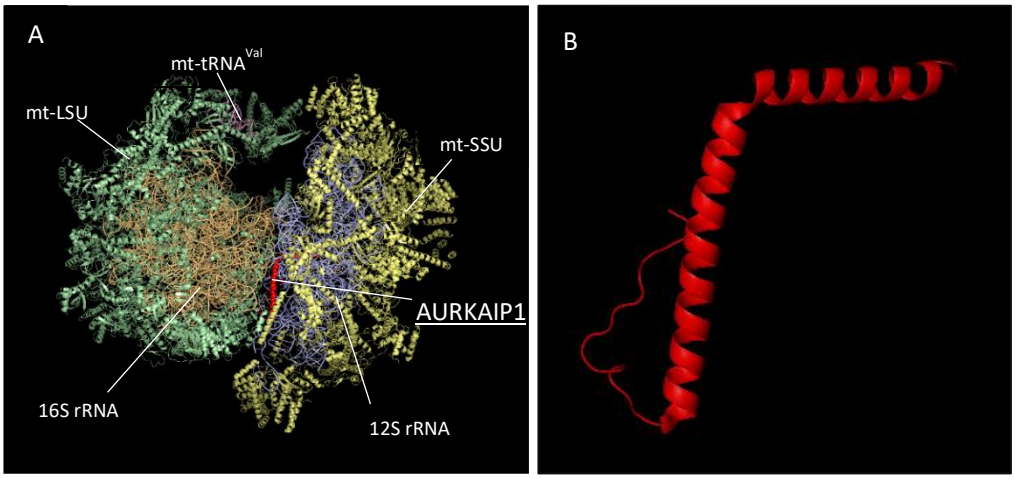

Figure 1.12 – Current structure of AURKAIP1 within the human mitoribosome. Complete structure of the human mitochondrial ribosome, originally published in Amunts *et al.* 2015. Structure pdb file 3J9M was imported into PyMOL and coloured. Mt-SSU = yellow, 12S rRNA = purple, mt-tRNA^{Val} = pink, mt-LSU = green, 16S rRNA = orange, AURKAIP1 = red. A = complete mitoribosome highlighting the location of AURKAIP1 (red). B = AURKAIP1 (mS38), showing amino acid residues 128-199 identified in the cryo-EM structure of the human mitoribosome.

mt-SSU (Figure 1.12A) but only amino acids 128 to 199 have been detected within the cryo-EM structures of the mitoribosomes (Figure 1.12B) (Koc *et al.* 2013, Amunts *et al.* 2015, Greber *et al.* 2015, Desai *et al.* 2017). This could suggest that AURKAIP1 has a long mitochondrial-signalling peptide at its N-terminus (Koc *et al.* 2013) or that the protein is cleaved twice upon import into the mitochondria.

AURKAIP1 contains a domain of unknown function at the C-terminus, DUF1713, that is also present in the yeast protein Cox24 (Figure 1.13, Barros *et al.* 2006, Koc *et al.* 2013). Little is known about the function of this domain, although it is most likely an RNA binding domain (Barros *et al.* 2006). In addition, this region is highly conserved between the two proteins and across species (Figure 1.13). Cox24 has recently been identified as a subunit of the mitoribosome in *S. cerevisiae* (Desai *et al.* 2017) but also has a function in the processing and the translation of MT-COXI mRNA (Barros *et al.* 2006). In humans, MT-COX1 mRNA does not need to be processed since mammalian mitochondrial genes do not contain introns.

In the cryo-EM structure of the human mitochondrial ribosome, AURKAIP1 forms one of two intersubunit bridges at the core of the mt-SSU, with its N-terminus interacting with 12S rRNA, notably helix 44 at the 3' end (Amunts *et al.* 2015). However, previous data from my host laboratory using expressed AURKAIP1-FLAG in both U2OS and HEK293T cell lines suggested that AURKAIP1 is cleaved to a 15kDa species by an unknown mechanism and may

Figure 1.13 – AURKAIP1 and Cox24 contain a conserved DUF1713 domain. Protein sequences for *H.sapiens* AURKAIP1 (Q9NWT8), *D.rerio* AURKAIP1 (), *M.musculus* AURKAIP1 (), *S.cerevisiae* Cox24 (P32344) and *S.pombe* Cox24 (Q9P7H5) were aligned using clustal omega (http://www.ebi.ac.uk/Tools/msa/clustalo) . The location of the DUF1713 domains (IPRO13177) domains in each sequence were taken from InterPro (www.ebi.ac.uk/interpro), and are highlighted in red above. Black asterisk (*) = fully conserved residue, colon(:) = residues with strongly similar properties, period (.) = residues with weakly similar properties.

not be a *bona fide* mitoribosomal protein (Thompson, 2014). This cleavage event, from a 25kDa full-length species to a 15kDa species, is most likely performed by one of the mitochondrial proteases.

1.5 Mitochondrial Proteases

Cell viability is dependent upon protein homeostasis within the cell and the individual cellular compartments. Proteases are used not only for protein catabolism but for modulating biochemical activities and this is also true for the mitochondrial proteases. In humans, mitochondria have maintained their own proteasome of which the vast majority of components are nuclear-encoded (Pagliarini *et al.* 2008) and in most cases, are highly conserved in eukaryotic cells (Käser and Langer, 2000). The mitochondrial proteases are

located within all mitochondrial subcompartments (Figure 1.14) and are involved in processes such as mitophagy, protein import, protein quality control and mitochondrial biogenesis.

The mitoproteases involved in protein import of nDNA-encoded mitochondrial proteins have already been discussed (1.4.1). Following protein import, there are additional proteases that are involved in further maturation of some mitochondrial matrix proteins. Mitochondrial intermediate peptidase (MIP) cleaves an octapeptide from some matrix proteins once the MTS has been cleaved off by MPP (Vögtle *et al.* 2011) in order to improve the stability of these proteins. For mtDNA-encoded proteins, methionine aminopeptidase 1D (METAP1D), a deformylase that is located within the mitochondrial matrix, removes the methionine residue at the N-terminus as part of the N-terminal methionine excision pathway generating functional, active proteins (Serero *et al.* 2003) prior to their insertion into the IMM.

Mitophagy is the selective degradation of damaged or excess mitochondria (Kissova *et al.* 2004). One of the proteases involved in mitophagy, USP30 (ubiquitin-specific peptidase 30, a cysteine protease), is located on the OMM (Figure 1.14). Briefly parkin, an E3 ubiquitin ligase, attaches ubiquitin onto target proteins e.g. TOMM20 when there is mitochondrial damage. USP30 hydrolyses the ubiquitin which inhibits mitophagy, since the target protein is no longer recognised by parkin. This process of ubiquitylation and deubiquitylation regulates mitophagy (Cunningham *et al*. 2015).

To date, there are four ATP-dependent proteases and two ATP-independent proteases that are involved in protein degradation within the mitochondria. Within the IMS, HTRA2 (high temperature requirement A2), an ATP-independent serine protease, plays an important role in degrading oxidised proteins (Vande Walle *et al.* 2008) and ATP23 (mitochondrial inner membrane protease Atp23 homologue), an ATP-independent protease, is thought to be involved in degrading lipid transfer proteins (Potting *et al.* 2010).

In the IMM, members of the AAA (ATPases associated with diverse cellular activities) degrade damaged IMM proteins: the intermembrane AAA (iAAA) and the matrix AAA (mAAA) ATP-dependent proteases. The iAAA has a catalytic site that faces the IMS (Gerdes *et al.* 2012) and in humans is a zinc metalloprotease, YME1L. YME1L, like ATP23, is also thought to be

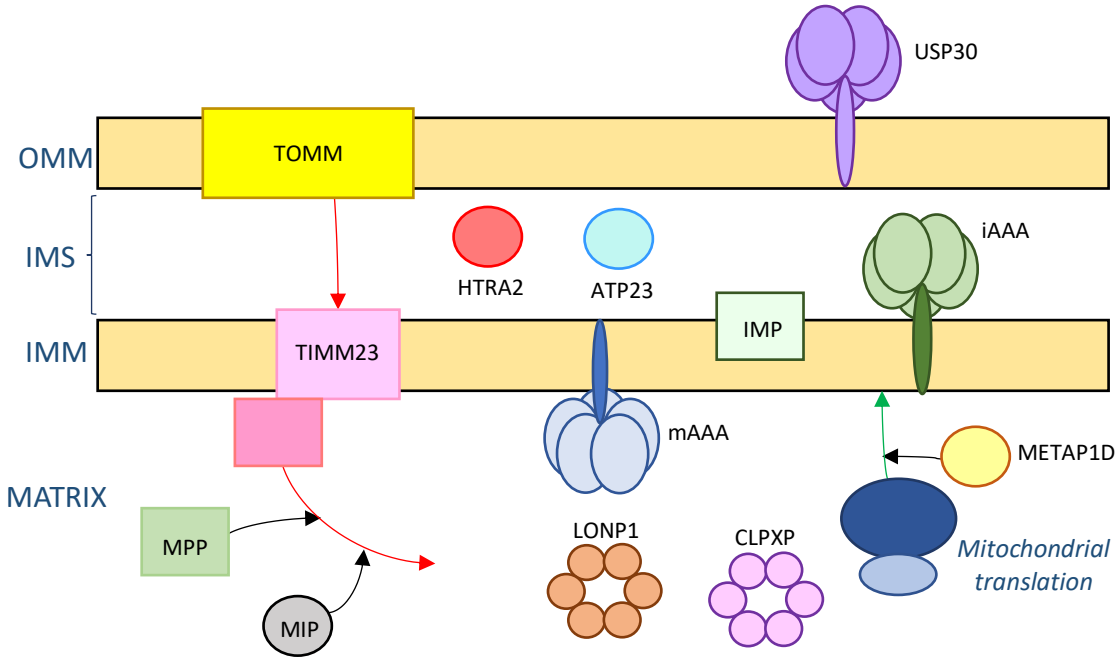

Figure 1.14 – Overview of human mitochondrial proteases. A 2D cartoon (not to scale) depicting some of the main proteases present in human mitochondria within different mitochondrial subcompartments. Red arrow = pathway of imported nuclear-encoded mitochondrial matrix proteins, green arrow = pathway of mitochondrial-encoded proteins. Proteases are explained further in the text.

involved in degrading lipid transfer proteins such as PRELI domain-containing protein 1 (PRELID1), which is associated with apoptosis resistance (Potting *et al.* 2013) and it has been suggested that both ATP23 and YME1L play a role in respiratory chain biogenesis (Zeng *et al.* 2007, Stiburek *et al.* 2012). YME1L also has a role in regulating mitochondrial dynamics, as YME1L1 mediates processing of OPA1 in the IMS together with the metalloendopeptidase OMA1 (Anand *et al.* 2014). The mAAA has its catalytic site orientated towards the matrix and in humans can be composed of AFG2-like protein 2 (AFG3L2) alone, or a combination of AFG3L2 and paraplegin (SPG7) (Koppen *et al.* 2007). Similar to YME1L1, AFG3L2 degrades damaged or misfolded OXPHOS complex subunits within the IMM (Hornig-Do *et al.* 2012) and in yeast, mAAA protease has been shown to be involved in the maturation of MrpL32 (bL32) (Nolden *et al.* 2005) suggesting that the mAAA protease may be involved in mitoribosome assembly in humans.

In the mitochondrial matrix, there are two further ATP-dependent proteases: CLPXP and LONP1. CLPXP consists of hexamers of two distinct proteins: CLPX and CLPP. CLPX recognises (Flynn *et al.* 2003), binds and partially unfolds the substrate (Baker and Sauer, 2012) before chaperoning the substrate to CLPP, the proteolytic subunit, for proteolysis (Barkow *et al.*

2009). Little is known about the function of CLPXP although a recent publication suggested that CLPXP is involved in mitoribosome assembly, by removing ERAL1 (Era-like 12S mitochondrial rRNA Chaperone 1), a 12S rRNA chaperone, from the mt-SSU in order for the full assembly of the mitoribosome to occur prior to mitochondrial translation (Szczepanowska *et al.* 2016).

1.5.1. LONP1

Human LONP1 is a mitochondrial, nuclear-encoded serine ATP-dependent protease whose gene, *PRSS15* or *LONP1,* is located on chromosome 19p13.3. The promoter region for *LONP1* contains binding sites for NRF2 (-623/+1), NF-κB (-2023/-1230) and potentially HIF-1 (Pinti *et al.* 2011, Fukuda *et al.* 2007). NRF2 (nuclear factor erythroid 2-related factor 2) is involved in regulating several antioxidant pathways, NF-κB is involved in controlling energy homeostasis by upregulating proteins involved in mitochondrial respiration, and HIF-1 has been shown to be a regulator of mitochondrial metabolism. The presence of these binding sites within the promoter region suggests that LONP1 is a highly regulated mitochondrial protein that is important in the cellular stress response (Ngo *et al.* 2009).

The LONP1 monomer is roughly 100kDa although it is thought that LONP1 is only an active protease as a hexamer. In addition, LONP1 is post-translationally regulated by SIRT3 (Sirtuin 3) via acetylation most likely at residue K917 (Gibellini *et al.* 2014). There are three evolutionary-conserved domains in LONP1 that have been identified (Figure 1.15): MTS, ATPase domain and the proteolytic domain. Within the ATPase domain, highly-conserved Walker A and Walker B motifs are primarily responsible for binding and hydrolysing ATP (Walker *et al.* 1982) (Figure 1.15). Human LONP1 shows significant homology to the bacterial La protease (García- Nafría *et al.* 2010) and the yeast Pim-1 (Suzuki *et al.* 1994) but in addition

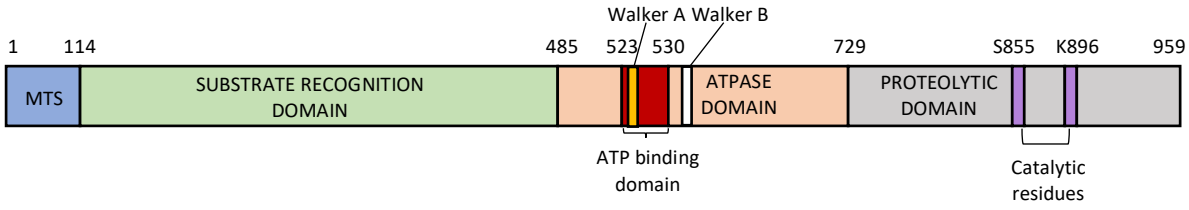

Figure 1.15 – The functional domains of LONP1. A cartoon depicting the functional domains of LONP1. Each domain is shown and their locations are taken from Venkatesh *et al.* 2012. MTS – mitochondrial targeting sequence. The Walker A and B motifs (orange and white respectively) in the ATPase domain, and the catalytic dyad (purple, serine 855 and lysine 896) in the proteolytic domain are shown.

to these, human LONP1 contains a substrate recognition domain at the N-terminus (Figure 1.14). When LONP1 is an active hexamer, the substrate is recognised by the substrate recognition domain, ATP is hydrolysed which induces a conformational change in the hexamer to allow the substrate to reach the proteolytic domain and the substrate is subsequently cleaved (Kereïche *et al.* 2016). A highly-conserved catalytic dyad of Ser855-Lys896 is located within the active site of proteolytic domain (Figure 1.15) that is required for the peptide bond hydrolysis (Botos *et al.* 2004). Generally, LONP1 degrades misfolded proteins but several more specific substrates have also been identified - oxidised mitochondrial proteins e.g. aconitase (Bota & Davies, 2002), StAR (steroidogenic acute regulatory protein, Granot *et al.* 2007) and phosphorylated TFAM (Matsushima *et al.* 2010) amongst others. Human LONP1 degrades TFAM when it is not associated with mtDNA, but in one study LONP1 has been shown to bind to mtDNA physiologically at the D-loop (Lu *et al.* 2007), notably mtDNA sequences that are G-rich e.g. G-quadruplexes (Chen *et al.* 2008). Although, it is currently unknown why LONP1 would bind to mtDNA.

1.6 Mitochondrial Diseases

Mitochondrial disease refers to a clinically heterogeneous group of genetic disorders that are characterised typically by defective oxidative phosphorylation, and caused by mutations in either the nDNA or mtDNA that can be inherited via all known mechanisms i.e. maternal, *de novo,* autosomal dominant and recessive, and X-linked. These mutations occur in mitochondrial proteins or proteins that are involved in mitochondrial function, with the current estimate of 1,158 proteins making up the mitoproteome (Calvo *et al.* 2016).

Since mtDNA is exclusively maternally-inherited, the Mendelian laws of inheritance do not apply (Giles *et al.* 1980). Mutations rates in mtDNA are roughly 15 times higher than in nDNA (Tuppen *et al*. 2009). To date, mutations in almost 300 genes have been identified in patients with mitochondrial disease, including 36 genes located in mtDNA (summarised in Craven *et al.* 2017), as point mutations in protein-coding genes, rRNA genes or tRNA genes and mtDNA rearrangements for e.g. deletions (Lott *et al.* 2013). Most pathogenic mtDNA mutations are heteroplasmic, in which mutant and wild-type mtDNA molecules co-exist in individual cells. When the number of mutant mtDNA molecules reaches a critical threshold in which the cell can no longer tolerate the mutant mtDNA molecules (typically >60%),

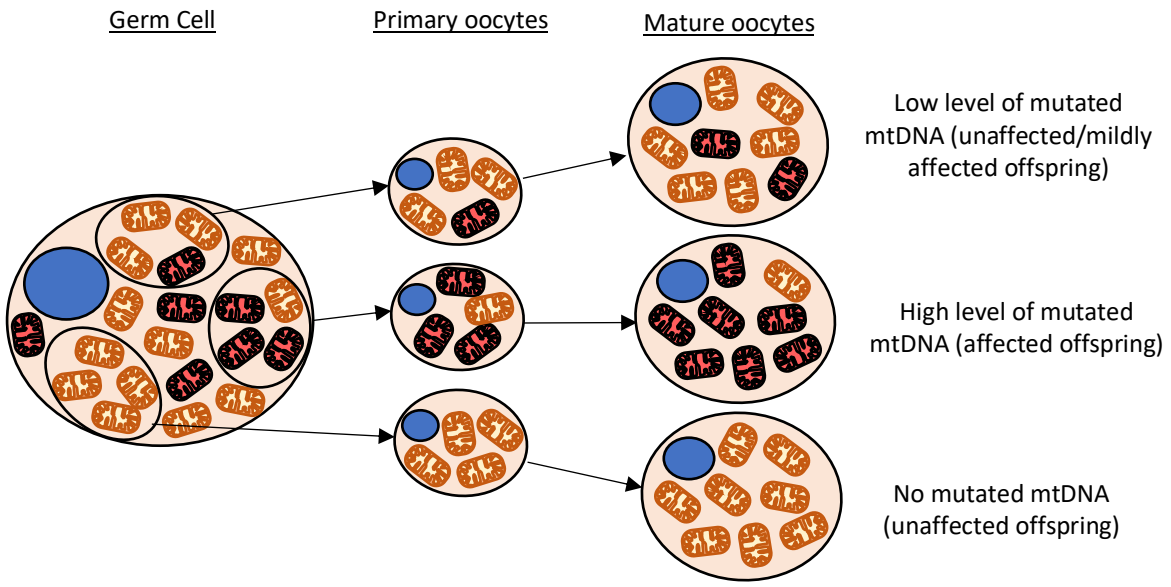

Figure 1.16 – Overview of the mitochondrial genetic bottleneck. A random selection of mtDNA molecules are transferred into each primary oocyte, resulting in mixed populations of wild-type and mutant mtDNA molecules in each. The maturation of oocytes is associated with rapid replication of these mtDNA molecules, which can lead to a shift in the proportion of mutant mtDNA molecules potentially reaching the critical threshold, resulting in mitochondrial disease. Orange mitochondria = contain wild-type mtDNA. Red mitochondria = contain mutant mtDNA. Blue circle = nucleus.

mitochondrial disease occurs (Stewart and Chinnery, 2015). This threshold level varies depending on the mutation, the disease, the organ involved and the individual (Craven *et al.* 2017). In addition, heteroplasmy levels can vary within and between generations due to the mitochondrial genetic bottleneck (Figure 1.16, Olivo *et al.* 1983). The age of onset varies from neonatal to adulthood and mitochondrial disease can affect one or multiple organ systems (Lightowlers *et al.* 2015), typically affecting organs with a high-energy requirement e.g. skeletal muscle and brain (Gorman *et al.* 2016). Considering these factors, and that there is a lack of correlation between genotype and phenotype, mitochondrial diseases are difficult to diagnose.

Due to the complexities of diagnosing mitochondrial disease, identifying the defective gene can sometimes prove difficult. Next Generation Sequencing (NGS) methods are now being implemented to aid in diagnosis, since many genes can be sequenced with a high-throughput. NGS technologies that are being implemented include: unbiased whole exome sequencing (Haack *et al.* 2010), in which only the exons and exon-intron boundaries are targeted, whole genome sequencing (Hartmannová *et al.* 2016), in which the coding and non-coding regions of the genome are analysed, and targeted panels of candidate genes (Lieber *et*

al. 2013), if clinical and functional data have suggested a possible disease of which there are known candidate disease genes. The NGS methods are being utilised in diagnostic and research settings and thus novel unidentified disease candidate genes are being identified. For example, mutations in *TMEM126B*, a previously unidentified complex I assembly factor, were found in patients with a previously unidentified complex I deficiency (Alston *et al.* 2016) and later validated with functional data.

Even though an increasing number of diverse gene mutations have been identified associating with mitochondrial disease, a multidisciplinary approach involving histochemistry, biochemistry and molecular genetics is employed for diagnosis (summarised in MacFarland *et al.* 2010). This approach is often required due to the clinical heterogeneity of mitochondrial disease although some clinical features can provide clues as to the nature of the mutation e.g. visual deterioration in a young adult suggests Leber's Hereditary Optic Neuropathy (LHON), which would result in the targeted sequencing of the three known LHON mtDNA mutations (Yu-Wai-Man *et al.* 2003). However, mitochondrial diseases tend to have multiple overlapping phenotypes such as muscle weakness and muscle biopsy findings such as a reduction in complex IV as revealed by COX/SDH staining or biochemistry. Further complications can arise in diagnosing patients such as a lack of family history, or a reduction in penetrance amongst other family members. Therefore, many patients with genetic diseases remain undiagnosed. One of the techniques that has been employed in identifying mutations in the exons (protein-coding) of genomes is whole exome sequencing (WES). Only ~2% of the human genome consists of exomes, the coding sequences of the genome, yet they account for ~85% of known disease-related variants (Bamshad *et al.* 2011) WES is therefore deemed to be a faster and more cost-effective method compared to whole genome sequencing (WGS), and an effective alternative to gene-panel tests if the phenotype is more general.

1.7 Aims of the Project

Many of the patients with a mitochondrial disease of unknown origin present with mitochondrial protein synthesis defects. It is therefore crucial that we increase our understanding of this process, where currently several areas of mitochondrial gene expression remain unknown. Recent cryo-EM structures of the mitoribosome, involved in mitochondrial translation, have identified new mitoribosomal proteins. I, therefore, decided to focus my project onto one of these uncharacterised proteins that has recently been identified as a member of the mt-SSU, AURKAIP1. Currently, there is conflicting data from within the literature and my host laboratory with regards to AURKAIP1. This could be due to the use of a human cell line expressing C-terminal FLAG-tagged AURKAIP1, since the FLAG-tag could interfere with the function of AURKAIP1. There are also some discrepancies in the size of AURKAIP1 within the mitochondria, since cryo-EM structures have only identified the N-terminal 71 amino acids of AURKAIP1, whereas AURKAIP1-FLAG was identified as a 15kDa species. The primary focus of my project was therefore to further characterise AURKAIP1 and determine its role within the mitoribosome.

During the course of my project, I generated data indicating a role for a mitochondrial matrix protease, LONP1, in the cleavage of AURKAIP1. A patient with mutations in LONP1 was also identified during my studies and was utilised to further investigate LONP1.

More specifically, the aims of my project were:

- To produce stable human cell lines that can express AURKAIP1 with or without a C-terminal FLAG-tag and to characterise the consequences of their overexpression.

- To determine whether AURKAIP1 associates with the mitoribosome.

- To identify the point site at which AURKAIP1 is cleaved using *in vitro* assays and siRNA depletion of known matrix proteases.

- To investigate a patient with mutations in *LONP1*, a mitochondrial matrix protease, and characterise the effects of these mutations on LONP1 function *in vitro*.

CHAPTER 2: MATERIALS AND METHODS

2.1 Cell Culture

2.1.1 *Mammalian Cell Lines and Tissues*

HEK293 Flp-In™/TREx™: The human embryonic kidney (HEK293T) cell line containing the Flp-In™/TREx™ system (Life Technologies) contains a constitutively active tetracycline (Tet) repressor and integrated Flip recombinase target (FRT) sites.

Tetracycline-inducible HEK293T cell lines: HEK293T-mS27-FLAG was prepared by Dr Mateusz Wydro (Richter *et al.* 2010). HEK293T-mL45-FLAG was prepared by Dr Nicole Mai (Mai, 2016). HEK293T-AURKAIP1 and HEK293T-AURKAIP1-FLAG were prepared as part of this project.

HeLa (ATCC®-CCL-2™): An immortalised human cervical cancer cell line originating from Henrietta Lacks (Gey *et al.* 1952).

U2OS (ATCC®-HTB-96™): An immortalised human osteosarcoma cell line (Ponten and Saksela, 1967).

143B (ATCC®-CRL-8303™): An immortalised human osteosarcoma cell line.

143B.206 Rho^0 (ρ^0): A 143B cell line that is devoid of mtDNA following extended ethidium bromide treatment (as described in King and Attardi, 1989).

Primary Skin Fibroblasts: All skin fibroblast cell lines were provided by the NHS Highly Specialised Service for Rare Mitochondrial Disorders, Newcastle-upon-Tyne with full ethical approval. Paediatric control cell lines used were: M1202-16, M1203-16, M1123-12 and M1171-13. LONP1 patient cell lines used were: M0938-13, M0561-16.

Skeletal Muscle Tissue: Samples were provided by the NHS Highly Specialised Service for Rare Mitochondrial Disorders, Newcastle-upon-Tyne with full ethical approval. Paediatric control tissue used: M0466-16, M0861-16. LONP1 patient tissue used: M0840-13.

Informed consent had previously been obtained by the NHS Highly Specialised Service for Rare Mitochondrial Disorders from patients and/or guardians for use of their cells and tissues for research purposes.

2.1.2 *Cell Culture Maintenance*

Cell culture work was performed in a class II Microflow cabinet and cells were monitored daily using an Axiovert25 inverted microscope (Zeiss). Cell lines were cultured at 37°C, 5% CO_2 with humidity in 24-well plates, 6-well plates (Cellstar) or 25cm^2, 75cm^2, 225cm^2 and 300cm^2 vented tissue culture flasks (Corning).

All cell lines were cultured in Dulbecco's modified Eagle's medium containing 1mM pyruvate, 2mM L-glutamine and 4500mg/L glucose (DMEM, D6540) supplemented with 10% foetal calf serum (FCS, Sigma-Aldrich, F7524), 1 x non-essential amino acids (NEAA, Sigma-Aldrich, M7145) and 50µg/ml uridine. HEK293T cell lines with inducible expression of AURKAIP1, AURKAIP1-FLAG, mL45-FLAG and mS27-FLAG were cultured in supplemented DMEM (as above) with 10µg/ml Blasticidin^S (Melford laboratories, B1105) and 100µg/ml Hygromycin^B (Invitrogen, 10687010) every third feed.

At 80-100% confluency, cell lines were passaged to ~30% confluency by harvesting in 1 x phosphate buffered saline (PBS)/1mM EDTA or 1 x trypsin-EDTA (Sigma-Aldrich, 59418C) for fibroblast cell lines. An equal volume of media was added and cells were pelleted at 230*g*, 4mins. Cell pellets were resuspended in fresh media and a fraction of the cells were seeded, the number of which was determined by the intended application.

2.1.3 *Cell Counting*

Cells were harvested (2.1.2) and resuspended in 5ml or 10ml fresh media. Of this cell suspension, 10µl was added to each chamber of a Neubauer improved haemocytometer. The number of cells in each square of the chamber were counted and averaged, then multiplied by 10^4 to determine the number of cells per ml of cell suspension.

2.1.4 *Cell Line Storage and Thawing*

Cell lines were harvested (2.1.2) at >80% confluency and the cell pellet was resuspended in 0.75 ml FCS supplemented with 10% dimethyl sulphoxide (DMSO) in cryostorage vials. The vials were stored in a Nalgene® Mr Frosty at -80°C overnight and then transferred to a liquid nitrogen storage tank for long-term storage.

Cell lines removed from liquid nitrogen storage were placed directly onto a 37°C heat block. Once defrosted, 5ml pre-warmed media was slowly added to the cells. The cell suspension was subsequently pelleted at 230*g* for 4 mins, resuspended in fresh media and transferred to a new flask.

2.1.5 *Mycoplasma Testing*

Cell cultures were tested for the presence of *Mycoplasma*. A 1ml aliquot of spent media was taken from the flask (minimum 24hrs with cells) and centrifuged at 230*g* for 4mins. The supernatant was transferred to a fresh tube and stored at 4°C until tested. The MycoAlert® *Mycoplasma* Detection Kit (Lonza, LTD7-218) was used according to manufacturer's instructions. If *Mycoplasma* was detected, cells were either thrown away or treated with 25µg/ml plasmocin™ (Invivogen, ant-mpp) every 3-4 days for 2 weeks in isolation. The media was subsequently retested to confirm that the culture was free from mycoplasma.

2.1.6 *Transfection with siRNA*

Transfection with small interfering RNA (siRNA) was performed on HeLa, HEK293T and U2OS cell lines in 6-well plates, T25cm^2 or T75cm^2 flasks. For 3 days treatment, reverse transfection was performed. For 6 days, forward transfection was performed following 3 days treatment by reverse transfection. Volumes of each reagent are stated below (Table 2.1).

Table 2.1: Volumes of reagents for siRNA transfection.

	6-well plate	**T25cm^2 flask**	**T75cm^2 flask**
No. of cells seeded (3 days)	150,000	350,000	1,000,000
No. of cells seeded (6 days)	30,000	75,000	200,000
OptiMEM®-Glutamax™	250µl	750µl	2.25ml
Lipofectamine RNAiMAX	2µl	6µl	18µl
siRNA (20µM)	2.5µl	7.5µl	22.5µl
Fresh media	1.245ml	3.736ml	11.209ml
Total volume	1.5ml	4.5ml	13.5ml

For reverse transfection, Opti-MEM®-GlutaMax™ (Gibco, 51985-026), siRNA (Appendix B) and lipofectamine RNAiMAX (Invitrogen, 13778150) were mixed and incubated at room temperature for 15mins. During this time, the cells were counted (2.1.3), diluted in fresh media and seeded (Table 2.1). The siRNA mix was added to the seeded cells slowly and the cells were incubated at 37°C, 5% CO_2 for 3 days.

For forward transfection, the media was aspirated off and fresh media was slowly added to the adherent cells. The siRNA mix was added as previously described, without disturbing the cells.

2.1.7 *Stable Transfection*

HEK293T cell lines (2.1.1) were independently transfected with one of two plasmid constructs that were generated in my host laboratory (Thompson, 2014): pcDNA5™/FRT/TO containing the full-length AURKAIP1 gene with or without a FLAG-tag at the C-terminus.

In a 6-well plate, 3 x 10^5 cells were seeded with 2ml supplemented DMEM media (2.1.2) and incubated overnight at 37°C, 5% CO_2 with humidity. Two wells were left untransfected as controls. To the remaining wells, 189.4µl DMEM (without supplements), 1.8µg pOG44 (Invitrogen), 200ng plasmid DNA and 10µl ViaFECT™ reagent (Promega, E4981) were mixed and incubated at room temperature for 15mins. The media in each well was replaced with 1.8ml fresh media and the ViaFECT™ mixture was added slowly to avoid disturbing the cells. The cells were incubated at 37°C, 5% CO_2 with humidity for 2 days after which the media was replaced, and selection performed by the addition of 10µg/ml Blasticidin^S (Melford Laboratories, B1105) and 100µg/ml Hygromycin^B (Invitrogen, 10687010) added. The media with added antibiotics was replaced every 3 days. After ~10days, individual clones were transferred to separate wells and cultured. Cells transfected with pcDNA5™/FRT/TO-AURKAIP1 and pcDNA5™/FRT/TO-AURKAIP1-FLAG are designated in this thesis as HEK-AUR1 and HEK-AUR1-FLAG respectively.

2.1.8 *Expression of Recombinant Protein in Mammalian Cell Lines*

HEK293T cell lines transfected with a DNA construct that allowed expression of recombinant proteins were split into two flasks at either 15% or 30% confluency. One of the two flasks was induced with tetracycline (1µg/ml) for either 3 days (from 30% confluency) or 6 days (from 15% confluency). The uninduced flasks were used as controls.

2.2 Bacterial Manipulation

2.2.1 Bacterial Culture and Storage

Bacterial cultures were grown in Lysogeny Broth (LB, 1% NaCl, 1% bacto-tryptone, 0.5% yeast extract, pH 7.0) as a liquid broth, or on LB plates containing 2% agar, with ampicillin (100µg/ml) at 37°C. For long-term storage, cultures were resuspended in 1.5ml LB media containing 18% glycerol and stored at -80°C.

2.2.2 *Transformation*

For constructs generated using the Strataclone Blunt PCR cloning kit (Agilent Technologies, 240207), StrataClone SoloPack competent cells were thawed on ice, and 1µl of the ligation mixture was added to the cells. For all other reactions, 40µl α-select silver efficiency (BIO-85026, Bioline) cells were thawed on ice per reaction, and 4µl of the ligation mixture was added to the cells. The transformation mixtures were incubated on ice for 20mins, heat-shocked at 42°C for 45secs and then incubated on ice for 2mins. Pre-warmed SOC media (250µl) was added to the mixture before incubation at 37°C for 1hr with agitation to allow the cells to recover. The transformation mixtures were centrifuged at 12,000*g* for 30secs, resuspended in 100µl SOC media and spread onto each LB agar plate with appropriate antibiotics. The plates were incubated overnight at 37°C.

2.2.3 *Expression of Recombinant Protein in Bacterial Cell LInes*

Bacterial cultures (100ml) were grown overnight at 37°C with appropriate antibiotics in a shaking incubator (Orbisafe TS Netwise). The 100ml culture was split into 2 x 5 litres flasks, each containing 2 litres of LB media (2.2.1) and grown until the cultures had reached an optical density at 600nm (OD_{600}) of 0.6. The cultures were induced with 1mM IPTG (final concentration) and incubated for 2.5hrs at 30°C at 160rpm in a shaking incubator. After 2.5hrs, the cultures were centrifuged at 3750*g* for 10mins at 4°C in an Avant J26 ultracentrifuge in a JLA-8.100 rotor**.** The pellets were resuspended in a small volume of PBS, combined and centrifuged at 3750*g* for 15mins at 4°C in 50ml falcon tubes. The supernatants were discarded and the pellets were frozen in liquid nitrogen and stored at -80°C until use.

2.2.4 *Bacterial Cell Lysis*

All samples were kept on ice at all times. In a 50ml falcon tube, 5ml bacterial cell pellets from a large-scale culture (2.2.3) were lysed initially in 3ml lysis buffer (50mM Tris-HCl pH 8.0, 10mM β-mercaptoethanol (β-ME), 0.1mM EDTA). The cell pellets were resuspended with a glass rod until the suspension was viscous. A further 27ml of lysis buffer was added in 3 stages and mixed as before. The suspension was homogenised using the UltraTurrax® T3 Homogeniser (Ika) for 3 x 10secs, with 20secs break in between. All samples were decanted into a pre-chilled 50ml falcon tube and centrifuged at 12,000*g* at 4°C for 1hr in Beckman-Coulter Avanti J25 centrifuge with the JA25-50 rotor. The supernatants were transferred to fresh tubes and used straight away.

2.2.5 Cracking Gel Bacterial Lysis

The cracking gel allowed for rapid screening of bacterial clones to determine if an insert was present in the transformed vector. Using a toothpick, a small sample of the clone was smeared onto the inside of a 0.5ml Eppendorf tube, before being restreaked onto a fresh agar plate with appropriate antibiotics. To each sample, 20µl cracking buffer (50mM NaOH, 0.5% SDS, 5mM EDTA) and 4µl 5 x DNA loading dye (35% glycerol, 0.02% bromophenol blue) was added. The tubes were incubated at 68°C for 30mins and then pelleted at 13,000*g* for 10mins. The supernatants were directly loaded onto a 0.7% agarose gel and separated by agarose gel electrophoresis (2.3.9) before visualisation on the ChemiDoc™ MP Imaging System (BioRad) using Image Lab™ Software.

2.3 DNA Manipulation

2.3.1 *Isolation of Plasmid DNA from Bacterial Cultures*

Bacterial cultures were grown in 5ml LB media with appropriate antibiotics overnight at 37°C at 180rpm in a floor-standing orbital shaker. The plasmid DNA was extracted from these cultures using the GeneJET® Plasmid Mini-Prep kit (Thermoscientific, K0503) according to the manufacturer's protocol. The eluate was used immediately or stored at -20°C.

2.3.2 *Restriction Digest*

Restriction endonuclease sites were selected by ensuring that they were not present in the amplified fragment, and were present in the multiple cloning site (MCS) of the vector. Restriction sites (Appendix G) were incorporated into the 5' end of primer sequences (Appendix C). Typically, 200ng - 1µg DNA (vector, amplified fragment or ligation fragment) was incubated with appropriate restriction endonucleases (Appendix G) in NEB restriction buffer 2 pH 7.9 (1 x buffer = 50mM NaCl, 10mM Tris-HCl, 10mM $MgCl_2$, 1mM DTT) in volumes of 10 - 50µl. The reactions were incubated at 37°C for 3hrs and then immediately placed on ice.

2.3.3 *Dephosphorylation of Vectors*

Vectors that were digested by restriction endonucleases required dephosphorylating to remove the 5'-PO_4 that remains following digestion. Removal of this PO_4 ensures that the vector does not re-ligate, and that the digested DNA fragment can be efficiently ligated into the digested vector. To a typical restriction digest reaction (20µl), 2µl 10% SDS, 2µl 1M Tris-HCl pH 9.0 and 1*U* alkaline phosphatase (10713023001, Roche) were added. The reaction was incubated at 37°C for 30mins, and

then 50°C for 30mins. The reaction was stopped by placing on ice, and the plasmid was isolated by phenol/chloroform extraction.

2.3.4 *Ligation*

Typical ligation reactions contained 50ng digested, dephosphorylated vector and digested DNA fragments at a molar ratio of 1:3 respectively. Reactions were carried out using the Rapid DNA Ligation kit (K1422, ThermoScientific®) according to manufacturer's instructions. Reactions were kept on ice until necessary for bacterial transformation (2.2.2).

Blunt PCR products (AURKAIP1-TransSyn) were ligated into pSC-amp/kan (Appendix A) using the StrataClone Blunt PCR cloning kit (Agilent Technologies, 240207) according to manufacturer's instructions. Briefly, 3µl StratClone Blunt Cloning Buffer, 2µl PCR product (20ng) and 1µl Strataclone Blunt Vector Mix amp/kan were mixed gently and incubated at room temperature for 5 mins. The reaction was immediately placed on ice.

2.3.5 *Phenol/Chloroform Extraction*

Typically, an equal volume of phenol (Sigma, P-4557) was added to the sample in a 1.5ml Eppendorf tube. The tube was vortexed for 15secs and centrifuged at 12,000*g* for 2mins. The aqueous phase was transferred to a clean tube, and an equal volume of a 1:1 mix of phenol and chloroform (Sigma, C2432) was added. The tubes were vortexed and centrifuged as above. The aqueous phase was transferred to a clean tube and an equal volume of chloroform was added. The tube was vortexed, centrifuged as before and the aqueous phase was transferred to a clean tube for DNA precipitation (2.3.6).

2.3.6 *Ethanol Precipitation*

To the DNA sample, 3M sodium acetate and 100% ice-cold ethanol (EtOH) were added to the DNA sample at 0.1 x and 2 x sample volumes respectively and incubated at -80°C for 2hrs – overnight. The samples were then centrifuged at 12000*g* for 10 mins at 4°C, the supernatants were discarded, and the pellets were washed in ice-cold 75% EtOH. The samples were centrifuged as above and the supernatants were removed. The pellets were left to air-dry, resuspended in 10-20µl dH_2O and either used immediately or stored at -20°C.

2.3.7 *Measuring Nucleic Acid Concentration*

DNA and RNA concentrations were determined using the Nano-drop (Spectrophotometer ND-1000) using 1µl of sample that was measured at wavelengths of 230nm and 260nm wavelengths. The

algorithm calculated concentrations based on 260nm, 1 A260 unit (1cm light path) being equivalent to 50µg/ml double-stranded DNA, 40µg/ml double-stranded RNA or 33µg/ml oligodeoxynucleotide.

2.3.8 *DNA Extraction from Whole Cells*

Mammalian cells were harvested, pelleted (2.1.2) and resuspended in 400µl 1 x TE buffer (10 mM Tris-HCl, pH 7.4, 1mM EDTA) with 1% SDS and 2mg/ml proteinase K (Roche, 25530-049). The samples were transferred to a 1.5ml Eppendorf tube, inverted 5 times and incubated at 37°C overnight with agitation. If the suspension was clear, phenol/chloroform extraction (2.3.5) and ethanol precipitation (2.3.6) were performed, and following resuspension the DNA concentration was measured (2.3.7).

2.3.9 *Agarose Gel Electrophoresis*

Agarose gel electrophoresis was used to analyse DNA using 1% - 4% agarose gels, depending on the size of the DNA species. Agarose (NBS Biologicals, NBS-AG500) was dissolved in 1 x TAE buffer (40mM Tris-acetate, 1mM EDTA pH 8.0) in a microwave until clear. Once cooled, EtBr was added to a final concentration of 0.5µg/ml. The liquid agarose was poured into a gel cast and allowed to set at 4°C. The samples were mixed in 6 x DNA loading dye (40% glycerol, 0.02% bromophenol blue, 0.02% xylene cyanol) prior to loading and electrophoresed alongside a 1kb ladder (Invitrogen) in 1 x TAE buffer at a constant voltage of 70V. The samples were visualised on the ChemiDoc™ MP Imaging System (BioRad) using Image Lab™ Software.

2.3.10 *Polymerase Chain Reaction (PCR)*

PCR reactions were performed on a PTC200 PCR Thermal Cycler and appropriate PCR conditions were used (Table 2.2). All primers were custom synthesised by Eurogentec (Appendix C) and stored as stock (100µM) and working concentration (10µM) primers were in distilled, deionised sterile water (ddH_2O) at -20°C.

Standard PCR reactions contained (final concentrations in brackets): 10-50ng DNA template, Taq buffer (1x), dNTPs (0.2mM), forward and reverse primers (0.5µM each, Appendix C), $MgCl_2$ (1mM), Taq polymerase (1*U*)**.** PCR reactions requiring a proof-reading enzyme contained (final concentrations in brackets): 50-100ng DNA template, Phusion HF buffer (1x), dNTPs (0.2mM), forward and reverse primers (0.5µM each, Appendix B), Phusion Hot Start II High Fidelity DNA Polymerase (1*U*), ddH_2O (to 50µl).

Table 2.2: PCR conditions used for proofreading PCR, general PCR, sequencing and qPCR.

Step	Proofreading PCR	General PCR	Sequencing	qPCR
Initial denaturation	98°C, 3mins	95°C, 3mins	95°C, 10mins	95°C, 10mins
Denaturation	98°C, 30secs	95°C, 1min	95°C, 10secs	94°C, 30secs
Annealing[a]	T_m, 30secs	T_m, 1min	60°C, 10secs	60°C, 30secs
Elongation	72°C, 30secs	72°C, 1min	72°C, 15secs	72°C, 15secs
No. of Cycles (total)	35	35	45	19
Final Elongation	72°C, 3mins	72°C, 5 mins	65°C, 50secs	72°C, 10mins
Final Hold	4°C, ∞	4°C, ∞	4°C, ∞	4°C, ∞

[a]Annealing temperatures for proofreading PCR and general PCR (T_m) were determined by the primers used for each reaction (Appendices C, D, E).

2.3.11 *Real-Time PCR (qPCR)*

Real-time PCR reactions were performed in the LightCycler® Nano (Roche). Briefly, 300ng total RNA was reverse transcribed to generate single-stranded cDNA using random hexamers (2.4.2). The qPCR was then performed as follows: 2µl reverse transcription reaction, forward and reverse primers (0.5µM each, Appendix D), 1 x Fast SYBR® Green Mastermix (Roche) and ddH_2O (to 20µl). Negative controls lacking cDNA were used for both primer pairs and appropriate qPCR conditions were used for the reaction (Table 2.2).

The cycle threshold (Ct) values were determined by the LightCycler® Nano (Roche) computer program for each sample. The levels of gene expression were determined using the normalised expression ratio ($2^{-\Delta\Delta Ct}$) equation (Livak and Shmittgen, 2001), comparing the Ct values of gene of interest to the Ct values of a standard housekeeping gene (8S rRNA or RNaseMRP) for each sample.

2.3.12 *Sanger Sequencing*

To each DNA construct (450ng), 3µl 5 x BigDye® Sequencing Buffer, 3µl 2.5 x BigDye® Ready Reaction Premix (Applied Biosystems) and 1µl 10µM forward or reverse primer (Appendix E) was added. The PCR was performed using a proof-reading enzyme (2.3.7) and samples were analysed on the ABI 3130xl Genetic Analyser (Applied Biosystems). Raw data was converted into a complete DNA sequence using the sequencing app, MySequence Version 1.3.2 (Shinjukunian).

2.3.13 *Whole Exome Sequencing, Analysis and Interpretation*

Whole Exome Sequencing was funded by the Lily Foundation and performed using the Illumina TruSeq Rapid Exome (45Mb) capture kit. Sequencing was performed using the Illumina HiSeq 2000 platform in 100bp reads, which were subsequently aligned to the human reference genome version

19 (UCSC hg19). Called variants were restricted to coding or splice-site variants with a minor allele frequency ≤ 1%, determined by variant databases (ExAC, NHLBI ESP, 1000G), with priority given to autosomal recessive homozygous or compound heterozygous variants in nuclear-encoded mitochondrial proteins. The pathogenicity of each variant was determined using PolyPhen-2 (genetics.bwh.harvard.edu/pph2/), Align GVGD (Tavtigian *et al.* 2006) and SIFT (sift.jcvi.org) and the identified candidate variants were confirmed with Sanger sequencing (2.3.12). Analysis was kindly performed by Dr Ewen Sommerville.

2.4 RNA Manipulation

2.4.1 *RNA Extraction from Whole Cells*

Cells were harvested, pelleted (2.1.2) and then resuspended in 1ml TRIzol® reagent (Invitrogen, 15596018) following manufacturer's instructions. Briefly, cell suspensions were incubated at room temperature for 5 mins and 200µl chloroform was added. Samples were shaken vigorously for 15secs and centrifuged at 12,000*g* for 15mins at 4°C. The aqueous phase was transferred to a fresh tube with 600µl isopropanol (Sigma, 278475) and 1µl glycogen (Ambion, AM9510). The sample was incubated at room temperature for 10mins and centrifuged at 12,000*g* for 15mins at 4°C. The supernatants were removed, and the pellets were washed in ice-cold 75% EtOH. The pellets were left to air dry, and resuspended in 10-50µl DEPC-treated water, depending on the pellet size. RNA concentrations were determined using the Nanodrop (2.3.3) and either used immediately or stored at -80°C.

2.4.2 *Reverse Transcription*

RNA (300ng - 3µg) was reverse transcribed to single-stranded cDNA using the Superscript™ First-Strand Synthesis System (Invitrogen, 11904-018) or Maxima H minus Reverse Transcriptase kit (Thermoscientific, EP0751) following manufacturer's standard protocol with either random hexamers or oligo-$dT_{(18)}$ primers.

2.4.3 *Ammonium Acetate Precipitation*

An equal volume of 5M NH_4OAc was added to the RNA samples and incubated on ice for 15mins. The samples were then centrifuged at 10,000*g* for 15mins at 4°C and the supernatants were removed. The pellets were washed in 200µl ice-cold 75% EtOH and centrifuged at 10,000*g* for 15mins at 4°C. The supernatants were removed and the samples were centrifuged at 10,000*g* for 1min at 4°C. The remaining supernatants were removed, the pellets were resuspended in 20µl DEPC H_2O and the RNA concentrations were determined using the Nanodrop (2.3.7).

2.4.4 *Denaturing Agarose Gel Electrophoresis*

Samples of isolated RNA were prepared in a total volume of 6µl DEPC H_2O, and made up to 20µl in 1 x MOPS (40mM MOPS acid, 10mM NaOAc, 1mM EDTA pH 7.2), 35% formamide, 5.5% formaldehyde. The samples were incubated at 55°C for 15mins after which ethidium bromide was added (final concentration of 0.1µg/µl), with an equal volume of RNA denaturing loading dye (80% formamide, 10mM EDTA, 0.5% bromophenol blue, 0.5% xylene cyanol).

In order to remove RNases, the gel apparatus was pre-soaked in 3% H_2O_2 for 10mins, rinsed in DEPC H_2O and left to air dry prior to use. The RNA samples were electrophoresed through a denaturing agarose gel (1% agarose, 0.925% formaldehyde, 1 x MOPS) at a constant voltage of 55V for 2hrs.

2.4.5 *High Resolution Northern Blot*

RNA was extracted from samples as described above (2.4.1), except that the pellets were resuspended in 5µl DEPC H_2O with 1*U* RiboSafe (Bioline, BIO-65027). Samples were left to incubate for 1hr on ice and then mixed with an equal volume of RNA denaturing loading dye (80% formamide, 10mM EDTA, 0.5% bromophenol blue, 0.5% xylene cyanol), incubated at 55°C, 5mins and immediately placed back on ice. Samples were loaded onto a 15% denaturing polyacrylamide gel (Table 2.3) and electrophoresed in 0.5 x TBE (50mM Tris base, 50mM boric acid, 1mM EDTA) at 3mA for 1hr, then 6mA for 2hrs.

Table 2.3: Reagents for a 15% denaturing polyacrylamide gel.

Stock Reagent	15% PAG	Final Conc'n
Urea	9.6g	8M
10 x TBE in DEPC H_2O	2ml	1 x
40% acrylamide/bisacrylamide 19:1	7.5ml	15%
25% APS in DEPC H_2O	24µl	0.03%
TEMED	24µl	0.12%
Nuclease-free water	Up to 20ml	-

Once complete, the gels and Genescreen Plus membranes (Perkin Elmer) were washed for 3 x 15mins in 0.25 x TBE. In order to remove RNases, a transfer tank (TE22, Mini Trans-Blot™, BioRad), cassette, sponges and flea were treated as above. The gels and membranes were subsequently sandwiched between 2 layers of 3MM Whatman filter paper and sponges in the cassette, and placed in the tank. The wet transfer was effected in 0.25 x TBE at 4°C at 150mA for 15mins, then 400mA for 30mins. The membranes were removed from the cassette, UV-crosslinked onto a Genescreen Plus

membrane (Perkin Elmer) at 120mJ for 60secs, wrapped in 3MM Whatman filter paper, Saran wrap and kitchen foil and stored at -20°C until use.

Table 2.4: Probes for high resolution northern blotting.

Probe	Internal/External[a]	Location on mt genome	Size
mt-tRNA^{Val}	Internal	m.1601-1655	54bp
mt-tRNA^{Leu}	Internal	m.3199-3352	153bp
mt-tRNA^{Phe}	External	m.523-677	154bp

[a]Probes were designed to span either inside (internal) or outside (external) the desired gene.

Prior to hybridisation with a radioactive probe, the membranes were removed from -20°C and blocked for 2hrs at 42°C with rotation in 10ml of pre-hybridisation solution (50% formamide, 5 x SSPE, 1% SDS, 5 x Denhardt's solution [50 x stock = 1% Ficoll type 400, 1% PVP, 1% BSA –Fraction V]). During this time, the ^{32}P-labelled DNA probes were prepared that targeted specific mitochondrial tRNA transcripts (Table 2.5). The DNA templates used for generating the radioactive probes were prepared using proof-reading PCR (2.3.10, Table 2.4), purified using the Stratagene StrataPrep kit (Agilent Technologies, 400771) and then stored at -20°C. For each probe, the DNA templates (100ng) were resuspended in DEPC H_2O to a final volume of 9µl and denatured at 95°C for 4mins. The templates were immediately placed on ice, mixed with 3µl 5 x random hexamer mix, 5*U* Klenow fragment (DNA polymerase I, Promega, M2201) and 2µl ^{32}P α-dCTP (=20µCi, Perkin Elmer NEG513H) and incubated at 37°C for 2hrs. The radiolabelled probes were subsequently purified using Illustra G-25 columns (GE Healthcare) according to manufacturer's instructions and the incorporation of activity into the final probe was estimated using a Cerenkov counter, of which 500,000cpm was added to the pre-hybridisation solution following blocking. The membranes and probes were incubated at 42°C overnight with rotation.

The membranes were then washed twice in 2 x SSPE (20 x stock = 3M NaCl, 0.2M NaH_2PO_4, 20mM EDTA) for 15mins at room temperature with rotation and then once in pre-warmed 2 x SSPE/2% SDS at 65°C for 15mins with rotation. The membranes were placed in a cassette with a PhosphoImage screen for 1 – 5 days (depending on the counts returned on the membrane) and the signal visualised using the Typhoon FLA 9500 (GE Healthcare) using ImageJ™ software.

2.5 Protein Manipulation

2.5.1 *Cell Lysis*

Mammalian cells were harvested (2.1.2), pelleted and stored on ice in 1.5ml Eppendorf tubes. The cell pellets were resuspended in 50-200µl cell lysis buffer (50mM Tris-HCl pH 7.5, 130mM NaCl, 2mM $MgCl_2$, 1mM PMSF, 1% NP-40, 1 x EDTA-free protease inhibitor cocktail [Pierce, 88666]) depending on size of the pellet. The resuspension was vortexed for 30secs and centrifuged at 564*g* for 5mins at 4°C. The supernatants were retained, snap frozen in liquid N_2 and stored at -20°C until use.

2.5.2 *Isolation of Mitochondria from Mammalian Cell Cultures*

Mammalian cells were grown in T75cm^2, T225cm^2 or T300cm^2 flasks until 80-90% confluent and harvested (2.1.2). The pellets were resuspended in 2ml homogenisation buffer (0.6M mannitol, 10mM Tris-HCl pH 7.4, 1mM EGTA, 0.1% BSA, 1mM PMSF) and homogenised with a homogeniser with 15 passes. The mix was centrifuged at 400*g* for 10mins at 4°C and the supernatants were retained on ice. The homogenisation step was repeated a further two times. The three supernatant fractions of each sample were centrifuged at 11000*g* for 10mins at 4°C and the supernatants were removed. The pellets were each resuspended in 100µl homogenisation buffer and the 3 fractions of each sample were pooled together. The combined fractions were subsequently centrifuged at 11000*g* for 5mins at 4°C and the resulting pellet was washed 3 times in 500µl homogenisation buffer without BSA. The supernatants were removed, and the resulting pellets were used instantly or snap frozen in liquid nitrogen and stored at -80°C.

2.5.3 *Mitochondria Shaving*

Cells were harvested (2.1.2) and a small volume of cells were retained and lysed, as the cell lysate. Mitochondria were isolated as previously described (2.5.2), except that the final supernatant was retained at the end, as the post-mitochondria supernatant. The pelleted mitochondria were resuspended in homogenisation buffer without BSA (HB –BSA) and the protein concentration was determined using a Bradford assay (2.5.9). The mitochondrial samples were diluted to 5µg/µl in 100µl HB – BSA and divided into 2 samples (sample 1 and sample 2). Sample 1 was left on ice (designated as the unshaved mitochondria). Sample 2 was incubated with 1.25µg proteinase K (Roche, 25530) for 30mins on ice. PMSF was added to sample 2 as a final concentration of 5mM and centrifuged at 11,000*g* for 10mins at 4°C. The supernatants were removed and the pellet was washed in 100µl HB – BSA + 5mM PMSF followed by centrifugation at 11,000*g* for 10mins at 4°C. The supernatants were

removed and the pellets were resuspended in the same volume of HB –BSA as sample 1. All samples were snap frozen in liquid nitrogen and stored at -80°C until required.

2.5.4 *Total Protein Extraction from Muscle Tissue*

Muscle tissue samples were kindly received from Newcastle-upon-Tyne NHS Diagnostics department and stored in liquid nitrogen. To pre-cool the apparatus, liquid nitrogen was poured into the centre of a pestle and mortar and left until all the nitrogen had evaporated. The tissue sample was placed into the centre of mortar along with a little liquid nitrogen and crushed into fine pieces. Drop-by-drop, 350µl RIPA buffer (1% Igepal CA-630, 0.5% sodium deoxycholate, 0.1% EDTA, 10mM β-mercaptoethanol, 10µg/ml PMSF, 15µl/ml Triton X-100, 1 x EDTA-free protease inhibitor cocktail in 1 x PBS) was added, followed by a further 350µl aliquot of RIPA buffer. Once defrosted, the suspensions were transferred to an ice-cold 2ml tube and vortexed for 6 x 10secs. The samples were incubated on ice for 45mins to allow for initial lysis to occur. During this time the homogeniser was assembled, cleaned in 75% ethanol and rinsed with ddH_2O. The samples were homogenised for 1 x 15secs at speed 3, incubated 1min on ice and homogenised again for 1 x 15secs, speed 3. The samples were incubated on ice for 10mins to allow the samples to settle prior to centrifugation at 14000*g*, for 10mins at 4°C. The supernatants were transferred to fresh ice-cold 1.5ml tubes (125µl in each aliquot) and the protein concentrations were measured by a Bradford assay (2.5.9). The samples were either used immediately, or snap frozen in liquid nitrogen and stored at -80°C.

2.5.5 *SDS-PAGE*

SDS-PAGE was performed using the Hoefer Mighty Small™ (GE Healthcare) or Bio-Rad Mini Protean Tetra® Cell systems. All samples were mixed with Laemmli buffer (final concentrations: 10% glycerol, 2% SDS, 125mM Tris-HCl pH 6.8, 0.01% bromophenol blue, 0.01% xylene cyanol, 50mM DTT) and denatured by incubating at 95°C for 3mins, or 37°C for 20mins. The samples were separated on polyacrylamide gels with a 12%, 15% or 18% resolving gel depending on the molecular weight of the protein, and a 3.75% stacking gel (Table 2.5). Electrophoresis was performed in 1 x SDS running buffer (192mM glycine, 25mM Tris, 0.1% SDS) at 100V through the stacking gel, and 150V through the resolving gel. The broad-range molecular weight coloured protein ladder (CSL-BBL, Cleaver Scientific Ltd) was used as a marker.

Table 2.5: Volumes of reagents for SDS-PAGE gels.

Stock Reagent	12% Resolving Gel	15% Resolving Gel	18% Resolving Gel	3.75% Stacking Gel
30% 29:1 acrylamide:bisacrylamide	2ml	2.5ml	3ml	0.625ml
3.75M Tris-HCl pH 8.5	0.5ml	0.5ml	0.5ml	-
0.5M Tris-HCl pH 6.8	-	-	-	1.25ml
ddH_2O	2.395ml	1.895ml	1.395ml	3.02ml
10% SDS	50µl	50µl	50µl	50µl
10% APS	50µl	50µl	50µl	50µl
TEMED	5µl	5µl	5µl	5µl

2.5.6 *Coomassie Brilliant Blue Staining*

Following electrophoresis, polyacrylamide gels were incubated at room temperature with agitation in Coomassie Brilliant Blue stain (45% methanol, 10% acetic acid, 0.2% Coomassie Blue R250) for 30mins. The gels were then washed three times in a de-staining solution (45% methanol, 10% acetic acid) for 20mins each. The signals were visualised with white light on the Chemi-Doc™ Imaging System (Bio-Rad) using ImageLab™ software.

2.5.7 *Silver Staining*

Following electrophoresis, polyacrylamide gels were incubated at room temperature with slight agitation in 50ml 50% methanol for 1hr, and then in freshly-made silver staining solution (0.1% $AgNO_3$, 10mM NH_4OH, 0.36% NaOH) for 15mins. The gel was incubated with the developer solution (0.05% citric acid, 0.04% formaldehyde) until the desired signals could be visualised. The reaction was then quenched with the stop solution (45% methanol, 10% acetic acid). The signals were visualised on the Chemi-Doc™ Imaging System (Bio-Rad) using ImageLab™ software.

2.5.8 *Western Blot and Immunodetection*

After samples were separated using SDS-PAGE (2.5.4), the gel was equilibrated in 1 x transfer buffer (192mM glycine, 25mM Tris, 0.02% SDS, 15% methanol). A PVDF membrane (Immobilin-P, Millipore), pre-wet in 100% methanol for 15secs and then transfer buffer for 15secs, was sandwiched against the gel between double thickness 3MM Whatman filter papers and gauze pads in a cassette. The wet transfer was effected in 1 x transfer buffer in the Mini Trans-Blot™ module (Bio-Rad) for 100V for 1hr at 4°C. The membrane was then blocked in 10ml 5% skimmed milk/TBS-T (Tris-buffer saline [50mM Tris, 150mM NaCl pH 7.6], 0.1% Tween-20) for 1hr with agitation at room temperature before

incubation overnight with the primary antibody (Appendix J) at 4°C with agitation. The membranes were washed 3 times for 15mins in TBS-T at room temperature with agitation to remove the excess primary antibody and then incubated with the secondary antibody (Appendix J) for 1hr. The membranes were finally washed 3 times for 15mins in TBS-T at room temperature with agitation to remove the excess secondary antibody. Detection was carried out using the ECL Prime kit (GE Healthcare) according to manufacturer's instructions and the chemiluminescent signals were visualised on the Chemi-Doc™ Imaging System (Bio-Rad) using ImageLab™ software.

The anti-AURKAIP1 antibody was produced by Eurogentech and purified by Dr Kyle Thompson (Thompson, 2014). Briefly, soluble AURKAIP1 elution was sent to Eurogentech using their speedy 28-day polyclonal antibody production protocol. Two rabbits were utilised and blood was taken at day 0 (pre-immune serum), day 21 (medium bleed) and day 28 (final bleed). Serum from the final bleed was subjected to further purification (detailed in Thompson, 2014). Briefly, approximately 900µg of soluble AURKAIP1 was purified using NHS-activated Sepharose 4 fast flow beads (detailed in Thompson, 2014). Serum from the final bleed was added to the beads, incubated overnight at 4°C. Affinity-purified antibodies were finally eluted with glycine buffer pH 2.5 (50mM Glycine pH2.5, 0.1% Triton X, 150mM NaCl) and immeditately neutralised with 1M Tris/HCl pH 9.0. The three sera were then pooled together and dialysed before the addition of 10% glycerol and 0.02% sodium azide (final concentrations) to produce the final antibody reagent.

2.5.9 *Bradford Assay*

The Bradford assay was used to estimate protein concentrations in samples. Experimental samples were measured in 1µl or 2µl with ddH_2O to a final volume of 800µl. A BSA standard curve was also prepared with 0, 2, 5, 10, 15 and 20µl BSA of a 1mg/ml stock solution to a final volume of 800µl in ddH_2O to give concentrations of 0, 2, 5, 10, 15 and 20µg/µl respectively. Each sample was mixed with 200µl Bradford Reagent (Bio-Rad), vortexed and incubated at room temperature for 5mins. Of each sample, 200µl aliquots were dispensed into a 96-well plate and analysed on the SpectraMax H3 microplate reader (Molecular Devices). The absorbance at 595nm was determined and in conjunction with the BSA standard curve, was used to calculate the protein concentration of the samples.

2.5.10 *Isokinetic Sucrose Gradient Separation*

A total of 0.5g and 1.5g sucrose were each dissolved in 5mls sucrose gradient buffer (50mM Tris-HCl pH 7.2, 10mM MgOAc, 40mM NH_4Cl, 100mM KCl, 1mM PMSF, 50µg/ml chloramphenicol) to generate 10% and 30% sucrose solutions respectively. For each gradient, 0.5mls of 10% sucrose solutions was added to an ultracentrifuge tube with a sterile syringe and needle. A 30% sucrose

solution was then carefully dispensed underneath using a sterile syringe and needle. The gradients were mixed using the Biocomp Gradient Maker 107 (TL55 program – short sucrose, 10-30% S1/1, 0:55/85.0/22) and incubated at 4°C for 1hr. Harvested and pelleted cells (2.1.2) were resuspended in lysate buffer (50mM Tris-HCl pH 7.4, 150mM NaCl, 1mM EDTA, 1% Triton X-100, 1 x EDTA-free protease inhibitor tablet, 10mM $MgCl_2$, 1mM PMSF) and incubated for 40mins at 4°C with agitation. The lysed cells were centrifuged at 12000*g* for 10mins at 4°C and the supernatants were retained. The protein concentrations of the supernatants were measured by the Bradford assay (2.5.9) and 700µg of the lysate was loaded onto each gradient in a total volume of 100µl. The gradients were centrifuged at 100,000*g* for 2hrs 15mins at 6°C in the Beckman Optima TLX ultracentrifuge with acceleration of 1, and deceleration of 4. The gradients were carefully removed from the ultracentrifuge and a total of eleven 100µl fractions were collected. The fractions were either used immediately or stored at -20°C.

2.5.11 *Trichloroacetic Acid (TCA) Precipitation of Proteins*

Trichloroacetic acid (TCA) precipitation was used to concentrate protein samples. An equal volume of 20% TCA was added to each sample, mixed by inversion and incubated on ice for 30mins. The samples were centrifuged at 16000*g* for 15mins at 4°C and the supernatants were carefully removed and discarded. Each sample was then washed three times with 1ml acetone. For each wash, 1ml ice-cold acetone was added, the samples were centrifuged at 16000*g* for 15mins at 4°C and supernatants were carefully removed and discarded. After the second wash, the precipitated proteins were scraped off the side of the microcentrifuge tubes with pipette tips to ensure that all the precipitated protein was pelleted. After the final wash, the samples were pulsed for 30secs and the remaining supernatant was discarded. The samples were left to air-dry on ice for 5mins and the pellets were resuspended in 20µl 1 x Laemmli buffer with 50mM DTT. The samples were used immediately or stored at -20°C.

2.5.12 *Immunoprecipitation (IP)*

Cells were grown in T75cm^2 flasks until 95% confluent and then harvested (2.1.2). The mitochondria were isolated from these cells (2.5.2), and the pellets were resuspended in 500µl lysis buffer (50mM Tris-HCl pH 7.4, 150mM NaCl, 1mM EDTA, 1% Triton X-100, 1 x EDTA-free protease inhibitor cocktail, 1mM PMSF, 1mM $MgCl_2$). The lysate was incubated for 30mins, 4°C with agitation. During this incubation, anti-FLAG® affinity gel (60µl, Sigma, FLAGIPT-1) was centrifuged at 5000*g* for 30secs at 4°C in hydrophobic 1.5ml tubes. The supernatants were carefully removed and the resin was washed 3 times in 1 x wash buffer (50mM Tris-HCl pH 7.4, 150mM NaCl, 1mM $MgCl_2$, 1mM PMSF, 1 x EDTA-free protease inhibitor tablet), 1*U* RiboSafe) followed by centrifugation at 5000*g* for 30secs at 4°C, removing the supernatants in between each wash. The mitochondrial lysates were centrifuged at

12000*g* for 10mins at 4°C and the supernatants were transferred to chilled 1.5ml tubes and kept on ice whilst the protein concentrations of the lysate were determined by a Bradford assay (2.5.9). Two 20µg samples were retained for each sample as the input, and 500µl (up to 2mg) of the mitochondrial lysates were added to the washed resins, and incubated with agitation for 2hrs at 4°C. The samples were centrifuged at 5000*g* for 30secs at 4°C and the supernatants were removed and retained as the flowthrough. The resin was washed 3 times with 500µl 1 x wash buffer, centrifuging at 5000*g* for 30secs at 4°C in between each wash and ensuring all wash buffer was removed. To elute the samples, 1 x PBS and 3 x FLAG® peptide solution (250ng/µl final concentration in 110µl) was added to the resins. The samples were incubated in a Thermomixer at 4°C, shaking at 1050rpm for 45mins, and flicking the tube every 5mins. The samples were centrifuged at 5000*g* for 30secs at 4°C and the supernatants were carefully transferred to chilled 1.5ml tubes. The supernatants are designated as the eluates. The beads were retained in 50µl 1 x PBS and all samples were stored at -20°C.

2.5.13 *Protein Purification using Nickel Resin*

For each sample, 4ml regenerated HIS-Select® Nickel Affinity Resin (Sigma-Aldrich, P6611) was added to 15ml 0mM imidazole solution (Table 2.6) in a 50ml falcon tube. The resin was centrifuged at 1455*g* for 10mins at 4°C in a Beckman Coulter Allegra X-15R ultracentrifuge. The supernatants were discarded and 15ml 5mM imidazole solution (Table 2.6) was added to each tube. The resins were centrifuged at 1455g, 10mins, 4°C and supernatant was discarded. Bacterial cell lysate (2.2.4) was added to the prepared resin and incubated at 4°C on a rotator for 45mins. The tubes were then centrifuged at 1455*g* for 10mins at 4°C. The supernatants were retained as the flowthrough and a 15ml 5mM imidazole solution + β-ME (Table 2.6) was added to the resins. The resins were incubated at 4°C on a rotator for 15mins, centrifuged at 1455*g* for 10mins at 4°C and supernatants were retained, designated as wash 1. A 25ml column was rinsed in ~3ml of 10mM imidazole solution + β-ME (Table 2.6). The resins were added to the columns and washed in ~20ml 10mM imidazole solution + β-ME (Table 2.6), with the flowthrough designated as wash 2. Approximately 8ml 250mM Imidazole solution + β-ME (Table 2.6) was added to the columns and the eluates were collected in 20 fractions (750µl for fractions 1 + 2, 500µl for fractions 3-20).

An equal volume of 1 x Laemmli buffer was added to 10µl of each sample, which were subsequently incubated at 99°C for 3mins and analysed by SDS-PAGE using a precast 4-20% gradient SDS-PAGE gel (BioRad, 567-8094). The gels were visualised on a ChemiDoc MP Imager using ImageLab™ (BioRad) to determine the efficiency of elution of the protein of interest. The fractions containing protein of interest were pooled together, frozen in liquid nitrogen and stored at -80°C.

Table 2.6: Imidazole solutions for Nickel columns.

Stock Reagent	0mM Imidazole	5mM Imidazole	10mM Imidazole	250mM Imidazole	Final Conc'n[a]
2 x Nickel Buffer[b]	50ml	50ml	50ml	50ml	1 x
0.5M EDTA	20µl	20µl	20µl	20µl	0.1mM
1M Imidazole	-	0.5ml	1ml	25ml	As stated
β-mercaptoethanol (+/-)	60µl	60µl	60µl	60µl	0.06%

[a]Volumes stated are for solutions of 100ml. Conc'n = concentration. [b]2 x Nickel Buffer = 50mM Tris-HCl pH 8.0, 20% glycerol, 0.8M NaCl.

2.5.14 *Protein Purification using Heparin Sepharose Column*

Purification was performed on the ÄKTApurifier™ with a Frac-950 (fraction collector), INV-907 (injection valve), M-925 (mixing valve) and PV-908 (outlet valve) (Amersham Biosciences) using the 5ml HiTRAP™ heparin HP columns and data was analysed using Unicorn 5.31 software (GE Healthcare). All solutions were filter-sterilised prior to use. Pumps A1 and B1, and the heparin column were washed in filtered dH_2O. Pump A1 was transferred to deliver Low Salt Buffer (Table 2.7) and pump B1 was moved to deliver High Salt Buffer (Table 2.7). Each pump was subsequently washed in their respective salt buffers. The heparin column was washed in 25ml Low Salt Buffer at a flow rate of 2ml/min. Using a 10ml syringe, 10ml dH_2O followed by 10ml Low Salt Buffer were injected through a filter to wash the injection valve. The sample that was purified using nickel resin (2.5.13) was removed from -80°C, made up to 40ml with No Salt Buffer (Table 2.7) and mixed 5 times by inversion. The sample was then injected as 3 x 10ml to allow the protein of interest to bind to the resin. The column was washed in 20ml of Low Salt Buffer at a flow-rate of 2ml/min. The samples were eluted with a gradient of 0-100% High Salt Buffer at a flow-rate of 2ml/min into 55 x 1ml fractions.

An equal volume of 1 x Laemmli buffer was added to 10µl of selected fractions, incubated at 99°C for 3mins and analysed by SDS-PAGE using a precast 4-20% gradient polyacrylamide gel (BioRad, 567-8094) to determine the efficiency of elution of the protein of interest.

Table 2.7: Salt buffers for Heparin columns.

No Salt Buffer	Low Salt Buffer	High Salt Buffer
0mM NaCl	100mM NaCl	1.4M NaCl
10% glycerol	10% glycerol	10% glycerol
20mM Tris-HCl pH 8.0	20mM Tris-HCl pH 8.0	20mM Tris-HCl pH 8.0
1mM EDTA	1mM EDTA	1mM EDTA
1mM DTT[a]	1mM DTT	1mM DTT

[a]DTT was added fresh on the day of purification.

2.5.15 *Protein Purification using Q Sepharose*

Purification was performed on the ÄKTApurifier™ with a Frac-950 (fraction collector), INV-907 (injection valve), M-925 (mixing valve) and PV-908 (outlet valve) (Amersham Biosciences) using the 1ml HiTRAP™ Q-HP columns and data was analysed using Unicorn 5.31 software (GE Healthcare). The HiTRAP™ Q-HP columns were washed in high salt buffer (Table 2.7) to remove any unbound protein from a previous run, at a flow rate of 1ml/min for 5mins and then washed in low salt buffer (Table 2.7) to remove the high salt at a flow rate of 1ml/min for 5mins. Using a 10ml syringe and a 0.45µm filter, the injection valve was rinsed by injecting 10ml filtered nanopure water, followed by 10ml low salt buffer. The samples that were purified using heparin Sepharose (2.5.14) were removed from -80°C, made up to 30ml with No Salt Buffer (Table 2.7) and mixed 5 times by inversion. The samples were then injected as 3 x 10ml to allow the protein of interest to bind to the resin. The columns were washed in 5ml low salt buffer at a flow rate of 1ml/min and the samples were eluted with a gradient of 0-43% high salt buffer at a flow rate of 1ml/min for 10mins into 40 x 250µl fractions. An equal volume of 1 x Laemmli buffer was added to 10µl of selected fractions, incubated at 99°C for 3mins and analysed by SDS-PAGE using a precast 4-20% gradient SDS-PAGE gel (BioRad, 567-8094) to determine the efficiency of elution of the protein of interest.

2.5.16 *Gel Filtration Analysis*

Gel filtration analysis by size exclusion chromatography was performed on the ÄKTApurifier™ with a Frac-950 (fraction collector), INV-907 (injection valve), M-925 (mixing valve) and PV-908 (outlet valve) (Amersham Biosciences) by using the 2.5ml Superose 6 Increase 3.2/300 column (GE Healthcare, 29-0915-98). All solutions were filter-sterilised prior to use. For identifying LONP1 monomers, the Superose 6 column was washed in 5ml high salt buffer (Table 2.9) with a flow rate of 0.04ml/min. Once the column was washed, purified protein (20µl) was injected into the column. The column was washed in 3ml high salt buffer at a flow-rate of 0.04ml/min and 60 x 50µl fractions were collected. For identifying LONP1 hexamers, 60µl of purified recombinant LONP1 protein (2.5.13) was dialysed in a Slide-a-Lyzer™ MINI 20K dialysis device (ThermoFisher, 10668284). Briefly, the dialysis device was soaked in nuclease-free water for 15mins. The dialysis device was transferred to a beaker of low salt buffer (Table 2.8), stirring at 4°C and 60µl recombinant LONP1 was added directly onto the membrane. The sample was left to dialyse for 2hrs. During this time, the Superose 6 column was washed in 5ml low salt buffer with a flow rate of 0.04ml/min. Once dialysed, 20µl sample was injected into the column. The columns were washed in 3ml low salt buffer at a flow-rate of 0.04ml/min and 50µl fractions were collected. Selected fractions were mixed with Laemmli buffer, incubated at 99°C,

3mins and analysed by SDS-PAGE using a precast 4-20% gradient SDS-PAGE gel (BioRad, 567-8094) to determine the efficiency of elution of the protein of interest.

Table 2.8: Salt buffers for gel filtration analysis.

Low Salt Buffer	High Salt Buffer
20mM Tris-HCl pH 8.0	20mM Tris-HCl pH 8.0
100mM NaCl	1M NaCl
10mM $MgCl_2$	10mM $MgCl_2$
2mM DTT	2mM DTT
10% glycerol	10% glycerol
2mM ATP	2mM ATP
Water to 250ml	Water to 250ml

2.5.17 *Microscale Thermophoresis (MST)*

Microscale thermophoresis was kindly performed by Dr Bradley Peter (University of Gothenburg, Sweden). TFAM was cysteine-labelled using a two-fold excess of NT-547-maleimide dye according to the manufacturer's instructions (NanoTemper Technologies). Twelve two-fold dilutions of unlabelled LONP1 (2.3 to 4650nM) were made in MST buffer (50mM Tris-HCl pH 8.0, 10mM $MgCl_2$, 10% (w/v) glycerol) supplemented with 4mM ATP or ATP-γS, a non-hydrolysable form of ATP. Dilutions were incubated with 200nM labelled TFAM for 10min at 24°C. Samples were analysed in triplicate using a Monolith NT.115 instrument (NanoTemper Technologies, Munich, Germany) with standard capillaries, 80% LED power and 60% MST power for 30secs at 24°C. Thermophoresis data were baseline-corrected and used to calculate K_d (dissociation constant), bound state and unbound state in the NanoTemper analysis software.

2.5.18 *Thermofluor Stability Assay*

The Thermofluor stability assay was kindly performed by Dr Bradley Peter (University of Gothenburg, Sweden). The fluorescent dye Sypro Orange (λ_{ex} = 490nm, λ_{em} = 570nm) was used to monitor the temperature-induced unfolding of wild-type and mutant LONP1. At higher temperatures, the proteins unfold and expose hydrophobic residues to which the dye binds, allowing for determination of thermal stability. LONP1 proteins (1.6μM) were set-up in 96-well plates in 5 x dye in assay buffer (50mM Tris-HCl, pH 8.0, 50mM NaCl) in the presence or absence of 10mM $MgCl_2$ and 4mM ATP. Differential scanning fluorimetry was performed in a C1000 Thermal Cycle using CFX96 real-

time software (BioRad) in 0.5°C increments with a 5secs equilibration time. The relative thermal stability (melting temperature/Tm) was determined as described in Matulis *et al.* 2005.

2.6 In Vitro Protein Import Assay

2.6.1. In Vitro Transcription

DNA fragments encoding AURKAIP1 and AURKAIP1-FLAG were amplified by PCR using a forward primer containing an SP6-promoter sequence together with the appropriate reverse primer (Appendix C). Amplified fragments were purified from the PCR mix using phenol/chloroform extraction (2.3.5), and following resuspension in nuclease-free water, the DNA concentration was determined using the Nanodrop. As a control sample, pSU9-DHFR (kindly donated by Professor Roland Lill, University of Marburg, Germany) was digested using *Pvu*II (New England Biosciences) for 4hrs in NEB Buffer 2, purified from the digestion mix by phenol/chloroform extraction (2.3.5), ethanol precipitated (2.3.6), resuspended in DEPC H_2O and the DNA concentration was determined using the Nanodrop (2.3.7). *In vitro* transcription reactions (20µl) were prepared using the AmpliScribe™ SP6 High Yield Transcription Kit (Epicentre Technologies, AS3107) in the order shown (Table 2.9) and incubated for 2hrs at 37°C. The resulting RNA from each reaction was precipitated (2.4.3) and the RNA concentration was determined using the Nanodrop (2.3.7). Each sample (2µl) was electrophoresed alongside 5µg HeLa RNA as a marker on a 1% denaturing agarose gel (2.4.4).

Table 2.9: Constituents for the *in vitro* transcription reaction.

Reagent	Sample	Final Concentration
RNase-free H_2O	Up to 20µl	-
10 x SP6 reaction buffer	2µl	1 x
100mM ATP	1µl	5mM
100mM CTP	1µl	5mM
100mM GTP	1µl	5mM
100mM UTP	1µl	5mM
100mM DTT	2µl	10mM
Linearised DNA	1µg	50ng/µl
10 x SP6 enzyme solution	2µl	1 x

2.6.2. *In Vitro Translation and Analysis*

Each reaction was set-up as detailed (Table 2.10) and incubated at 30°C for 1hr. Each reaction was immediately placed on ice, and 2µl of each reaction was electrophoresed on a 15% polyacrylamide gel (2.4.4) at 100V through the stacking gel, and then 150V through the resolving gel. The gels were then

incubated at room temperature on a rocker at a slow speed for 15mins in 20ml fixing solution (50% MeOH, 10% acetic acid), soaked for 5mins in 20ml pre-drying solution (7% acetic acid, 7% MeOH, 1% glycerol) and vacuum-dried at 65°C for 2hrs until dry. The gels were exposed to a PhosphorImage screen overnight or up to 4 days and signals were visualised using the Typhoon FLA9500 system and ImageQuant™ software.

Table 2.10: Constituents for the *in vitro* translation reaction.

Reagent	Volume	Final Concentration
Rabbit Reticulocyte Lysate[a]	10µl	-
^{35}S-EasyTag protein mix	3.5µl	35µCi
Amino acids minus Met	0.5µl	25µM
RNA substrate	*X*µl	100ng/µl (=2µg)
RiboSafe	0.5µl	1*U*
Nuclease-free water	Up to 20µl	-

[a]Rabbit reticulocyte lysate (Promega, L4960) is nuclease-treated.

2.6.3. Isolation of Rat Liver Mitochondria

The liver was extracted from a humanely-sacrificed rat and minced in ~20ml ice-cold MSE buffer (220mM mannitol. 70mM sucrose, 10mM HEPES-KOH pH 7.4, 2mM EGTA, 1mM PMSF, 0.1% BSA). All steps were carried out on ice in the cold room at 4°C. The buffer was replaced 3-4 times to remove the released blood. Using a glass/Teflon homogeniser, the sample was homogenised 3-5 times in 20ml volume on top speed to produce an even-textured homogenate. The sample was centrifuged at 400*g* for 4mins at 4°C in a Sorvall SS34 rotor. The turbid supernatant was transferred to SS34 tubes and centrifuged at 8500*g* for 10mins at 4°C. The supernatant was discarded and the pellet was carefully resuspended in 5ml MSE buffer, avoiding the red blood cells. The pellets were pooled together into a SS34 tube, which was filled with MSE buffer without BSA, designated as wash 1. The sample was centrifuged at 8500*g* for 10mins at 4°C, the supernatant was discarded and the resulting pellet was initially resuspended in 5ml MSE buffer without BSA, and then the tube was filled to the top with the same buffer, designated as wash 2. The sample was centrifuged at 8500*g* for 10mins at 4°C and the supernatant was removed. The final mitochondrial pellet was resuspended in a small volume of MSE buffer without BSA in a pre-chilled 2ml Eppendorf tube. The isolated mitochondria were kept on ice for immediate use and the protein concentration was determined by a Bradford assay (2.5.9).

2.6.4. *In Vitro Protein Import*

Each reaction was set-up on ice as detailed (Table 2.11), but omitting proteinase K, into a 0.5ml eppendorf tube and incubated at 30°C, 1hr. All tubes were directly placed on ice. Selected samples (Table 2.12) were then incubated with 5µg proteinase K (Roche, 25530-49) at 37°C for 30mins. To stop

the reaction, PMSF was added to each tube (final concentration of 1mM). All samples were centrifuged at 13,000*g* for 10mins at 4°C after which the supernatant was removed and the pellets were resuspended in 1 x Laemmli buffer (2.5.4). These samples were subsequently analysed following separation through a 15% polyacrylamide gel (2.5.4). The gels were exposed to a PhosphorImage screen overnight or up to 4 days and the signals were visualised using the Typhoon FLA9500 system and ImageQuant™ software.

Table 2.11: Reaction constituents for *in vitro* protein import.

Component	+ FCCP, - Prot. K	- FCCP, - Prot. K	+ FCCP, + Prot. K	- FCCP, + Prot. K
***In vitro* translated protein**	3µl	3µl	3µl	3µl
10mg/ml rat liver mitochondria	10µl	10µl	10µl	10µl
100mM ATP	1µl	1µl	1µl	1µl
100mM NADH	2µl	2µl	2µl	2µl
1M succinate	2µl	2µl	2µl	2µl
5mM FCCP	1µl	-	1µl	-
Protein Import Reaction Buffer[a]	80µl	80µl	80µl	80µl
ddH_2O	-	1µl	-	1µl
Proteinase K (5mg/ml)	-	-	1µl	1µl

[a]Protein import reaction buffer (final concentrations) = 100µM GTP, 1mM creatine phosphate, 15µg/ml creatine kinase, 1mM DTT in isolation buffer. Isolation buffer = 220mM mannitol, 70mM sucrose, 10mM HEPES-KOH pH 7.4, 2mM EDTA, 1mM $MgCl_2$.

2.7 In Vitro Protein Activity Assays

2.7.1. *In Vitro ATPase Assay*

In vitro ATPase assays were performed using the Malachite Green Phosphate Assay kit (BioAssay systems, POMG-25H) according to manufacturer's instructions. Briefly, samples were prepared +/- ATP with 0, 0.5, 1 or 2µg recombinant LONP1 and with or without 6.5pmol TFAM in a total volume of 20µl per reaction and loaded on to Nunclan 96-wells flat transparent plates. A standard curve with phosphate concentrations of 0 - 40µM were also prepared. The samples were incubated in the plate at 37°C for 30mins. A working reagent was prepared by mixing reagent A with reagent B in the ratio of 100:1, and 80µl of this mix was added to each sample. The plates were incubated at room temperature for 25mins and then analysed on the Tecan Infinite M200 at 630nm with 25 flashes, using Magellan 6 software.

2.7.2. *In Vitro TFAM Degradation Assay*

Mastermixes were prepared for 8 x 10µl reactions to include: 9.5pmol recombinant LONP1 protein, +/- 6.5pmol TFAM and 2 x Buffer A or B (Table 2.12). Recombinant LONP1 and TFAM proteins were diluted in Buffer B (Table 2.12) if necessary. The samples were incubated at 37°C for 0, 5, 10, 15, 30, 45, 60 and 75mins respectively and then immediately placed on ice. Samples were separated on a precast 4-20% gradient SDS-PAGE gel (BioRad, 567-8094) and visualised on a ChemiDoc MP Imager using ImageLab™ (BioRad) to determine the efficiency of TFAM degradation.

Table 2.12: Constituents of TFAM degradation assay buffers.

Stock	2 x Buffer A (+ ATP)	2 x Buffer B (- ATP)	Final 2 x Conc'n
5M NaCl	4µl	4µl	100mM
1M Tris-HCl pH 8.0	10µl	10µl	50mM
0.5M $MgCl_2$	4µl	4µl	10mM
1mg/ml BSA	20µl	20µl	0.1mg/ml
100mM ATP	4µl	-	2mM
Nuclease-free water	158µl	162µl	-

CHAPTER 3: Levels of AURKAIP1 are Tightly Controlled

3.1 Introduction

A preliminary siRNA screen of candidate mitochondrial proteins was performed in my host laboratory in both HeLa and ρ^0 cells. Since ρ^0 lack mtDNA, a cell growth defect seen in HeLa and not ρ^0 would suggest that the candidate protein had a potential role in mitochondrial gene expression. AURKAIP1 was identified as one of the proteins that may have a role in mitochondrial gene expression via this preliminary siRNA screen, as a growth defect was seen in HeLa cells, but not in ρ^0. At this time little was known about AURKAIP1, and my project aimed to characterise this protein and identify its function.

AURKAIP1 was originally identified as an ubiquitously-expressed nuclear protein through experiments using ectopic expression of recombinant AURKAIP1 with an N-terminal FLAG-tag, expressed in NIH 3T3 and COS fibroblast cells (Kiat *et al.* 2002). Using FLAG-AURKAIP1, transiently transfected within a pcDNA3 (Invitrogen) vector for continuous expression, Kiat *et al.* demonstrated that AURKAIP1 localised to the nucleus and negatively-regulated Aurora-A kinase, a mitotic serine/threonine kinase (Kiat *et al.* 2002) that is involved in centrosome maturation and separation (Glover *et al.* 1995), promotion of mitotic entry (Hirota *et al.* 2003) and tumourigenesis (Bischoff *et al.* 1998). AURKAIP1 was shown to interact with Aurora-A kinase *in vivo* promoting its degradation via the proteasome-dependent pathway. Further research also revealed that AURKAIP1 was also a binding partner of GSK-3β, another serine/threonine kinase, and that GSK-3β bound and phosphorylated AURKAIP1. Phosphorylated AURKAIP1 was thought to downregulate Aurora-A kinase, as a way of regulating the stages of early mitosis (Fumoto *et al.* 2008) and therefore, GSK-3β was thought to regulate levels of Aurora-A kinase via AURKAIP1.

After this research was published, a MitoCarta study identified AURKAIP1 as a candidate mitochondrial protein (Pagliarini *et al.* 2008) and later the Human Protein Atlas Project (Uhlen *et al.* 2010) concluded that AURKAIP1 had both nuclear and mitochondrial localisation. Since most mitochondrial targeting sequences (MTSs) are located at the N-terminus of nuclear-encoded mitochondrial proteins, Kiat *et al*. may have interfered with the MTS by generating an N-terminal FLAG-tagged protein and thus causing AURKAIP1 to mislocalise to the nucleus.

AURKAIP1 was first shown to localise to mitochondria by utilising a HEK293T cell line that stably expressed AURKAIP1 protein with a C-terminal GFP-tag (Szklarczyk *et al.* 2012) that co-localised with TMRM (tetramethylrhodamine methyl ester), a red fluorescent dye that is taken up by active mitochondria, and is therefore used as a marker for the mitochondrial network (Scaduto and Grotyohann, 1999). Subsequently, AURKAIP1 was identified in preparations of bovine mitochondrial ribosomes via capillary liquid chromatography-mass spectrometry (capLC-MS/MS) (Koc *et al.* 2013) implying that AURKAIP1 not only localised to the mitochondria but that it associated with the mitochondrial ribosome. However, in my host laboratory, endogenous AURKAIP1 could not be detected in cell lysates or mitochondrial lysates using a custom-made or Sigma anti-AURKAIP1 antibody, and thus in order to study AURKAIP1 further an overexpressing cell line had to be utilised. In a previous PhD study (Thompson, 2014), a cell line that could inducibly express AURKAIP1 with a C-terminal FLAG-tag (AURKAIP1-FLAG) was produced by Dr Kyle Thompson. When expression of AURKAIP1 was induced (tetracycline, 1µg/ml, for 3 days), there was a severe reduction in the steady state levels of mitoribosomal proteins, particularly those of the mt-LSU (Thompson, 2014). However, since these data were produced using a C-terminal FLAG tagged protein, and recent publications suggested that AURKAIP1 was located at the interface between the two mitoribosomal subunits (Amunts *et al.* 2015, Greber *et al.* 2015), it was possible that the FLAG tag, rather than elevated levels of AURKAIP1, was causing the severe reduction in mitoribosomal proteins by interfering with the function of AURKAIP1.

Previous work performed by my host laboratory had determined that depletion of AURKAIP1 resulted in a severe cell growth defect, a reduction in COXI, COXII and ND1 protein levels but no change in mtDNA copy number (Thompson, 2014). The current data therefore suggests that levels of AURKAIP1 are very tightly controlled since too much or too little AURKAIP1 is detrimental to the cell.

In this chapter, I will validate previously obtained data from my host laboratory by using an alternative AURKAIP1 overexpressing cell line lacking the C-terminal FLAG-tag so that it is more representative of the endogenous species and to confirm whether the effects of siRNA depletion of AURKAIP1 seen both in the preliminary screen and by Dr Kyle Thompson using siRNA targeted to different regions of the *AURKAIP1* gene.

3.2 Results

3.2.1 *Expression of AURKAIP1 and AURKAIP1-FLAG in HEK293T cell lines*

Constructs of pcDNA™5/FRT/TO-AURKAIP1-FLAG and pcDNA™5/FRT/TO-AURKAIP1 were readily available in my host laboratory. These constructs were checked by Sanger sequencing (Appendix H) before being used to transfect HEK293T cells. Individual clones of HEK293T-pcDNA™5/FRT/TO-AURKAIP1-FLAG (HEK-AUR1-FLAG) and HEK293T-pcDNA™5/FRT/TO-AURKAIP1 (HEK-AUR1) were isolated, propagated and then induced with tetracycline for 3 days to identify expression of either AURKAIP1-FLAG or AURKAIP1.

Uninduced (U) and induced (I) cells were harvested and lysates were produced which were subjected to western blotting with a custom anti- AURKAIP1 antibody (Thompson, 2014). HEK-AUR1 clones 1 and 2 as well as HEK-AUR1-FLAG clone 5 expressed high levels of AURKAIP1 and AURKAIP1-FLAG respectively, detectable as a 15kDa species (Figure 3.1). HEK-AURKAIP1 clones 4 and 5 also expressed AURKAIP1 as a 15kDa species, but only at low levels. HEK-AURKAIP1 clones 1 and 2, and HEK-AURKAIP1-FLAG clone 5 were subsequently used throughout this project.

3.2.2 *Effects of AURKAIP1 and AURKAIP1-FLAG overexpression*

Previous work in my host laboratory had shown that after only 3 days overexpression of AURKAIP1-FLAG, there was a decrease in the steady state levels of the components of the

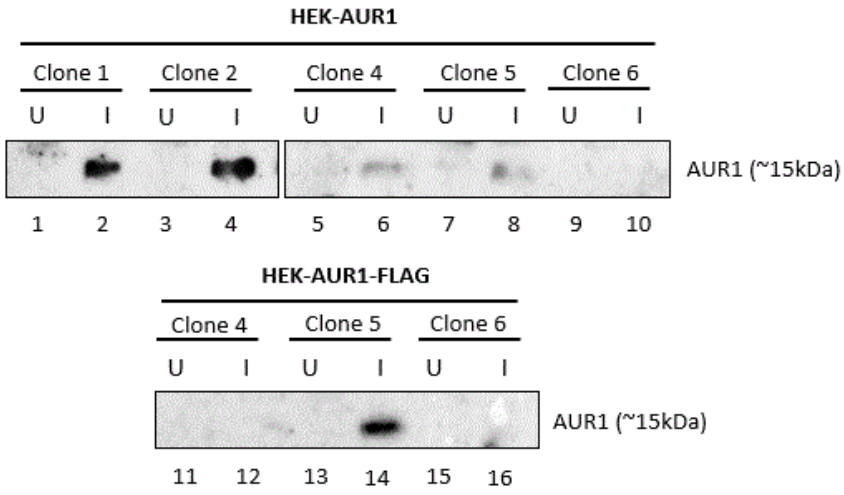

Figure 3.1 – Expression of AURKAIP1 and AURKAIP1-FLAG in HEK293T cells. Cell lysates (60µg) taken from uninduced (U) and induced (I) cells. Induced cells were grown in 1µg/ml tetracycline for 3 days. Lysates were subjected to 15% SDS-PAGE western blotting and incubated with anti-AURKAIP1 antibody.

mt-LSU and mt-SSU (Thompson, 2014). I therefore induced HEK-AUR1 clones 1 and 2 and AURKAIP1-FLAG clone 5 were for 3 days with tetracycline (1µg/ml) and immunoblotted with antibodies that recognised mitoribosomal proteins of the mt-LSU and mt-SSU (Figure 3.2). In all 3 clones, there was a dramatic decrease in the steady state levels of mt-LSU proteins, a decrease in the levels of mt-SSU proteins and potentially a reduction in mitochondrial translation or an increase in mtDNA degradation, indicated by the reduction in steady state levels of COXII. There was a greater effect on the mt-SSU proteins with AURKAIP1-FLAG expression compared to AURKAIP1 overexpression, suggesting that the FLAG tag may have affected the steady state levels of mt-SSU.

Since the steady state levels of the mt-LSU and mt-SSU proteins were decreased upon induction of AURKAIP1 and AURKAIP1-FLAG, real-time PCR was used to determine whether this was possibly due to decreased mitochondrial rRNA. The levels of the 16S rRNA and 12S rRNA of the mt-LSU and mt-SSU respectively were analysed following 3 days of induction of

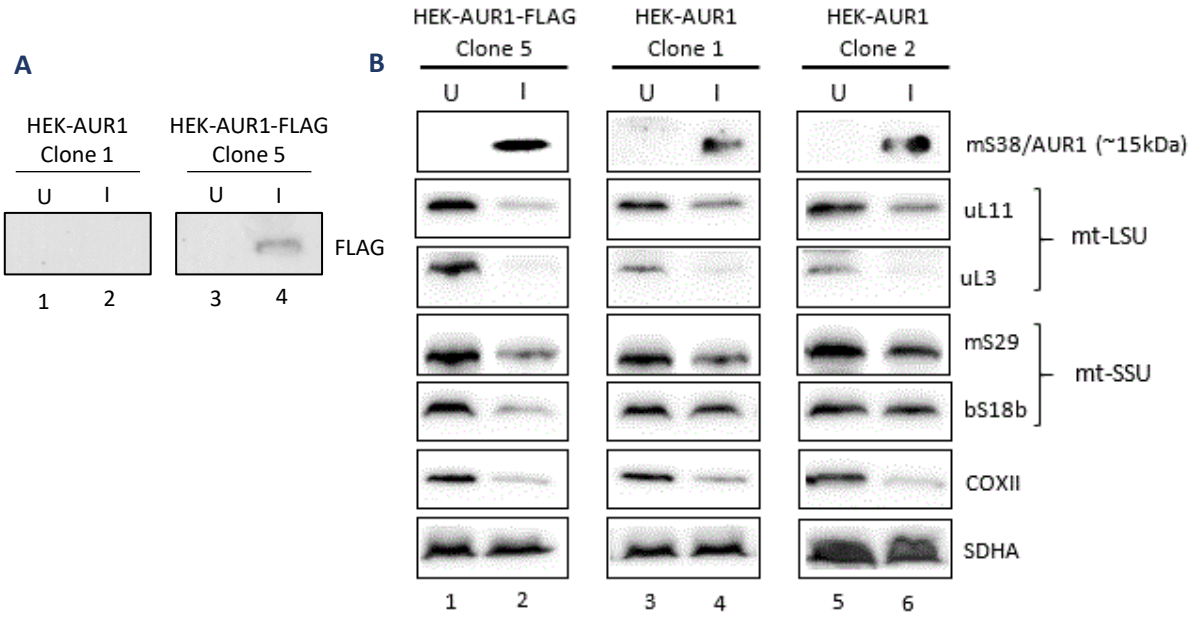

Figure 3.2 – Effects of AURKAIP1-FLAG and AURKAIP1 overexpression on mitochondrial proteins. Cell lysates (60µg) generated from uninduc ed (U) and induced (I) cells (3 days) were subjected to 15% SDS-PAGE western blotting and incubated with antibodies as indicated. SDHA was used as a loading control.

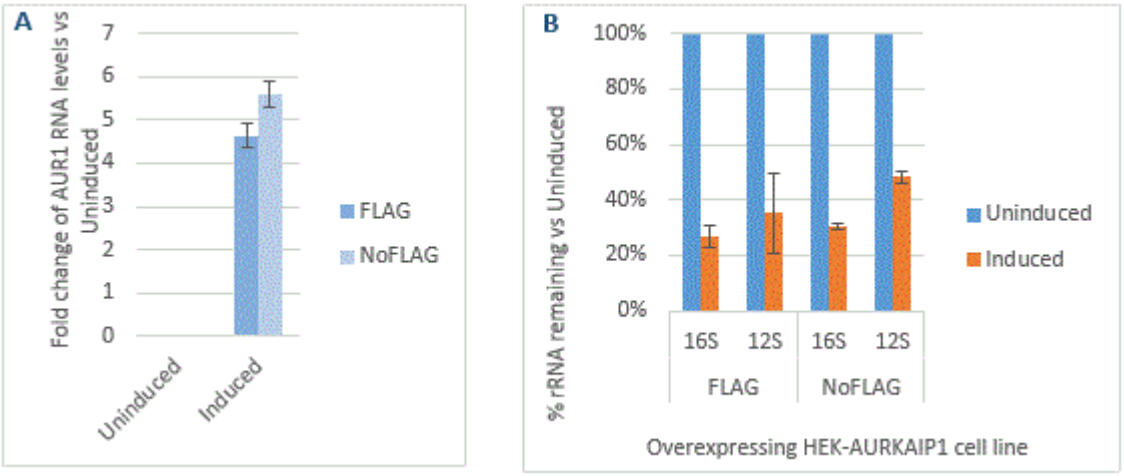

Figure 3.3 – Effects of AURKAIP1-FLAG and AURKAIP1 expression on mitoribosomal rRNA species. RNA was isolated from uninduced and induced (3 days) HEK-AURKAIP1 (NoFLAG) and HEK-AURKAIP1-FLAG (FLAG) cell lines. Reverse transcription and qPCR was performed with A = AUR1 and 18S rRNA primers and B = 18S rRNA, 16S rRNA and 12S rRNA primers. 18S rRNA was used to normalise the data using ΔΔCt (2.3.11). Standard error bars are indicative of three technical repeats.

AURKAIP1 and AURKAIP1-FLAG after 3 days (tetracycline, 1µg/ml). Levels of 16S rRNA and 12S rRNA were reduced when compared to uninduced samples (Figure 3.3). There was a greater reduction in 16S rRNA compared to the 12S rRNA in both AURKAIP1 and AURKAIP1-FLAG, consistent with the observation that the mt-LSU was more affected than the mt-SSU upon AURKAIP1 overexpression. There was a stronger effect on both 16S and 12S rRNA when AURKAIP1-FLAG was expressed compared to untagged AURKAIP1, which reflected the steady state levels of the mt-LSU and mt-SSU proteins respectively (Figure 3.3B).

From these results, overexpression of both AURKAIP1 and AURKAIP1-FLAG cause disruption to the mitoribosome, with decreased levels of both mitoribosomal proteins and the mitoribosomal RNA species. Since AURKAIP1 has been identified as a mtSSU protein (Koc *et al.* 2013), HEK293T cell lines that could inducibly express either mL45-FLAG or mS27-FLAG for the mt-LSU and mt-SSU respectively were utilised to identify whether overexpression of other mitoribosomal proteins had the same effect on the mitoribosome upon overexpression. Both cell lines expressed a protein with a C-terminal FLAG-tag. Overexpression of either HEK-mS27-FLAG or HEK-mL45-FLAG did not cause a decrease in the polypeptide levels of either mitoribosomal subunit, nor in the steady state levels of COXII, suggesting either a decrease in the translation of mtDNA-encoded proteins or an increase in stability (Figure 3.4). There was a slight increase in uL3 with mL45-FLAG expression, and mS29 with mS27-FLAG suggesting that more mt-LSU and mt-SSU is generated upon induction of these recombinant proteins

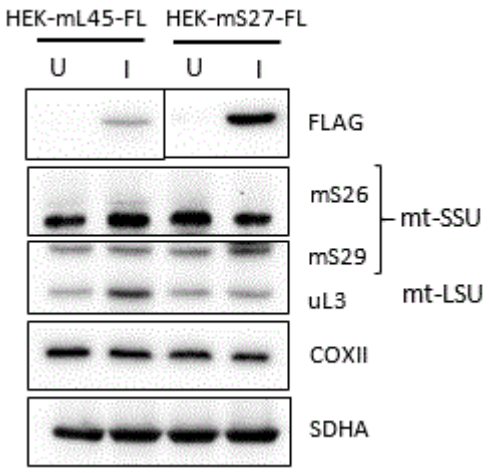

Figure 3.4 – Effect of mL45-FLAG and mS27-FLAG overexpression on mitoribosomal proteins. Cell lysates (60µg) were generated from uninduced (U) and induced (I, 3 days) HEK293T cells with inducible mS27-FLAG or mL45-FLAG expression. Lysates were subjected to 12% SDS-PAGE western blotting and incubated with antibodies as stated.

respectively. Since this effect was not seen with either AURKAIP1 or AURKAIP1-FLAG overexpression, AURKAIP1 may not be a typical mitoribosomal subunit.

3.2.3 *Effects of AURKAIP1 depletion in mammalian cell lines*

Previous work performed in my host laboratory had depleted AURKAIP1 using three different siRNAs, with siRNA2 being used for the majority of the experiments (Thompson, 2014). Using these siRNAs, cell growth was severely affected. The sequence of siRNA2 however has 100% homology to CARD11 (caspase recruitment domain-containing protein 11, Figure 3.5), a protein that contains a CARD domain that interacts with BCL10 (B-cell lymphomia/leukaemia 10) and is involved in apoptosis signalling (Bertin *et al.* 2001). For this

```
AUR1_siRNA2          1 GTACCGGAAGCTGGTGAAG 19
AURKAIP1_t1        745 GTACCGGAAGCTGGTGAAG 763
AURKAIP1_t2        664 GTACCGGAAGCTGGTGAAG 682
AURKAIP1_t3        568 GTACCGGAAGCTGGTGAAG 586
CARD11_t1         2736 GTACCGGAAGCTGGTGAAG 2754
CARD11_t2         2675 GTACCGGAAGCTGGTGAAG 2693
                       ********************
```

Figure 3.5 – AURKAIP1 siRNA2 has 100% homology to CARD11. Amino acid sequences were compared using Clustal Omega. AURKAIP1 sequences NM_017900.2 (t1), NM_001127229.1 (t2) and NM_001127230 (t3) and CARD11 sequences NM_001324281.1 (t1) and NM_032415.5 (t2) were used. Black asterisk represents 100% identity between all sequences.

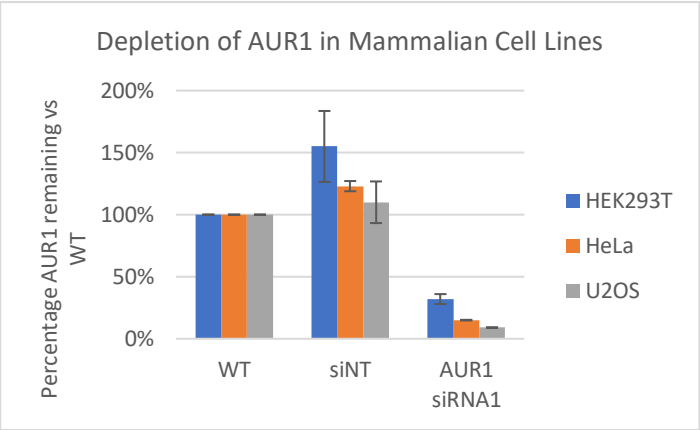

Figure 3.6 – AURKAIP1 siRNA1 is efficient at depleting AURKAIP1. AURKAIP1 was depleted in HEK293T, HeLa and U2OS cell lines using AURKAIP1 siRNA1 (33nM) for 3 days to test the efficiency of the siRNA. RNA was extracted, reverse transcribed and subjected to real-time PCR using AUR1 and 18S rRNA primers. The percentage of AURKAIP1 mRNA remaining compared to wild-type (WT) is depicted here. Untransfected (wild-type) and cells transfected with non-targeting siRNA (siNT) are used as controls. Experimental repeats were performed in triplicate.

reason, AURKAIP1 siRNA1 was used to deplete AURKAIP1 in mammalian cell lines, that upon a BLAST search, had 100% homology only to AURKAIP1.

Endogenous AURKAIP1 could not be detected using any available anti-AURKAIP1 antibodies. Therefore, real-time PCR was used as a substitute to determine whether the transcript encoding AURKAIP1 was depleted in different mammalian cell lines. The efficiency of siRNA1 to deplete AURKAIP1 mRNA was tested after 3 days of treatment, using RNA extracted from HEK293T, HeLa and U2OS cells. This was reverse-transcribed to generate cDNA that was used as the template for quantitative real-time PCR. HeLa and U2OS cells showed the greatest average level of AURKAIP1 depletion with 15% and 9% remaining respectively (Figure 3.6).

Since AURKAIP1 siRNA1 showed robust and reproducible levels of depletion of AURKAIP1 (Figure 3.6), mammalian cell lines were depleted of AURKAIP1 for 3 days using AURKAIP1 siRNA1 (Figure 3.8) to determine the effects on cell growth. After 3 days, there was a slight reduction in cell number and a change in cell morphology in both HEK293T and HeLa cell lines (Figure 3.7, 2 upper panels). There is a slight decrease in the confluency of the siNT-treated cells, which could be due to the siRNA transfection reagent, lipofectamine. The lipofectamine reagent that is used for the siRNA transfection forms liposomes surrounding the siRNA. These liposomes can merge with the phospholipid bilayer in the cell membrane, transporting the siRNA into the cell, which is thought to be required for optimal levels of transfection (Bauer *et al.* 2006) allowing transport of the siRNA into the cell. However, cytotoxicity can be a side effect of the lipofectamine reagent (Rasmussen *et al.* 2006). HEK293T cell lines show a more significant phenotype when subjected to treatment with AURKAIP1 siRNA compared to siNT, with a greater reduction in cell number and a change in cell shape which is suggestive of apoptosis (Figure 3.7).

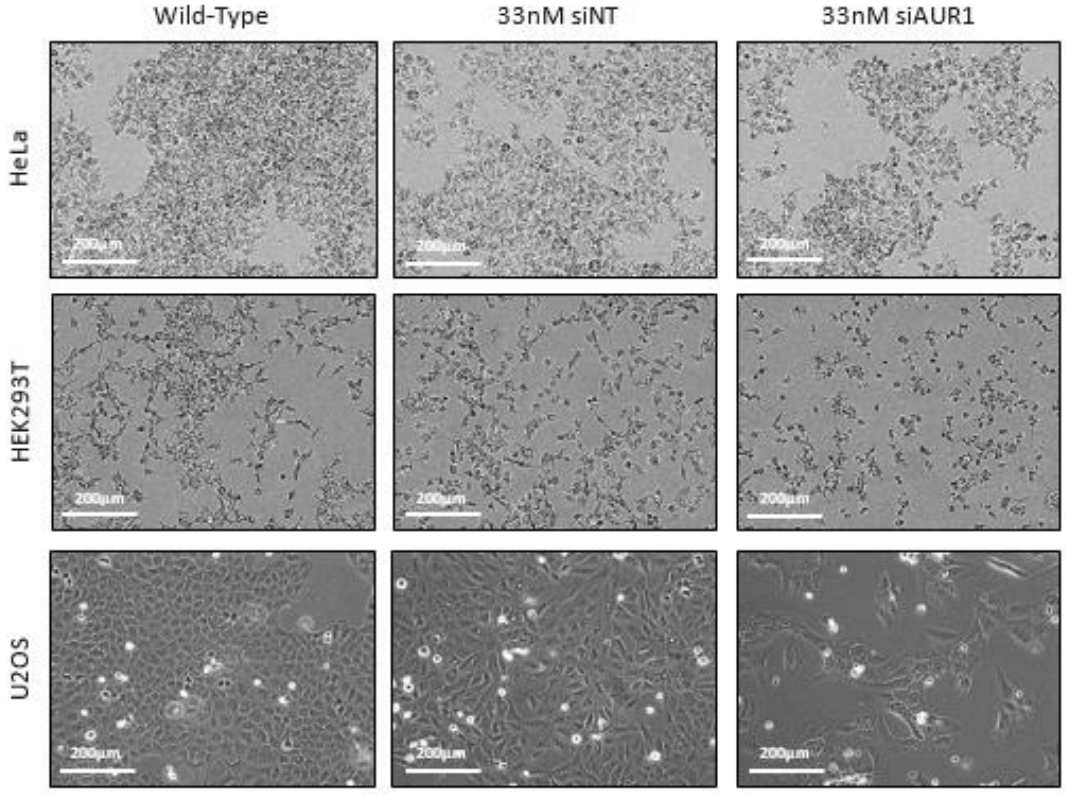

Figure 3.7 – Effects of AURKAIP1 siRNA1 in mammalian cell lines after 3 days. HeLa, HEK293T and U2OS cells were either untreated (wild-type), or treated with 33nm siNT or AURKAIP1 siRNA for 3 days. Images are representative of biological and technical repeats.

To analyse any changes in the steady state levels of mitoribosomal proteins, and to determine whether there was a possible effect of mitochondrial translation, cell lysates were taken from HeLa, HEK293T and U2OS cell lines after treatment with AURKAIP1 siRNA1 for 3 days. The cell lysates were subjected to western blotting (Figure 3.8), but no significant change in the steady state levels of mitoribosomal proteins, or mitochondrial translation, as determined by the levels of COXII, was observed. If AURKAIP1 is an essential mitoribosome protein, and the turnover of mitoribosomes is slow than within the timeframe of the experiment, there could still be AURKAIP1 within the mitochondria even after the treatment with AURKAIP1 siRNA1 for mitochondrial translation to occur.

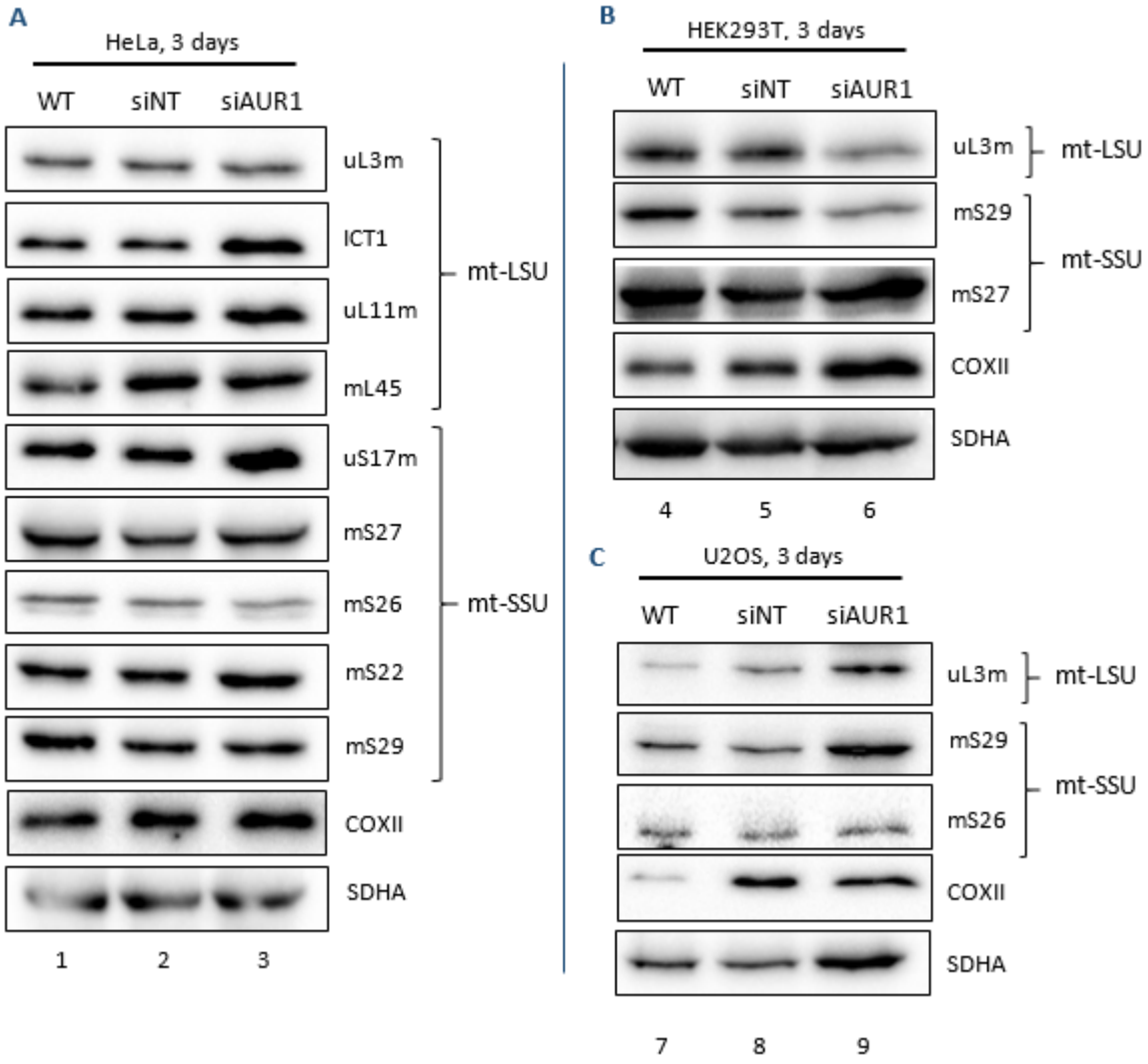

Figure 3.8 – Treatment with AURKAIP1 siRNA1 does not change steady state levels of mitoribosomal proteins or mitochondrial-encoded COXII. Mammalian cells were untreated (WT) or treated with 33nm non-targeting siRNA (siNT) or 33nm AURKAIP1 siRNA1 (siAUR1) for 3 days in 6-well plates. Cells were harvested, lysed and subjected to western blotting following 12% SDS-PAGE. Antibodies for the mt-LSU, mt-SSU, mitochondrial translation (COXII) and loading control (SDHA) were used. Lysates were analysed from HeLa cells (A), HEK293T cells (B) and U2OS cells (C).

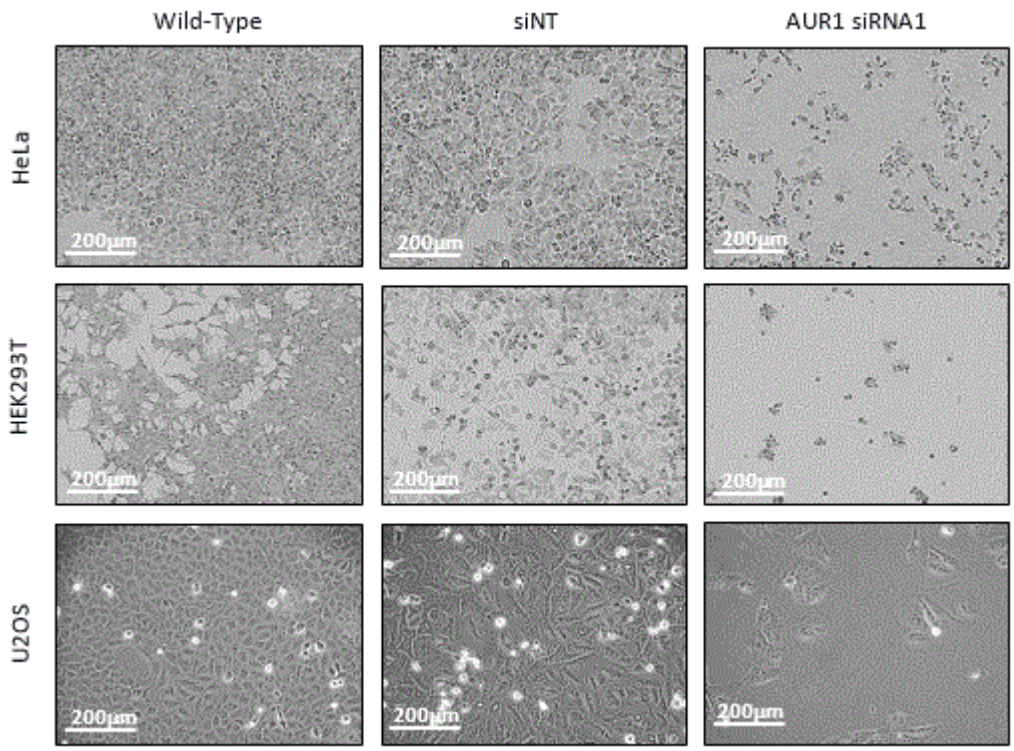

Figure 3.9 – Effect of AURKAIP1 depletion on mammalian cell lines after 6 days. Mammalian cells were untreated (WT) or treated with 33nm non-targeting siRNA (siNT) or 33nm AURKAIP1 siRNA1 (AURKAIP1 siRNA1) for 6 days in 6-well plates. Cells were reverse transfected with siRNA on day 0, and forward transfected with the same siRNA on day 3.

Treatment with AURKAIP1 siRNA1 for 3 days caused a cell growth defect, as well as a decrease in the steady state levels of COXII when compared to the control protein, SDHA (Figure 3.8C) as was seen previously (Thompson, 2014). There were no detectable changes in steady state levels of mitoribosomal proteins. Depleting AURKAIP1 for 3 days may not have been long enough for an effect to be seen with regards to mitoribosomal protein steady state levels. Therefore, the depletion treatment with siRNA1 against AURKAIP1 was extended to 6 days. After this time, HEK293T, HeLa and U2OS cells all displayed a more severe growth defect (Figure 3.9) with very few attached, live healthy cells visible. This was particularly the case for HEK293T cells.

Unfortunately, due to the severity of the growth defect and cell death there was insufficient material from HEK293T cells for further investigations. Cells from both U2OS and HeLa cells were harvested, lysed and subjected to western blotting. HeLa cells, showed no significant change in the steady state levels of mitoribosomal proteins, or in mtDNA-encoded protein COXII (Figure 3.10A) when compared to treatment with siNT and untreated cells. In

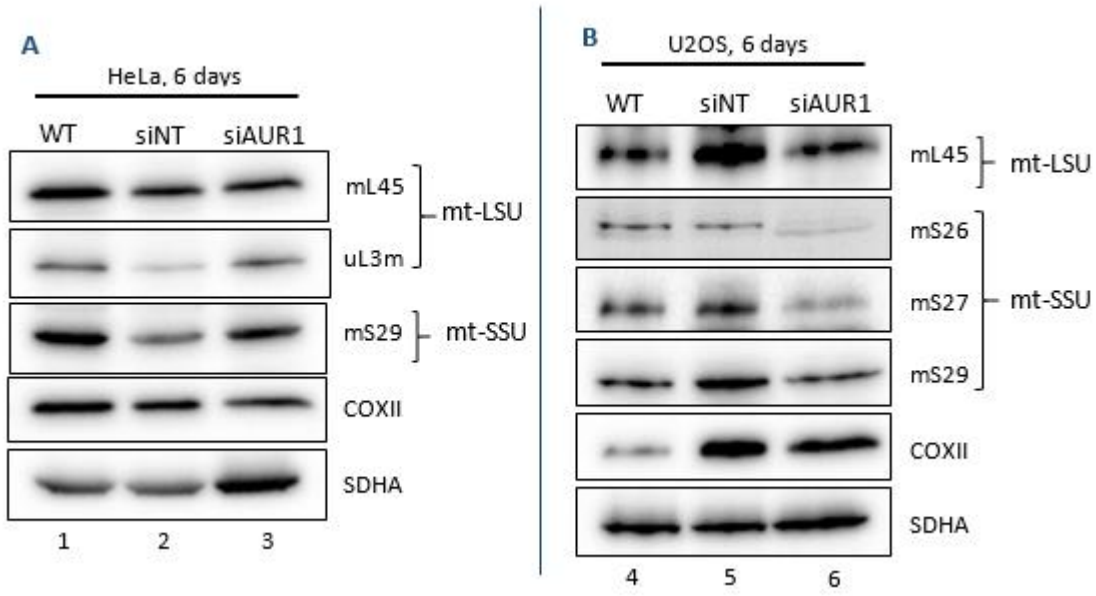

Figure 3.10 – Effect of AURKAIP1 depletion for 6 days on mitoribosomal proteins in mammalian cell lines. Mammalian cells were untreated (WT) or treated with 33nm non-targetting siRNA (siNT) or 33nm AURKAIP1 siRNA1 (siAUR1) for 7 days in 6-well plates. Cells were harvested, lysed and subjected to western blotting on a 12% polyacrylamide gel. Antibodies for the mt-LSU, mt-SSU, mitochondrial translation (COXII) and loading control (SDHA) were used. A = Lysates from HeLa cells. B = Lysates from U2OS cells.

U2OS cells, there was a decrease in the steady state levels of mS26 and mS27 of the mt-SSU (Figure 3.10B) but only a slight decrease in mitochondrial COXII. Since there was a greatest amount of depletion of AURKAIP1 in U2OS cells (Figure 3.6) compared to other mammalian cell lines, the more efficient depletion of AURKAIP1 in U2OS cell lines may have more of an effect on the mitoribosome.

Since there was little change in the steady state levels of the mitoribosomal proteins, a sucrose gradient was performed on U2OS cells treated with AURKAIP1 siRNA1 for 6 days to determine whether mt-tRNA^{Val}, a structural component of the mt-LSU, was affected and to determine whether there was an effect on mitoribosome assembly. U2OS cells were treated with siNT or AURKAIP1 siRNA1 for 6 days and the mitochondria were isolated from these cells. The isolated mitochondria were lysed and separated on a 10-30% isokinetic sucrose gradient. RNA was isolated from the fractions of the sucrose gradient and analysed by high resolution northern blotting. The sucrose gradient conditions had been optimised by my host laboratory to separate protein complexes according to their size such that the mt-SSU (fractions 4 and 5) and mt-LSU (fractions 6 and 7) are distinguishable. Oligonucleotide sequences that targeted

mt-tRNA^{Val} and mt-tRNA^{Leu} were generated using PCR and radiolabelled with ^{32}P-γATP to visualise the relative positions of these two mt-tRNA species.

Upon depletion of AURKAIP1, there was no evidence of a change in the steady state levels of mt-tRNA^{Val} and there was no dissociation of the mitoribosome as a similar proportion of mt-tRNA^{Val} compared to controls was still located in the mt-LSU in fractions 6 and 7 (Figure 3.11) relative to the free fractions (fractions 1-3). The signal in fraction 7 appears weaker in the siAUR1 sample, but this is most likely due to the strength of the overall signal rather than a decrease in the mt-LSU. The western blot was performed on the same samples to confirm that the distribution of the mt-SSU and mt-LSU correlated with the distribution of mt-tRNA^{Val}. The distribution of both the mt-SSU in fractions 4 and 5 and the mt-LSU in fractions 6 and 7 was the same in both the siNT and AURKAIP1 siRNA1-treated cells and showed a co-migration of mt-tRNA^{Val} with mt-LSU components.

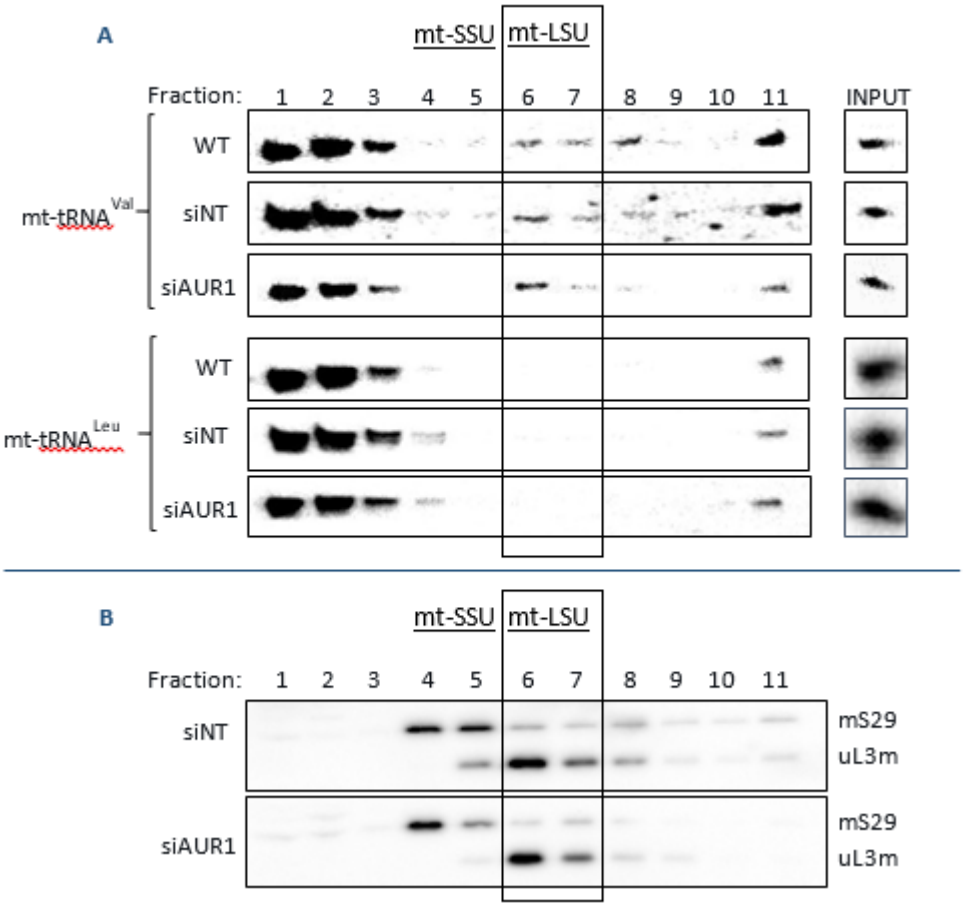

Figure 3.11 – Treatment with AURKAIP1 siRNA1 for 6 days has no effect on mitoribosome assembly. U2OS cells were untreated (WT), treated with 33nm non-targeting siRNA (siNT) or with AURKAIP1 siRNA1 (siAUR1) for 7 days. Mitochondrial lysate (750µg) were separated on a 10-30% isokinetic sucrose gradient. Post-centrifugation, eleven fractions (100µl) with RNA extracted from 50µl of each fraction, subjected to high resolution northern blotting and incubated with radiolabelled probes as indicated (A). The probe against mt-tRNA^{Leu} was used as a control. The remaining 50µl of each fraction was TCA precipitated and subjected to western blotting with antibodies against the mt-SSU (mS29) and the mt-LSU (uL3m).

3.3 Discussion

The data presented in this chapter has shown that both overexpressed AURKAIP1 and AURKAIP1-FLAG cause disruption to the mitoribosome and to mitochondrial translation. Further, depletion of AURKAIP1 with AURKAIP1 siRNA1 impairs cell growth and causes cell death. These data are consistent with previous work performed in my host laboratory using a different AURKAIP1-FLAG overexpresser and a different siRNA targeting AURKAIP1 respectively (Thompson, 2014). The preliminary screen performed in my host laboratory, in which AURKAIP1 depletion resulted in a cell growth defect in HeLa cells but not in ρ^0 cells, suggested a role for AURKAIP1 in mitochondrial gene expression. However, with the different siRNA, the decrease in the steady state levels of COXII could not be recapitulated.

The phenotype seen with AURKAIP1 overexpression is unusual for a mitoribosomal protein, since overexpression of other mitoribosomal proteins caused an increase in their respective subunit but no effect on mitochondrial translation. Data from another PhD student in my host laboratory showed that overexpression of mL45-FLAG resulted in an increase in the steady state levels of mt-LSU proteins, but no significant changes to levels of other mitoribosomal components and no detectable alteration in levels of COXII (Mai, 2016). AURKAIP1 therefore must have a role in mitochondrial gene expression that is not typical of a mitoribosomal protein. At present, AURKAIP1 is assigned to the mt-SSU, although curiously overexpression results in a decrease of the mt-LSU components. Current data produced in my host laboratory has shown that the mt-LSU associates with the IMM, potentially through the interaction of mL45 to the IMM (Mai, 2016). What is unclear with regards to mitoribosome assembly, is whether the mt-LSU or mt-SSU are assembled first. If AURKAIP1 is a mt-SSU protein, it may assemble initially with the mt-SSU before the mt-LSU assembles to form the monosome. When AURKAIP1 or AURKAIP1-FLAG is overexpressed, excess AURKAIP1 may also associate with the mt-LSU and thus prevent the two subunits from coming together. Since the mt-LSU is degraded, this hypothesis assumes that the mt-SSU is more stable than the mt-LSU.

Depletion of AURKAIP1 using siRNA1 caused a dramatic cell growth defect but there was no apparent change in the steady state levels of mitoribosomal proteins. Since endogenous AURKAIP1 cannot be detected using the available AURKAIP1 polyclonal antibody (Thompson, 2014; Sigma Aldrich, HPA031821) it is not possible to accurately determine the levels of

AURKAIP1 following depletion with AURKAIP1 siRNA1. Real-time PCR was therefore used as a surrogate to determine the efficiency of depletion of the AURKAIP1 mRNA as it was not possible to accurately determine the depletion level of the protein.

Since siRNA treatment is not 100% efficient, and a cell growth defect is apparent even after 3 days' treatment with AURKAIP1 siRNA1, the cells that remain after 7 days after treatment with AURKAIP1 siRNA1 may represent an untransfected population. Although structural data has confirmed AURKAIP1 to be a mitochondrial protein (Amunts *et al.* 2015, Greber *et al.* 2015, Desai *et al.* 2017), previous research performed by Lim *et al.* had indicated that AURKAIP1 was a nuclear protein that was involved in cell cycle. This was based on an N-terminal FLAG-tagged protein for their experiments that may have interfered with a potential mitochondrial targeting sequence, which is often found at the N-terminus. However, it cannot be ruled out that AURKAIP1 may have dual functionality. Several cytosolic ribosomal proteins have dual functionality and most often associated with the cell cycle. For example, in the cytosol, human ribosomal protein S3A (hRPS3A) depletion can induce apoptosis with characteristic morphological characteristics e.g. cell shrinkage and nuclear and cell fragmentation (Naora *et al.* 1998). Moreover, recent data has shown that human ribosomal protein S3 (hRPS3) is involved in Cdk2-mediated cell cycle regulation (Han *et al.* 2017). In the mammalian mitochondrial ribosome, several mt-SSU and mt-LSU proteins have been implicated in the regulation of the cell cycle. These include mS29 and mS30, which are both reported to be involved in apoptosis (Cavdar Koc *et al.* 2001). It should be noted that there is currently debate in the literature as to whether mS29 (DAP3) is involved in apoptosis due to its localisation to the mitochondrial matrix and mitoribosome (Berger and Kretzler, 2002), and that mitochondria are involved in apoptosis later in the cascade.

Originally, AURKAIP1 was identified as a protein that interacted with Aurora-A kinase, a mitotic serine/threonine kinase that contributes to the regulation of the cell cycle (Kiat *et al.* 2002). AURKAIP1 was thought to promote degradation of this kinase via a proteasome-dependent pathway. If AURKAIP1 does have two functions and two localisations, this would explain my data with both overexpression and depletion of AURKAIP1. If this was the case, then the AURKAIP1 present in the cytosol would play a role in regulating the cell cycle and therefore depletion of AURKAIP1 results in apoptosis as Aurora A kinase is no longer degraded. The fraction of the AURKAIP1 population that is present within the mitochondria could

potentially be involved in assembly of the mitoribosome and when there is too much AURKAIP1, the mitoribosome fails to assemble. This is a hypothesis that I will investigate in the next chapter.

My data presented here confirmed previous data that AURKAIP1 is an essential protein and unlike other mitoribosomal proteins, the levels of AURKAIP1 must be very tightly controlled. If there is too much AURKAIP1 within the cell, the steady state levels of the mt-LSU decrease and if there is too little AURKAIP1, cell growth is inhibited and cells undergo apoptosis. However, previous work in my host laboratory had been unable to demonstrate an association of AURKAIP1-FLAG with the mitoribosome upon overexpression and therefore determined that it was a mitochondrial matrix protein (Thompson, 2014). In the next chapter I will describe experiments using the HEK-AURKAIP1 cell line. I will investigate whether overexpressed AURKAIP1 may associate with the mitoribosome, since there is an absence of a C-terminal FLAG-tag that could have interfered with mitoribosome assembly. My next chapter will therefore describe whether AURKAIP1 is a *bona fide* mitoribosomal protein and whether overexpressed endogenous AURKAIP1, rather than AURKAIP1-FLAG, can interact with the mitoribosome.

CHAPTER 4: Is AURKAIP1 a component of the mature mammalian mitoribosome?

4.1 Introduction

Initial work by Koc *et al.* 2013 suggested that AURKAIP1 was a member of the mt-SSU of the mitoribosome having identified AURKAIP1 using capLC-MS/MS (capillary liquid chromatography tandem-mass spectrometry) and confirming by western blot. However, in this publication, no size markers were used for the western blot image. The same AURKAIP1 antibody (HPA031821, Sigma) that was used to confirm the presence of AURKAIP1 within the mt-SSU as a 15kDa species was used by my host laboratory (Thompson 2014) and only a 27kDa protein could be detected in the mt-SSU (Thompson, 2014).

Since the start of this project, there have been three publications showing detailed cryo-EM structures of the human (Amunts *et al.* 2015), porcine (Greber *et al.* 2015) and yeast (Desai *et al.* 2017) mitoribosomes respectively that have identified AURKAIP1 (also known as mS38) within the mitoribosome as a member of the mt-SSU using densitometry and mass spectrometry. However, only amino acids 128-199 (~9kDa) of the C-terminus of AURKAIP1 could be identified in these structures. Furthermore, to produce homogeneous structures in cryo-EM it is necessary to discard a large percentage of single molecule images that do not conform to the consensus image. Thus, more than c.95% of the single molecule mitoribosome images were discarded prior to the generation of final publishable structures of the human or porcine mitoribosomes. AURKAIP1 could therefore only be present in the consensus structure of the mitoribosomes, potentially because AURKAIP1 enhances the homogeneity of the mitoribosome in these preparations, and could reflect a mitoribosome structure that is not fully mature. Previous data from my host laboratory suggested that AURKAIP1-FLAG does not associate with the mitoribosome upon induction but this have may been due to the addition of a C-terminal FLAG-tag, since my data in the previous chapter has shown that the overexpression of AURKAIP1-FLAG has a more profound effect on the mitoribosome, particularly on the mt-SSU, and therefore may prevent AURKAIP1 from associating with the mitoribosome, leading to degradation of mt-LSU and mt-SSU. Overexpressed natural AURKAIP1 lacking the C-terminal FLAG had a less profound effect on the mt-SSU but still

caused a decrease in the steady state levels of the proteins of the mt-LSU. This effect is not seen with the overexpression of other mitoribosomal proteins (Chapter 3).

AURKAIP1 contains a domain of unknown function at the C-terminus, DUF1713, that is also present in the yeast protein Cox24p (Figure 4.1) and is thought to be associated with RNA binding. Both proteins have been shown to be subunits of the mitoribosome in human and yeast respectively. The mitoribosome itself contains 3 RNA species: 16S rRNA and mt-tRNA^{Val} in the mt-LSU, and 12S rRNA in the mt-SSU. All three species are co-transcribed along with mt-tRNA^{Phe} in a major polycistronic RNA unit. The 16S rRNA and 12S rRNA are released following cleavage of mt-tRNAs presumably my mtRNase P (5') and ELAC2 (3') and are modified at various sites before integration into the nascent mitoribosome (1.3.2). The published cryo-EM structures of the mitoribosomes places AURKAIP1 at the interface between the mt-LSU and mt-SSU where much of the 16S rRNA and 12S rRNA are located (Amunts *et al.* 2015, Greber *et al.* 2015, Desai *et al.* 2017). Potentially, AURKAIP1 could therefore be involved in the processing of these RNA species, or as a chaperone due to the presence of the DUF1713 domain. Using a technique called CLIP (cross-linking and immunoprecipitation), it is possible to identify interacting RNA species by cross-linking the RNA using ultraviolet (UV) light to the overexpressed RNA binding protein, purifying the protein, isolating the RNA species that have bound and identifying them by sequencing the isolated RNA fragments.

In this chapter, I investigated whether overexpressed AURKAIP1 lacking a C-terminal FLAG-tag associated with the mitoribosome itself and determined whether AURKAIP1-FLAG interacted with any mitochondrial RNA species.

4.2 Results

4.2.1 *Overexpressed AURKAIP1 does not associate with the mitoribosome*

In the previous chapter, I demonstrated that both overexpressed AURKAIP1-FLAG and AURKAIP1 resulted in a decrease in the steady state levels of mitoribosomal proteins. Using a sucrose gradient, which separates protein complexes according to their mass, I was able to determine whether overexpressed AURKAIP1 and AURKAIP1-FLAG associate with the mitoribosome, as inferred by the cryo-EM structures of the human, porcine and yeast mitoribosomes.

Mitochondrial lysates from induced HEK-AURKAIP1-FLAG cells were separated on a 10-30% sucrose gradient. My host laboratory has optimised this technique so that the mt-SSU, mt-LSU and the monosome are visible in distinct fractions. Using our custom anti-AURKAIP1 antibody, I could detect AURKAIP1-FLAG in fractions 1 and 2 only, and not associated with either the individual subunits or the fully assembled monosome (Figure 4.1B). This was also repeated and confirmed using anti-FLAG (data not shown). The steady state levels of the mitoribosomal proteins were reduced upon induction, as was seen previously, and the endogenous AURKAIP1 species could not be detected in the uninduced sample. This data agrees with previous observations that AURKAIP-FLAG does not associate with the mitoribosome (Thompson, 2014). However, here there are 3 species that are identified with the anti-AURKAIP1 antibody: 25kDa, 20kDa and 15kDa species respectively (Figure 4.1B). Koc *et al.* had suggested that AURKAIP1 is cleaved to a 15kDa species (Koc *et al.* 2013) as was shown by their bovine liver mitoribosomal preparations and this may be the case with overexpressed AURKAIP1-FLAG. However, this 15kDa species is not detected in the mature mitoribosomes.

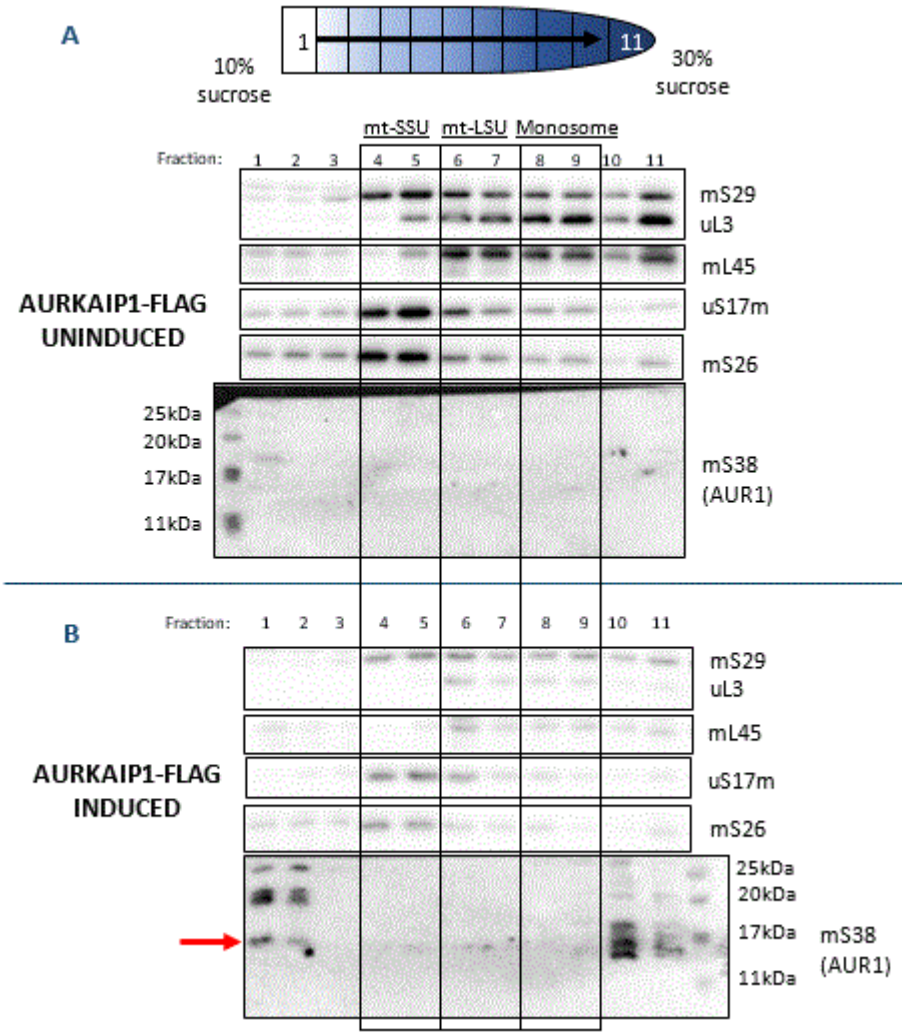

Figure 4.1 – AURKAIP1-FLAG does not associate with the mitoribosome. Mitochondrial lysates (750µg) from HEK-AURKAIP1-FLAG cells that were uninduced (A) and induced (B) for 3 days with tetracycline (1µg/ml) were separated on a 10-30% sucrose gradient. Eleven 100µl fractions were taken, TCA precipitated and subjected to western blotting on a 15% polyacrylamide gel. The membranes were immunoblotted with antibodies recognising mitoribosomal antibodies as shown. AURKAIP1 (15kDa species) is shown with a red arrow.

Using the HEK-AURKAIP1 cell line, overexpressed AURKAIP1 also did not associate with the mitoribosome and was detected in fractions 1, 2 and 3 (Figure 4.2). As with AURKAIP1-FLAG, the anti-AURKAIP1 antibody could detect 3 AURKAIP1 species of 25kDa, 20kDa and 15kDa in the induced sample, but was unable to detect endogenous AURKAIP1 in the uninduced sample. The steady state levels for the mt-LSU proteins were reduced in fractions 6 and 7 compared to the uninduced sample, supporting the data from chapter 3. Interestingly, overexpression of AURKAIP1 causes a reduction in the mt-SSU proteins of fraction 4, which could indicate a reduction in a partially-assembled mt-SSU. Similarly, there was a reduction in the mt-LSU proteins associated with the fully assembled monosome when compared to the

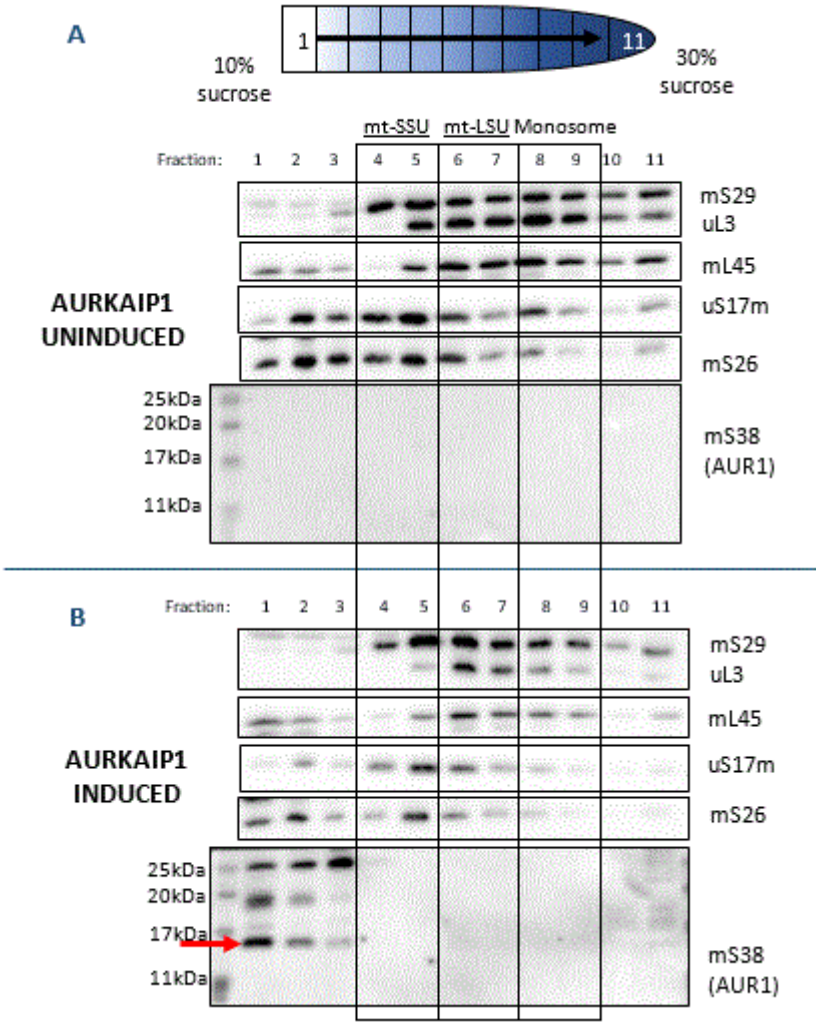

Figure 4.2 – Overexpressed AURKAIP1 does not associate with the mitoribosome. Mitochondrial lysates (750µg) from HEK-AURKAIP1 cells that were uninduced (A) and induced (B) for 3 days with tetracycline (1µg/ml) were separated on a 10-30% sucrose gradient. Eleven 100µl fractions were taken, TCA precipitated and subjected to western blotting on a 15% polyacrylamide gel. The membranes with immunoblotted with antibodies recognising mitoribosomal antibodies as shown. AURKAIP1 (15kDa species) is shown with a red arrow.

uninduced sample (Figure 4.2, fractions 8 and 9). The reduction of mitoribosomal proteins of the mt-LSU in fractions 8 and 9 of the sucrose gradients could indicate a problem with mitoribosome assembly upon overexpression of AURKAIP1 and AURKAIP1-FLAG.

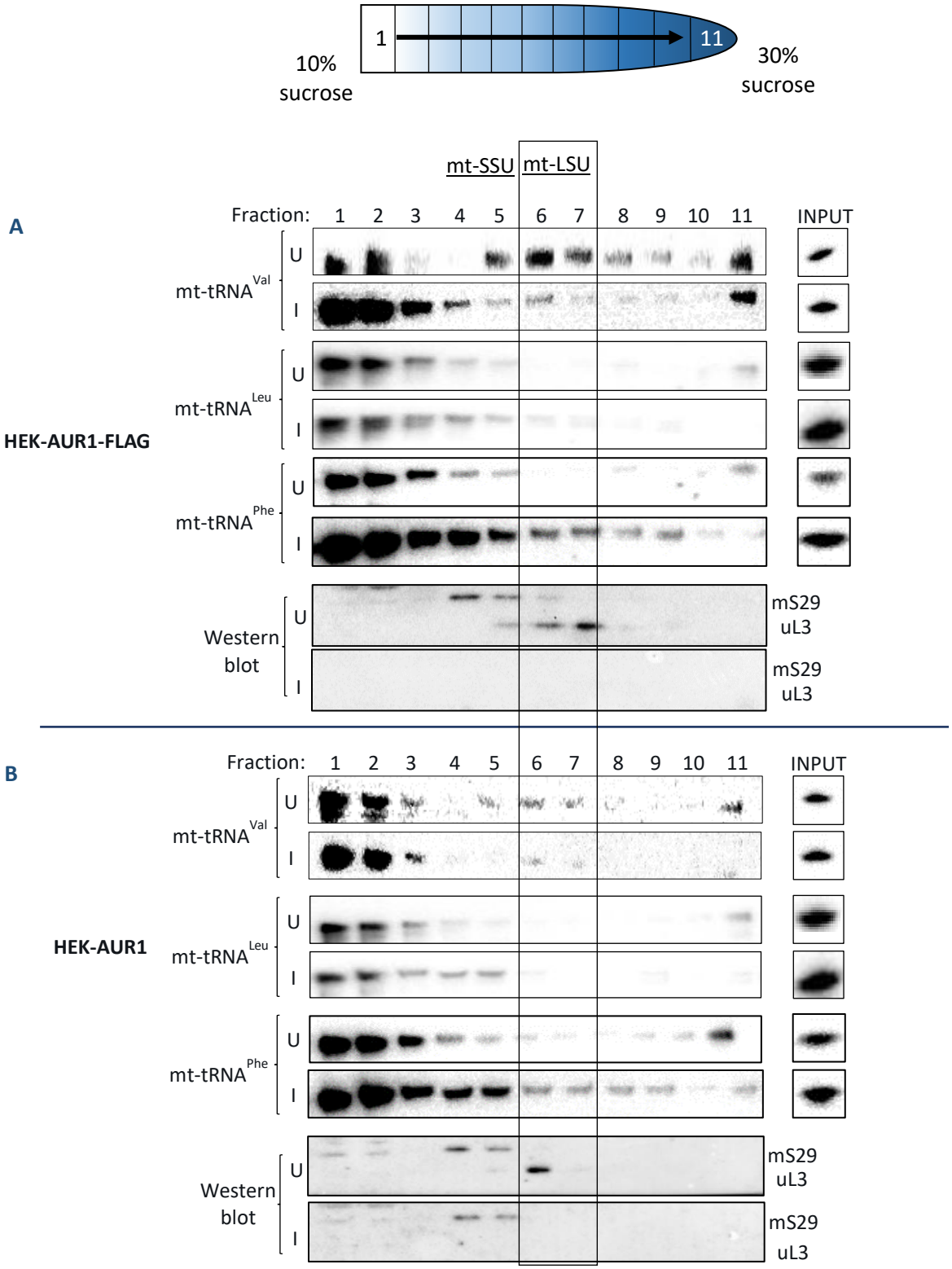

Figure 4.3 – Mt-tRNA^{Val} is no longer associated with the mitoribosome upon AURKAIP1 and AURKAIP1-FLAG overexpression. Mitochondrial lysates (750µg) from uninduced and induced HEK-AURKAIP1-FLAG (A) and HEK-AURKAIP1 (B) cells was separated on a 10-30% sucrose gradient. Eleven 100µl were taken and RNA extracted from each fraction. Samples were subjected to high resolution northern blotting and incubated with ^{32}P-γATP radiolabelled probes as shown. Mt-tRNA^{Leu} was used as a control mt-tRNA. One tenth of each fraction was subjected to western blotting and immunoblotted with antibodies recognising mS29 (mt-SSU) and uL3 (mt-LSU).

4.2.2 *AURKAIP1-FLAG associates with mitoribosomal RNA species*

The sucrose gradients performed with mitochondrial lysates resolve the distribution of the mt-LSU and mt-SSU proteins but do not reveal the distribution of mt-tRNA^{Val}, a structural tRNA of the mt-LSU. To confirm that overexpression of AURKAIP1 or AURKAIP1-FLAG prevents the formation of mt-LSU, sucrose gradients were performed as previously described, and RNA was extracted from the eleven fractions. The isolated RNA was subjected to high resolution northern blotting and probed for mt-tRNA^{Val}, mt-tRNA^{Phe} and mt-tRNA^{Leu}.

In the uninduced control samples (U) for both HEK-AURKAIP1 and HEK-AURKAIP1-FLAG, mt-tRNA^{Val} was visible in fractions 6 and 7, where the mt-LSU is located (Figure 4.3). Upon induction, the levels of mt-tRNA^{Val} in these fractions decreased, and there was an increase in fractions 1 and 2 for both AURKAIP1 and AURKAIP1-FLAG overexpression. However, AURKAIP and AURKAIP1-FLAG overexpression result in a decrease in the steady state levels of the mt-LSU in particular (Figure 4.3). The proportion of mt-tRNA^{Val} associated with the mitoribosome has therefore decreased although the total amount of mt-tRNA^{Val}, as shown in the input (Figure 4.3), did not change. Upon overexpression of both AURKAIP1 species there was an increase in the total amount of mt-tRNA^{Phe}, of which some is now associated with the mt-LSU, as confirmed by the increased levels of mt-tRNA^{Phe} in fractions 6 and 7. As the mt-tRNA^{Val} disassociated with the remaining mitoribosome, the mt-tRNA^{Phe} replaced the mt-tRNA^{Val}. This phenomenon is unique to mt-tRNA^{Phe}, since there was no change in total levels, or location on the sucrose gradient in the control mt-tRNA, mt-tRNA^{Leu}. One cannot disclude, however, that the increase it mt-tRNA^{Phe} in fractions 6 and 7 could potentially be due to a larger amount overall of mt-tRNAPhe, rather than specifically being in the mt-LSU, as shown by a trailing signal down the gradient (Figure 4.3B).

Currently, my data has shown that overexpressed AURKAIP1 and AURKAIP1-FLAG do not associate with the mitoribosome, and that there is a reduction in the mt-tRNA^{Val} that associates with the mt-LSU, with most mt-tRNA^{Val} being present in the free fractions of the sucrose gradient, fractions 1, 2 and 3. However, the cryo-EM structures place AURKAIP1 in between the mt-LSU and mt-SSU, near to the 16S rRNA and 12S rRNA of the mt-LSU and mt-SSU respectively. The DUF1713 domain located at the C-terminus of AURKAIP1, suggests that potentially AURKAIP1 could be an RNA binding protein. From my previous data (Figure 4.3),

AURKAIP1 could be binding mt-tRNA^{Val} and sequestering mt-tRNA^{Val} in the mitochondrial matrix. In order to determine whether AURKAIP1 could bind mitoribosomal RNA species, a CLIP assay was performed.

Dr Agata Rozanska performed a CLIP assay using overexpressed AURKAIP1-FLAG from a HEK293T cell line. Unfortunately, the HEK-AURKAIP1 cell line as there was not a suitable antibody available to perform the immunoprecipitation to isolate AURKAIP1 bound to RNA species following UV crosslinking. Thus, beads containing anti-FLAG were used for the immunoprecipitation instead.

As a control, mt-Luciferase-FLAG had previously been used for immunoprecipitation using the same anti-FLAG beads, and there were no RNA species represented that corresponded to mtDNA (Hornig-Do *et al.* 2014).

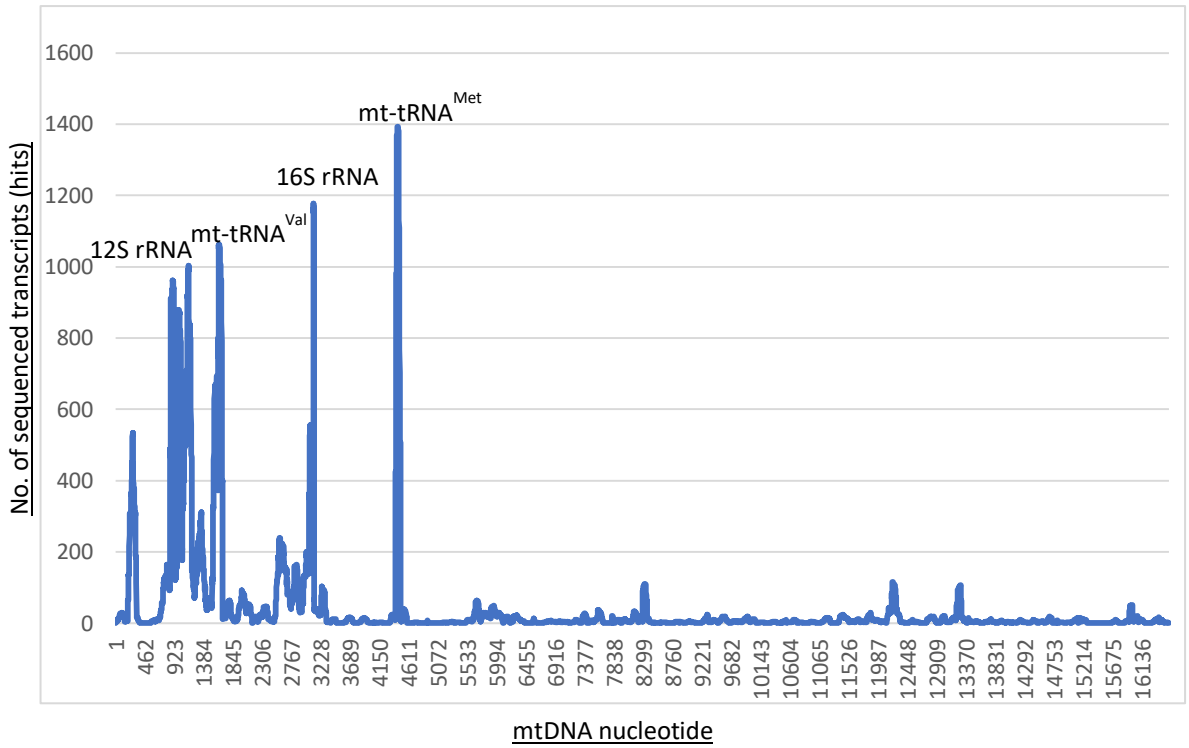

Figure 4.4 – AURKAIP1-FLAG binds to mitoribosomal RNA species. Experiment was performed by Dr Agata Rozanska, and the graph was generated by Dr John Grady after filtering the data to remove outliers. AURKAIP1-FLAG was induced with tetracycline for 3 days, UV-crosslinked and purified using immunoprecipitation. The RNA species were isolated, and sequenced by Ion Torrent™ sequencing (ThermoFisher). The number of transcripts sequenced for each nucleotide (hits) on the mtDNA was summarised into a graph using the program, R. Genes with the highest number of hits are labelled.

From the transcripts that were isolated, the RNA species that were highly represented and therefore bound to AURKAIP1-FLAG, were the 16S rRNA, mt-tRNA^{Val} and the 12S rRNA from the mitoribosome (Figure 4.4). There were also several transcripts detected that represented mt-tRNA^{Met}. A peak for mt-tRNA^{Met} was also identified in the control CLIP assay, so it is likely that the peak for mt-tRNAMet identified using AURKAIP1-FLAG is artefactual, although due to the high number of hits, an interaction between AURKAIP1-FLAG and mt-tRNA^{Met} cannot be discounted. Given the proposed location of AURKAIP1 within the mitoribosome, the hits for the 16S rRNA and 12S rRNA agree with the cryo-EM structures (Figure 4.5) since they are also located at the interface between the mt-LSU and mt-SSU. As a control, mt-Luciferase-FLAG had previously been used for immunoprecipitation using the same anti-FLAG beads, and there were no RNA species represented that corresponded to mtDNA (Hornig-Do *et al.* 2014).

There was also a distinct peak for transcripts representing mt-tRNA^{Val}, which is not located close to AURKAIP1 on the structure of the human mitoribosome (Figure 4.5). The UV-

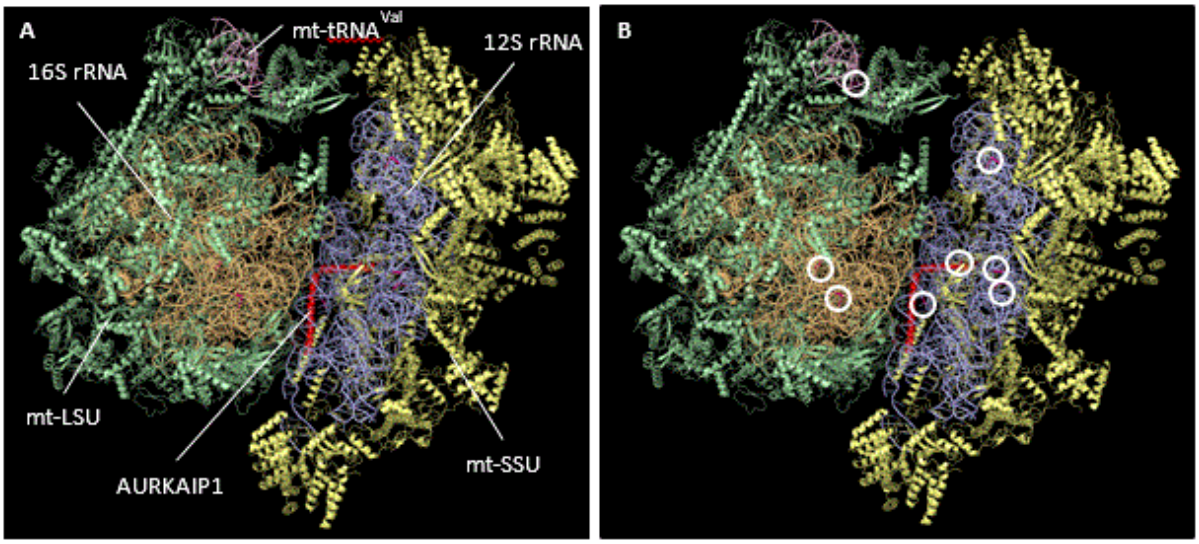

Figure 4.5 – CLIP data agrees with published structure of the human mitoribosome. The complete cryo-EM structure of the human mitoribosome, originally published by Amunts *et al.* 2015, was imported into PyMOL and coloured (PDB file = 3J9M). A = Structure of the human mitoribosome. B = Structure of the human mitoribosome, with the peak hits identified by CLIP indicated by white circles. AURKAIP1 = red, mt-LSU = green, 16S rRNA = orange, mt-SSU = yellow, 12S rRNA = blue.

crosslinking may have caused mt-tRNA^{Val} to interact with AURKAIP1-FLAG if they were in close proximity or that AURKAIP1-FLAG was interacting with mt-tRNA^{Val} outside of the mitoribosome.

4.2.3 Mycoplasma stress increases levels of a mitoribosomal protein

AURKAIP1 can only be visualised with our antibodies if overexpressed, as the endogenous levels of AURKAIP1 are particularly low, the antibodies available to detect AURKAIP1 are inefficient at recognising AURKAIP1, or the epitopes recognised by the antibody are lost upon cleavage of AURKAIP1 following import. Intriguingly, at an early stage of my studies a species at 27kDa had been detected by our custom anti-AURKAIP1 antibody (Eurogentec) in one aliquot of both HEK-AURKAIP1-FLAG and HEK-AURKAIP1 cell lysates, but not in HEK293T wild-type cells (Figure 4.6A). This 27kDa protein had not been previously seen in other aliquots of my clones but was shown to be localised to the mitochondrial matrix, since the species was present even in shaved mitochondria (Figure 4.6B).

Upon routine testing for *Mycoplasma* contamination on all cell cultures, it was discovered that both HEK-AURKAIP1 and HEK-AURKAIP1-FLAG cell lines tested positive for *Mycoplasma*. As a result, the cultures were treated with plasmocin (25µg/ml) for two weeks

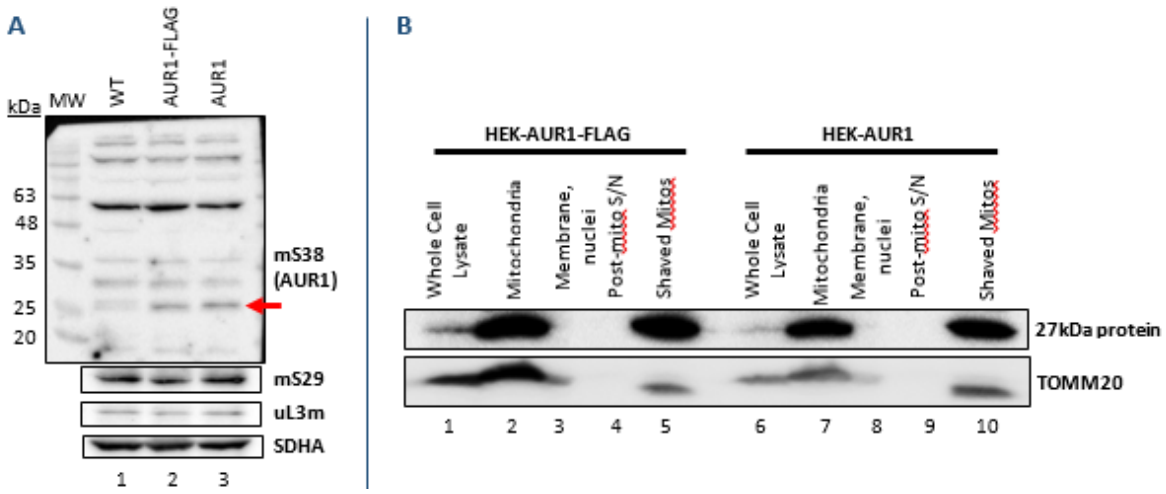

Figure 4.6 – A 27kDa mitochondrial protein is recognised by anti-AURKAIP1 antibody. A = Cell lysates (60µg) were separated on a 15% polyacrylamide gel and subjected to western blotting. Antibodies are stated. SDHA was used as a loading control. The 27kDa species is highlighted with a red arrow. B = 20µg of whole cell lysate, mitochondrial lysate, cell membrane/nuclei, post-mitochondrial supernatant (S/N) and shaved mitochondria (mitos) were separated on a 15% polyacrylamide gel and subjected to western blotting. TOMM20 was used as marker to ensure the outer membranes of the mitochondria were degraded (lanes 5 and 10).

before being re-tested to confirm that the cell lines were *Myoplasma*-free. Cell lysates taken during this treatment period showed that the 27kDa mitochondrial protein was expressed as a result of *Mycoplasma* contamination (Figure 4.7) and that the levels of *Mycoplasma* (Figure 4.11B) were correlated with the steady state levels of this 27kDa protein (Figure 4.7).

However, since AURKAIP1 was currently undetectable in standard cell lines, the contaminated cell line provided a unique cell model for potentially investigating AURKAIP1. For these experiments, the cell lines were grown in a separate incubator and all equipment was routinely cleaned with 1% Trigene solution and 75% ethanol prior and after use to limit the spread of contamination to other cell lines. The contaminated cell lines are referred to as HEK-AUR1^{M} and HEK-AUR1-FLAG^{M} respectively.

This 27kDa species was recognized by the custom anti-AURKAIP1 antibody and localized to the mitochondria without the need for induction of AURKAIP1 or AURKAIP1-FLAG. Since this species was present only in *Mycoplasma*-infected cell lines, this 27kDa protein could be endogenous unprocessed AURKAIP1, or produced from leaky expression of the pcDNA5/FRT/TO-AURKAIP1 or –AURKAIP1-FLAG constructs. Therefore, a sucrose gradient was performed to see whether this 27kDa species associated with the mitoribosome.

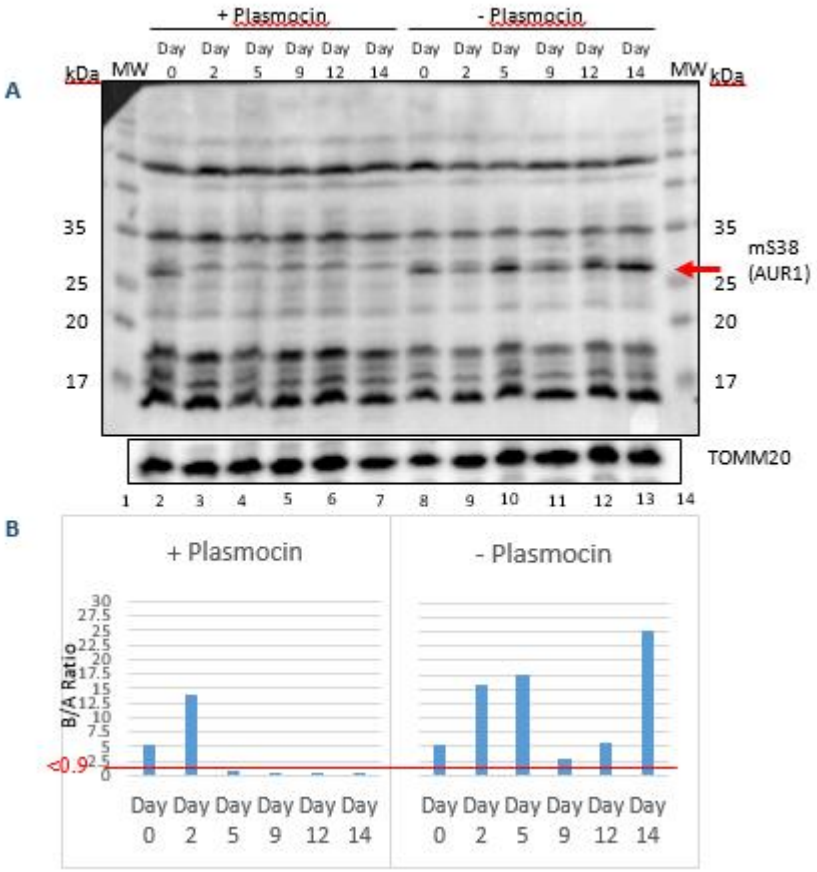

Figure 4.7 – The 27kDa unknown mitochondrial protein is no longer detected upon plasmocin treatment to remove *Mycoplasma*. HEK-AURKAIP1-FLAG^{M} cell line was treated with or without plasmocin (25µg/ml) for 2 weeks. A = Cells were harvested from the flask at day 0, 2, 5, 9, 12 and 14, lysed and 60µg of cell lysate separated by SDS-PAGE on a 15% polyacrylamide gel and subjected to western blotting. Membrane was immunoblotted with anti-AURKAIP1 and anti-TOMM20. TOMM20 was used as a loading control. B = Media was taken from the HEK-AURKAIP1-FLAG flask at day 0, 2, 5, 9, 12 and 14 and tested for B = Media was taken from the HEK-AURKAIP1-FLAG flask at day 0, 2, 5, 9, 12 and 14 and tested for *Mycoplasma* contamination using the MycoAlert™ kit. A B/A ratio of <0.9 indicates that the cells are free from *Mycoplasma*.

Sucrose gradients were performed on the uninduced cell lysates of both HEK-AURKAIP1 and HEK-AURKAIP1-FLAG. In both cell lines, the 27kDa species migrated with the mt-LSU (fractions 6 and 7, Figure 4.8) and the fully assembled monosome (fraction 8, Figure 4.10). Since AURKAIP1 is located at the interface between the mt-SSU and mt-LSU, this 27kDa species could represent AURKAIP1 with the hypothesis being that AURKAIP1 is involved in late mitoribosome assembly, acting as an anchor between the mt-SSU and mt-LSU.

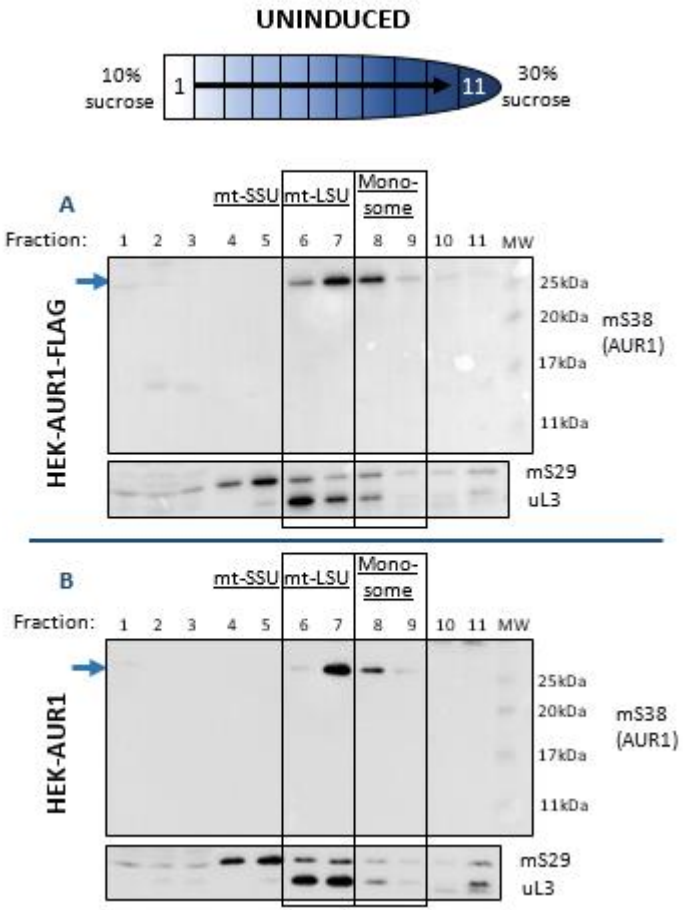

Figure 4.8 – A 27kDa mitochondrial protein migrates with the mt-LSU in uninduced AURKAIP1 cell lines. Mitochondrial lysates (750µg) from uninduced HEK-AURKAIP1-FLAG (A) and HEK-AURKAIP1 (B) cells were separated on a 10-30% sucrose gradient. Eleven 100µl fractions were taken, TCA precipitated and subjected to western blotting on a 15% polyacrylamide gel. The membranes were immunoblotted with antibodies recognising AURKAIP1 (AUR1, mS38), mS29 (mt-SSU) and uL3 (mt-LSU). The 27kDa species is highlighted with a blue arrow.

To confirm whether the 27kDa species was generated from leaky expression of the pcDNA5/FRT/TO™ construct, sucrose gradient fractions from uninduced HEK-AURKAIP1-FLAG together with whole cell lysate harvested from an induced HEK-mL45-FLAG cell line (Mai, 2016) were incubated with the anti-FLAG antibody. The antibody was able to detect mL45-FLAG, but the 27kDa species was not present in any of the sucrose gradient fractions (Figure 4.9). This confirmed that the 27kDa species was not induced from the pcDNA5/FRT/TO-AURKAIP1-FLAG construct.

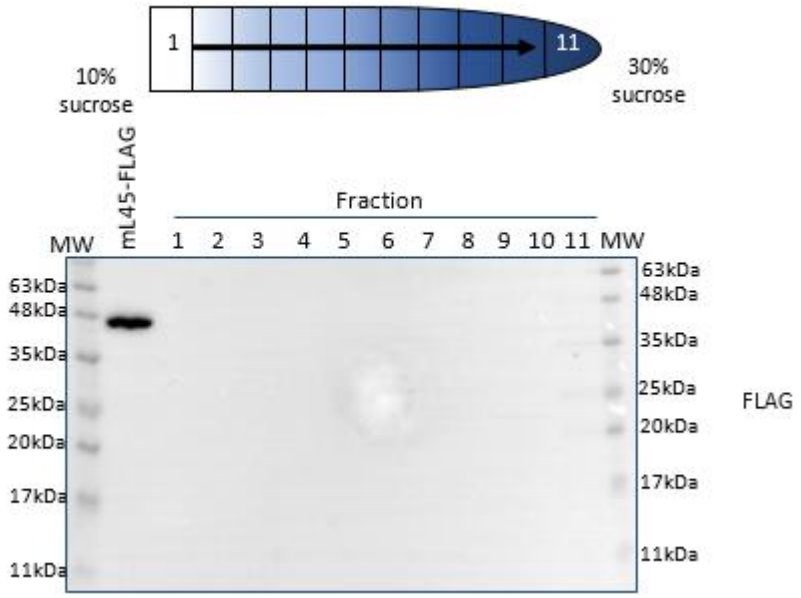

Figure 4.9 – Generation of the 27kDa species is not due to leaky expression of AURKAIP1-FLAG. Mitochondrial lysates (750µg) from uninduced HEK-AURKAIP1-FLAG (A) and HEK-AURKAIP1 (B) cells were separated on a 10-30% sucrose gradient. Eleven 100µl fractions were taken and TCA precipitated. Cell lysate (50µg) from HEK-mL45-FLAG induced for 3 days with tetracycline (1µg/ml) was added as a control for the presence of a FLAG-tag. The samples were subjected to western blotting on a 15% polyacrylamide gel and incubated with anti-FLAG.

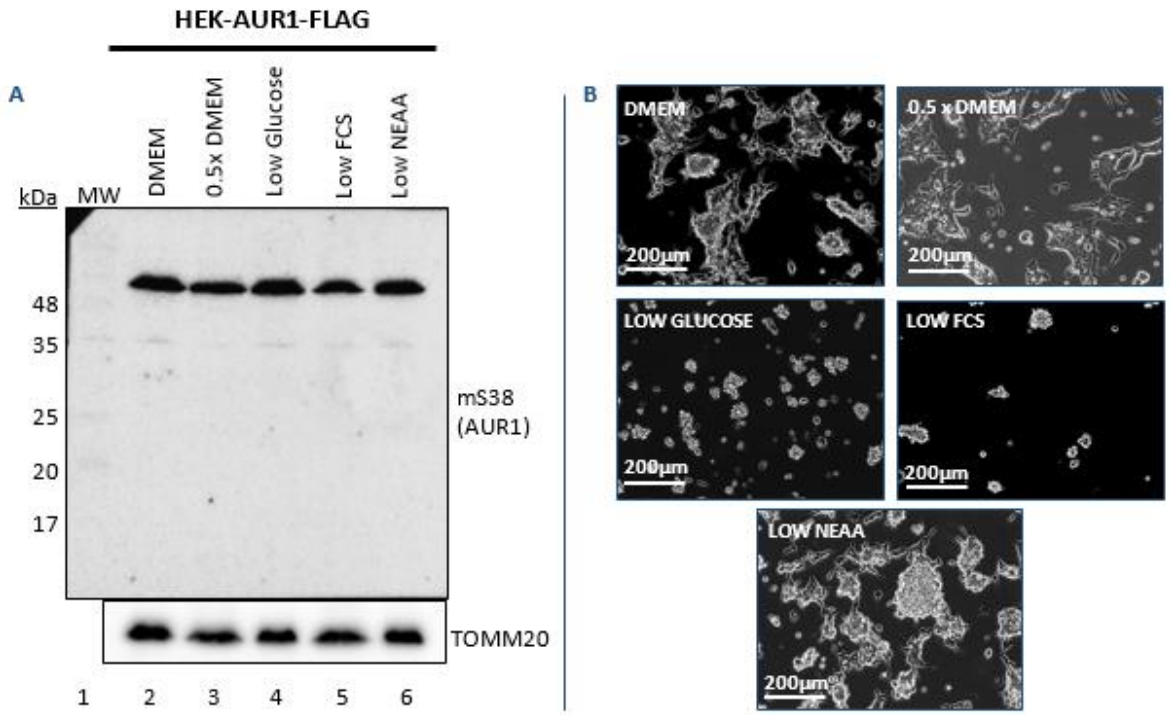

Figure 4.10 – Cellular stress does not result in expression of the 27kDa mitochondrial protein. *Mycoplasma* negative HEK-AURKAIP1-FLAG cells were grown for 3 days in normal DMEM, 0.5 x DMEM (DMEM diluted 1:1 with 1 x PBS), or DMEM media containing low glucose (5mM), low FCS (2%) or low NEAA (0.002 x). A = Cells lysates (60µg) were subjected to western blotting on a 15% polyacrylamide gel and immunoblotted with antibodies as shown. TOMM20 was used as a loading control. B = Images taken of HEK-AURKAIP1-FLAG cells grown in each of the different media conditions.

Since *Mycoplasma* contamination was present, the resulting stress on the cells may have caused the upregulation of the full-length endogenous AURKAIP1. In order to try and mimic the cell stress caused by the *Mycoplasma*, HEK-AURKAIP1-FLAG cells were grown in DMEM media with different amounts of glucose, foetal calf serum and non-essential amino acids. The cells were harvested, lysed and subjected to western blotting. As shown in Figure 4.10, a 27kDa species was undetectable using the anti-AURKAIP1 antibody under these conditions, consistent with the 27kDa species being expressed as a result of the *Mycoplasma* contamination, or is a *Mycoplasma* protein itself which was recognised by our custom anti-AURKAIP1 antibody.

The 27kDa species was only visible in *Mycoplasma*-infected cells and it was still unclear whether this protein was AURKAIP1 or another protein entirely, despite localising to the mitochondria, fractionating with the mitoribosome and being recognised by the anti-AURKAIP1 antibody. In attempt to identify the protein, mass spectrometry was employed. The

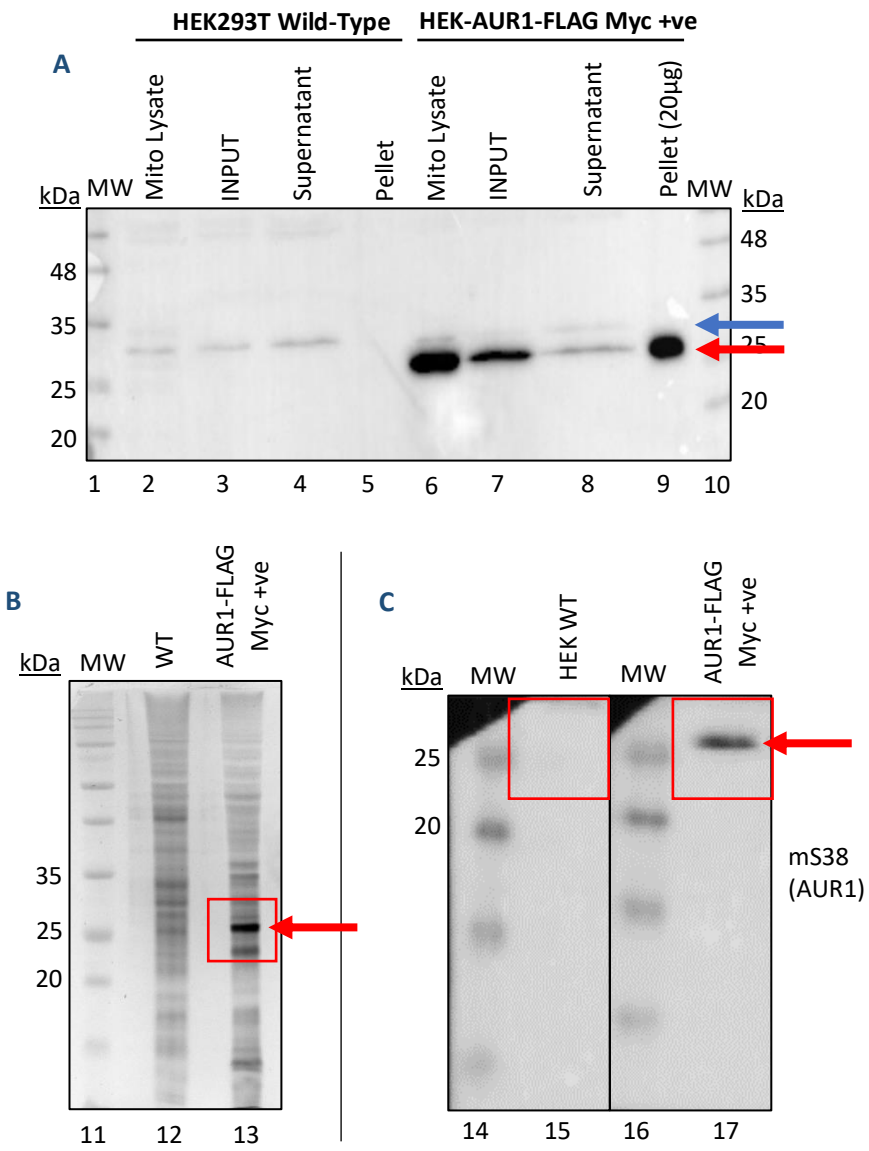

Figure 4.11 – Preparation of *Mycoplasma*-contaminated lysates for mass spectrometry. Mitochondrial lysates (Mito Lysate) from HEK293T wild-type cells and *Mycoplasma* positive HEK-AURKAIP1-FLAG cells were used. A = Lysates were centrifuged at 12,000*g* for 10mins at 4°C. The supernatant was taken (INPUT) and centrifuged at 200,000*g* for 1hr at 4°C. The supernatant and pellet fractions were taken. 20µg of each sample was separated on a 15% polyacrylamide gel and subjected to western blotting. The membrane was immunoblotted with anti-AURKAIP1 antibody. Unspecific band = blue arrow, 27kDa mitochondrial protein = red arrow. B = Mitochondrial lysate (10µg) from HEK293T wild-type (WT) and HEK-AUR1-FLAG *Mycoplasma* positive (AUR1-FLAG Myc +ve) cells were separated on a 12% polyacrylamide gel. The proteins were visualised using silver staining. A band indicating the 27kDa species is indicated (red arrow). C = Mitochondrial lysates (30µg) were separated on a 12% polyacrylamide gel and subjected to western blotting using anti-AURKAIP1 antibody. A band indicating the 27kDa species is indicated (red arrow). Corresponding areas excised for tandem mass spectrometry are indicated by the red squares. MW = molecular weight marker, kDa = kiloDaltons.

remaining mitochondrial lysate of HEK-AURKAIP1-FLAG^{M} that was utilised for a sucrose gradient (Figure 4.7A) was prepared for mass spectrometry analysis by centrifugation at a high

speed. The high centrifugation speed separated out the heavy complexes as a pellet to further purify the 27kDa species, since it segregated on the sucrose gradient with either the mt-LSU, or a complex of a similar mass (Figure 4.7A).

Using the anti-AURKAIP1 antibody, the 27kDa species was visualised in the HEK-AURKAIP1-FLAG^{M} mitochondrial lysate and purified in the pellet fraction (Figure 4.11A). HEK293T wild-type mitochondrial lysate was used as a control. A larger species of about 30kDa was detected in both samples but was not present in the pellets (Figure 4.11A, lanes 5 and 9). A small amount of the pellet fraction was initially checked by silver stain (Figure 4.11B) and then by western blot (Figure 4.11C) to determine if the 27kDa species could still be visualised.

Table 4.1: Mass spectrometry does not identify AURKAIP1 as the 27kDa species in *Mycoplasma* positive cells.

Unique Proteins	Protein	AUR1-FL (%)	HEK WT (%)	No. of Peptides
FRIH_HUMAN	Ferritin heavy chain	44.3	0	9
SSRB_HUMAN	Translocon-associated protein subunit beta	16.4	0	8
P29_MYCHR	Probable ABC transporter ATP-binding protein p29	38.9	0	7
SCO1_HUMAN	SCO1 homolog (copper chaperone)	28.9	0	6
RHOA_HUMAN	Transforming RhoA precursor	39.4	0	6
CYB5B_HUMAN	Cytochrome b5 type B precursor	31.5	0	5
ROA2_HUMAN	Heterogeneous nuclear ribonucleoproteins A2/B1	14.4	0	5
MAAI_HUMAN	Maleylacetoacetate isomerase	19.4	0	5
RM02_HUMAN	39S ribosomal protein L2, mitochondrial	22.6	0	4
K2C6B_HUMAN	Keratin, type II cytoskeletal CB	8.5	0	4

A table summarising the top 10 unique proteins in the HEK-AURKAIP1-FLAG *Mycoplasma* positive sample. MYCHR = *Mycoplasma hyorhinis*, HUMAN = *Homo sapiens*.

Samples of HEK293T wild-type and HEK-AURKAIP1-FLAG *Mycoplasma*-positive cells were cut out from polyacrylamide gels (indicated by the red squares, Figure 4.13) and sent to Dr Hans Wessels (Radboud University, Nijmegen, Netherlands) for targeted mass spectrometry. The data was compared to *H. sapiens* and various *E. coli* and *Mycoplasma* databases. In the HEK293T wild-type sample, 492 proteins and 1985 peptides were identified and in the HEK-AURKAIP1-FLAG^{M} sample 464 proteins and 2019 peptides were identified. However, AURKAIP1 was not identified as a unique protein in the HEK-AURKAIP1-FLAG^{M} cells (Table 4.1, Appendix N). In the list of unique proteins, there was one human mitoribosomal protein, uL2m (RM02_HUMAN, Table 4.1). However, when aligned to AURKAIP1, there was

Figure 4.12 – Few sequence similarities appear between uL2m and AURKAIP1. Amino acid sequences for uL2m (Q5T653) and AURKAIP1 (Q9NWT8) were aligned using Clustal Omega (http://www.ebi.ac.uk/Tools/msa/clustalo/). Black asterisk = fully conserved residue, colon (:) = residues with strongly similar properties, period (.) = residues with weakly similar properties. Region of similarity is highlighted in the blue box.

no significant stretch of amino acids in uL2m that could be an epitope for the AURKAIP1 antibody to recognise the mt-LSU protein (Figure 4.12).

Of the proteins that were enriched in the HEK-AURKAIP1-FLAG^{M} sample, AURKAIP1 was also not identified (Table 4.2). The proteins that were enriched primarily corresponded to the 26S cytosolic proteasome. The cytosolic proteasome has been shown to be upregulated when cells are infected with intracellular bacteria (Iovino *et al.* 2014) so it is possible that subunits of the 26S cytosolic proteasome are upregulated in response to *Mycoplasma* infection also. Of the proteins that were enriched in the HEK-AURKAIP1-FLAG^{M} sample, there were none that identified in the *E. coli* or *Mycoplasma* databases.

Table 4.2: AURKAIP1 is not enriched in HEK-AURKAIP1-FLAG^{M} cells

Enriched Proteins	Protein	AUR1-FL (%)	HEK WT (%)	Ratio Peptides A/H
PSB7_HUMAN	Proteasome subunit beta type-7	54.2	20.9	8
AR6P1_HUMAN	ADP-ribosylation factor-like protein 6-interacting protein 1	17.7	3.9	7
PSB4_HUMAN	Proteasome subunit beta type-4	37.1	11	6.5
PSB6_HUMAN	Proteasome subunit beta type-6	38.9	13.8	6.333
PSB2_HUMAN	Proteasome subunit beta type-2	751	31.8	5
DCXR_HUMAN	L-xylulose reductase	72.1	41	4.8
PSA3_HUMAN	Proteasome subunit alpha type-3	27.8	12.2	4.5
PGAM1_HUMAN	Phosphoglycerate mutase 1	43.7	16.5	4
ERP29_HUMAN	Endoplasmic reticulum resident protein 29	26.1	10.3	4
ETHE1_HUMAN	Persulphide dioxygenase ETHE1, mitochondrial	36.2	11.4	4

A table summarising the top 10 enriched proteins in the HEK-AURKAIP1-FLAG *Mycoplasma* positive sample. A/H = AUR1-FL/HEK WT.

4.3 Discussion

In this chapter I have investigated whether overexpressed AURKAIP1 and AURKAIP1-FLAG associated with the mitoribosome, as has been shown in the cryo-EM structures of the mitoribosome (Amunts *et al.* 2015, Greber *et al.* 2015, Desai *et al.* 2017). Previous work using AURKAIP1-FLAG had indicated that AURKAIP1-FLAG did not associate with the mitoribosome, and thus overexpressed AURKAIP1 lacking the FLAG-tag was used in case the FLAG-tag had interfered with mitoribosome assembly. I confirmed that AURKAIP1-FLAG does not associate with the mitoribosome as previously seen (Thompson, 2014) as the 15kDa AURKAIP1-FLAG species was not detected in the mt-SSU and mt-LSU fractions as indicated by mS29 and uL3m. Following fractionation of mitochondria lysate, AURKAIP1-FLAG could only be detected in sucrose gradient fractions 1 and 2, suggesting that AURKAIP1-FLAG localised to the mitochondrial matrix. Overexpressed AURKAIP1 also did not associate with the mitoribosome, as the 15kDa AURKAIP1 species was only present in fractions 1, 2 and 3. However, there was a specific decrease in the levels of mitoribosomal proteins that localised to fraction 4, representing the early assembled mt-SSU, and fraction 7, representing the late assembled mt-LSU. The process of mitoribosome assembly is largely unknown, although various RNA-binding proteins and assembly factors have been identified (1.3.2). Potentially AURKAIP1 could be involved in this assembly process and being located at the interface of the mt-SSU and mt-LSU, AURKAIP1 could have a role in the assembly of both subunits and the full monosome as a possible RNA binding protein through its DUF1713 domain.

The human mitoribosome lacks the 5S rRNA species and instead contains mt-tRNA^{Val} in the mt-LSU (Amunts *et al.* 2015). Porcine mitoribsomes typically contain mt-tRNA^{Phe}, whereas the macaque and rat mitoribosomes prefer mt-tRNA^{Val} (Rorbach and Gao *et al.* 2016). Upon induction of both AURKAIP1 and AURKAIP1-FLAG, mt-tRNA^{Val} became dissociated from the mt-LSU and mt-tRNA^{Phe} partially associated with the remaining mt-LSU instead. This phenomenon is not unusual in human cells; Rorbach and Gao *et al.* demonstrated that in a 143B cybrid cell line harbouring a homoplasmic m.1624C>T mutation in *MTTV*, in which the steady state levels of mt-tRNA^{Val} are greatly reduced, mt-tRNA^{Phe} associated with the mitoribosome instead. However, in the case of overexpressed AURKAIP1 and AURKAIP1-FLAG, the steady state levels of mt-tRNA^{Val} have not been reduced, but there was more a greater proportion of mt-tRNA^{Val} that was not associated with the mt-LSU when compared to the

uninduced samples. Overexpressed AURKAIP1 and AURKAIP1-FLAG also did not associate with the mitoribosome when analysed by sucrose gradients, and one possibility is that overexpressed AURKAIP1 and AURKAIP1-FLAG are binding to and sequestering mt-tRNA^{Val} in the matrix.

The DUF1713 domain identified in AURKAIP1 is present in Cox24p, the yeast protein that is involved in splicing COXI mRNA and thus could be representative of an RNA-binding protein. The CLIP data suggested that AURKAIP1-FLAG bound to 12S rRNA, 16S rRNA and mt-tRNA^{Val}. The areas of 12S and 16S rRNA that AURKAIP1-FLAG bound to are located at the interfaces of the mt-SSU and mt-LSU, indicating that AURKAIP1-FLAG does localise to this area of the mitoribosome, albeit temporarily. However, mt-tRNA^{Val} is not located in the close vicinity of AURKAIP1 if the cryo-EM structure of the mitoribosome is a true reflection of the fully mature mitoribosome. AURKAIP1 may have the potential function therefore of a mt-tRNA^{Val} chaperone, binding to mt-tRNA^{Val} when mt-tRNA^{Val} is cleaved off the rRNA transcripts (1.2.3) until ready for assembly into the mitoribosome. When AURKAIP1 and AURKAIP1-FLAG are overexpressed, there is more AURKAIP1 than is required and thus more mt-tRNA^{Val} is bound and sequestered in the mitochondrial matrix. Without mt-tRNA^{Val}, the partially-assembled mt-LSU would degrade, which in turn could lead to the degradation of the mt-SSU if fully-assembled mitoribosomes were not being produced.

Physiologically, endogenous AURKAIP1 may act as the chaperone to mt-tRNA^{Val} and before associating with the mitoribosome as a *bona fide* mt-SSU subunit. However, when the cryo-EM structures of the mitoribosomes were determined, only homogeneous structures are analysed which typically accounts for ~2% of all available molecular images. AURKAIP1 may stabilise the fully assembled monosome under experimental conditions, and is thus the reason why AURKAIP1 is present in the structure but may not be the true situation *in vivo*. One caveat to AURKAIP1 being a *bona fide* mitoribosomal subunit is that the steady state levels of AURKAIP1 appear very low when visualising AURKAIP1 in either cell or mitochondrial lysates via western blot with the custom AURKAIP1 antibody or Sigma antibody. Since AURKAIP1 can be detected when AURKAIP1 or AURKAIP1-FLAG is induced, the custom antibody certainly recognises epitopes on AURKAIP1, although it is unclear whether the antibody recognises the C- or N-terminus, or many epitopes within the structure.

As the steady state levels of AURKAIP1 do not seem to reflect the steady state levels of other mitoribosomal proteins, AURKAIP1 is more challenging to investigate as it difficult to visualise. When a species at 27kDa appeared in one vial each of *Mycoplasma*-contaminated AURKAIP1 or AURKAIP1-FLAG, it was possible that the increase in stress to the cells would result in an increase in AURKAIP1 to stabilise the mitoribosome and would thus provide a good model system to investigate the function of AURKAIP1.

The vector pcDNA5/FRT/TO™ is known to result in low leaky expression (Meyer-Ficca *et al.* 2001) and potentially the low level of AURKAIP1 or AURKAIP1-FLAG expression was at a suitable level that AURKAIP1 behaved in a physiological manner, since depletion of AURKAIP1 and overexpression of AURKAIP1 both result in detrimental effects to the cell. The FLAG antibody could not identify this 27kDa species, suggesting that this species was not due to leaky expression of the pcDNA5/FRT/TO vector and could be the endogenous AURKAIP1. Full-length AURKAIP1 is predicted to be ~23kDa (199 amino acids) and since some proteins tend to migrate slightly higher or lower than predicted when analysed by western blot, potentially this species could represent the full-length species. To date, only amino acids 128-199 of AURKAIP1 have been identified in the crystal structures of the mitoribosomes but the exact size of AURKAIP1 is currently unknown. Upon further analysis, this species turned out to be an unidentified protein that was not AURKAIP1.

Figure 4.13 – *Mycoplasma* proteins also contain the DUF1713 domain. The FASTA sequences for AURKAIP1 from *H. sapiens* (Q9NWT8), and uncharacterised proteins from *M. leprae* (P0A5D0) and *M. tuberculosis* (P9WKT4 and P9WKT5) were aligned using clustal omega (https://www.ebi.ac.uk/Tools/msa/clustalo/). The DUF1713 domain is highlighted (red box).

Unfortunately, the mass spectrometry was unable to identify the individual protein conclusively. If the protein is of human origin, then potentially it is one of the subunits of the proteasome which would be upregulated upon infection with *Mycoplasma.* However, this would be surprising since the 27kDa species was found in the mitochondrial matrix, colocalised to fractions containing mitoribosomes and was recognised by our custom antibody. A second option is that the species is a *Mycoplasma* protein since there are several *Mycobacterium* proteins that also contain a DUF1713 domain (Interpro: IPR013177) (Figure 4.13). However, Dr Wessels was unable to find a hit on searching a *Mycoplasma* proteomics database that corresponded with a protein of similar mass. In addition, the custom antibody that was generated from the purification of AURKAIP1 was produced in *E. coli* cells (Thompson, 2014). Since it is difficult to produce a pure fraction of protein from bacterial cells despite several purification steps, the sample used to generate the polyclonal custom AURKAIP1 antibody would have contained some bacterial proteins. Thus, the antibody may recognise an epitope from one of these contaminant bacterial proteins. Once again, however, Dr. Wessels compared data against the *E. coli* database and was unable to find a suitable candidate. To date, we are unsure as to the identity of this 27kDa protein but it was clearly expressed as a function of *Mycoplasma* contamination.

A major problem in investigating AURKAIP1 is that it is unclear what size AURKAIP1 is when it enters the mitoribosome. The unidentified 27kDa species could have represented the full-length species of AURKAIP1 that associated with the mitoribosome, or alternatively the 15kDa species that is seen with AURKAIP1 and AURKAIP1-FLAG overexpression may be the correct size but this would indicate that AURKAIP1 is therefore not a *bona fide* mitoribosomal protein. Using *in vitro* assays, it may be possible to confirm where AURKAIP1 is cleaved *in vitro* to indicate what size AURKAIP1 is *in vivo* once it is imported into the mitochondria to could be determine if the AURKAIP1 and AURKAIP1-FLAG 15kDa species are the correct size, despite not localising to the mitoribosome. Both possibilities seem unlikely, although data available from mass spectrometry has only been able to identify peptides from 128-199 amino acids of the AURKAIP1 protein in the mitochondrial matrix. Combining the data altogether, it is likely that AURKAIP1 goes through a major cleavage event upon import prior to association with the mitoribosome and that this cleavage event may result in the loss of any epitopes that are recognised by our custom anti-AURKAIP1 antibody. Using *in vitro* assays, it may be possible to

confirm where AURKAIP1 is cleaved *in vitro* to indicate what size AURKAIP1 is *in vivo* once it is imported into the mitochondria. Additionally, this approach would determine if AURKAIP1 and AURKAIP1-FLAG 15kDa species are the correct size, despite not localising to the mitoribosome.

CHAPTER 5: Determining the true size of AURKAIP1

5.1 Introduction

During the course of my PhD investigations, cryo-EM structures of the mitoribosome from human (Amunts *et al.* 2015), porcine (Greber *et al.* 2015) and yeast (Desai *et al.* 2017) have been published. All of which have identified AURKAIP1 as a mitoribosomal protein that is located at the interface between the mt-LSU and mt-SSU. Previous data from my host laboratory, current data suggested that AURKAIP1 was not a *bona fide* mitoribosomal protein and that there are very low endogenous levels of AURKAIP1 within the cell. Utilising AURKAIP1 fused with a C-terminal FLAG tag, Dr Kyle Thompson identified that AURKAIP1-FLAG localised to the mitochondrial matrix and was present as a 15kDa protein, ~10kDa smaller than the full-length species. I have confirmed this data using a cell line capable of overexpressing AURKAIP1, as shown in the previous chapter.

In each of the published crystal structures the region corresponding to amino acids 128-199 of the full-length AURKAIP1 were identified, which correlates to a ~9kDa protein. AURKAIP1 is predicted to have an N-terminus MTS of 77 amino acids, according to TargetP (www.cbs.dtu.dk/services/TargetP), which would be predicted to be cleaved upon import by MPP, for example. If mature AURKAIP1 is ~9kDa, then at least one more cleavage event would have to occur. My work presented thus far, together with previous work from my host laboratory, has shown that overexpressed AURKAIP1 and AURKAIP1-FLAG is a 15kDa species (Chapter 3, Thompson, 2014) that localises to the mitochondria. Since the full-length AURKAIP1 species is predicted to be ~24kDa, overexpressed AURKAIP1 and AURKAIP1-FLAG must have undergone at least one cleavage event. The cryo-EM structures of the mitoribosomes only represent a sub-population, since homogeneous structures are used for the final analysis and some peptide regions in these structures may also be flexible, and cannot be visualised since they may not be the same in the homogeneous structures. Peptide sequences upstream of the 128-199 amino acids identified from AURKAIP1 may therefore be unresolved and unidentified. It is therefore difficult to determine the true size of AURKAIP1 within the mitoribosome from these data. The overexpressed AURKAIP1 and AURKAIP1-FLAG could therefore still represent the true size of AURKAIP1 within the mitoribosome.

Endogenous AURKAIP1 is difficult to detect using current methodologies. Since it is not possible to look at the endogenous form of AURKAIP1 as it is expressed in such low levels in the cell (Thompson, 2014), and the AURKAIP1 antibodies available are unable to detect endogenous AURKAIP1 using western blotting, one way to determine the pattern of AURKAIP1 cleavage is to use an *in vitro* approach. The full-length AURKAIP1 gene is amplified by PCR either using a forward primer that contains an RNA polymerase recognition site (for either T3, T7 or SP6 RNA polymerase), or the AURKAIP1 gene is cloned into a vector that already contains an RNA polymerase recognition site. The respective recognition site is recognised by T3, T7 or SP6 RNA polymerase which when incubated with ribonucleoside triphosphates (rNTPs) allows for *in vitro* transcription. The amplified RNA species can then be *in vitro* translated in the presence of radiolabelled ^{35}S-methionines/cysteines (^{35}S-met/cys) to generate a radiolabelled, full-length AURKAIP1 protein. Using this substrate with active mitochondria prepared from rat liver, it is possible to determine whether AURKAIP1 is cleaved *in vitro* upon import into the active mitochondria since a smaller, radiolabelled species would be detected when the sample was separated by SDS-PAGE if a cleavage event has occurred.

Other than using an *in vitro* method to determine the pattern of AURKAIP1 cleavage, an additional approach is to try and identify the mitochondrial protease that is involved in the cleavage event. AURKAIP1 has a role in mitochondrial gene expression, albeit the function is yet to be determined and three of the mitochondrial matrix ATP-dependent proteases, CLPXP, AFG3L2 and LONP1, have been shown to be involved in mitochondrial translation. CLPXP and AFG3L2 are also thought to be involved in mitoribosome maturation with CLPP acting as a chaperone for ERAL1 in mammalian cells (Szczepanowska *et al.* 2016). AFG3L2 is also involved in the cleavage of *Mrpl32* in yeast (Nolden *et al.* 2005). LONP1 has been shown to be involved in mtDNA maintenance, by controlling the levels of TFAM and may bind to mtDNA itself (Lu *et al.* 2007). With these three mitochondrial matrix proteases being involved in mitochondrial translation, there is a possibility that one of them may associate with AURKAIP1, by either cleaving AURKAIP1 to the 9kDa species prior to assembly into the ribosome in a similar manner to AFG3L2 with *Mrpl32*, or chaperoning AURKAIP1 to the mitoribosome as with CLPP and ERAL1.

The aim of this chapter was to investigate whether AURKAIP1 can be identified in purified mitoribosomes and if so, whether the N-terminus of AURKAIP1 can be determined. In

addition, I aimed to investigate whether *in vitro* translated AURKAIP1 is cleaved upon import into active isolated mitochondria, in order to determine the true size of AURKAIP1 within the mitochondrial matrix and determine whether any of the mitochondrial matrix proteases is involved in the processing of AURKAIP1.

5.2 Results

5.2.1 *Determining the cleavage of AURKAIP1 in vitro*

The size of AURKAIP1 within the mitoribosome, or indeed the mitochondria, is currently debated within the literature (Koc *et al.* 2013, Amunts *et al.* 2015). Since AURKAIP1 has been identified as a mitoribosomal protein, one approach was to purify the mitoribosome using a cell line that could overexpress a mitoribosomal subunit, and was known to be able to purify the mitoribosome through immunoprecipitation, followed by LC-MS/MS (liquid chromatography mass spectrometry) combined with N-terminal labelling and sequencing. By labelling the N-termini of the purified proteins, these peptides could be sequenced and thus identifying the final cleavage point of each protein before associating with the mitoribosome.

HEK-mS27-FLAG was induced for 3 days and purified via immunoprecipitation as described above. Previous work performed by my host laboratory showed that mS27-FLAG is able to purify the monosome as well as the mt-SSU. The eluate from immunoprecipitation of mS27-FLAG was separated by SDS-PAGE on a 12% polyacrylamide gel and stained with silver stain to visualise the proteins. In addition, a protein calibration curve was concurrently separated by using known amounts of BSA (bovine serum albumin) on the same gel in order to estimate the quantity of protein present in the eluate (Figure 5.1). The eluate, along with anti-FLAG M2

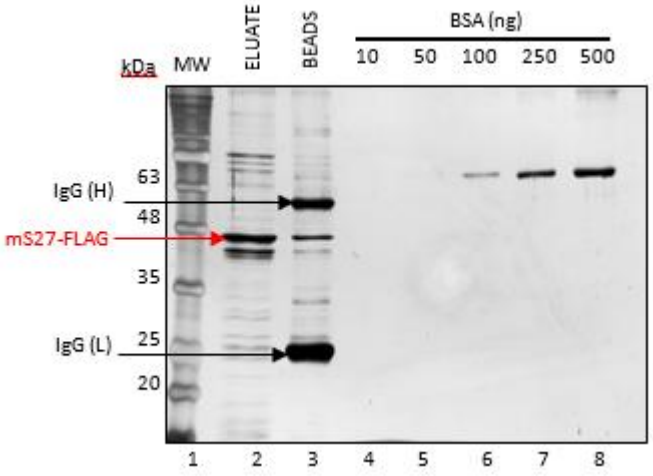

Figure 5.1 – Immunoprecipitation of the mitoribosome via mS27-FLAG for N-terminal sequencing of MRPs. Silver stain of an immunoprecipitation of mS27-FLAG, separated on 12% polyacrylamide gel by SDS-PAGE. Heavy and light chains of the anti-FLAG M2 that coats the beads are indicated (IgG H + L respectively). Expected size of mS27-FLAG (red) = 46kDa. ELUATE = 10µl of 110µl elution in 1 x phosphate buffered saline (PBS) post-elution with 3 x FLAG peptide. BEADS = 5µl of 50µl anti-FLAG M2 bead suspension in 1 x PBS post-elution. BSA = bovine serum albumin, and is used to estimate the quantity of protein present in the eluate.

beads used for the experiment, were sent to Professor Christine Carapito (University of Strasbourg, France) for doublet N-terminal oriented proteomics (dN-TOP). Briefly, proteins were separated by SDS-PAGE and the N-terminus labelled with TMPP (trimethoxyphenyl phosphonium) (Bertaccini *et al.* 2013). The proteins were subsequently digested with trypsin to form short peptide fragments and subsequently analysed by LC-MS (liquid chromatography mass spectrometry). In the first experiment, Professor Carapito's group were able to determine that AURKAIP1 was present but AURKAIP1 contains many arginine and lysine residues. Since trypsin, which is used to digest the peptide fragments for sequencing, cut at these residues, the peptide fragments produced were too small for further analyses, despite other mitoribosomal proteins being successfully labelled with TMPP (Appendix M). The immunoprecipitation was repeated and a second set of samples were sent to be digested with an alternative endopeptidase, Asp-N (flavastacin), that cleaves the N-terminal side of aspartate residues. A peptide corresponding to amino acids 172-183 (DLRRIWLKAGLK) was identified, however it was still not possible to determine the N-terminal cleavage point of AURKAIP1 since the fragment was not labelled with TMPP.

5.2.2 *Optimising in vitro translation*

Since it was not possible to identify the cleavage point using basic proteomics, an *in vitro* approach was adopted. Using radiolabelled protein with an MTS that has been transcribed and translated *in vitro,* the approximate cleavage site of a mitochondrial protein can be determined using freshly-prepared rat liver mitochondria. The construct pGEM4-SU9-DHFR (pSU9-DHFR), which consists of mouse dihydrofolate reductase (DHFR) fused to the N-terminal MTS presequence of ATP synthase subunit 9 from *Neurospora crassa*, was used as the control. This protein is known to be successfully translated *in vitro,* and is known to be cleaved upon import into isolated rat liver mitochondria. SU9-DHFR is considered the gold standard for this experiment. The *AURKAIP1* gene with and without a FLAG-tag was amplified using PCR. A forward primer was designed to target the 5' terminus of *AURKAIP1* with the addition of the SP6 promoter ahead of the AURKAIP1 sequence, to facilitate *in vitro* transcription by SP6 polymerase. The same reverse primers designed for the cloning of HEK-AUR1 and HEK-AUR1-FLAG (Thompson, 2014) respectively were used to target the 3' terminus of *AURKAIP1* (Appendix C). PCR was performed with HeLa cDNA as the template to generate SP6-AUR1 and SP6-AUR1-FLAG DNA templates.

Previous work performed by my host laboratory suggested that *in vitro* transcription was more efficient if the pSU9-DHFR construct was linearised (Rorbach, 2008). Therefore, pSU9-DHFR was digested for 2.5hrs and 5hrs with *Pvu*II to ensure full digestion prior to *in vitro* translation. The sample that was digested for 2.5hrs was used for subsequent reactions.

SP6-AUR1, SP6-AUR1-FLAG and SU9-DHFR DNA templates were used in AmpliScribe™ *SP6 in vitro* transcription reactions (EpiCentre, following manufacturer's protocol) to produce RNA transcripts. Linearised pSU9-DHFR was more efficient at producing an RNA transcript compared to undigested, as previously found in my host laboratory, and thus the construct was fully digested with *Pvu*II. RNA transcripts were generated from linearised SU9-DHFR, SP6-AUR1 and SP6-AUR1-FLAG (Figure 5.2A). Rabbit reticulocyte lysate, amino acids and ^{35}S-Met were combined with the RNA transcripts and incubated at 37^{o}C to produce radioactive-labelled protein by *in vitro* translation. The *in vitro* translation was more efficient in the control, SU9-DHFR, compared to SP6-AUR1 or SP6-AUR1-FLAG (Figure 5.2B, C) although specifics product were seen for both SP6-AURKAIP1 and SP6-AURKAIP1-FLAG.

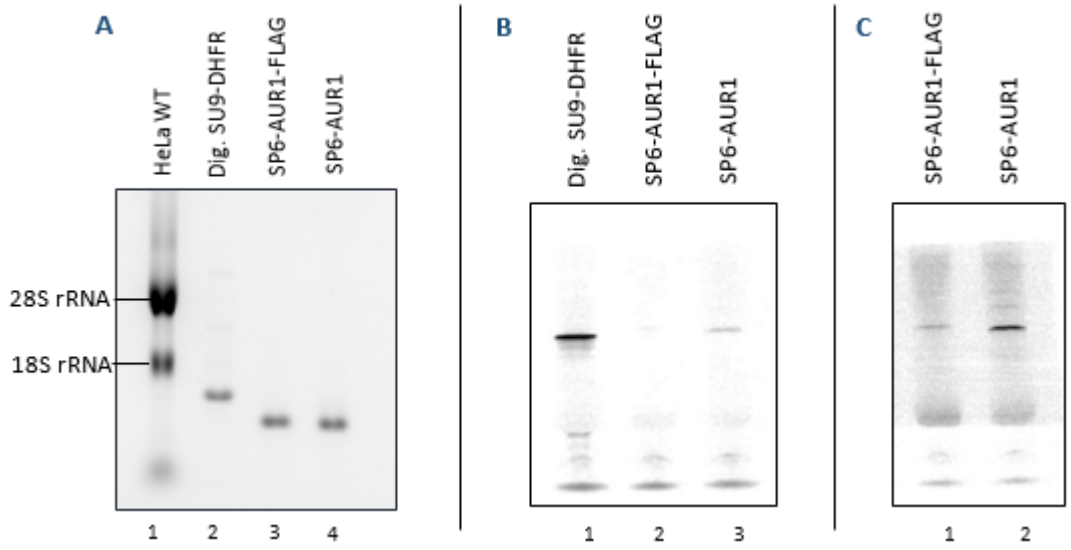

Figure 5.2 – *In vitro* transcription and translation of AURKAIP1 and AURKAIP1 FLAG. A - 5µg HeLa RNA and 1/10 *in vitro* transcription reactions analysed on 1% denaturing agarose gel. 28S rRNA = 5025bp, 18S rRNA = 1868bp, SU9-DHFR = 950bp, SP6-AUR1 = 628bp, SP6-AUR1-FL = 656bp. B – *in vitro* translation of SU9-DHFR (26kDa), SP6-AUR1-FLAG and SP6-AUR1 (~25kDa). Samples analysed on 15% polyacrylamide gel, fixed in 50% MeOH, dried, exposed to a PhosphorImage screen and developed for 4 days. Signals were visualised on the Typhoon FLA9500 system using ImageQuant™ software. C – higher exposure of *in vitro* translation of SP6-AUR1 and SP6-AUR1-FLAG from (B).

Since *in vitro* translation of SP6-AURKAIP1 produced the highest amounts product, I tried to optimise the reaction by altering the amount of template RNA. *In vitro* translation was repeated with 3µl and 0.3µl RNA transcripts but similar levels of SP6-AURKAIP1 were achieved

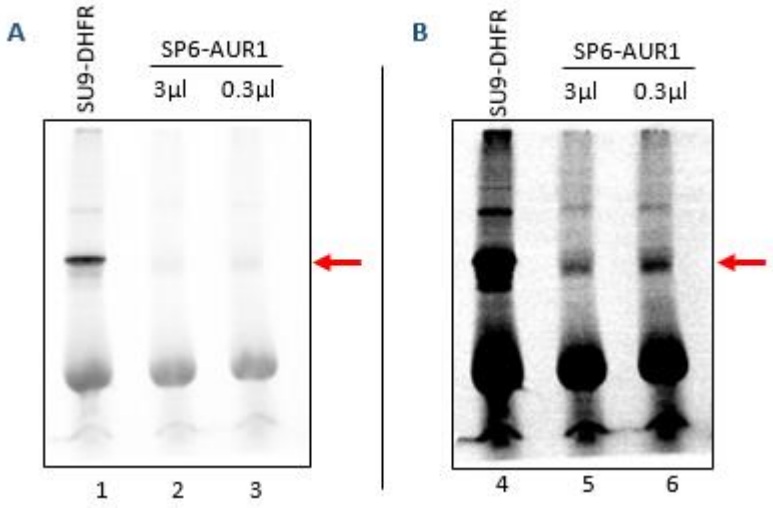

Figure 5.3 – Improving the efficiency of *in vitro* translation for SP6-AURKAIP1. One tenth of each *in vitro* translation reaction for SU9-DHFR (3µl) and SP6-AUR1 (3µl or 0.3µl) were separated by SDS-PAGE in a 15% polyacrylamide gel. The gels were dried, and exposed to a PhosphorImage screen for 5 days. A = normal brightness. B = darker brightness. Red arrow = SP6-AURKAIP1. SU9-DHFR = 950bp, SP6-AUR1 = 628bp, SP6-AUR1-FL = 656bp.

(Figure 5.3). Therefore, the original *in vitro* translated SP6-AURKAIP1 was used for the *in vitro* import assay.

Active mitochondria were isolated from fresh rat liver homogenate, to maintain the membrane potential and the ability to import mitochondrial proteins. Four reactions were each set-up for SU9-DHFR and SP6-AURKAIP1. As controls, FCCP was used to inhibit mitochondrial import and proteinase K was used to degrade proteins that were outside of the mitochondria. The first reaction contained FCCP, which inhibits mitochondrial import so only the full-length, uncleaved species should be seen (Figure 5.6, lanes 2 and 7). The second reaction contains both FCCP and proteinase K, a protease that degrades proteins not imported into the mitochondria. In this lane, there should be no protein visible since the species would not be imported and yet all degraded (Figure 5.6, lanes 3 and 8). The third reaction contains neither FCCP or proteinase K, and therefore both the full-length species that has not been imported into the mitochondria, and the cleaved species should be visible (Figure 5.6, lanes 4 and 9). The final reaction contains only proteinase K, and thus only the species that has been imported into the mitochondria and cleaved should be detected (Figure 5.6, lanes 5 and 10).

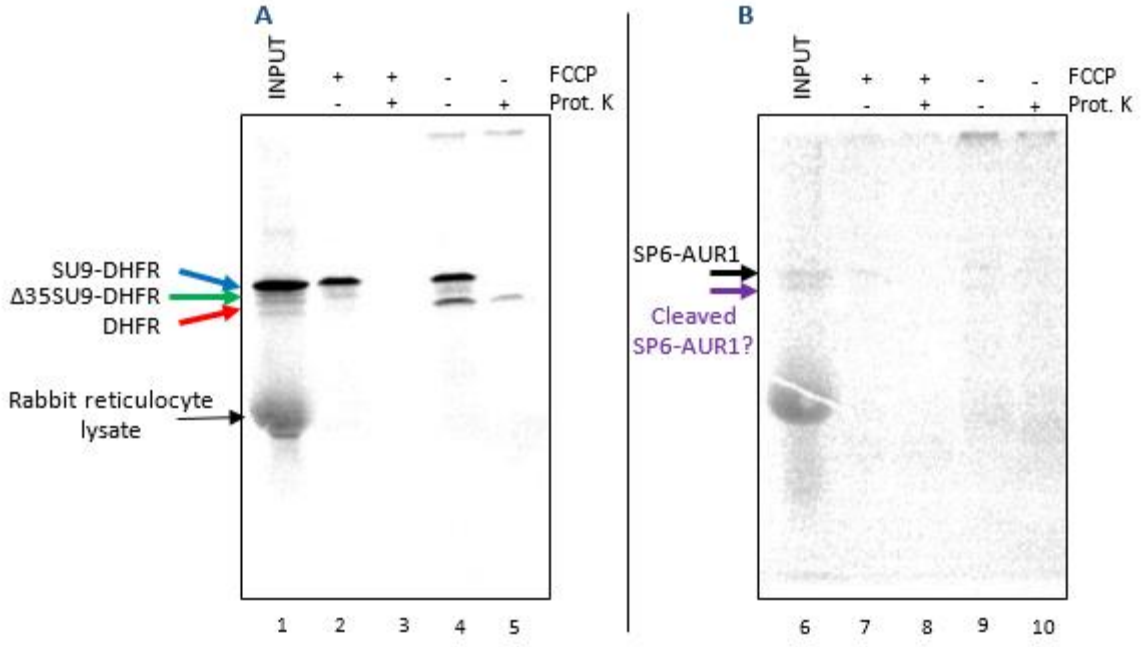

Figure 5.4 – SU9-DHFR, but not AURKAIP1, is visibly cleaved upon *in vitro* import. SU9-DHFR and SP6-AURKAIP1 that had been *in vitro* translated were incubated in the presence or absence of FCCP and proteinase K as shown with active mitochondria. Mitochondrial lysates were separated out by SDS-PAGE on a 15% polyacrylamide gel. Gels were dehydrated, and exposed to a PhosphorImage screen for 5 days. A = SU9-DHFR. Blue arrow = SU9-DHFR, green arrow = Δ35SU9-DHFR, red arrow = DHFR. B = SP6-AURKAIP1. Black arrow = immature SP6-AURKAIP1, purple arrow = potential cleaved AURKAIP1 species.

SU9-DHFR is used as the gold standard control for this experiment. The DHFR protein undergoes two cleavage events at residues 35 and 66 (Schmidt and Neuport, 1984) to produce an intermediate and mature protein respectively which can both be detected.

In the SU9-DHFR sample, the three species were detected in the input (Figure 5.4, lane 1). With the addition of FCCP, the full-length and Δ35 species were detected, indicating that the initial cleavage event most likely occurs in the cytosol (Figure 5.4, lane 2). When both FCCP and proteinase K were added, no proteins were detected since they would have all been degraded (Figure 5.4, lane 3). Without FCCP or proteinase K added, all three species can be detected; the full-length, intermediate species and the mature species (Figure 5.4, lane 4). Finally, the addition of proteinase K degrades all protein that has not been imported into the active isolated mitochondria. Only the DHFR species resulting from two cleavage events is detected, since the SU9-DHFR and Δ35SU9-DHFR species would have degraded outside the mitochondria (Figure 5.4 lane 5). In the SP6-AUR1 sample, unfortunately the protein could not be detected clearly. In the input lane, it appears that there are two species (Figure 5.4, lane 6) but these are closer in size than predicted. If AURKAIP1 was cleaved to a ~9kDa species, then the rabbit reticulocyte lysate that contains excess ^{35}S-Met/Cys may be covering the signal of the SP6-AURKAIP1. When this sample is incubated with active mitochondria, the second, smaller band could still be detected (Figure 5.4, lane 9). However, since there was not a clear detected signal from the reaction that contained only proteinase K (Figure 5.4, lane 10), leaving only the imported species, it is not possible to conclude the cleavage pattern of AURKAIP1 from this data.

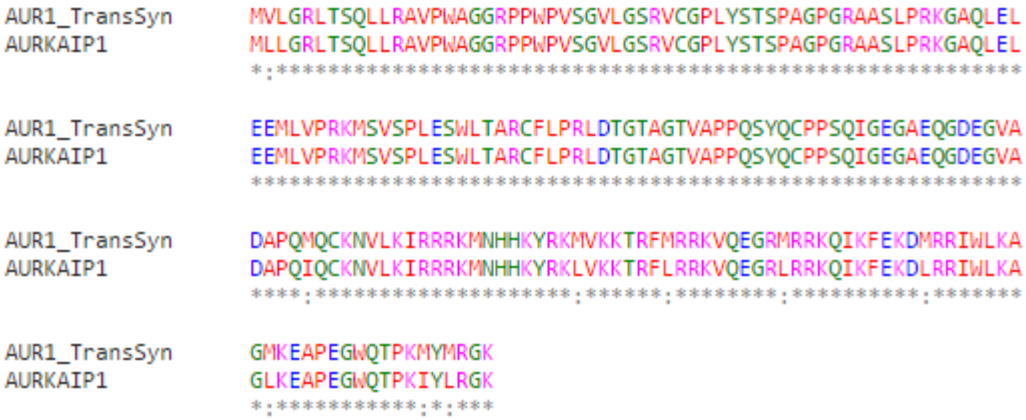

Figure 5.5 – Synthesised AURKAIP1 has increased methionine residues. SP6-AURKAIP1 was custom synthesised with leucine and isoleucine residues replaced with methionine residues. The amino acid sequence of the synthesised sequence (AUR1_TransSyn) was compared using to the AURKAIP1 amino acid sequence (Q9NWT8) using Clustal Omega (https://www.ebi.ac.uk/Tools/msa/clustalo/). Asterisk (*) = single, fully-conserved residue, colon (:) = conservation between groups with strongly similar properties.

Since it was not possible to generate radiolabelled SP6-AURKAIP1 which could be detected despite attempts at optimisation, a third approach was used. The radiolabel used for *in vitro* translation is ^{35}S-Met/Cys that labels both methionine and cysteine. However, methionine residues are generally better incorporated compared to cysteine residues. By changing leucine or isoleucine residues to methionines in the SP6-AURKAIP1 sequence, it may be possible to enhance the radioactive signal without interfering with the structure of AURKAIP1. Since the predicted MTS is in the N-terminus, only isoleucine and leucine residues in the C-terminus were changed to prevent interference with the MTS. The new sequence was termed SP6-AUR1-TransSyn (Figure 5.5).

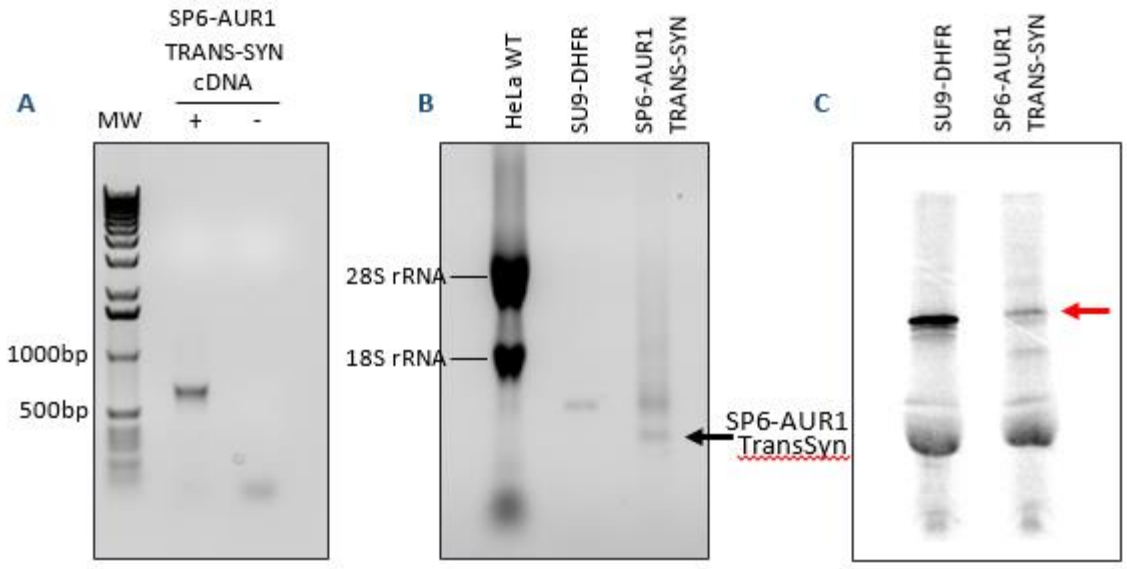

Figure 5.6 – *In vitro* transcription and translation of SP6-AUR1-TransSyn. A = PCR (2µl of a 50µl reaction) of SP6-AUR1-TransSyn using the single-stranded synthesised AURKAIP1 oligonucleotide. Samples were separated on 1% agarose gel. Expected size = 628bp. B = *In vitro* transcription using digested SU9-DHFR (expected size = 950bp) and the purified SP6-AUR1-TransSyn PCR product (expected size = 628bp). RNA samples are separated on a 1% denaturing agarose gel. 5µg HeLa RNA was also separated as a marker. 28S rRNA = 5025bp, 18S rRNA = 1868bp C = *In vitro* translation of SU9-DHFR and SP6-AUR1-TransSyn (red arrow). Protein samples were separated on a 15% polyacrylamide gel.

SP6-AUR1-TransSyn was transcribed and translated *in vitro* alongside digested SU9-DHFR (Figure 5.6). Despite a single PCR product (Figure 5.8A) *in vitro* transcription produced two RNA products (Figure 5.8B). However, the RNA samples were used for *in vitro* translation. SP6-AUR1-TranSyn did produce a stronger signal, but due to the presence of multiple other products the sample was not used for the *in vitro* import assay, since it would not be possible to identify the true cleaved AURKAIP1 species. (Figure 5.6C).

5.2.3 *Depletion of matrix proteases*

Since it was not possible to determine whether AURKAIP1 was cleaved *in vitro* using the *in vitro* import assay, the mitochondrial matrix proteases were investigated to determine if any of them were involved in cleaving AURKAIP1. Overexpressed AURKAIP1 and AURKAIP1-FLAG are detectable only as a 15kDa species, whereas the full-length species is ~25kDa and the species that has been visualised in the mitoribosome is ~9kDa. Potentially, there may be two cleavage events on AURKAIP1 before it is inserted into the mitoribosome, as shown by my previous data (Chapter 4), and one of the matrix proteases could be involved. To test this

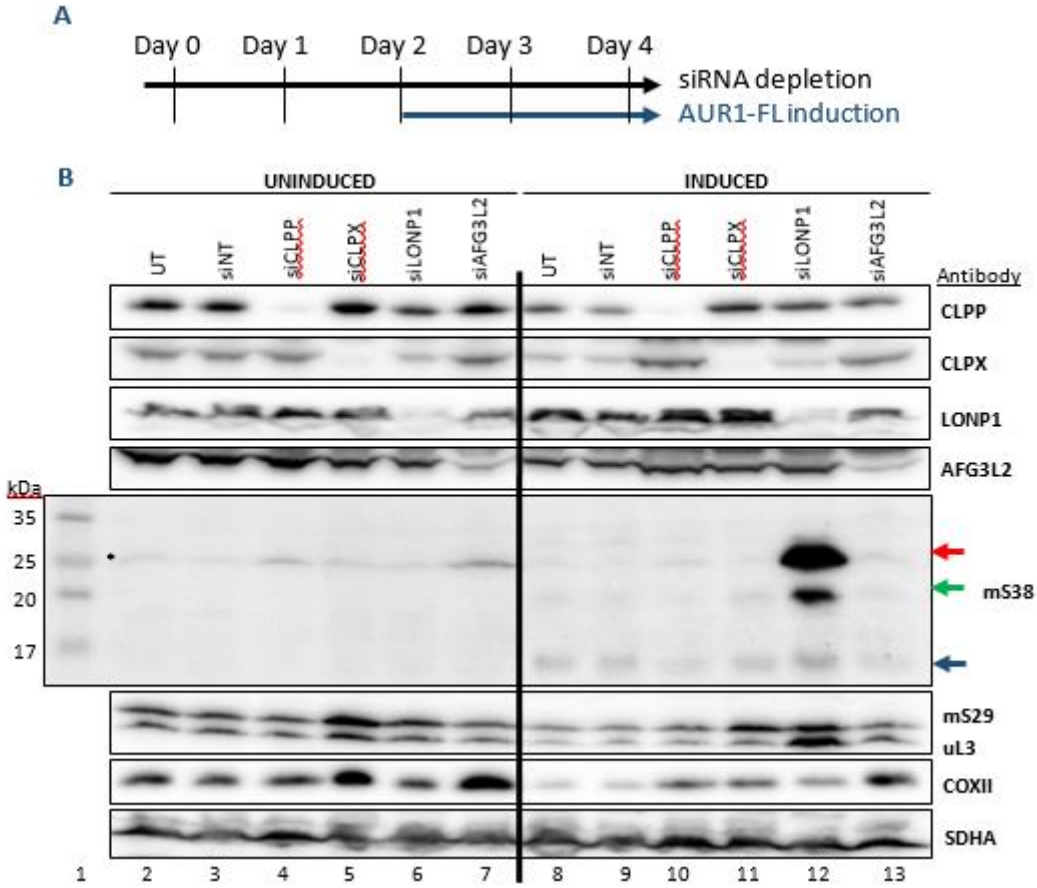

Figure 5.7 – LONP1 degrades overexpressed AURKAIP1-FLAG to a 15kDa species. A = Overview of the experiment. In 6-wells plates, HEK-AURKAIP1-FLAG cells were treated with siRNA (non-targetting, ClpP, ClpX, LONP1 and AFG3L2) for 4 days. At Day 2, half the samples were induced with 1µg/ml tetracycline for 2 days. B = Samples were harvested, lysed and separated on a 15% polyacrylamide gel by SDS-PAGE and analysed by western blot. The membrane was incubated with antibodies as stated. Red arrow = 25kDa AURKAIP1-FLAG species, green arrow = 20kDa AURKAIP1-FLAG species, blue arrow = 15kDa AURKAIP1-FLAG species. UT = untreated.

hypothesis, four of the mitochondrial matrix proteases were depleted using siRNA, at the same time that AURKAIP1-FLAG was overexpressed (Figure 5.7A). Depletion of LONP1 resulted in an increase in the levels of the full-length 25kDa AURKAIP1 species and an intermediate 20kDa species (Figure 5.7B). This was also repeated with AUR1-NoF (data not shown). However, there was no increase in the 25kDa species in the uninduced control samples with LONP1 depletion. LONP1 could still be cleaving the endogenous species, but with the current antibodies available this is not possible to detect. Repeats of this experiment were also performed using the FLAG antibody, and the same species were visible in the induced AURKAIP1-FLAG samples following LONP1 depletion. In order to verify that the 25kDa species was indeed AURKAIP1-FLAG, samples of uninduced and induced HEK-AURKAIP1-FLAG lysates

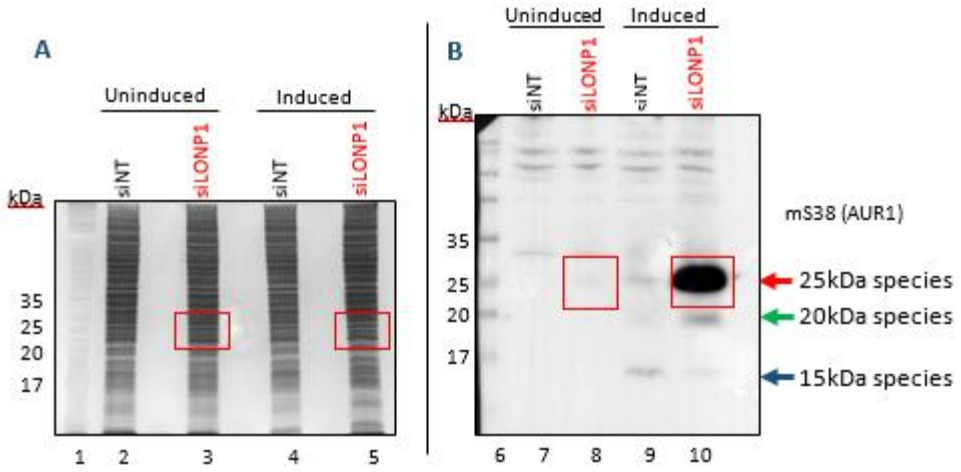

Figure 5.8 – Identifying 25kDa AURKAIP1-FLAG species upon depletion of LONP1 using mass spectrometry. Uninduced and induced HEK-AURKAIP1-FLAG lysates treated with either non-targeting (siNT) or LONP1 (siLONP1) siRNA as described in Figure 5.6 were separated on a 15% polyacrylamide gel by SDS-PAGE and analysed by silver staining (A) or western blot using anti-AURKAIP1 antibody (B). Red box = corresponding area of gel excised for mass spectrometry analysis. Red arrow = 25kDa AURKAIP1-FLAG species, green arrow = 20kDa AURKAIP1-FLAG species, blue arrow = 15kDa AURKAIP1-FLAG species.

treated with either siNT or siLONP1 were analysed by silver staining and western blot to confirm the presence of the 25kDa species in the induced, siLONP1 sample (Figure 5.9). Uninduced and induced HEK-AUR1-FLAG lysates treated with siLONP1 were subsequently separated by SDS-PAGE and gel sections sent to the Nijmegen proteomics facility (Dr Hans Wessels) for analysis by mass spectrometry (Figure 5.8).

Mass spectrometry analysis identified 608 proteins from 2595 peptides in the uninduced sample, and 268 proteins from 1044 peptides in the induced sample (Appendix O). Analysis confirmed the presence of AURKAIP1 in the induced, siLONP1 HEK-AURKAIP1-FLAG lysate (Figure 5.9). In my previous chapter (Chapter 3) I had shown that the levels are tightly controlled. Therefore, LONP1 may be involved in processing overexpressed AURKAIP1-FLAG because the levels of the protein are too high. The 25kDa and 20kDa species, although only detected when AURKAIP1 was overexpressed, could still be components of the mitoribosome.

5.2.4 *Novel AURKAIP1-FLAG species do not associate with the mitoribosome*

Upon LONP1 depletion, a 25kDa and a 20kDa AURKAIP1-FLAG species can be detected using our custom AURKAIP1 antibody. The 25kDa species was also confirmed to be AURKAIP1 using mass spectrometry. To determine if either of these species associated with the mitoribosome, mitochondrial lysates were prepared from induced HEK-AURKAIP1-FLAG cells that had also been treated with non-targeting or LONP1 siRNA (as described in Figure 5.9). These lysates were resolved on sucrose gradients (Figure 5.10). Western blot analysis of each of the fractions identified that neither the 25kDa nor the 20kDa AURKAIP1-FLAG species associated with the mitoribosome (Figure 5.10B). The 25kDa species was identified in fraction 4 of the siLONP1 sample, indicating that potentially the full-length species was associated with the early mt-SSU, but this is more likely to be due to carryover from fractions 1-3, due to the large amount of the protein that was present in the sample.

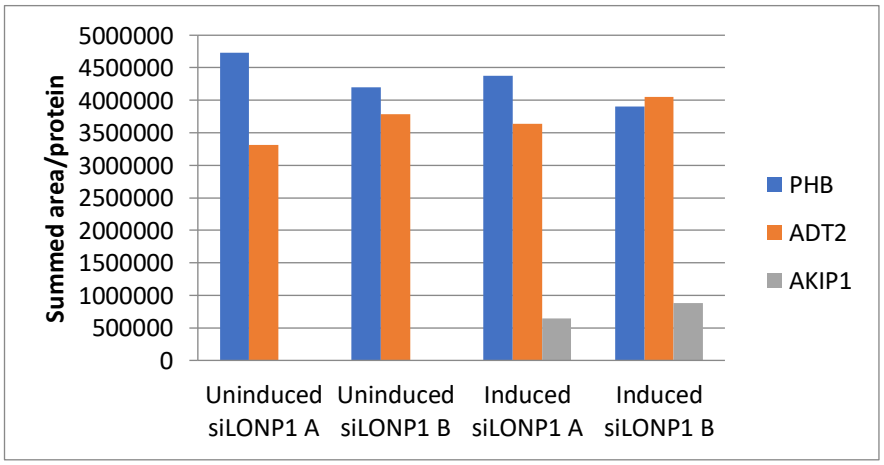

Figure 5.9 – LONP1 is involved in the degradation of overexpressed AURKAIP1-FLAG. Controls were: PHB (polyhydroxybutyrate) and ADT2 = (ADP/ATP translocase 2). AKIP1 = AURKAIP1. Values for summed area/protein were taken for each protein. Two repeats (A and B) were analysed.

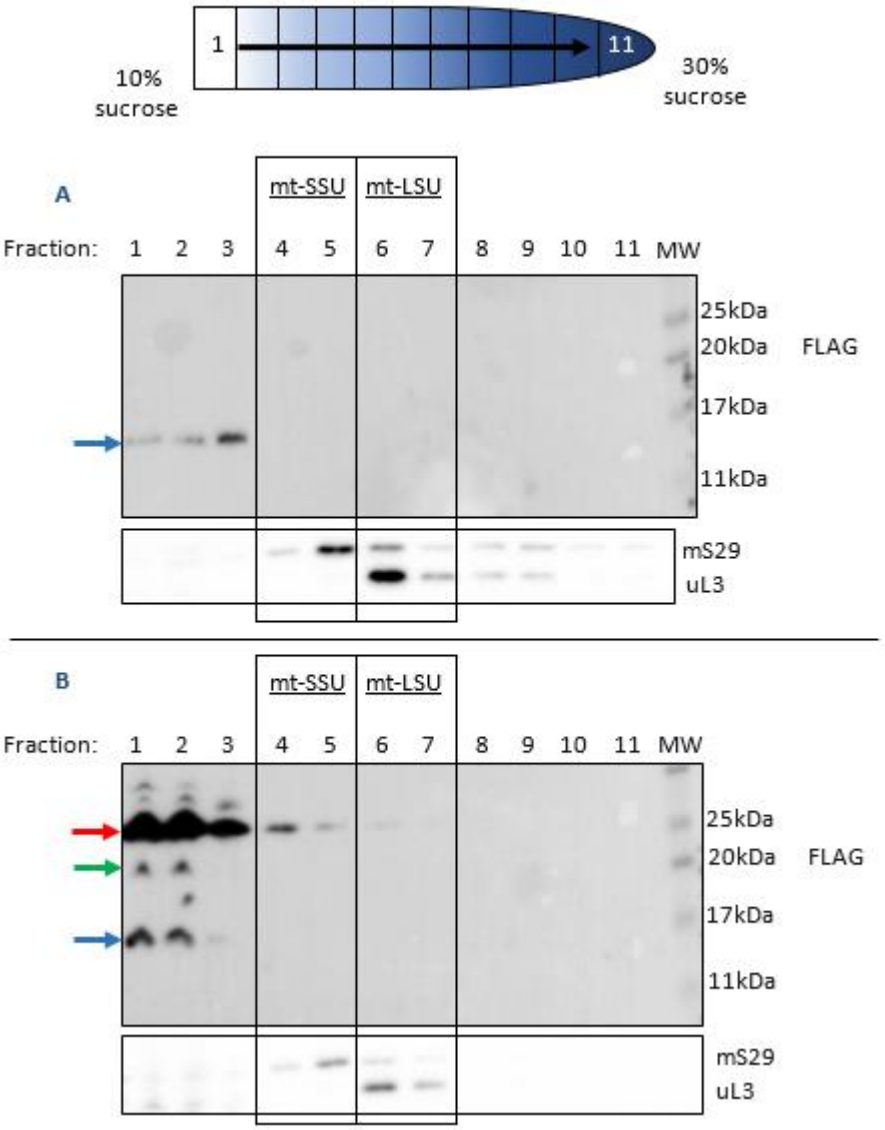

Figure 5.10 – Exogenous AURKAIP1-FLAG species do not associate with the mitoribosome. Mitochondrial lysate (750µg) of induced HEK-AURKAIP1-FLAG treated with non-targeting siRNA (siNT, A) or LONP1 siRNA (siLONP1, B) was separated through a 10-30% sucrose gradient. Eleven fractions were taken, TCA precipitated and half of each sample was loaded on 15% SDS-PAGE gels. Membranes were subjected to western blotting with antibodies as shown. Mitoribosomal proteins mS29 and uL3 are used as markers for the mt-SSU and mt-LSU respectively. Red arrow = 25kDa AURKAIP1 species, green arrow = 20kDa AURKAIP1 species, blue arrow = 15kDa AURKAIP1 species.

5.3 Discussion

I have confirmed that AURKAIP1 associates with the mitoribosome, as determined by LC-MS of immunoprecipitated mS27-FLAG. However, the N-terminus of AURKAIP1 could not be determined as the identified peptides was not labelled with TMPP for sequencing. Trypsin was originally used for the cleavage of the peptides prior to mass spectrometry, which cleaves C-terminal to arginine and lysine residues (Figure 5.11A). By using trypsin, this resulted in peptides that were too small to be analysed (Figure 5.11B). There are six other proteases that

A

Protease	Origin	Cleavage	Residues
Trypsin	Porcine pancreas	C-terminal	Arginine and lysine, except when followed by a proline
Chemotrypsin	Bovine pancreas	C-terminal	Tyrosine, phenylalanine, tryptophan
LysC	*Lysobacter enzymogenes*	C-terminal	Lysine
LysN	*Grifola frondosa*	N-terminal	Lysine
AspN	*Flavobacterium menigosepticum*	N-terminal	Aspartate
GluC	*Staphylococcus aureus*	C-terminal	Glutamate, aspartate
ArgC	*Clostridium histolyticum*	C-terminal	Arginine, lysine.

B

MLLGRLTSQLLRAVPWAGGRPPWPVSG
VLGSRVCGPLYSTSPAGPGRAASLPRKGA
QLELEEMLVPRKMSVSPLESWLTARCFLP
RLDTGTAGTVAPPQSYQCPPSQIGEGAE
QGDEGVADAPQIQCKNVLKIRRRKMNH
HKYRKLVKKTRFLRRKVQEGRLRRKQIKFE
KDLRRIWLKAGLKEAPEGWQTPKIYLRGK

C

MLLGRLTSQLLRAVPWAGGRPPWPVSG
VLGSRVCGPLYSTSPAGPGRAASLPRKGA
QLELEEMLVPRKMSVSPLESWLTARCFLP
RLDTGTAGTVAPPQSYQCPPSQIGEGAE
QGDEGVADAPQIQCKNVLKIRRRKMNH
HKYRKLVKKTRFLRRKVQEGRLRRKQIKFE
KDLRRIWLKAGLKEAPEGWQTPKIYLRGK

D

MLLGRLTSQLLRAVPWAGGRPPWPVSG
VLGSRVCGPLYSTSPAGPGRAASLPRKGA
QLELEEMLVPRKMSVSPLESWLTARCFLP
RLDTGTAGTVAPPQSYQCPPSQIGEGAE
QGDEGVADAPQIQCKNVLKIRRRKMNH
HKYRKLVKKTRFLRRKVQEGRLRRKQIKFE
KDLRRIWLKAGLKEAPEGWQTPKIYLRGK

E

MLLGRLTSQLLRAVPWAGGRPPWPVSG
VLGSRVCGPLYSTSPAGPGRAASLPRKGA
QLELEEMLVPRKMSVSPLESWLTARCFLP
RLDTGTAGTVAPPQSYQCPPSQIGEGAE
QGDEGVADAPQIQCKNVLKIRRRKMNH
HKYRKLVKKTRFLRRKVQEGRLRRKQIKFE
KDLRRIWLKAGLKEAPEGWQTPKIYLRGK

Figure 5.11 – Endoproteases used for cleaving peptides for mass spectrometry. A – Table detailing the seven common proteases that are used for mass spectrometry. B – Lysine (red) and arginine (blue) residues present within the AURKAIP1 sequence that are digested by trypsin (lysine, arginine), LysC and LysN (lysine). C – Aspartate (purple) residues present within the AURKAIP1 sequence that are digested by AspN (aspartate). D – Glutamate (orange) residues present within the AURKAIP1 sequence that are digested by GluC (aspartate, aspartate). E – Trytophan (pink), tyrosine (blue) and phenylalanine (F) residues present in the AURKAIP1 sequence that are digested by chymotrypsin.

are often used for mass spectrometry (Giansanti *et al.* 2016, Figure 5.11) of which AspN was a suitable candidate for analysing AURKAIP1 as the endopeptidase would have produced long enough fragments for analysis (Figure 5.11C).

However, only one peptide corresponding to residues 172-183 (DLRRIWLKAGLK) was identified. Previous mass spectrometry analyses on the cryo-EM structures of the mitoribosomes had also identified AURKAIP1 peptides from residues 128-199. Either the N-terminus of AURKAIP1 is not well-suited for mass spectrometry analyses, or AURKAIP1 is cleaved to a protein of ~9kDa as indicated by the cryo-EM structures. To increase the chances of identifying more AURKAIP1 peptides, a protein-protein cross-linker e.g. DSP (dithiobis(syccinimidyl propionate)) could be used on the induced HEK-mS27-FLAG cells prior to harvesting and immunoprecipitation. DSP contains an *N*-hydroxysuccinimide ester at both the N- and C-termini which reacts with primary amines that are typically located on lysine residues, forming stable amide bonds. If the interaction between AURKAIP1 and the mitoribosome is weak, then DSP will cross-link AURKAIP1 to the mitoribosome via these amide bonds so that more protein is present in the eluate of the immunoprecipitation (Gingras *et al.* 2007).

Unfortunately, I was unable to determine the cleavage point of AURKAIP1 using the *in vitro* import assay. The efficiency of *in vitro* translation of SP6-AURKAIP1-FLAG and SP6-AURKAIP1 were both low despite attempts at optimising the protocol with both increased and decreased amounts of RNA template, as well as altering the sequence to contain more methionines for ^{35}S-Met/Cys labelling. Due to time restraints, it was not possible to optimise the protocol further, but other factors can be altered to improve translation efficiency. Firstly, the RNA concentration within the reaction can be optimised further. *In vivo,* AURKAIP1 appears to be present at low levels within the cell and it may be that efficient translation occurs with a reduced amount of template within the reaction. Secondly, magnesium and potassium concentrations can be optimised within the *in vitro* translation reaction to try and improve the yield of AURKAIP1 protein. The ribosome uses both magnesium and potassium ions as cofactors (Lightfoot, 1988) and in the current reaction, magnesium is present as 0.35mM MgOAc, whereas potassium is present as 56mM KOAc (2.6.2). Similar to PCR, optimal concentrations of these two ions will change depending on the template (Nierhaus, 2014) with optimal potassium concentrations ranging from 30-120mM and additional magnesium can be

added as 0.5-2.5mM (final concentration). Thirdly, AURKAIP1 has several rare codons (Table 5.1). Despite rabbit reticulocyte lysate containing tRNAs for rare codons, lowering the temperature of the reaction may enable these tRNAs to be incorporated into the ribosome when required more efficiently by slowing down the reaction. Since it is not possible to visualise AURKAIP1 using conventional methods, the *in vitro* import assay will be a useful tool in predicting the mature size of AURKAIP1 within the mitochondria once optimised.

Table 5.1: Rare codon usage within AURKAIP1 mRNA sequence.

Amino Acid	Rare Codon[a]	Frequency of Occurrence
Arginine	CGA	0
	CGG	7
	AGG	5
	AGA	2
Glycine	GGA	2
	GGG	9
Isoleucine	AUA	1
Leucine	CUA	1
Proline	CCC	8
Threonine	ACG	2

[a]Number of rare codons present in the AURKAIP1 sequence was determined using the "Rare Codon Calculator" (http://people.mbi.ucla.edu/sumchan/caltor.html).

I was able to confirm that overexpressed AURKAIP1-FLAG were both being degraded by LONP1 via two cleavage events from the full-length 25kDa species to an intermediate 20kDa species and finally to a 15kDa species. However, LONP1 does not seem to act on the endogenous AURKAIP1 species, since there was no increase of a 25kDa endogenous species in the uninduced samples upon LONP1 depletion. Potentially, this could indicate that the overexpressed proteins are either misfolded, oxidatively-damaged or that there is too much AURKAIP1 within the cell. By protein quality control pathways within the cell and the mitochondria, the damaged or excess protein therefore needs to be degraded and removed. Within the mitochondrial matrix, LONP1 and CLPXP are involved in protein quality control. CLPXP is involved in the mitochondrial unfolded protein response (UPR^{mt}), in which a disturbance in protein homeostasis activates a signalling pathway to the nucleus (Zhao *et al.* 2002). LONP1 is not a component of the UPR^{mt} but has been shown to be the primary matrix protease that degrades misfolded, not aggregated, mitochondrial proteins (Bezawork-Geleta *et al.* 2015). Since the sequences of both constructs had been confirmed with Sanger

sequencing, it is unclear as to why the overexpressed proteins, and not the endogenous AURKAIP1 protein, are being degraded specifically by LONP1.

Since it is difficult to study mitochondrial proteins *in vivo* without using RNAi, or overexpressed proteins, patient cell lines that harbour mutations in the respective proteins are often utilised. Using whole exome sequencing, a patient with compound heterozygous mutations in *LONP1* was identified. The patient's muscle and primary fibroblasts were available for further analysis. Since this protein has been shown to be important in processing overexpressed AURKAIP1-FLAG in my experiments shown here, I will analyse these samples to confirm the inheritance of these mutations, and determine the effect of these mutations on mitochondrial function in order to further understand the functions of LONP1.

CHAPTER 6: INVESTIGATING A PATIENT WITH LONP1 MUTATIONS

6.1 Introduction

Utilising patient cell lines harbouring mutations in mitochondrial proteins allows us to investigate mitochondrial protein function in more detail without altering cell homeostasis using molecular biology techniques. This is very much the case for mitochondrial proteases such as LONP1, and mutations in several mitochondrial ATP-dependent proteases have been identified. In iAAA (YME1L), which mediates the processing of OPA1 in the IMS together with OMA1 (Rainbolt *et al.* 2015), a homozygous missense mutation (c.616C>T, p.R149W) was identified in a highly conserved region of the MTS of *YME1L1* in four siblings from a Saudi Arabian family, resulting in infantile-onset mitochondriopathy. In these four siblings, mitochondriopathy presented as intellectual disability, motor developmental delay, speech delay, optic nerve hypoplasia, and hearing impairment.

The mAAA protease is composed of two subunits, AFG3L2 and SPG7, of which mutations have been identified in both. AFG3L2 is highly expressed in cerebellar Purkinje cells (Sacco *et al.* 2010) and mutations in *AFG3L2* have been associated with dominant hereditary spastic ataxia type 28 (Di Bella *et al.* 2010) and spastic ataxia-neuropathy syndrome (Pierson *et al.* 2013). SPG7 (paraplegin) is also highly expressed in Purkinje cells (Sacco *et al.* 2010) and mutations in *SPG7* result in the autosomal recessive hereditary spastic paraplegia (ARHSP) and chronic progressive ophthalmoplegia due to impaired mtDNA maintenance (Pfeffer *et al.* 2014).

The matrix protease CLPXP is made up of the two subunits, CLPX and CLPP. No mutations have so far been identified in CLPX in humans, but mutations in CLPP have been associated with Perrault syndrome, an autosomal recessive disease that causes hearing loss and ovarian failure (Jenkinson *et al.* 2013). Interestingly, mutations in several other mitochondrial genes including LARS2 (Pierce *et al.* 2013), HARS2 (Pierce *et al.* 2011) and Twinkle primase-helicase (Morino *et al.* 2014) also result in Perrault syndrome.

Mutations in *LONP1* that have been identified are typically associated with CODAS (cerebral, ocular, dental, auricular, skeletal) syndrome. This disease was first identified in 1991

(Shebib *et al.* 1991) in an endogenous German Mennonite community and was characterised by a distinctive phenotype consisting of developmental delay (cerebral), cataracts, ptosis (ocular), delayed tooth eruption, anomalous cusp morphology (dental), malformed helices, hearing loss (auricular), short stature, coronal clefts in the lower vertebrae (T11-S2) and hip dysplasia (skeletal). As a part of the Lily Foundation-funded WES of patients with mtDNA depletion, a patient was identified with two novel LONP1 mutations. I will investigate the effects of these LONP1 mutations on the OXPHOS complexes.

6.2 Results

6.2.1 Identifying a patient with LONP1 mutations

Since the first case of CODAS syndrome, identified by Shebib *et al.*, several reports of patients with similar phenotypes have been published (Innes *et al.* 2001, Cabral de Almeida *et al.* 1995, Marlin *et al.* 2010). CODAS syndrome was later associated with mutations in the mitochondrial matrix protease, LONP1, with the mutations identified as being located throughout the ATPase and proteolytic domains (Figure 6.1). These mutations (Figure 6.1) have all resulted in CODAS syndrome. One atypical case has recently been published in a patient who harboured a compound heterozygous mutation in *LONP1* (p.Ser100GInfs*46; p.Arg786Trp, Figure 6.1), and whose phenotype was described as atypical CODAS syndrome, overlapping with Marinesco-Sjögren syndrome (Inui *et al.* 2017), a disorder that is typically characterised by mild-moderate intellectual disability, skeletal abnormalities including scoliosis and short stature (Alter *et al.* 1962). The patient harbouring the apparent mutation in *LONP1* had myopathy, ataxia, scoliosis, cataracts, developmental delay and delayed/absent

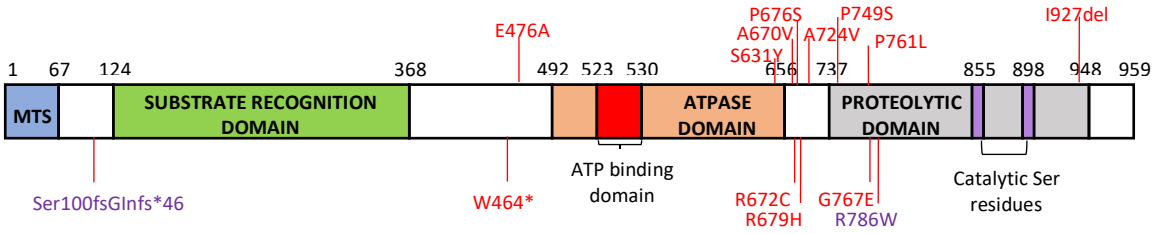

MUTATIONS	HETEROZYGOUS /HOMOZYGOUS	REFERENCES
Ser100fsGlnfs*46; R786W	Heterozygous	Inui *et al.* 2017
P749S; G767E	Heterozygous	Dikoglu *et al.* 2015
P761L; P761L	Homozygous	Nimmo *et al.* 2017
S631Y; A724V	Heterozygous	Strauss *et al.* 2015
E476A; P749S	Heterozygous	Dikoglu *et al.* 2015
A670V; I927del	Heterozygous	Dikoglu *et al.* 2015
R672C; R672C	Homozygous	Dikoglu *et al.* 2015
A670V; A670V	Homozygous	Dikoglu *et al.* 2015
W464*; R679H	Heterozygous	Dikoglu *et al.* 2015
P676S; P676S	Homozygous	Shebib *et al.* 1991, Strauss et al. 2015

Figure 6.1 – *LONP1* mutations have been identified throughout the LONP1 protein domains. LONP1 mutations that have been published in the literature are shown here. Each mutation has been mapped (not to scale) to the respective domain in LONP1. Each domain is shown and their locations are taken from Venkatesh *et al.* 2012.

puberty. At my host laboratory, there was one patient that was identified to harbour two potential *LONP1* mutations using WES.

The proband was a male who was born in 2013 to non-consanguineous parents. The patient presented with congenital lactic acidosis, muscle weakness and a brain MRI that showed a Leigh-like syndrome pattern, with bilateral hypertensity that can be seen in cortical areas and the basal ganglia.

Quantitative real-time PCR was used to quantify mtDNA copy number and a severe mtDNA depletion was discovered, with the proband harbouring <10% mtDNA versus age-matched controls (Professor Robert Taylor, personal communication). Thus, the patient's DNA was sequenced using a targeted screen of genes that when mutated are known to be causative of mtDNA depletion. These genes were *SLC25A4, MPV17, SUCLG1, SUCLA2, TK2 and RRM2B* (Table 6.1), but no mutation was discovered in the patient.

Table 6.1: Known genes that are associated with depletion of mtDNA copy number when mutated.

GENE	PROTEIN	DISEASE	REFERENCES
SLC25A4	ANT1, adenine nucleotide transporter 1	Adult-onset PEO[a] childhood-onset mitochondrial myopathy and cardiomyopathy	Napoli *et al.* 2001 Komaki *et al.* 2002 Siciliano *et al.* 2003 Deschauer *et al.* 2005 Thompson *et al.* 2016
MPV17	MPV17, mitochondrial inner membrane protein	Neuropathy and leukoencephalopathy; Hepatocerebral mitochondrial DNA depletion syndrome	Blakely *et al.* 2012 Spinazzola *et al.* 2006 Wong *et al.* 2007 El-Hattab *et al.* 2010
SUCLG1	SUCLG1, succinate-coA ligase α sununit	Fatal infantile lactic acidosis with mitochondrial DNA depletion	Ostergaard *et al.* 2007 Rivera *et al.* 2010 Rouzier *et al.* 2010
SUCLA2	SUCLA2, succinate-coA ligase β subunit	Encephalopathy with elevated methylmalonic acid and mtDNA depletion; Mild methylmalonic aciduria, Leigh-like encephalomyopathy, dystonia and deafness	Elpeleg *et al.* 2005 Lamperti *et al.* 2012 Ostergaard *et al.* 2007 Carrozzo *et al.* 2007
TK2	TK2, Thymidine kinase 2	Fatal mitochondrial DNA depletion myopathy;	Mancuso *et al.* 2002 Mancuso *et al.* 2003 Wang *et al.* 2005 Blakely *et al.* 2008
RRM2B	P53R2, p53-controlled ribonucleotide reductase	Mitochondrial DNA depletion syndrome; adult-onset PEO[a]	Bourdon *et al.* 2007 Bornstein *et al.* 2008 Acham-Roschitz *et al.* 2009 Tyynismaa *et al.* 2009

[a]PEO = progressive external ophthalmoplegia.

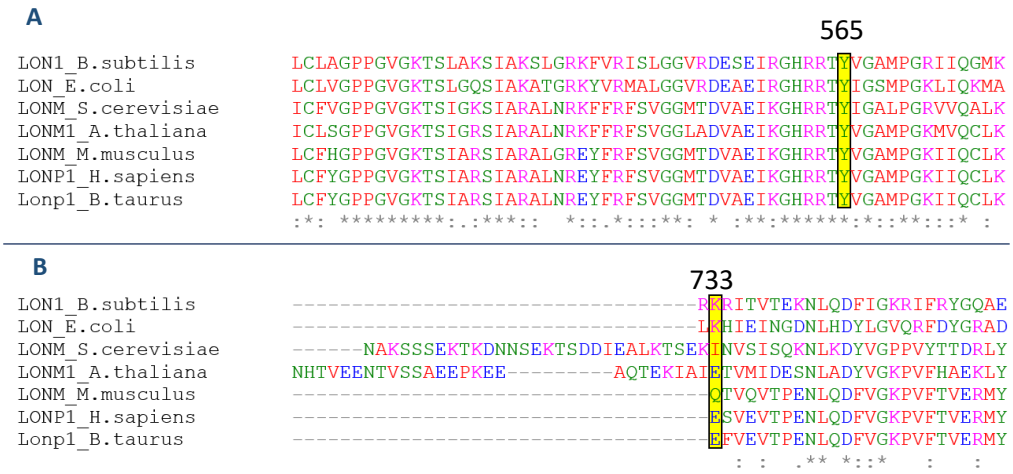

Figure 6.2 – *LONP1* variants in the proband are not both conserved across all species. Protein sequences for *B. subtilis* LON1 (P37945), *E. coli* Lon (P0A9M0), *S. cerevisiae* LonM (PIM1, P36775), *A. thaliana* LONM1 (P93655), *M. musculus* LONM (Q8CGK3), *H. sapiens* LONP1 (P36776) and *B. taurus* Lonp1 (Q59HJ6) were aligned using Clustal omega (http://www.ebi.ac.uk/Tools/msa/clustalo/). A = Tyr565His is highlighted in a yellow box. B = Glu733Lys is highlighted in a yellow box. Black asterisk = fully conserved residue, colon (:) = residues with strongly similar properties, period (.) = residues with weakly similar properties.

Since a mutation was not identified, the proband's DNA was analysed by WES. WES filtering identified two compound heterozygous missense variants in *LONP1* gene, encoding Lon peptidase 1 (LONP1), a mitochondrial matrix protease. The identified mutations were c.1693T>C (p.Tyr565His) (rs144125085) and c.2197G>A (p.Glu733Lys). The p.Tyr565 residue is located within a highly conserved region of the ATPase domain (Figure 6.2), and is itself highly conserved. Polyphen-2 also predicted that this mutation would be probably damaging (Table 6.2). On the contrary, the p.Glu733 residue is not highly conserved, is only located within a moderately-conserved region (Figure 6.2) and polyphen-2 predicted the mutation to be benign (Table 6.2).

Table 6.2: Variants identified in *LONP1* in the proband using WES.

VARIANT	ANNOTATION	POPULATION	ALLELE COUNT	ALLELE NUMBER	MAF	POLYPHEN-2 (HumVar)
c.1693T>C, p.Tyr565His (rs144125085)	Missense	European (non-Finnish)	1	118492	0.000008439	0.983 (probably damaging)
c.2197G>A, p.Glu733Lys	Missense	European (non-Finnish); South Asian	2	119658	0.00001671	0.006 (benign)

The ExAC (Exome Aggregation Consortium) browser (www.exac.broadinstitute.org) was used to determine the minor allele frequency (MAF) for both variants. Both variants were heterozygous. For

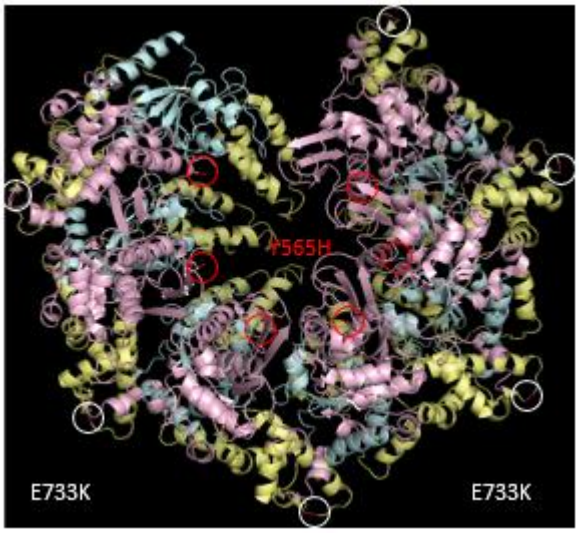

Figure 6.3 – The p.Tyr565His mutation affects an important residue in LONP1. The p.Tyr565His (Y565H, red) and p.Glu733Lys (E733K,white) mutations are shown on the hexameric structure of LONP1 from *Bacillus subtilis*. Structure file 3M6A was imported into PyMol and coloured. Mutations are highlighted. Blue = ATPase domain, yellow = P domain.

p.Tyr565His, rs144125085 is the SNP identifier number. PolyPhen-2 (Adzhubei *et al.* 2010; http://genetics.bwh.harvard.edu/pph2/) was used to determine the pathogenicity of each variant.

These two mutations are located within the ATPase domain (p.Tyr565His) and the proteolytic domain (p.Glu733Lys) of LONP1 respectively. When modelled onto the hexameric structure of LONP1 from *B. subtilis*, which has a high level of homology with the *H. sapiens* ATPase and proteolytic domains, the p.Tyr565 residue was suggested to be located on the innermost ring of the LONP1 hexamer (Figure 6.3) and since this area is highly conserved, the mutation in this residue could affect an important function. The p.Glu733 residue was located on the outermost ring of LONP1 (Figure 6.3) and although the mutation in this residue was not deemed pathogenic, it may still play a role in the function of LONP1.

6.2.2 Determining the inheritance of the LONP1 mutations

Unfortunately, it was not possible to obtain parental DNA samples from the LONP1 patient to determine the inheritance patterns of these two mutations directly. As an alternative, the LONP1 alleles from the patient were cloned and sequenced individually as one fragment to determine if the mutations were on the same, or different, alleles. RNA was extracted from primary fibroblasts and reverse transcribed to cDNA in order to remove the introns from the amplified fragments and ensuring that both mutation sites were located on the same fragment. Using this cDNA, primers targeting exons 10 and 15 (Appendix C), which spanned the region where the two mutations were located, were used to generate PCR products. The fragments together with the pcDNA5/FRT/TO™ vector were digested and ligated together.

The ligation mixture was transformed into α-Select *E. coli* cells and colonies were checked for the presence of a plasmid containing an insert using a cracking gel. The plasmid was extracted and subsequently digested to confirm the presence of the LONP1 fragment. Positive clones were analysed by Sanger sequencing using CMV forward and BGH reverse primers, whose sequences are located 5' and 3' of the multiple cloning site of pcDNA5/FRT/TO™ respectively. Sanger sequencing revealed that only one mutation was present on each allele (Figure 6.4, Appendix I), suggesting that the mutations were inherited in an autosomal recessive manner.

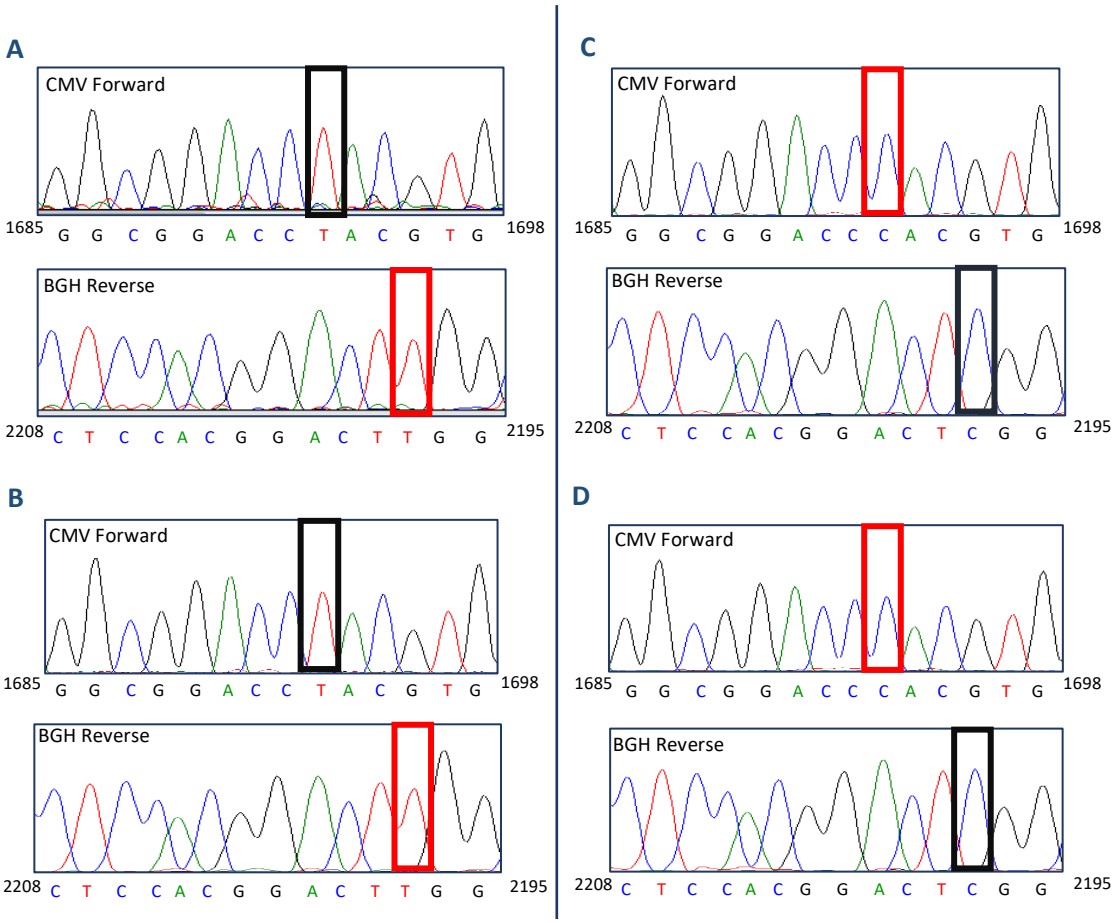

Figure 6.4 – *LONP1* mutations are located on different alleles. Isolated plasmids were amplified using BigDyes™ reagents and analysed by Sanger sequencing. Primers targeting the CMV and BGH sequences located on the pcDNA5/FRT/TO™ plasmid were used for the forward and reverse reactions respectively. A = clone 3. Contains the c.2197G>A mutation only (red box). B = clone 11. Contains the c.2197G>A mutation only (red box). C = clone 7. Contains the c.1693T>C mutation only (red box). D = clone 8. Contains the c.1693T>C mutation only (red box). Black box denotes the wild-type sequence. Not all clones that were sequenced are shown.

6.2.3 *The effects of LONP1 mutations in skeletal muscle and skin fibroblasts*

The proband's primary fibroblast cells and a skeletal muscle biopsy were available for further studies. Immunohistochemistry was performed on skeletal muscle biopsy samples. COX/SDH staining is one of the gold standards in diagnosing mitochondrial disease (Old and Johnson, 1989). The combined staining targets cytochrome *c* oxidase (complex IV, COX) which has key subunits encoded by the mtDNA (Anderson *et al.* 1981), and succinate dehydrogenase (complex II, SDH) which has subunits encoded entirely the nuclear genome. COX/SDH staining on this patient revealed a slight increase in SDH activity (Figure 6.5A) and patchy COX-deficient fibres (Figure 6.5B). A haematoxylin and eosin *stain* revealed areas of degenerated muscle (black arrows, Figure 6.5D) as can be seen by the lighter staining of the muscle fibres and the cluster of purple staining, indicative of the nuclei of invading immune cells. (Ross, 2011).

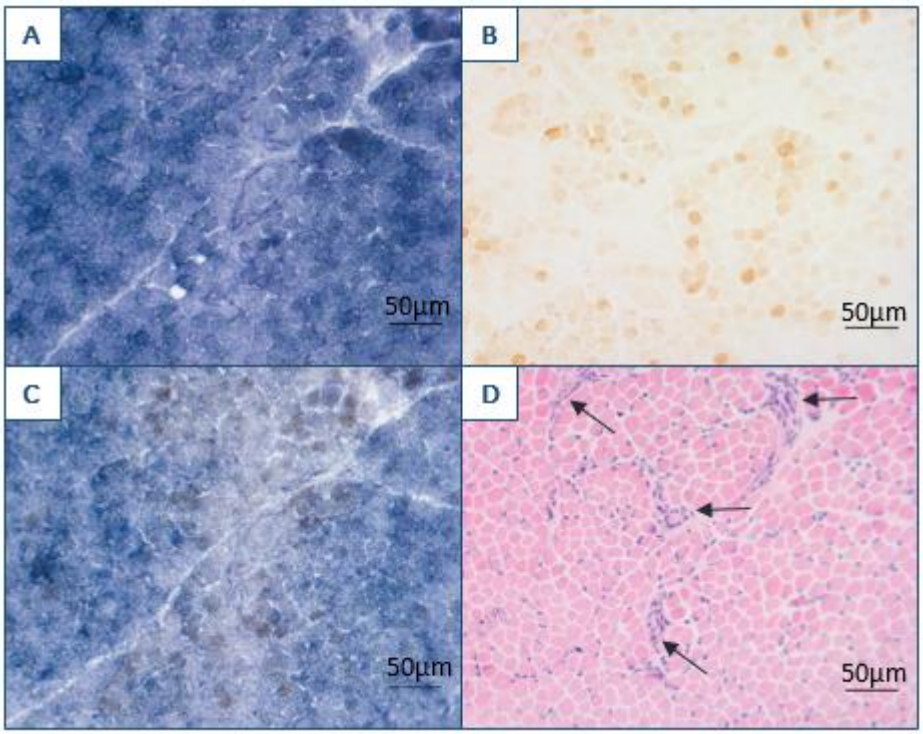

Figure 6.5 – Skeletal muscle of LONP1 patient displays degenerated muscle fibres and a COX deficiency. Immunohistochemistry was performed by Mr Gavin Falkous (NHS Highly Specialised Mitochondrial Diagnostic Service, Newcastle-upon-Tyne) on 10µm transversely orientated serial cryosections of skeletal muscle biopsy samples. A = SDH staining. B = COX staining. C – COX/SDH staining. D = haematoxylin and eosin staining. Black arrows = areas indicative of the inflammasome.

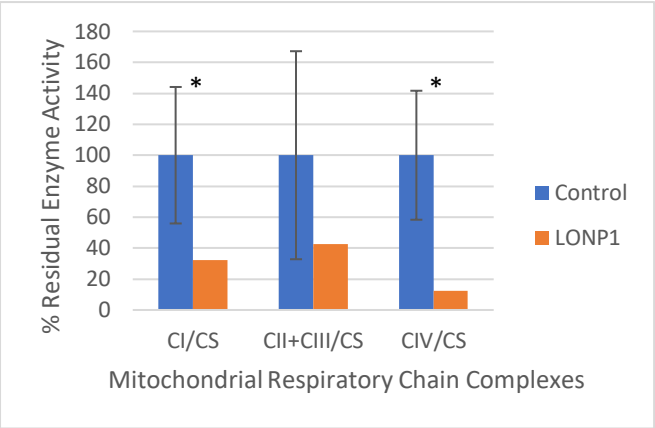

Figure 6.6 – Skeletal muscle in LONP1 patient shows a decrease in the respiratory activities of complexes I and IV. Mitochondrial respiratory chain activities of OXPHOS complexes were measured and normalised to citrate synthase (CS). Complex I, complexes II + III and complex IV were analysed. This was performed by Dr Iain Hargreaves (The National Hospital for Neurology and Neurosurgery, University College London Hospitals NHS Foundation Trust, London). Significant differences ($p<0.05$) are marked with a black asterisk in CI/CS and CIV/CS.

Biochemical assays of mitochondrial respiratory chain activities of complexes I, II, III and IV (Kirby *et al.* 2007) were performed using muscle homogenates by Dr Langping He (NHS Mitochondrial Diagnostic Laboratory, Newcastle-upon-Tyne). These studies revealed severe deficiencies in the activities of complex I and complex IV (Figure 6.6). Further confirmation of the complex I and complex IV defects were seen using the quadruple immunofluorescence assay (Rocha *et al.* 2015), performed by Miss Sila Hopton (NHS Mitochondrial Diagnostic Laboratory, Newcastle-upon-Tyne). The quadruple immunofluorescence assay utilises

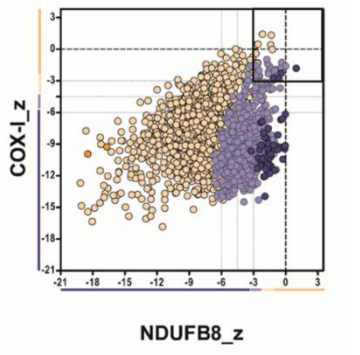

Figure 6.7 – Complexes I and IV are severely depleted in skeletal muscle sections. MRC (mitochondrial respiratory chain) profile produced from data generated using quadruple immunofluorescence assay that was performed on skeletal muscle sections. Each dot represents an individual muscle fibre and coded according to the mitochondrial mass (very low = dark purple, low – light purple, normal – yellow, high = orange). Images were used in conjunction with IMARIS software to determine the levels of COXI and NDUFB8 in individual fibres.

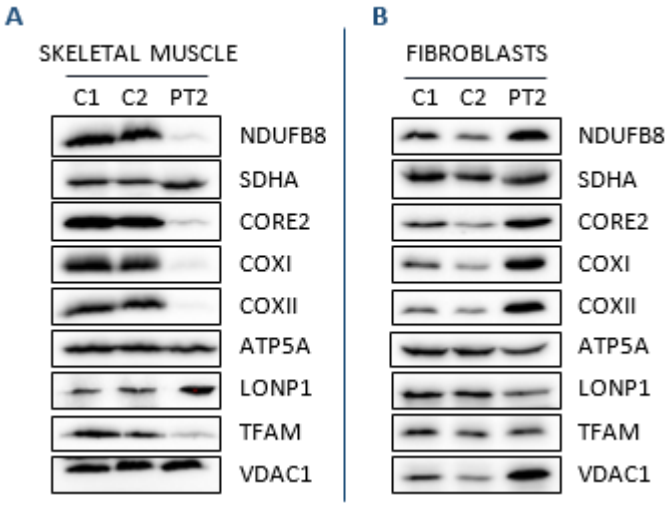

Figure 6.8 – Effects of *LONP1* mutations on OXPHOS complexes in tissue and cell lines. A = skeletal muscle lysates (30µg) from control 1 (C1, M0466-16), control 2 (C2, M0861-16) and patient 2 (PT2, M0840-13) were subjected to western blotting on a 12% polyacrylamide gel. B = Primary skin fibroblasts (70µg) from control 1 (C1, M1123-12), control 2 (C2, M1171-13) and patient 2 (PT2, M0938-13) were subjected to western blotting on a 12% polyacrylamide gel. Membranes were immunoblotted with antibodies targeting LONP1, TFAM and subunits of the OXPHOS complexes: NDUFB (complex I), SDHA (complex II), CORE2 (complex III), COX I and COXII (complex IV) and ATP5A (complex V, F_1). VDAC1 was used as a loading control.

fluorescent antibodies targeting complex I (NDUFB8), complex IV (COX-I), porin (mitochondrial mass marker) and laminin (cell membrane marker) on the same 20µm section. The patient's skeletal muscle tissue biopsy revealed a severe complex I and complex IV defect when analysed (Figure 6.7).

For this proband, skeletal muscle tissue and a primary skin fibroblast cell line were available for further analysis. When analysed by western blot, the skeletal muscle of the proband showed a severe defect in the steady state levels of subunits comprising complexes I, III and IV when compared to age-matched controls (Figure 6.8). The skin fibroblasts however showed no defects by western blot (Figure 6.8B) but skin fibroblasts do not always show mitochondrial disease phenotypes due to tissue-specific effects (Antonicka *et al.* 2006, Zhang and Falk, 2014). Interestingly, in skeletal muscle the steady state levels of LONP1 were slightly increased but the steady state levels of TFAM, a known substrate of LONP1 that is involved in transcription, mtDNA stability and mtDNA replication (1.2.2), were decreased. The reduced steady state levels of TFAM could reflect the reduction in mtDNA copy number that was originally seen using quantitative real-time PCR. Overall, the data suggests that LONP1 protein

is stable, but that there may be a defect in function that is related to mtDNA copy number, possibly through TFAM.

6.3 Discussion

For CODAS syndrome, there has yet to be a clear genotype-phenotype correlation identified from the published cases (Dikoglu *et al.* 2015). Although the patient described in this chapter has mutations in *LONP1*, the clinical phenotype is not characteristic of CODAS syndrome. However, the literature shows variability in patients described as having CODAS syndrome, particularly with differences in the presence of skeletal-ocular form and developmental delay (Dikoglu *et al.* 2015). The patient presented in this chapter may therefore have atypical CODAS syndrome, or another condition not previously associated with mutations in *LONP1.* Indeed, the clinical presentation reflected a more classical mitochondrial disease phenotype, with lactic acidosis, muscle weakness and a Leigh-like MRI.

Two novel mutations were identified in the *LONP1* gene, localising to the ATPase and proteolytic domains respectively. From cloning the individual alleles and analysing them by Sanger sequencing, it appears that these compound heterozygous missense mutations identified in the proband were inherited in an autosomal recessive manner since individual alleles only contained one of the two mutations. However, without the parental samples this cannot be confirmed. The p.Tyr565His mutation localises to the innermost circle of the hexameric LONP1 on the ATPase domain and predictions by PolyPhen-2 suggest that this mutation is pathogenic. Other *LONP1* mutations that have been identified in the ATPase domain have not localised to this specific region, but rather to the C-terminal end of the ATPase domain (amino acids 630-660), or the region between the ATPase and proteolytic domains (amino acids 660-750, Figure 6.1). The p.Glu733Lys mutation localises to the outermost ring of the LONP1 hexamer in the proteolytic domain and although polyphen-2 identified the mutation as benign, the mutation may still be pathogenic.

In the skeletal muscle of this patient, steady state levels of LONP1 slightly increased and steady state levels of TFAM have reduced dramatically. The mutations may therefore result in an increase in the proteolytic activity of LONP1, which could increase the rate of TFAM degradation, causing the reduction of mtDNA copy number since there would be less TFAM to coat the mtDNA molecules. This data suggests that LONP1 is involved in regulating the levels of TFAM and therefore mtDNA, albeit indirectly.

There are a few examples of functional work on specific LONP1 mutations or samples from patients with CODAS syndrome in the literature. In one study, Dikoglu *et al.* reported mutations in *LONP1* from seven patients, each with CODAS syndrome. Dikoglu *et al.* had modelled these mutations onto a structure of *B. subtilis* LonA, which as a high degree of homology with the human LONP1 protein, and had observed that the mutations in *LONP1* clustered around the ATP-binding and proteolytic domains of the enzyme. In a second study, Strauss *et al.* produced EBV-immortalised B-lymphoblast cell lines from the peripheral blood of a proband with CODAS syndrome harbouring homozygous p.Arg721Gly;p.Arg721Gly mutations (Strauss *et al.* 2015). However, it should be noted that CODAS syndrome does not typically affect B-lymphoblast cells (Strauss *et al.* 2015). Steady state levels of LONP1 and TFAM were unchanged in this cell line, and mtDNA copy number was reduced. In addition, this study had claimed that COXII was aggregated and insoluble in this CODAS cell line. Previous studies in both yeast and mammalian cells had suggested that LONP1 was involved in the assembly of complex IV by its additional function as a chaperone for COXII (Hori *et al.* 2002, Rep *et al.* 1996). Strauss *et al.* suggested that the failure of the mutated LONP1 to degrade or chaperone COXII may be the cause of the reduced spare respiratory capacity that was observed in these cells.

Using muscle histochemistry, quadruple immunofluorescence assay and western blots, the LONP1 patient presented in this chapter highlighted a deficiency in complexes I, III and IV. Steady state levels of LONP1 were unchanged, as was seen in the CODAS cell line by Strauss *et al.*, but unlike the CODAS cell line steady state levels of TFAM were greatly reduced. The p.Tyr565His or the p.Glu722Lys mutant forms may therefore play a key function in the structure of LONP1 that affects its proteolytic activity. The severe deficiencies in complexes I, III and IV that were indicated by quadruple immunofluorescence assay, western blot and respiratory chain activity could be a consequence of the reduction in mtDNA copy number, as previously discussed. However, it is more likely that since LONP1 is known to have a number of substrates, some of which may not yet have been identified, and potentially a number of functions besides proteolysis including as a COXII chaperone, a mutation in LONP1 could have an effect on a number of mitochondrial and cellular processes. In order to investigate the consequences of these mutations further, recombinant wild-type and mutated LONP1 proteins were produced *in vitro* and will be subjected to further analysis and investigation.

CHAPTER 7: CHARACTERISING LONP1, A MATRIX PROTEASE

7.1 Introduction

As mentioned previously (Chapter 1), LONP1 is a mitochondrial matrix protease that is thought to be active as a hexamer, and has been reported to be involved in the degradation of various substrates including aconitase, TFAM and StAR. In the previous chapter, the skeletal muscle of the proband showed a decrease in the steady state levels of TFAM but not in the steady state levels of LONP1.

TFAM is a high-mobility group-box (HMGB) protein, a subclass of HMG proteins which are known to be DNA-binding proteins and are typically highly abundant (Goodwin *et al.* 1973). TFAM is most often associated with its role in mitochondrial transcription, by initially binding upstream promoter sequences and recruiting POLRMT to the promoter sites on mtDNA (1.2.2). When TFAM binds to these promoter sequences, it introduces a 180° kink at the promoter region to provide access for POLRMT to bind (Ngo *et al.* 2011). Within mitochondrial nucleoids, where TFAM is highly abundant (Bogenhagen *et al.* 2008, Garrido *et al.* 2003), TFAM packages the mtDNA, binding along the molecule and bending the DNA (Kukat *et al.* 2015, Figure 7.1) with one mtDNA molecule per nucleoid. With regards to LONP1, it has been postulated that LONP1 degrades TFAM when it is phosphorylated and not bound to DNA.

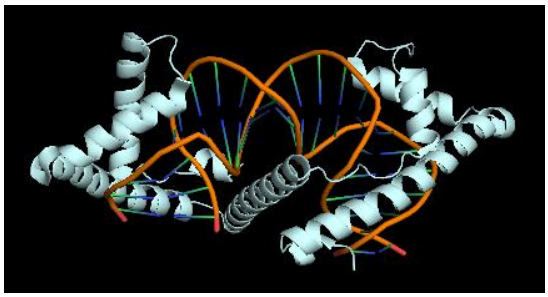

Figure 7.1 – TFAM introduces a 180° turn in mtDNA. Structure of TFAM (light blue) bound to the LSP of mtDNA (orange). PDB structure 3TQ6 was imported into PyMOL and coloured as appropriate.

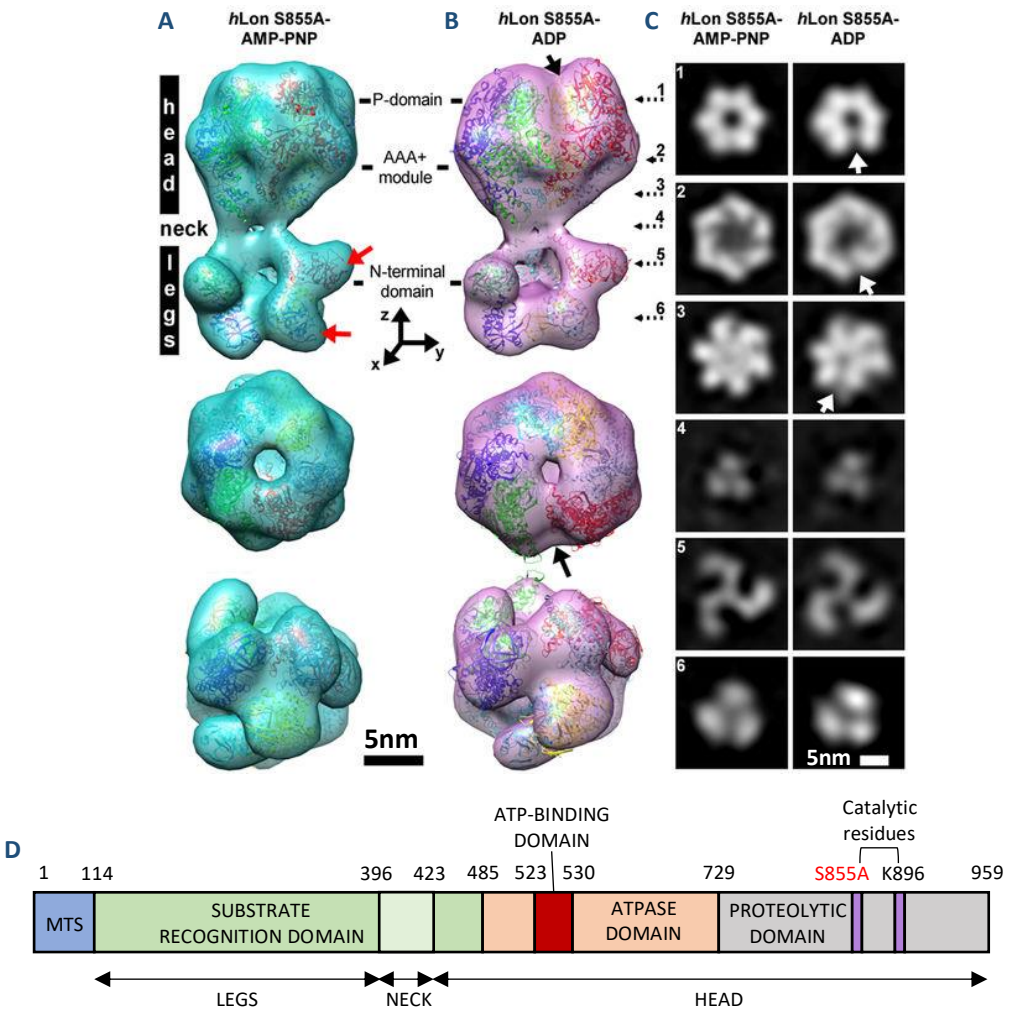

Figure 7.2 – Cryo-EM structures of proteolytically inactive human mutant LONP1. Figure adapted from Kereïche *et al.* 2016. Human LONP1 harbouring a Ser855Ala mutation to deem the protein catalytically inactive was used. Surface representation of the reconstructed cryo-EM structure of a human LONP1-Ser855Ala with non-hydrolysable ATP, AMP-PNP to 15Å (A) and hydrolysed ATP, ADP, to 21Å (B). Proteolytic and ATPase domains were fitted as shown in *B. subtilis* structures (PDB = 3M6A), N-terminal domains were fitted as with residues 1-219 of *E. coli* N-terminal domain (PDB = 3JLC). Black arrow/white arrow = opening for substrate, C = Cross-sections of the reconstructed structures. Dashed arrows represent the section as shown in (B). D = Location of the legs, neck and head of the human LONP1-S855A structure as well as the mutated catalytic residue (red).

In *Drosophila melanogaster,* Lon overexpression results in a reduction in the steady state levels of TFAM as well as a reduction in copy number, whereas a reduction in Lon by RNAi results in an increase in the steady state levels of TFAM (Matsushima *et al.* 2010). Additionally, studies have indicated that LONP1 may be a DNA-binding protein (Lu *et al.* 2007, Chen *et al.* 2008) and one study suggested that LONP1 may bind to the antisense strands of the HSP and LSP, located on mtDNA in the D-loop (Fu *et al.* 1998). These data suggest that

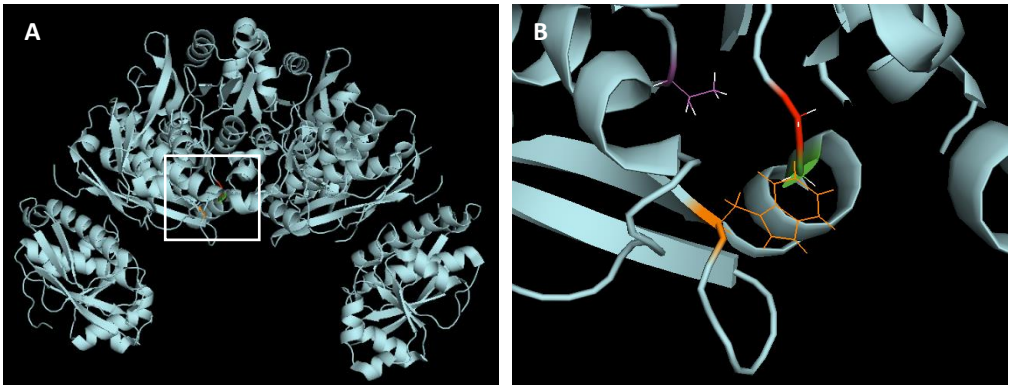

Figure 7.3 – Structure of the human LONP1 proteolytic domain. A = Structure of the human LONP1 proteolytic domain, as published by García-Navría *et al.* 2010 (PDB structure 2X36). Visualised using PyMOL. White square = area of the glycine loop. B = The glycine loop, highlighting residues that were mutated by Ambro *et al.* 2014. Mutations are Gly893 (red), Gly894 (green), Trp770 (orange) and Thr880 (purple).

LONP1 may play a role in mitochondrial gene expression other than in the regulating levels of TFAM.

Mechanistic studies have been performed only using purified wild-type and mutated bacterial and human LONP1 in order to try and understand further how LONP1 functions. Patterson-Ward *et al.* generated two proteolytically-inactive *E. coli* Lon protease proteins, mutating the serine residue of the catalytic dyad to either alanine or tryptophan (S679A, S679W) (Patterson-Ward *et al.* 2007). In both mutants, they demonstrated that Lon protease binds to the peptide substrate in a two-step process i.e. a rapid initial peptide binding event, followed by a conformational change. The S679W mutation, due to the indole side chain of tryptophan, demonstrated a conformational change within the proteolytic site itself. These data supported a mechanism by which ATP first binds to the allosteric site of Lon protease, and energy derived from ATP hydrolysis is used to induce a conformational change that allows the substrate to reach the proteolytic site. A similar study was also performed using the human LONP1 protein, in which the serine residue of the catalytic dyad was also mutated to alanine to make the protein catalytically inactive (S855A, Kereïche *et al.* 2016, Figure 7.1). Similar to the *E. coli* Lon protease, when ATP is hydrolysed to ADP there is a conformational change in the N-terminal domain which allows access to the proteolytic domain (Figure 7.2).

Further work was performed by Ambro *et al.* in which they focussed on a particular loop that is found in the proteolytic domain and is in close proximity to the active site (Figure 7.3A,

Ambro *et al.* 2014). By mutating residues on and interacting with this loop (Figure 7.3B), they discovered that this loop was also involved in a conformational change upon substrate binding. They also demonstrated that this loop only undergoes a conformational change when cleaving large peptides e.g. β-casein, but does not move when cleaving small, fluorogenic peptides, highlighting a structural flexibility for LONP1 when cleaving differently-sized substrates.

Very few functional studies have been performed using patient mutations that have been identified in LONP1. Most reports regarding *LONP1* mutations have focussed on the clinical phenotypes of the patients and the identification of the mutations via sequencing methodologies. Strauss *et al.* had performed protease assays using purified recombinant human LONP1 with p.Pro676Ser, p.Arg721Gly, p.Ser631Tyr or p.Ala724Val mutations, all of which were found in patients with CODAS syndrome. Using fluorogenic S3, a decapeptide reporter substrate that can be cleaved by LONP1, all four mutants demonstrated reduced peptidase activity when compared to wild-type recombinant human LONP1. In addition, recombinant LONP1 harbouring the p.Pro676Ser and p.Arg721Gly mutations were able to degrade steroidogenic acute regulatory protein (StAR), but were not able to degrade TFAM. Using Epstein-Barr virus-transformed B-lymphoblastoid cell lines generated from p.Arg721Gly homozygous CODAS patient cell lines, Strauss *et al.* confirmed that the cells showed abnormal mitochondrial ultrastructure that included swollen intercristal spaces and vesiculated cristae (Strauss *et al.* 2015). Lysates from these cells, when analysed by western blotting, were shown to have decreased steady state levels of COXII, but normal steady state levels of other subunits from all OXPHOS complexes.

The LONP1 patient described in the previous chapter (Chapter 6) is unlike the patients presented in Strauss *et al.* not only for the different mutations present, but also the phenotypical presentation. As the WES pipeline identifies putative pathogenic mutations, it was important to confirm pathogenicity. When dealing with putative recessive mutations, the gold standard is to infect defective cell lines with the wild-type copy of the gene that is mutated in the patient and to confirm that the deficiency is rescued. Unfortunately, in this case it was not possible, as the primary fibroblast cell line did not express any defect, a common problem often associated with mitochondrial disease. Therefore, to confirm pathogenicity, it was necessary to examine these LONP1 mutations *in vitro* to determine their

effects on the multimerization and proteolytic activity of the enzyme. Further, these mutations may reveal additional information about the function of LONP1 when analysed.

In this chapter, I investigated the activities of the two LONP1 mutations described in chapter 6 using *in vitro* functional studies.

7.2 Results

7.2.1 *Purification of recombinant LONP1 proteins*

Recombinant wild-type LONP1-His (WT), LONP1-Y565H-His (Y565H) and LONP1-E733K-His (E733K) that lacked the MTS (Δ1-114 amino acids residues, Strauss *et al.* 2015) were cloned into the pET20b+ vectors by Miss Monica Olsson (University of Gothenburg, Sweden) and *E. coli* cells were transformed with these constructs. Cells were induced with IPTG and the recombinant LONP1 proteins produced were purified using nickel affinity resin via the 6 x histidine tags on the C-terminal of the recombinant LONP1 proteins (Figure 7.4). Following elution with imidazole (a histidine analogue), fractions that contained the LONP1 protein (c.100kDa) were pooled together and further purified using heparin columns.

Heparin is a large polyanion that bears similarity to nucleic acid polymers. Herparin columns are therefore traditionally used as a purification step for DNA or RNA binding proteins. The recombinant LONP1 proteins were eluted using increasing concentrations of salt (Figure 7.5, 2.5.14). All three recombinant proteins could be purified in this manner, with the recombinant wild-type and mutant LONP1 proteins predicted to be the same size of 100kDa.

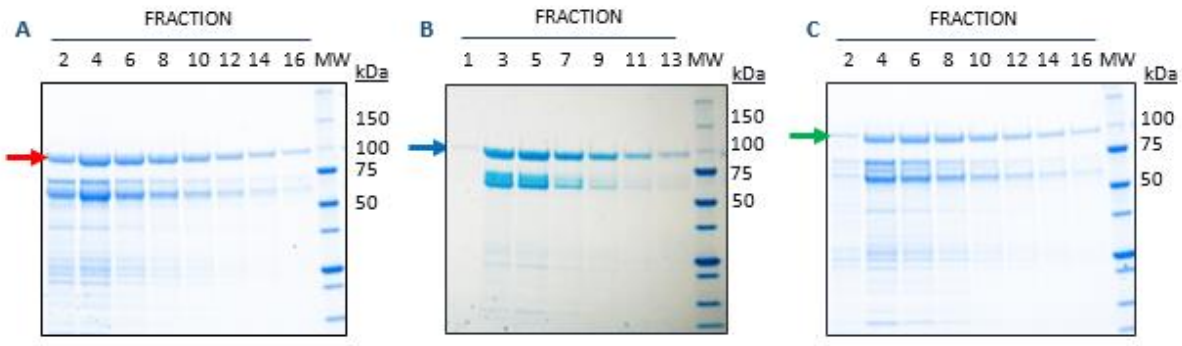

Figure 7.4 – Purifying recombinant LONP1-His proteins using nickel resin. A = wild-type LONP1-His (red arrow). Fractions 2-16 were pooled together. B = LONP1-Y565H-His (blue arrow). Fractions 3-13 were pooled together. C = LONP1-E733K (green arrow). Fractions 4-16 were pooled together.

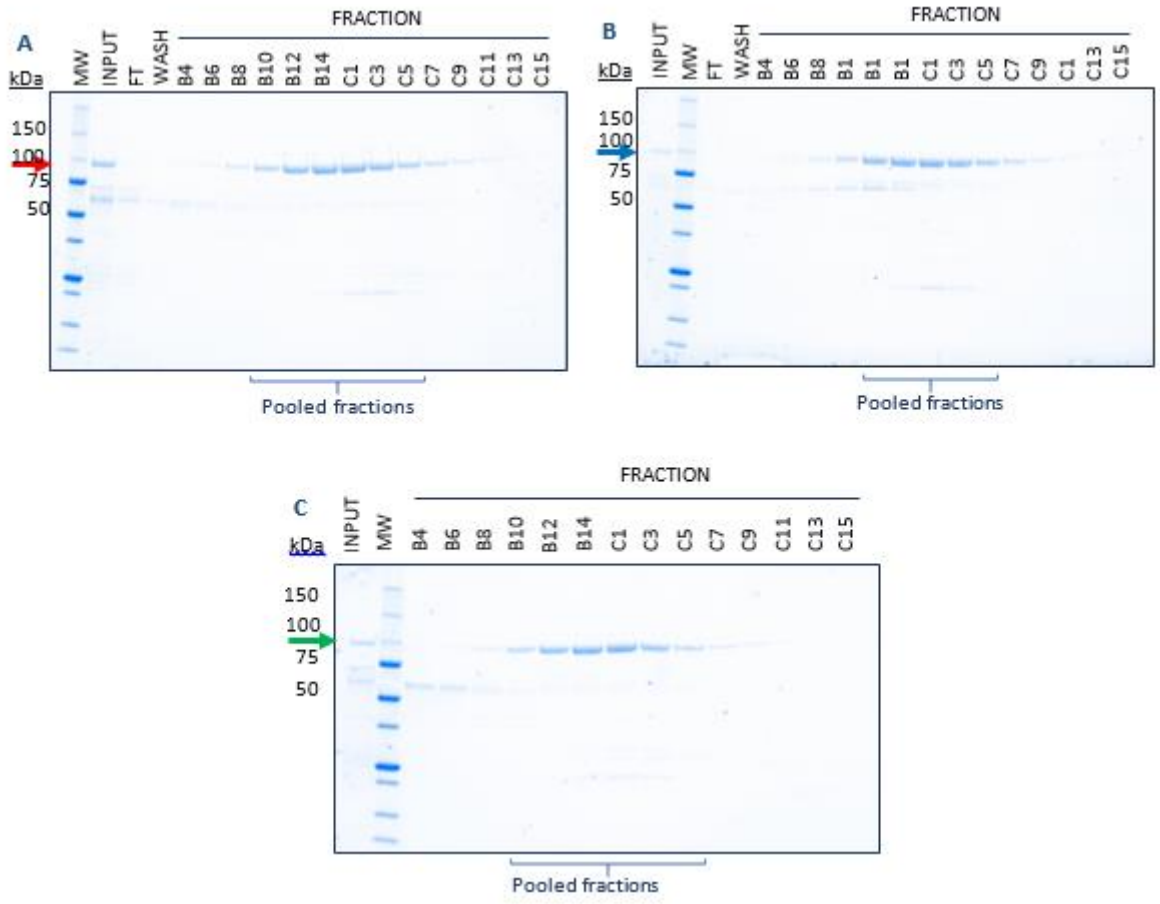

Figure 7.5 – Purifying recombinant LONP1-His proteins using heparin sepharose. A = wild-type LONP1-His (red arrow). Fractions B10-C5 were pooled together. B = LONP1-Y565H-His (blue arrow). Fractions B1-C5 were pooled together. C = LONP1-E733K (green arrow). Fractions B10-C5 were pooled together.

A final purification step was performed using a Q sepharose anionic exchange column to remove any further impurities from the samples (Figure 7.6, 2.5.15). After purification, some minor impurities still remained but the samples were sufficiently pure to perform further investigations using *in vitro* activity assays.

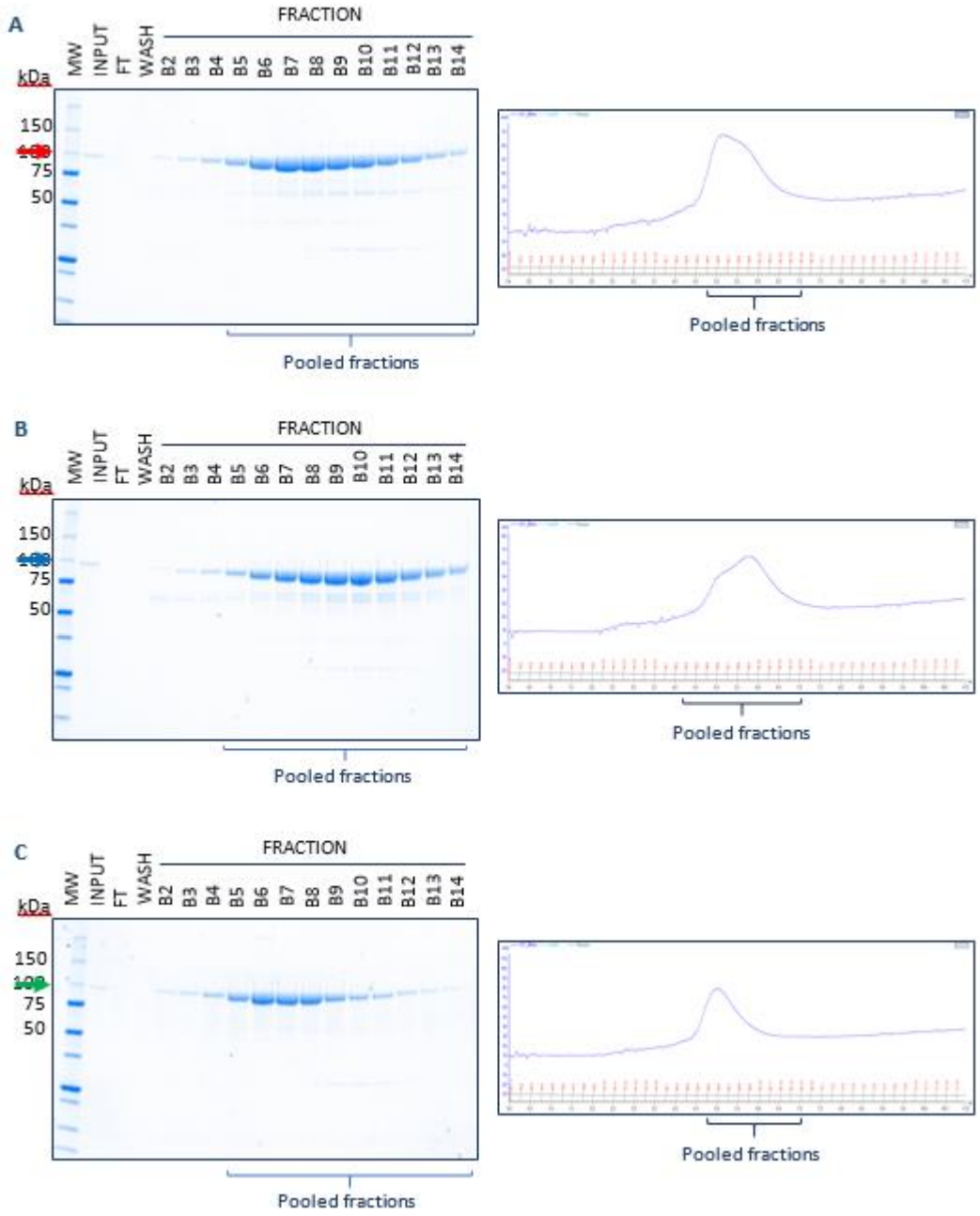

Figure 7.6 – Purifying recombinant LONP1-His proteins using Q sepharose. A = wild-type LONP1-His (red arrow). Fractions B5-B14 were pooled together. B = LONP1-Y565H-His (blue arrow). Fractions B5-B14 were pooled together. C = LONP1-E733K (green arrow). Fractions B5-B14 were pooled together. A trace generated by the Unicorn software indicating the eluted protein by an increase in absorbance units is shown for each sample. FT = flowthrough., MW = molecular weight marker.

7.2.2 *Effects of LONP1 mutations on LONP1 hexamerisation*

Once the LONP1 proteins were purified, each was assessed for their ability to form hexamers. By using a gel filtration column and altering the salt conditions in the buffer, the LONP1 proteins would either favour a multimeric or monomeric confirmation, as determined by comparing to a gel filtration standard. In low salt, all three proteins appeared to adopt the hexameric form (Figure 7.7A). In high salt, most of the recombinant LONP1 proteins dissociated into the monomeric form, although a small fraction of hexamers could still be visualised in each sample (Figure 7.7B). This was confirmed using densitometry analysis

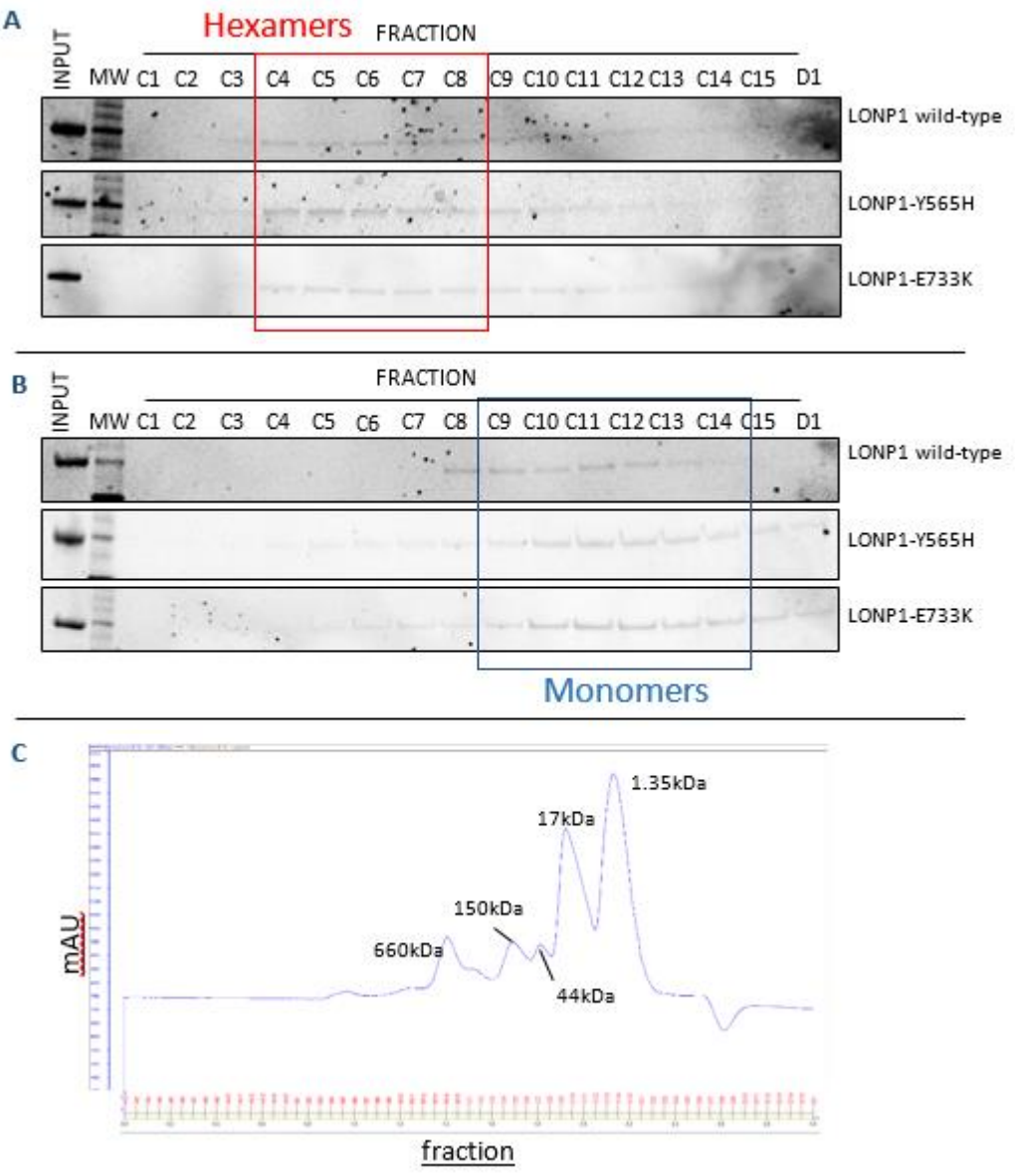

Figure 7.7 – Recombinant LONP1 proteins can be separated out into monomers. Gel size exclusion chromatography was performed with 60µl dialysed, purified LONP1-WT, LONP1-Y565H or LONP1-E733K protein. A = 50mM NaCl + 4mM ATP. B =1M NaCl -ATP. C = a standard curve.

(performed by Dr Bradley Peter, University of Gothenburg, Sweden) in which under high salt conditions, all 3 LONP1 proteins were predominantly monomers (Figure 7.8A). In low salt conditions, however, LONP1-WT and LONP1-E733K predominantly formed hexamers but LONP1-Y565H showed some defects in oligomerisation, as most LONP1-Y565H remained as monomers (Figure 7.8B).

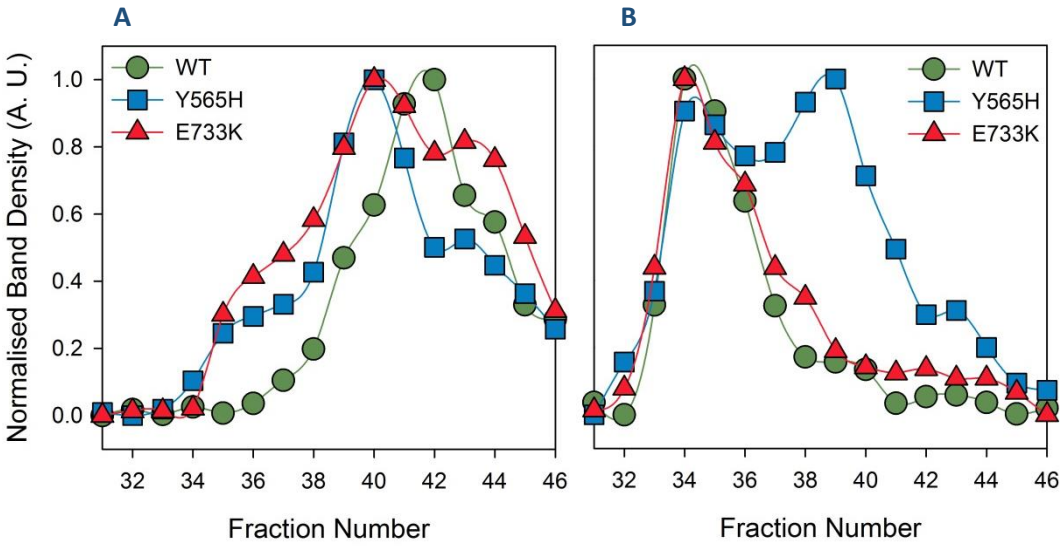

Figure 7.8 – *LONP1* mutation affects the relative stability of LONP1 oligomerisation. Densitometry analysis was performed on LONP1-WT, LONP1-Y565H and LONP1 E733K. A – High salt (1M NaCl) buffer. B – Low salt (50mM NaCl) buffer. LONP1 proteins appear as monomers, and LONP1-Y565H displays monomeric and hexameric species.

7.2.3 *Effects of LONP1 mutations on ATP hydrolysis in vitro*

The mutations that were identified in the patient localised to the ATPase domain (Y565H) and the proteolytic domain (E733K) respectively. To determine the effect of the mutations on the ATP hydrolysis function of LONP1, purified recombinant wild-type and mutant LONP1 proteins were incubated with or without ATP and analysed using the malachite green phosphate assay (2.7.1). This assay measured the levels of phosphate released from the hydrolysis of ATP to ADP and P_i. Both LONP1-Y565H and LONP1-E733K could hydrolyse ATP. LONP1-Y565H appeared to hydrolyse more ATP but this was not statistically significant when

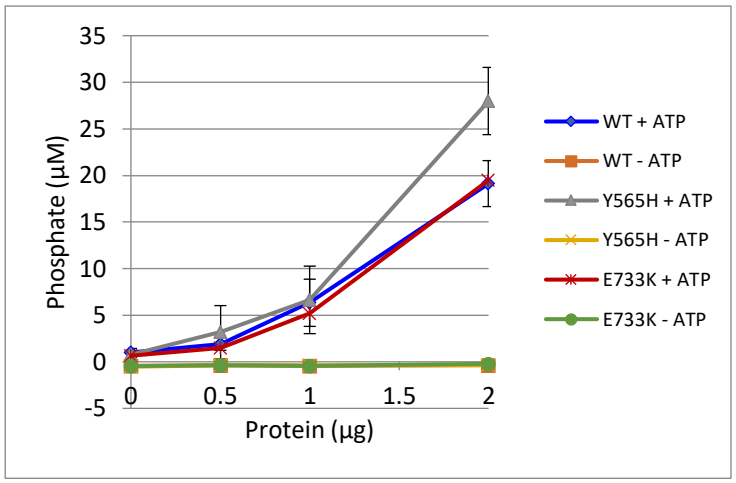

LONP1	pmol/µg/min
WT + ATP	17.8
WT – ATP	0
Y565H + ATP	24.3
Y565H – ATP	0
E733K + ATP	16.5
E733K - ATP	0

Figure 7.9 – Mutant recombinant LONP1 can hydrolyse ATP. Purified LONP1 proteins (0-2µg) were prepared with or without ATP using the Malachite Green Phosphate Assay kit in 100µl reactions. A standard curve of 0-40µM phosphate concentration was also prepared, and the samples were analysed on the Tecan Infinite M200 at 630nm using Magellan 6 software. Standard error bars are from 3 technical repeats. Table represents no. of pmol of ATP hydrolysed per µg of LONP1 per min. Baseline rates were calculated using –ATP reactions respectively.

compared to wild-type (p=0.5872) or LONP1-E733K (p=0.5409) (Figure 7.7) which had comparable rates of ATP hydrolysis (p=0.8699).

A known substrate of LONP1 is TFAM and it has been suggested in *E. coli* Lon protease that the presence of a substrate may increase the rate of ATP hydrolysis compared to ATP alone (Wohlever *et al.* 2014). The malachite green phosphate assay was repeated in the presence and absence of TFAM, in addition to the presence and absence of ATP. Recombinant TFAM-His (cloned into pET3A) was purified by Miss Monica Olsson (University of Gothenburg, Sweden, Shi *et al.* 2012) and stored at -20°C. The rates of ATP hydrolysis were unaffected by the addition of TFAM for each of the recombinant LONP1 proteins (Figure 7.10).

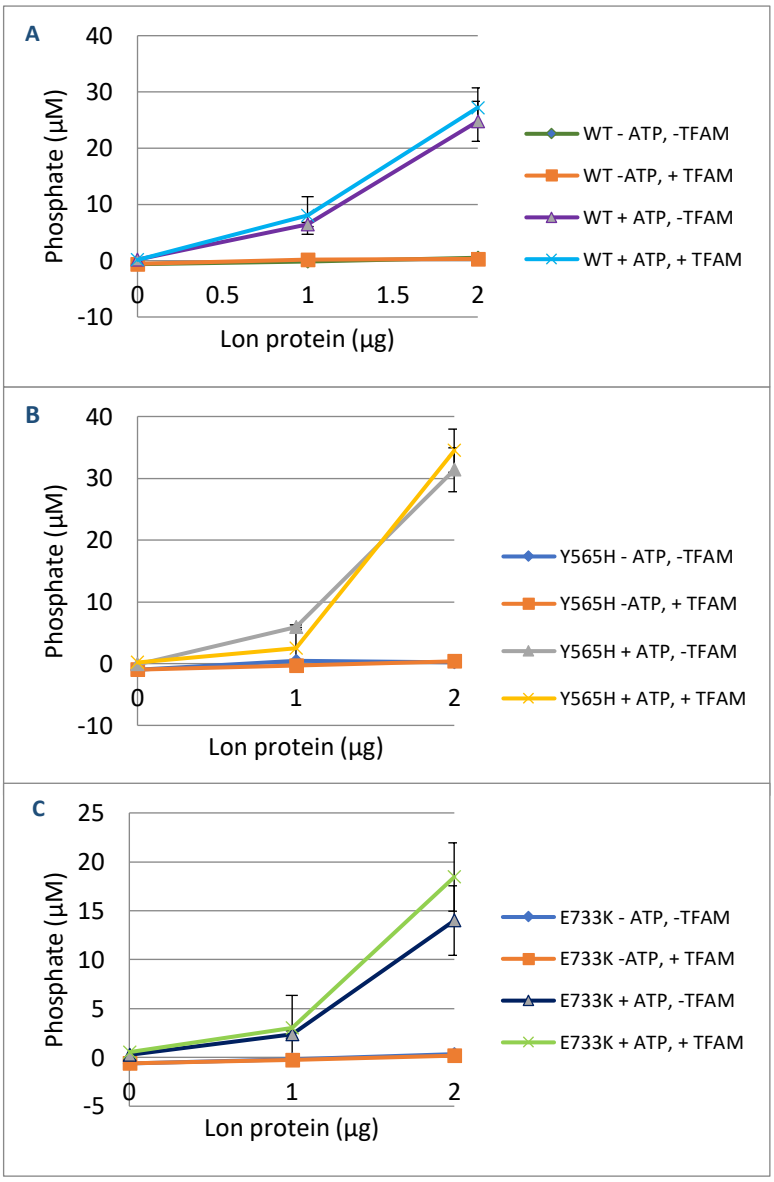

LONP1-WT	pmol/µg/min
+ TFAM + ATP	30.7
– TFAM + ATP	31.0
+ TFAM – ATP	0
– TFAM – ATP	0

LONP1-Y565H	pmol/µg/min
+ TFAM + ATP	32.7
– TFAM + ATP	35.0
+ TFAM – ATP	0
– TFAM – ATP	0

LONP1-E733K	pmol/µg/min
+ TFAM + ATP	16.3
– TFAM + ATP	19.2
+ TFAM – ATP	0
– TFAM – ATP	0

Figure 7.10 – Presence of TFAM does not affect rates of ATP hydrolysis *in vitro*. Purified LONP1 proteins (0-2µg) were prepared with or without ATP, with or without TFAM, using the Malachite Green Phosphate Assay kit in 100µl reactions. A standard curve of 0-40µM phosphate concentration was also prepared, and the samples were analysed on the Tecan Infinite M200 at 630nm using Magellan 6 software. Tables show no. of pmol of ATP hydrolysed per µg of LONP1 per minute. Standard error bars are representative of two repeats. Baseline rates were calculated using +/- TFAM -ATP respectively.

7.2.4 *Mutant recombinant proteins cannot degrade TFAM in vitro*

LONP1-WT, LONP1-Y565H and LONP1-E733K proteins were incubated with TFAM (2.7.2) to determine whether the mutations individually affected the proteolytic function of LONP1. As LONP1 is an ATP-dependent protease, the experiment was performed both with and without 1mM ATP as a control, in the presence and absence of TFAM. A time course was used to track the degradation of TFAM from 0 – 75mins. LONP1-WT and LONP1-E733K degraded TFAM in the presence of ATP, consistent with its role as an ATP-dependent protease, whereas LONP1-Y565H could not degrade TFAM at all, even after 75mins (Figure 7.11).

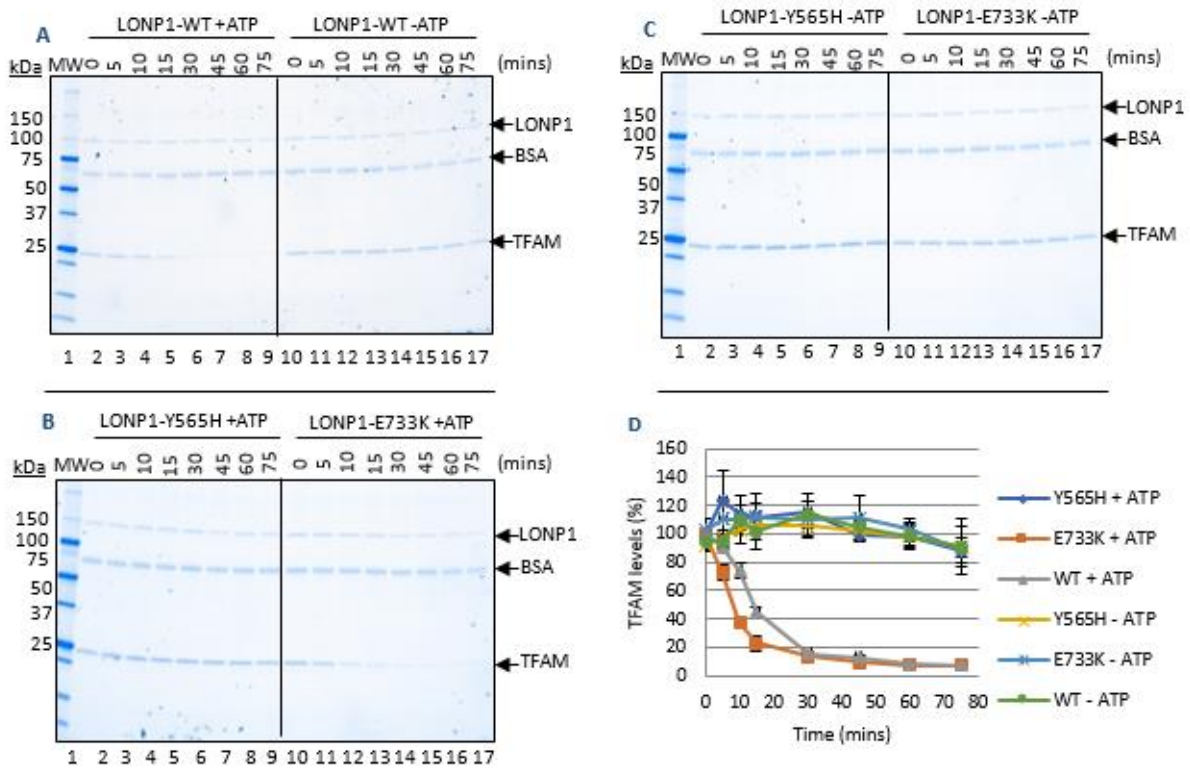

Figure 7.11 – LONP1-Y565H is unable to degrade TFAM *in vitro*. TFAM degradation assay was performed with each protein at the same time. A = LONP1-WT +/- ATP. B = LONP1-Y565H and LONP1-E733K + ATP. C = LONP1-Y565H and LONP1-E733K –ATP. D = Quantification of the levels of TFAM remaining based on the gel images. Band intensities were measured using ImageLab, and were normalized to band intensities at 0mins. Standard error bars are representative of 3 technical repeats.

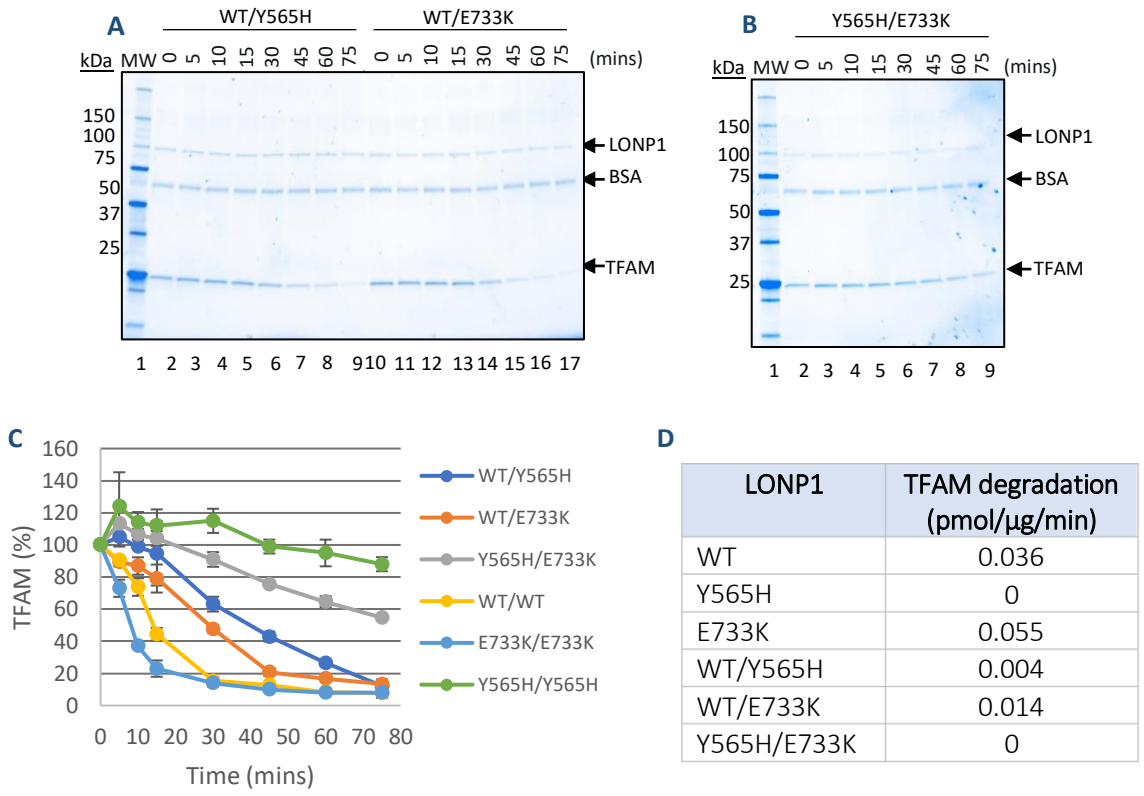

LONP1	TFAM degradation (pmol/µg/min)
WT	0.036
Y565H	0
E733K	0.055
WT/Y565H	0.004
WT/E733K	0.014
Y565H/E733K	0

Figure 7.12 – Mixed mutant recombinant LONP1 hexamers cannot degrade TFAM. TFAM degradation assay was performed with mixed LONP1 hexamers, with ATP. A – LONP1-WT and LONP1-Y565H were mixed. B – LONP1-Y565H and LONP1-E733K were mixed. C – Quantification of the levels of TFAM remaining based on the gel images. Band intensities were measured using ImageLab, and were normalised to band intensities at 0mins. Data from Figure 7.11 is also included, and represents the average of 3 technological repeats. D – The rate of TFAM degraded per 1µg LONP1 protein per minute (initial first order rates were used).

In order to mimic the protein that is seen in the patient, a mixed LONP1 hexamer of both LONP1-E733K and LONP1-Y565H was produced. To facilitate the production of mixed hexamers, the individual homomeric hexamers were broken down to their monomers by increasing NaCl concentrations to 1M, equimolar amounts of the relevant monomers mixed, and then the salt gradually removed by dialysis. The mixed recombinant LONP1 hexamers were then subjected to the protease assay with TFAM as the substrate. When combined with LONP1-WT, either the LONP1-Y565H or LONP1-E733K mixed hexamers could degrade TFAM after 75mins (Figure 7.12A). When the two mutant proteins were mixed, there was a slight degradation of TFAM after 75mins, but the majority remained undegraded (Figure 7.12B). When compared to the homogeneous hexamers, LONP1-Y565H showed the least amount of proteolytic function *in vitro*, followed by LONP1-Y565H/E733K. Interestingly, LONP1-WT/E733K was less effective at degrading TFAM than LONP1-WT, suggesting that LONP1-E733K may be affecting the function of LONP1 albeit slightly.

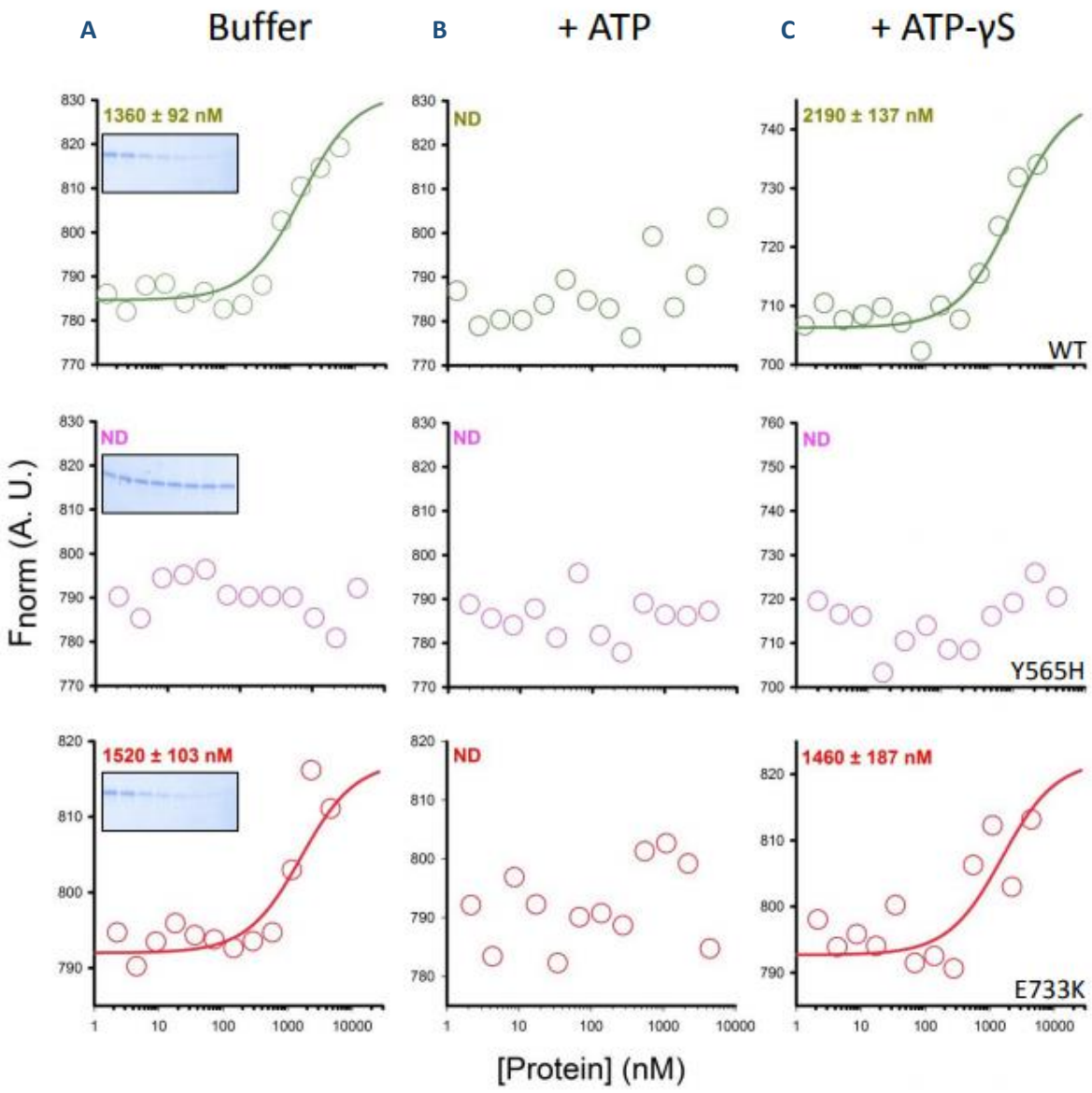

Figure 7.13 – LONP1-Y565H is unable to bind to TFAM. Microscale thermophoresis was kindly performed by Dr Bradley Peter (University of Gothenburg, Sweden). LONP1-WT, LONP1-Y565H and LONP1-E733K were analysed in the presence of TFAM in buffer alone (A), with added ATP (B) and with added ATP-γS (C).

These experiments determined that TFAM can be degraded *in vitro*, but not whether the recombinant LONP1 proteins bound to TFAM. Microscale thermophoresis utilises fluorescently-labelled TFAM to analyse protein interactions. A temperature gradient is used and the strength of the interaction between the LONP1 proteins and TFAM can be determined by analysing the changes in thermophoretic movement of unbound TFAM compared to bound TFAM along a capillary. As shown in Figure 7.13, in buffer alone without ATP, both LONP1-WT (KD = 1.4µM) and LONP1-E733K (KD = 1.5µM) were able to bind TFAM with similar affinities

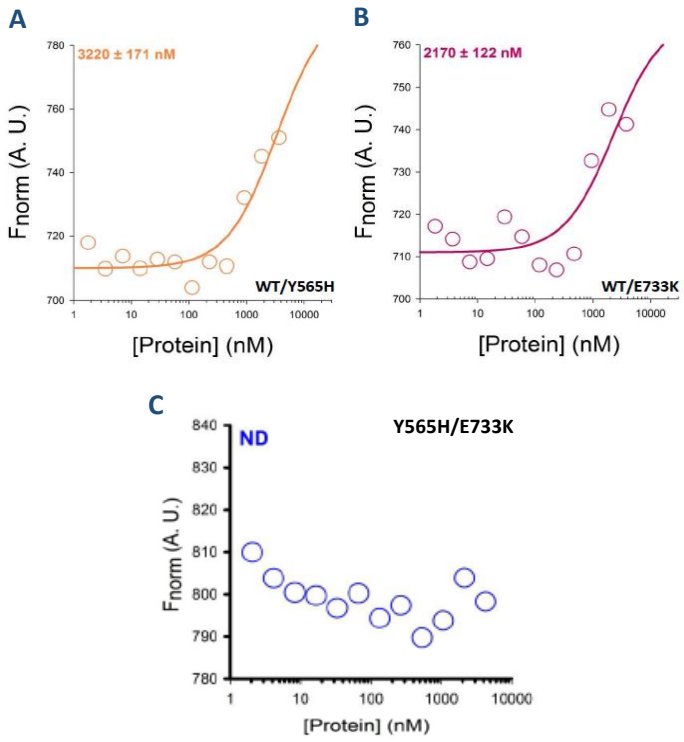

Figure 7.14 – Mixed mutant recombinant LONP1 hexamers are unable to bind TFAM. Microscale thermophoresis was kindly performed by Dr Bradley Peter (University of Gothenburg, Sweden). Mixed LONP1 hexamers were incubated with ATP-γS. A – LONP1-WT/Y565H. B – LONP1-WT/E733K. C – LONP1-Y565H/E733K.

whereas no binding was detectable for LONP1-Y565H, indicated by the lack of consistent change in absorbance units as the concentration of TFAM was increased (Figure 7.13A). When MST was performed with ATP, there was no TFAM bound to any of the LONP1 proteins, because TFAM was degraded in the presence of ATP in both the LONP1-WT and LONP1-E733K samples and LONP1-Y565H could not bind TFAM (Figure 7.13B). In the presence of a non-hydrolysable analog of ATP, ATP-γS, TFAM still bound with similar affinities to LONP1-WT and LONP1-E733K, but no binding was measurable for LONP1-Y565H (Figure 7.13C). In order to mimic the LONP1 proteins present in the parental samples, heterogeneous hexamers were used. Mixing of LONP1-Y565H and LONP1-WT resulted in a weaker binding affinity for TFAM (Figure 7.14). I did not determine the population spread of the various permutations for the mixed hexamer, and it could even have been possible that no mixed hexamers were formed, with all hexamers being essentially monomers. However, irrespective this situation would model the LONP1 in the matrix of one of the unaffected parents of the patient. The second parent would have a mix of LONP1-WT and LONP1-E733K, which resulted in a similar affinity

to either homohexamer (KD = 2.2μM). Intriguingly, binding of TFAM to the equimolar mixture of the two mutant forms of LONP1 was undetectable. This result is consistent with the recessive but profound clinical presentation of the child who expressed the two mutant alleles. Together, they were unable to bind the substrate, consistent with the very low protease activity measured in the mixture of the two mutant alleles.

7.3 Discussion

In this chapter, I have reported the expression and purification of His-tagged wild-type LONP1-WT (wild-type), LONP1-Y565H and LONP1-E733K in order to investigate the pathogenicity of the two mutations that were identified in the patient described in Chapter 6.

Individually, all three proteins could hydrolyse ATP *in vitro*. For LONP1-Y565H, this was unexpected since this mutation localised to the ATPase domain and was considered to be pathogenic by PolyPhen-2 (Chapter 6). The presence of a substrate, TFAM, did not alter the ability of the LONP1 proteins to hydrolyse ATP, although only LONP1-WT and LONP1-E733K could bind and subsequently degrade TFAM, suggesting that the Y565H mutation is associated with a severe substrate binding defect. One caveat, however, is that although the rates were consistent between the LONP1 proteins, the amount of free phosphate should have doubled with double the amount of LONP1 protein, and should show a linear relationship. One likely explanation is that 0.5µg and 1µg LONP1 protein hydrolysed too little ATP for the assay, and is therefore representative of the background hydrolysis in the assay. Ideally, the ATP hydrolysis assays would need to be repeated using 4µg and 8µg LONP1 proteins, but undortunately due to time restraints this was not possible. The rates of ATP hydrolysis reported here were the average amounts of ATP hydrolysed for 0.5, 1 and 2µg LONP1 respectively.

The LONP1-E733K mutant appeared to behave in a similar manner to LONP1-WT, although the mixed hexamer LONP1-WT/E733K was less efficient at degrading TFAM than LONP1-WT, indicating that this mutation may interfere with the structure of LONP1, despite being located at the periphery of the LONP1 hexamer (Chapter 6).

Gel filtration analysis indicated that hexamers could only be detected in the presence of ATP and in a low salt buffer, and that the hexamer formation was not particularly stable, since monomers were also present under these conditions. All three recombinant proteins however could form hexamers, indicating that the mutations did not affect hexamer formation however LONP1-Y565H was less efficient, as determined by densitometry analysis. By using high salt conditions without ATP, each protein could be forced into monomers and allow for the formation of mixed hexamers upon dialysis and the addition of ATP into the buffer. Even though LONP1-Y565H was unable to degrade TFAM alone, when combined with LONP1-WT

the mixed hexamers could degrade TFAM albeit at a slower rate than LONP1-WT alone. If mixed hexamers do form, then the Y565H mutation alone reduces the efficiency of either substrate binding or substrate degradation in a mixed hexamer. The microscale thermophoresis indicated that LONP1-Y565H alone was unable to bind to the substrate, even in the presence of non-hydrolysable ATP, ATP-γS, but LONP1-WT/Y565H could (Figure 7.13). In both cases, there is a possibility that only LONP1-WT hexamers are degrading the TFAM. The Y565H mutation could interfere with the binding pocket of the LONP1 hexamer, since the mutation is located on the inner ring of LONP1, or effect the second conformational change that LONP1 adopts once ATP has been hydrolysed. However, under these conditions it cannot be ruled out that only LONP1-WT hexamers have formed, and since there is half as much LONP1-WT in the sample the rate of TFAM binding, as shown by microscale thermophoresis, and the rate of TFAM degradation will therefore be slower as shown by the TFAM proteolysis assay.

The Y565H mutation is located in a conserved aromatic-hydrophobic (Ar-ϕ) motif which is an axial pore loop (Kereïche *et al.* 2016), that is highly conserved amongst hexameric ATP-dependent proteases e.g. ClpX (Bar-Nun and Glickman, 2012; Martin *et al.* 2016). This loop is located within the ATPase domain and acts as a gateway into the catalytic site of the protease domain. The loop extends from all 6 monomers into the central chamber and upon ATP hydrolysis, a structural conformation occurs in which the loop moves, "opening" the gate and allowing the peptide to enter (Kereïche *et al.* 2016). In LONP1, the sequence for this motif is 'RTYVG' whereas in ClpX, the sequence is 'GYVG', but in both cases the tyrosine residue however is deemed to be vital for the function of each protease. When a Y153A mutation was introduced into the motif in ClpX, ClpX was unable to degrade the substrate, even though the mutant still maintained ATP hydrolysis activity. Interestingly, ATP hydrolysis activity increased from 10-fold to 40-fold (Siddiqui *et al.* 2004). In LONP1-Y565H, there was a slight increase in ATP hydrolysis, although it was not statistically significant, as well as a loss of TFAM degradation which closely mimics the Y153A mutant studied by Siddiqui *et al.* in ClpX. From the microscale thermophoresis data (Figure 7.12), the LONP1-Y565H mutant could not bind TFAM in the presence of non-hydrolysable ATP or ATP, suggesting that the 'gate' to the proteolytic domain remained closed throughout. For the mixed mutant of LONP1-Y565H/E733K, the gate still remains closed and TFAM is unable to bind to LONP1. However, it

is unclear as to whether this is because hexamers have not formed with the mixed monomers, or that the heterogeneous hexamers have formed but are inactive.

The LONP1-WT/E733K and LONP1-WT/Y565H are representative of the proteins found in each parent. Both proteins could hydrolyse ATP and degrade TFAM, albeit less efficiently than LONP1-WT. This is consistent since neither parent were affected with mitochondrial disease. The patient harbours both mutations and I have demonstrated that the mixed hexamer cannot degrade TFAM. Unfortunately, there was insufficient time to determine if the mixed hexamer also hydrolysed ATP. In addition, it was not possible to determine with the whether the reconstituted hexamers were truely heterogeneous hexamers or homogeneous. There was also insuffiecient time to test the hexamer reconstitution on homogeneous LONP1-WT and LONP1-E733K proteins. Thus, the results could be due to reduced levels of LONP1-WT alone, rather than a true effect of mixed hexamers

If TFAM cannot be degraded, then one would hypothesise that TFAM levels would increase, but an increase in TFAM has not been associated with mtDNA depletion, as has been observed in skeletal muscle of the proband, but leads to an increase in mtDNA copy number (Ikeda *et al.* 2015). LONP1 may yet have an unidentified role in mitochondrial gene expression which results in the effects observed in the skeletal muscle of the proband, but further research would still be required.

CHAPTER 8: FINAL CONCLUSIONS

The work presented in this thesis has focused on the characterisation of two proteins, AURKAIP1 and LONP1, which are involved in ribosome assembly, proteolysis and pathogenesis within human mitochondria. I initially focussed on human AURKAIP1 (mS38), a newly-identified component of the mt-SSU of the mitoribosome. During my project, data generated through my investigations into AURKAIP1 led into work on LONP1, a mitochondrial matrix protease. The data obtained about the two proteins are summarised below.

8.1 AURKAIP1

I generated two HEK293T cell lines that could overexpress AURKAIP1 either with or without a C-terminal FLAG-tag. In both cell lines, induction with tetracycline resulted in disruption to the mitoribosome. Even after 3 days' induction, steady state levels of mitoribosomal proteins were dramatically decreased, notably those of the mt-LSU. Induction of AURKAIP1 that lacked the C-terminal FLAG had less of an effect. In both cell lines, 12S rRNA and 16S rRNA were also decreased. Steady state levels of the mtDNA-encoded protein COXII were also reduced, indicating that AURKAIP1 overexpression resulted in a defect in mitochondrial translation. However, depletion of AURKAIP1 using siRNA did not affect the steady state levels of mitoribosomal proteins, but caused severe cell growth defects and cell death in U2OS, HEK293T and HeLa cell lines.

These data suggest that levels of AURKAIP1 are tightly controlled within the cell, since too much or too little AURKAIP1 is detrimental to mitochondrial translation and to cell growth respectively. It is uncertain as to whether the cell growth defects observed upon AURKAIP1 depletion are a direct cause of the reduction in AURKAIP1, or a secondary effect. However, the severeity and rapidness of onset suggests that AURKAIP1 does have an important function in the cell cycle. The cell growth defect could potentially be linked to the observation that AURKAIP1 is a regulator of Aurora-A kinase. Despite localising to the mitochondria, there are proteins with dual subcellular localisation for example DDX28, a mitoribosomal assembly factor that localises both to the mitochondria and to the nucleolus (Valgardsdottir *et al.* 2001). Indeed, many mitoribosomal proteins have been associated with apoptosis for e.g. mL41, mS29, mS40, mL37 (Yoo *et al.* 2015, Carim *et al.* 1999, Chintharlapalli *et al.* 2005, Levshenkova

et al. 2004) either suggesting that the mitoribosome and mitochondrial translation are themselves involved in apoptosis, or that these mitoribosomal proteins do have dual functionality (Kim *et al.* 2017). The cell growth defect observed when depleting AURKAIP1 is unlikely to be as a result of the function of the mitoribosome in apoptosis, since depletion of other mitoribosomal proteins does not induce rapid cell death for e.g. mL45 (Mai, 2016). It is more likely that AURKAIP1 possesses a function within the nucleus. If this is the case, then based on the work by Fumoto *et al.*, depletion of AURKAIP1 could lead to an increase in Aurora-A kinase activity since they suggested that AURKAIP1 negatively-regulated Aurora-A. The work produced by Katayama *et al.* would, however, suggest a decrease in activity since AURKAIP1 was suggested to promote the stability of Aurora-A. Since the cells undergo autophagy when AURKAIP1 is depleted, the more likely function would be to stabilise Aurora-A kinase. Currently, this function remains elusive.

Overexpressed AURKAIP1-FLAG resulted in the depletion of steady state levels of the mitoribosomal proteins. This is most likely due to lack of mitoribosome biogenesis and subsequent degradation of the MRPs which in turn would impair mitochondrial translation and lead to degradation of the 16S and 12S rRNA since they would no longer be protected by the MRPs. Additionally, as identified by the CLIP assay, AURKAIP1-FLAG was able to bind regions of 12S rRNA, 16S rRNA and mt-tRNA^{Val}. The highest hits were located at regions of RNA that were at the interface between the mt-LSU and mt-SSU, agreeing with the location of AURKAIP1 that has been suggested in the cryo-EM structures of the mitoribosomes. In addition, AURKAIP1 and AURKAIP1-FLAG overexpression resulted in mt-tRNA^{Val} dissociating from the mitoribosome with mt-tRNA^{Phe} taking its place. One potential hypothesis for these data is that AURKAIP1 is an RNA chaperone for mt-tRNA^{Val}. AURKAIP1 contains the DUF1713 domain which is also seen in the yeast protein Cox24 and is thought to be a homolog of AURKAIP1. Cox24, however, is used in the splicing of COXI transcripts, which is not required in humans since there are no introns in the mitochondrially-encoded genes. However, AURKAIP1 could be involved in stabilising mt-tRNA^{Val} once it is cleaved off from the rRNA species, as demonstrated in the tRNA punctuation model. During overexpression of AURKAIP1, mt-tRNA^{Val} is sequestered in the mitochondrial matrix, which in turn prevents mitoribosome assembly. Since mt-tRNA^{Phe} can replace mt-tRNA^{Val} (Rorbach and Gao *et al.* 2016), and mt-

$tRNA^{Phe}$ is present in the porcine mitoribosome (Greber *et al.* 2015), there must be an additional explanation as to why the mitoribosome disassembles so quickly.

A second potential hypothesis is that AURKAIP1 is a mitoribosomal assembly factor. The cryo-EM structures only represent a small proportion of the mitoribosome conformations and AURKAIP1 may be present in the cryo-EM structure because this is the most stable conformation during experimental preparations. Since the cryo-EM structures place AURKAIP1 surrounded by rRNA with only one potential protein interaction with mS15 at the 3' terminus of AURKAIP1, it is likely that AURKAIP1 associates with the mitoribosome via its RNA binding domain. Therefore, AURKAIP1 may assemble with the mt-SSU during late assembly via 12S rRNA, or may associate with the mt-LSU via the 16S rRNA. ERAL1 is thought to stabilise 12S rRNA (Dennerlein *et al.* 2010) but as yet, no RNA-binding protein has been identified to stabilise the 16S rRNA.

Both overexpressed AURKAIP1 and AURKAIP1-FLAG were recognised by our custom anti-AURKAIP1 antibody as a 15kDa species, even though the full-length species is predicted to be c.25kDa. The 15kDa species did not associate with the mt-SSU, mt-LSU or monosome when mitochondrial lysate was separated out through a sucrose gradient, yet LC-MS of purified mitoribosome using overexpressed mS27-FLAG could identify AURKAIP1 in the eluate. The size of AURKAIP1 within the mitochondria remains a mystery. Even though overexpressed AURKAIP1 and AURKAIP1-FLAG are detected as a 15kDa species, I determined that LONP1 was degrading both proteins from a 25kDa species to a 15kDa species by two cleavage events. However, via western blot it was not possible to determine if LONP1 was also involved in cleaving the endogenous species. One possibility is that the overexpressed AURKAIP1-FLAG is present in such great amounts that only these species can be detected, or alternatively the endogenous species is translated in such low amounts that it could not be visualised, regardless of LONP1 depletion. The anti-AURKAIP1 antibody may not recognise the cleaved species if the epitopes only localise to the N-terminus of AURKAIP1. Within the cryo-EM structures, AURKAIP1 has been detected as a 9kDa protein although this is yet to be confirmed by any other method. At the interface, there does not appear to be sufficient space for a 15kDa protein to fit so it is likely that AURKAIP1 is cleaved.

8.2 LONP1

During my studies, LONP1 was found to cleave overexpressed AURKAIP1-FLAG. To further characterise LONP1, I investigated samples from a paediatric patient who presented with severe mitochondrial disease, Through WES, two novel compound heterozygous mutations, p.Tyr565His; p.Glu733Lys, in *LONP1* were identified which I confirmed demonstrated autosomal recessive inheritance. The patient did not present with typical CODAS syndrome although the phenotype was characteristic of a severe mitochondrial disorder, notably with depletion of mtDNA. Skeletal muscle showed biochemical defects in OXPHOS activity, which was reflected in the severe decrease in steady state levels of subunits from complexes I, III and IV using western blotting. Interestingly, steady state levels of LONP1 were albeit slightly increased and yet levels of TFAM were reduced. The patient fibroblasts did not exhibit a mitochondrial disease phenotype, which is a known phenomenon in some fibroblast cell lines (Rodenburg, 2011). Since it was not possible to confirm pathogenesis by rescuing the phenotype in the patient cell line, *in vitro* functional studies were performed. Mature LONP1 proteins lacking the N-terminal MTS were expressed with a C-terminal His-tag and purified.

The p.Tyr565His mutation localised to a highly conserved residue in pore loop 1, containing a dipeptide aromatic-hydrophobic motif that is seen in many AAA+ proteases (Bar-Nun, 2012). This motif was shown to be vital for the movement of the substrate into the proteolytic domain, as well as undergoing conformational changes following ATP hydrolysis. My data demonstrated that recombinant LONP1-Y565H could hydrolyse ATP, but was unable to bind or to degrade TFAM, confirming the role of this residue in the movement of the substrate for subsequent proteolysis. The presence of TFAM did not alter the rate of ATP hydrolysis *in vitro*, suggesting that ATP is initially hydrolysed but the subsequent conformational change cannot occur in order to degrade TFAM.

The Glu733Lys mutation is in a less conserved residue located at the periphery of the LONP1 hexamer, and was predicted to be a non-pathogenic mutation. Indeed, LONP1-E733K behaved in a similar manner to LONP1-WT. However, when combined with the LONP1-WT protein to form a mixed hexamer, LONP1-WT/E733K was less efficient at degrading TFAM than

either LONP1-WT or LONP1-E733K alone, suggesting that the mutation does cause a structural change that does affect proteolysis efficiency.

The LONP1-Y565H/E733K mixed hexamer that mimicked the protein that would form within the proband was unable to bind and to degrade TFAM. The E733K mutation may allow for the formation of LONP1 hexamers with monomers carrying the Y565H mutation, since LONP1-WT/Y565H could bind and degrade TFAM *in vitro*, with the most likely explanation being that only LONP1-WT hexamers had formed in this sample.

In vitro studies have confirmed that the Y565H mutation is inactive in degrading TFAM on its own and when combined with the E733K mutation. The mutation affects the ability of LONP1 to degrade substrates, although ATP can still be hydrolysed. It is likely that there are other substrates of LONP1 that are yet to be identified that contribute to the disease phenotype observed in the proband. The decrease in the steady state levels of the OXPHOS complexes and the decrease in respiratory chain activity is consistent with the depletion of mtDNA. The levels of TFAM and mtDNA are related, since TFAM is degraded by LONP1 when not associated with mtDNA, and mtDNA is degraded when not associated with TFAM as it is left exposed. One of the functions of LONP1 is thought to be in maintaining the optimum mtDNA:TFAM ratio through degradation of TFAM (Matsushima *et al.* 2010). However, it is unclear how mutations in LONP1 this would lead to mtDNA depletion. In *Drosophila* Schneider cells, inducing mtDNA depletion in a Lon knockdown cell line did not result in the degradation of TFAM (Matsushima *et al.* 2010). It is likely that there are many unknown substrates of LONP1 involved in currently unidentified pathways that could lead to mtDNA depletion, which would produce the phenotype seen in the proband.

REFERENCES

Acham-Roschitz, B., Plecko, B., Lindbichler, F., Bittner, R., Mache, CJ., Sperl, W., Mayr, JA. "A novel mutation of the *RRM2B* gene in an infant with early fatal encephalomyopathy, central hypomyelination and tubulopathy" *Molecular Genetics and Metabolism* 98:300-304 (2009).

Adzhubei, IA., Schmidt, S., Peshkin, L., Ramensky, VE., Gerasimova, A., Bork, P., Kondrashov, AS, Sunyaev, SR. "A method and server for predicting damaging missense mutations" *Nature Methods* 7(4):248-249 (2010).

Al-Furoukh, N., Goffart, S., Szibor, M., Wanrooij, S., Braun, T. "Binding to G-quadruplex RNA activates the mitochondrial GTPase NOA1" *Biochimica et Biophysica Acta* 1833(12):2933-2942 (2013).

Alston, CL., Compton, AG., Formosa, LE., Strecker, V., Oláhová, M, Haack, TB., Stouffs, K., Diakumis, P., Ciara, E., Cassiman, D., Romain, N., Yarham, JW., He, L., De Paepe, B., Vanlander, AV., Seneca, S., Feichtinger, RG., Płoski, R., Rokicki, D., Pronicka, E., Haller, RG., Van Hove, JL., Bahlo, M., Mayr, JA., Van Coster, R., Prokisch, H., Wittig, I., Ryan, MT., Thorburn, DR., Taylor, RW. "Biallelic mutations in TMEM126B cause severe complex I deficiency with a variable clinical phenotype" *American Journal of Human Genetics* 99(1):217-227 (2016).

Alter, M., Talbert, OR., Croffead, G. "Cerebellar ataxia, congenital cataracts, and retarded somatic and mental maturation" *Neurology* 12(12):836 (1962).

Ambro, L., Pevala, V., Ondrovičová, G., Bellová, J., Kunová, N., Kutejová, E., Bauer, J. "Mutations to a glycine loop in the catalytic site of human Lon changes its protease, peptidase and ATPase activities" *FEBS Journal* 281:1784-1797 (2014).

Amunts, A., Brown, A., Bai, XC., Llácer, JL., Hussain, T, Emsley, P., Long, F., Murshudov, G., Scheres, SHW., Ramakrishnan, V. "Structure of the yeast mitochondrial large subunit" *Science* 343(6178):1485-1489 (2014).

Amunts, A., Brown, A., Toots, J., Scheres, SHW., Ramakrishnan, V. "The structure of the human mitochondrial ribosome" *Science*, 348(6230):95-98 (2015).

Anand, R., Wai, T., Baker, MJ., Kladt, N., Schauss, AC., Rugarli, E., Langer, T. "The *i*-AAA protease YME1L and OMA1 cleave OPA1 to balance mitochondrial fusion and fission" *Journal of Cell Biology* 204(6):919-929 (2014).

Anderson, S., Bankier, AT., Barrell, BG., De Bruijn, MHL., Coulson, AR., Drouin, J., Eperon, PC., Nierlich, DP., Roe, BA., Sanger, F., Schreier, PH., Smith, AJH., Staden, R., Young, IG. "Sequence and organization of our human mitochondrial genome" *Nature* 290:457-465 (1981).

Andersson, SGE., Zomorodipour, A., Andersson, JO., Sicheritz-Pontén, T., Alsmark, ACM., Podowski, RM., Näslund, AK., Eriksson, A-S., Winkler, HH., Kurland, CG. "The genome sequence of *Rickettsia prowazekii* and the origin of mitochondria" *Nature* 396:133-140 (1998).

Anger, AM., Armache, J-P., Berninghause, O., Habeck, M., Subklewe, M., Wilson, DN., Beckmann, R. "Structures of the human and *Drosophila* 80S ribosome" *Nature* 497:80-85 (2013).

Antonicka, H., Sasarman, F., Kennaway, NG., Shoubridge, EA. "The molecular basis for tissue specificity of the oxidative phosphorylation deficiencies in patients with mutations in the mitochondrial translation factor EFG1" *Human Molecular Genetics* 15:1835-1846 (2006).

Antonicka, H., Østergaard, E., Sasarman, F., Weraarpachai, W., Wibrand, F., Pedersen, AMB., Rodenburg, RJ., van der Knapp, MS., Smeitink, JAM., Chrzanowska-Lightowlers, ZMA., Shoubridge, EA. "Mutations in *C12orf65* in patients with encephalomyopathy and a mitochondrial translation defect" *American Journal of Human Genetics* 87(1):115-122 (2010).

Antonicka, H., Sasarman, F., Nishimura, T., Paupe, V., Shoubridge, EA. "The mitochondrial RNA-binding protein GRSF1 localises to RNA granules and is required for posttranscriptional mitochondrial gene expression" *Cell Metabolism* 17:386-398 (2013).

Antonicka, H., Shoubridge, EA. "Mitochondrial RNA granules are centers for posttranscriptional RNA processing and RNA biogenesis" *Cell Reports* 10:920-932 (2015).

Arnold, I., Pfeiffer, K., Neupert, W., Stuart, RA., Schägger, H. "Yeast mitochondrial F_1F_0-ATP synthase exists as a dimer: identification of three dimer-specific subunits" *EMBO Journal* 17:7170-7178 (1998).

Baer, RJ., Dubin, DT. Methylated regions of hamster mitochondrial ribosomal RNA: structural and functional correlates" *Nucleic Acids Research* 9:323-337 (1981).

Baker, TA., Sauer, RT. "ClpXP, an ATP-powered unfolding an protein-degradation machine" *Biochimica et Biophysica Acta* 1823(1):15-28 (2012).

Balsa, E., Marco, R., Perales-Clemente, E., Szklarczyk, R., Calvo, E., Landázuri, MO., Enríquez, JA. "NDUFA4 is a subunit of complex IV of the mammalian electron transport chain" *Cell Metabolism* 16(3):378-386 (2012).

Bamshad, MJ., Ng, SB., Bigham, AW., Tabor, HK., Emond, MJ., Nickerson, DA., Shendure, J. "Exome sequencing as a tool for Mendelian gene discovery" *Nature Review Genetics* 12(11):745-755 (2011).

Bar-Nun, S., Glickman, MH. "Proteasomal AAA-ATPases: structure and function" *Biochimica et Biophysica Acta* 1823:67-82 (2012).

Barat, M., Rickwood, D., Dufresne, C., Mounolou, JC. "Characterization of DNA-protein complexes from the mitochondria of *Xenopus laevis* oocytes" *Experimental Cell Research* 157:207-217 (1985).

Barkow, SR., Levchenko, I., Baker, TA., Sauer, RT "Polypeptide translocation by the AAA+ ClpXP protease machine" *Chemistry and Biology* 16:605-612 (2009).

Barrell, BG., Bankier, AT., Drouin, J. "A different genetic code in human mitochondria" *Nature* 282:189-194 (1979).

Barros, MH., Myers, AM., Van Driesche, S., Tzagoloff, A. "COX24 codes for a mitochondrial protein required for processing of the COX1 transcript" *Journal of Biological Chemistry* 281:3743-3751 (2006).

Bauer, MF., Hofmann, S., Neupert, W., Brunner, M. "Protein translocation into mitochondria: the role of TIM complexes" *Trends in Cell Biology* 10:25-31 (2000).

Bauer, M., Kristensen, BW., Meyer, M., Gasser, T., Widmer, HR., Zimmer, J., Ueffing, M. "Toxic effects of lipid-mediated gene transfer in ventral mesencephalic explant cultures" *Basic and Clinical Pharmacology and Toxicology* 98:395-400 (2006).

Benz, R. "Permeation of hydrophilic solutes through mitochondrial outer membranes: review on mitochondrial porins" *Biochimica et Biophysica acta* 1197:167-196 (1994).

Berger, T. and Kretzler, M. "Interaction of DAP3 and FADD only after cellular disruption" *Nature Immunology* 3:3-4 (2002).

Bertaccini, D., Vaca, S., Carapito, C., Arsène-Ploetze, F., Van Dorsselaer, AV., Schaeffer-Reiss, C. "An improved stable isotope N-terminal labelling approach with light/heavy TMPP to automate proteogenomics data validation: dN-TOP" *Journal of Proteome Research* 12(6):3063-3070 (2013).

Bertin, J., Wang, L., Guo, Y., Jacobson, MD., Poyet, J-L., Srinivasula, SM., Merriam, S., DiStefano, PS., Alnemri, ES. "CARD11 and CARD14 are novel caspase recruitment domain (CARD)/membrane-associated guanylate kinase (MAGUK) family members that interact with BCL10 and activate NF-κB" *Journal of Biological Chemistry* 276:11877-11882 (2001).

Bezawork-Geleta, A., Brodie, EJ., Dougan, DA., Truscott, KN. "LON is the master protease that protects against protein aggregation in human mitochondrial through direct degradation of misfolded proteins" *Scientific Reports* 5:17397 (2015).Bischoff, JR., Anderson, L., Zhu, Y., Mossie, K., Ng, L., Souza, B., Schryver, B., Flanagan, P., Clairvoyant, F., Ginther, C., Chan, CSM., Novotny, M., Slamon, DJ., Plowman, GD. "A homologue of *Drosophila aurora* kinase is oncogenic and amplified in human colorectal cancers" *EMBO Journal* 17(11):2971-3216 (1998).

Bischoff, JR. and Plowman, GD. "The Aurora/Ipl1p kinase family: regulators of chromosome segregation and cytokinesis" *Trends in Cellular Biology* 9(11):454-459 (1999).

Blakely, E., He, L., Gardner, JL., Hudson, G., Walter, J., Hughes, I., Turnbull, DM., Taylor, RW. "Novel mutations in the *TK2* gene associated with fatal mitochondrial DNA depletion myopathy" *Neuromuscular Disorders* 18(7):557-560 (2008).

Blakely, EL., Butterworth, A., Hadden, RDM., Bodi, I., He, L., McFarland, R., Taylor, RW. "*MPV17* mutation causes neuropathy and leukoencephalopathy with multiple mtDNA deletions in muscle" *Neuromuscular Disorders* 22(7):587-591 (2012).

Bogenhangen, DF., Rousseau, D., Burke, S. "The layered structure of human mitochondrial DNA nucleoids" *Journal of Biological Chemistry* 283(6):3665-3675 (2008).

Bogenhagen, DF., Martin, DW., Koller, A. "Initial steps in RNA processing and ribosome assembly occur at mitochondrial DNA nucleoids" *Cell Metabolism* 19:618-629 (2014).

Bornstein, B., Area, E., Flanigan, KM., Ganesh, J., Jayakar, P., Swoboda, KJ., Coku, J., Naini, A., Shanske, S., Tanji, K., Hirano, M., DiMauro, S. "Mitochondrial DNA depletion syndrome due to mutations in the *RRM2B* gene" *Neuromuscular Disorders* 18:453-459 (2008).

Borutaite, V., Brown, GC. "Mitochondrial regulation of caspase activation by cytochrome oxidase and tetramethylphenylenediamine via cytosolic cytochrome *c* redox state" *Journal of Biological Chemistry* 282(43):31124-31130 (2007).

Bota, DA., Davies, KJA. "Lon protease preferentially degrades oxidized mitochondrial aconitase by an ATP-stimulated mechanism" *Nature Cell Biology* 4:674-680 (2002).

Bota, DA, Davies, KJA. "Mitochondrial Lon protease in human disease and aging: Including an etiologic classification of Lon-related diseases and disorders" *Free Radical Biology and Medicine"* 100:188-198 (2016).

Botos, I., Melnikov, EE., Cherry, S., Tropea, JE., Khalatova, AG., Rasulova, F., Dauter, Z., Maurizi, MR., Rotanova, TV., Wlodawer, A., Gustachina, A. "The catalytic domain of *Escherichia coli* Lon protease has a unique fold and a Ser-Lys dyad in the active site" *Journal of Biological Chemistry* 279:8140-8148 (2004).

Bourdon, A., Minai, L., Serre, V., Jais, JP., Sarzi, E., Aubert, S., Chrétien, D., de Lonlay, P., Paquis-Flucklinger, V., Arakawa, H., Nakamura, Y., Munnich, A., Rötig, A. "Mutation of RRM2B, encoding p53-controlled ribonucleotide reductase (p53R2) causes severe mitochondrial DNA depletion" *Nature Genetics* 39:776-780 (2007).

Bowmaker, M., Yang, MY., Yasukawa, T., Reyes, A., Jacobs, HT., Huberman, JA., Holt, IJ. "Mammalian mitochondrial DNA replicates bidirectionally from an initiation zone" *Journal of Biological Chemistry* 278:50961-50969 (2003).

Brown, A., Amunts, A., Bai, XC., Sugimoto, Y., Eqwards, PC., Murshudov, G., Scheres, SH., Ramakrishnan, V. "Structure of the large ribosomal subunit from human mitochondria" *Science* 346:718-722 (2014).

Brown, A., Rathore, S., Kimanius, D., Aibara, S., Bai, X-C., Rorbach, J., Amunts, A., Ramakrishnan, V. "Structures of the human mitochondrial ribosome in native states of assembly" *Nature Structural and Molecular Biology* [Epub ahead of print] (2017).

Brzezniak, LK., Bijata, M., Szczesney, RJ., Stepien, PP. "Involvement of human ELAC2 gene product in 3' end processing of mitochondrial tRNAs" *RNA Biology* 8(4):616-626 (2011).

Burri, L., Strahm, Y., Hawkins, CJ., Gentle, IE., Puryer, MA., Verhagen, A., Callus, B., Vaux, D., Lithgow, T. "Mature DIABLO/Smac is produced by the IMP protease complex on the mitochondrial inner membrane" *Molecular Biology of the Cell* 16(6):2926-2933 (2005).

Cabral de Almeida, JC., Vargas, FR., Barbosa-Neto, JG., Llerana Jr., JC. "CODAS syndrome: a new distinct MCA/MR syndrome with radiological changes of spondyloepiphyseal dysplasia. Another case report" *American Journal of Medical Genetics* 55:19-20 (1995).

Capaldi, RA., Aggeler, R., Turina, P., Wilkens, S. "Coupling between catalytic sites and the proton channel in F1F0-type ATPases" *Trends in Biochemical Science* 19(7):284-289 (1994).

Capt, C., Passamonti, M., Breton S. "The human mitochondrial genome may code for more than 13 peptides" *Mitochondrial DNA Part A* 27(5):3098-3101 (2015)

Carim, L., Sumoy, L., Nadal, M., Estivill, X., Escarceller, M. "Cloning, expression and mapping of PDCD9, the human homolog of *Gallus gallus* pro-apoptotic protein p52" *Cytogenetics Cell Genetics* 87:85-88 (1999).

Carrozzo, R., Dionisi-Vici, C., Steuerwald, U., Lucioli, S., Deodata, F., Di Giandomenico, S., Bertini, E., Franke, B., Kluijtmans, LAJ., Meschini, MC., Rizzo, C., Piemonte, F., Rodenburg, R., Santer, R., Santorelli, FM., van Rooij, A., Vermunt-de Koning, D., Morava, E., Wevers, RA. "*SUCLA2* mutations are associated with mild methylmalonic aciduria, Leigh-like encephalomyopathy, dystonia and deafness" *Brain* 130(3):862-874 (2007).

Cavdar Koc, E., Ranasinghe, A., Burkhart, W., Blackburn, K., Koc, H., Moseley, A., Spremulli, LL. "A new face on apoptosis: death-associated protein and PDCD9 are mitochondrial ribosomal proteins" *FEBS Letters* 492(1-2):166-170 (2001).

Chacinska, A., Pfannschmidt, S., Wiedemann, N., Kozjak,V., Sanjuán Szklarz, LK., Schulze-Specking, A., Truscott, KN., Guiard, B., Meisinger, N., Pfanner, N. "Essential role of Mia40 in import and assembly of mitochondrial intermembrane space proteins" *EMBO Journal* 23:3735-3746 (2004).

Chen, SH., Suzuki, CK., Wu, SH. "Thermodynamic characterisation of specific interactions between human Lon protease and G-quartet DNA" *Nucleic Acids Research* 36(4):1273-1287.

Chintharlapalli, SR., Jasti, M., Malladi, S., Parsa, KV., Ballestero, RP., Gonzalez-García, M. "BMRP is a Bcl-2 binding protein that induces apoptosis" *Journal of Cellular Biochemistry* 94:611-626 (2005).

Christian, BE., Spremulli, LL. "Evidence for an active role of IF3mt in the initiation of translation in mammalian mitochondria" *Biochemistry* 48(15):3269-3278 (2009).

Christian, BE., Spremulli, LL. "Preferential selection of the 5'-terminal start codon on leaderless mRNAs by mammalian mitochondrial ribosomes" *Journal of Biological Chemistry* 285:28379-28386 (2010).

Christian, BE., Spremulli, LL. "Mechanism of protein biosynthesis in mammalian mitochondria" *Biochimica et Biophysica Acta* 1819(9-10):1035-1054 (2012).

Claros, MG., Perea, J., Shu, Y., Samatey, FA., Popot, JL., Jacq, C. "Limitations to *in vivo* import of hydrophobic proteins into yeast mitochondria. The case of a cytoplasmically synthesized apocytochrome *b*" *European Journal of Biochemistry* 228:762-771 (1995).

Clayton, DA. "Replication of animal mitochondrial DNA" *Cell* 28:693-705 (1982).

Cogliati, S., Frezzam, C., Soriano, ME., Varanita, T., Quintana-Cabrera, R., Corrado, M., Cipolat, S., Costa, V., Casarin, A., Gomes, LC., Perales-Clemente, E., Salviati, L., Fernandez-Silva, P., Enriquez, JA., Scorrano, L. "Mitochondrial cristae shape determines respiratory chain supercomplexes assembly and respiratory efficiency" *Cell* 155:160-171 (2013).

Conway, DJ., Fanello, C., Lloyd, JM., Al-Joubori, BM., Baloch, AH., Somanath, SD., Roper,C., Oduola, AM., Mulder, B., Povoa, MM., Singh, B., Thomas, AW. "Origin of *Plasmodium falciparium* malaria is traced by mitochondrial DNA" *Molecular and Biochemical Parasitology* 111(1):163-171 (2000).

Craven, L., Alston, CL., Taylor, RW., Turnbull, DM. "Recent advances in mitochondrial disease" *Annual Review of Genomics and Human Genetics* AHEAD OF PRINT (2017)

Cunningham, CN., Baughman, JM., Phu, L., Tea, JS., Yu, C., Coons, M., Kirkpatrick, DS., Bingol, B., Corn, JE. "USP30 and parkin homeostatically regulate atypical ubiquitin chains on mitochondria" *Nature Cell Biology* 17(2):160-169 (2015).

Dalla Rosa, I., Durigon, R., Pearce, SF., Rorbach, J., Hirst, EM., Vidoni, S., Reyes, A., Brea-Calvo, G., Minczuk, M., Woellhaf, MW., Herrmann, JM., Huynen, MA., Holt, IJ., Spinazzola, A. "MPV17L2 is required for ribosome assembly in mitochondria" *Nucleic Acids Research* 42(13):8500-8515 (2014).

Dennerlein, S., Rozanska, A., Wydro, M., Chrzanowska-Lightowlers, ZMA., Lightowlers, RN. "Human ERAL1 is a mitochondrial RNA chaperone involved in the assembly of the 28S small mitochondrial ribosomal subunit" *Journal of Biochemistry* 430(pt3):551-558 (2010).

Desai, N., Brown, A., Amunts, A., Ramakrishnan, V. "The structure of the yeast mitochondrial ribosome" *Science* 355(6324):528-531 (2017).

Deschauer, M, Hudson, G., Müller, T., Taylor, RW., Chinnery, PF., Zierz, S. "A novel ANT1 gene mutation with probably germline mosaicism in autosomal domain progressive external ophthalmoplegia" *Neuromuscular disorders* 15:311-315 (2005).

Di Bella, D., Lazzaro, F., Brusco, A., Plumari, M., Battaglia, G., Pastore, A., Finardi, A., Cagnoli, C., Tempia, F., Frontali, M., Veneziano, L., Sacco, T., Boda, E., Brussino, A., Bonn, F., Castellotti, B., Baratta, S., Mariotti, C., Gellara, C., Fracasso, V., Magri, S., Langer, T., Plevani, P., Di Donato, S., Muzi-Falconi, M., Taroni, F. "Mutations in the mitochondrial protease gene *AFG3L2* cause dominant hereditary ataxia SCA28" *Nature Genetics* 42(4):313-321 (2010).

Dikoglu, E., Alfaiz, A., Gorna, M., Bertola, D., Chae, JH., Cho, T-J., Derbent, M., Alanay, Y., Guran, T., Kim, O-H., Llerenar Jr., JC., Yamamoto, G., Superti-Furga, G., Reymond, A., Xenarios, I., Stevenson, B., Campos-Xavier, B., Bonafé, L., Superti-Furga, A., Unger, S. "Mutations in *LONP1*, a mitochondria matrix protease, cause CODAS syndrome" *American Journal of Medical Genetics* 167A:1501-1509 (2010).

Doble, BW., Woodgett, JR. "GSK-3: tricks of the trade for a multi-tasking kinase" *Journal of Cell Science* 116:1175-1186 (2003).

Doda, JN., Wright, CT., Clayton, DA. "Elongation of displacement-loop strands in human and mouse mitochondrial DNA is arrested near specific template sequences" *PNAS* 78(10):6116-6120 (1981).

Dvoráková-Holá, K., Matusková, A., Kubala, M., Otyepka, M., Kucera, T., Vecer, J., Herman, P., Parkhomenko, N., Kutejova, E., Janata, J. "Glycine-rich loop of mitochondrial processing peptidase alpha-subunit is responsible for substrate recognition by a mechanism analogous to mitochondrial receptor Tom20" *Journal of Molecular Biology* 396(5):1197-1210 (2010).

El-Hattab, AW., Li, F-Y., Schmitt, E., Zhang, S., Craigen, WJ., Wong, L-JC. "*MPV17*-associated hepatocerebral mitochondrial DNA depletion syndrome: New patients and novel mutations" *Molecular Genetics and Metabolism* 99(3):300-308 (2010).

Elpeleg, O., Miller, C., Hershkovitz, E., Bitner-Glindzicz, M., Bondi-Rubinstein, G., Rahman, S., Pagnamenta, A., Eshhar, S., Saada, A. "Deficiency of the ADP-forming succinyl-CoA synthase activity is associated with encephalomyopathy and mitochondrial DNA depletion" *American Journal of Human Genetics* 76:1081-1086 (2005).

Englmeier, R., Pfeffer, S., Förster, F. "Structure of the human mitochondrial ribosome studied *in situ* by cryoelectron tomography" *Structure* 25:1-8 (2017).

Falkenberg, M., Gaspari, M., Rantanen, A., Trifunovic, A., Larsson, N-G., Gustafsson, CM. "Mitochondrial transcription factors B1 and B2 activate transcription of mtDNA" *Nature Genetics* 31:289-294 (2002).

Falkenberg, M., Larsson, N-G., Gustafsoon, CM. "DNA replication and transcription in mammalian mitochondria" *Annual Review of Biochemistry* 76:679-699 (2007).

Fan, ACY., Kozlov, G., Hoegl, A., Marcellus, RC., Wong, MJH., Gehring, K., Young, JC. "Interaction between the human mitochondrial import receptors Tom20 and Tom70 *in vitro* suggests a chaperone displacement mechanism" *Journal of Biological Chemistry* 286:32208-32219 (2011).

Faure, E., Delaye, L., Tribolo, S., Levasseur, A., Seligmann, H., Barthélémy, RM. "Probable presence of an ubiquitous cryptic mitochondrial gene on the antisense strand of the cytochrome oxidase I gene" *Biology Direct* 24:56 (2011).

Flynn, JM., Neher, SB., Kim, YI., Sauer, RT., Baker, TA. "Proteomic discovery of cellular substrates of the ClpXP protease machine" *Molecular Cell* 11:671-683 (2003).

Foury, F., Roganti, T., Lecrenier, N., Purnelle, B. "The complete sequence of the mitochondrial genome of *Saccharomyces cerevisiae*" *FEBS Letters* 440:325-331 (1998).

Frey, TG., and Mannella, CA. "The internal structure of mitochondria" *Trends in Biochemical Science* 25:233-241 (2000).

Frohman, MA. "Role of mitochondrial lipids in guiding fission and fusion" *Journal of Molecular Medicine* 93:263-269 (2015).

Fukuda, R., Zhang, H., Kim, J-W., Shimoda, L., Dang, CV., Semenza, GL. "HIF-1 regulates cytochrome oxidase subunits to optimise efficiency of respiration in hypoxic cells" *Cell* 129(1):111-122 (2007).

Fumoto, K., Lee, PC., Saya, H., Kikuchi, A. "AIP regulates stability of Aurora-A at early mitotic phase coordinately with GSK3beta" *Oncogene* 27(32):4478-4487 (2008).

Fung, S., Nishimura, T., Sasarman, F., Shoubridge, EA. "The conserved interaction of C7orf30 with MRPL14 promotes biogenesis of the mitochondrial large ribosomal subunit and mitochondrial translation" *Molecular Biology of the Cell* 24(3):184-193 (2013).

Fusté, JM., Wanrooij, S., Jemt, E., Granycome, CE., Cluett, TJ., Shi, Y., Atanassova, N., Holt, IJ., Gustafsson, CM., Falkenberg, M. "Mitochondrial RNA polymerase is needed for activation of the origin of light-strand DNA replication" *Molecular Cell* 37:67-78 (2010).

Galkin, AS., Grivvenikova, VG., Vinogradov, AD. "H+/2e- stoichiometry in NADH-quinone reductase reactions catalysed by bovine heart submitochondrial particles" *FEBS Letters* 451:157-161 (1999).

García-Nafría, J., Ondrovicová, G., Blagova, E., Levdikov, VM., Bauer, JA., Suzuki, CK., Kutejová, E., Wilkinson, AJ., Wilson, KS. "Structure of the catalytic domain of the human mitochondrial Lon protease: proposed relation of oligomer formation and activity" *Protein Science* 19(5):987-999 (2010).

Garrido, N., Griparic, L., Jokitalo, E., Wartiovaara, J., van der Bliek, AM., Spelbrink, JN. "Composition and dynamics of human mitochondrial nucleoids" *Molecular Biology of the Cell* 14(4):1583-1596 (2003).

Gaur, R., Grasso, D., Data, PP., Krishna, PDV., Das, G., Spencer, A., Agrawal, RK., Spremulli, L., Varshney, U. "A single mammalian mitochondrial translation initiation factor functionally replaces two bacterial factors" *Molecular Cell* 29:180-190 (2008).

Gerdes, F., Tatsuta, T., Langer, T. "Mitochondrial AAA proteases – towards a molecular understanding of membrane-bound proteolytic machines" *Biochimica et Biophysica Acta* 1823:49-55 (2012).

Gey, GO., Coffman, WD., Kubicek, MT. "Tissue culture studies of the proliferative capacity of cervical carcinoma and normal epithelium" *Cancer Research* 12:364-365 (1952).

Giansanti, P., Tsiatsiani, L., Low, TY., Heck, AJR. "Six alternative proteases for mass spectrometry-based proteomics beyond trypsin" *Nature Protocols* 11:993-1006 (2016).

Gibellini, L., Pinti, M., Beretti, F., Pierri, CL., Onofrio, A., Riccio, M., Carnevale, G., De Biasi, S., Nasi, M., Torelli, F., Boraldi, F., De Pol, A., Cossarizza, A. "Sirtuin 3 interacts with Lon protease and regulates its acetylation status" *Mitochondrion* 18:76-81 (2014).

Giles, RE., Blanc, H., Cann, HM., Wallace, DC. "Maternal inheritance of human mitochondrial DNA" *PNAS* 77:6715-6719 (1980).

Gingras, A-C., Gstaiger, M., Raught, B., Aebersold, R. "Analysis of protein complexes using mass spectrometry" *Nature Reviews Molecular Cell Biology* 8.8:645-654 (2007).

Glover, DM., Leibowitz, MH., McLean, DA., Parry, H. "Mutations in aurora prevent centrosome separation leading the formation of monopolar spindles" *Cell* 81:95-105 (1995).

Gohil, VM. And Greenberg, ML. "Mitochondrial membrane biogenesis: phospholipids and proteins go hand-in-hand" *Journal of Cellular Biology* 184:469-472 (2009).

Goodwin, GH., Sanders, C., Johns, EW. "A new group of chromatin-associated proteins with a high content of acidic and basic amino acids" *European Journal of Biochemistry* 38:14-19 (1973).

Gorman, GS., Chinnery, PF., DiMauro, S., Hirano, M., Koga, Y., McFarland, R., Suomalainen, A., Thorburn, DR., Zeviani, M., Turnbull, DM. "Mitochondrial disease" *Nature Reviews Disease Primers* 2:16080 (2016).

Granot, Z., Melamed-Book, N., Bahat, A., Orly, J. "Turnover of StAR protein: Roles for the proteasome and mitochondrial proteases" *Molecular and Cellular Endocrinology* 265-266:51-58 (2007).

Gray, MW. "The bacterial ancestry of plastids and mitochondria" *Bioscience* 33:693-699 (1983).

Greber, BJ., Boehringer, D., Leitner, A., Bieri, P., Voigts-Hoffman, F., Erzberger, JP., Lebundgut, M., Aebersold, R., Ban, N. "Architecture of the large subunit of the mammalian mitochondrial ribosome" *Nature* 505:515-519 (2014).

Greber, BJ., Bieri, P., Leibundgut, M., Leitner, A., Aebersold, R., Boehringer, D., Ban, N. "The complete structure of the 55S mammalian mitochondrial ribosome" *Science* 348(6232):303-308 (2015).

Haack, TB., Danhauser, K., Haberberger, B., Hoser, J., Strecker, V., Boehm, D., Uziel, G., Lamantea, E., Invernizzi, F., Poulton, J., Rolinski, B., Iuso, A., Biskup, S., Schmidt, T., Mewes, HW., Wittig, I., Meitinger, T., Zeviani, M., Prokisch, H. "Exome sequencing identifies ACAD9 mutations as a cause of complex I deficiency" *Nature Genetics* 42(12):1131-1134 (2010).

Hage, AE. and Tollervey, D. "A surfeit of factors: why is ribosome assembly so much more complicated in eukaryotes than bacteria?" *RNA Biology* 1:10-15 (2004).

Hägerhäll, C. "Succinate:quinone oxidoreductases, variations on a conserved theme" *Biochimica et Biophysica Acta* 1320:107-141 (1997).

Hammarsund, M., Wilson, W., Corcoran, M., Merup, M, Einhorn, S., Grandér, D., Sangfelt, O. "Identification and characterization of two novel human mitochondrial elongation factor genes, hEFG2 and hEFG1, phylogenetically conserved through evolution" *Human Genetics* 109(5):542-550 (2001).

Han, SH., Chung, JH., Kim, J., Kim, KS., Han, YS. "New role of human ribosomal protein S3: Regulation of cell cycle via phosphorylation by cyclin-dependent kinase 2" *Oncology Letters* 13(5):3681-3687 (2017).

Hartmann, RK., Gößringer, M., Späth, B., Fischer, S., Marchfelder, A. "The making of tRNAs and more – RNase P and tRNase Z" *Progress in Nucleic Acid Research and Molecular Biology* 85:319-368 (2009).

Hartmannová, H., Piherová, L., Tauchmannová, K., Kidd, K., Acott, PD., Crocker, JF., Oussedik, Y., Mallet, M., Hodaňová, K., Stránecký, V., Přistoupilová, A., Barešová, V., Jedličková, I., Živná, M., Sovová, J., Hůlková, H., Robins, V., Vrbacký, M., Pecina, P., Kaplanová, V., Houštek, J., Mráček, T., Thibrault, Y., Bleyer, AJ., Kmoch, S. "Acadian variant of Fanconi syndrome is caused by mitochondrial respiratory chain complex I deficiency due to a non-coding mutation in complex I assembly factor NDUFAF6" *Human Molecular Genetics* 25(18):4062-4079 (2016).

Hashimoto, Y., Niikura, T., Tajima, H., Yasukawa, T., Sudo, H., Ito, Y., Kita, Y., Kawasumi, M., Kouyama, K., Doyu, M., Sobue, G., Koide, T., Tsuji, S., Lang, J., Kurohawa, K., Mishimoto, I. "A rescue factor abolishing neuronal cell death by a wide spectrum of familial Alzheimer's disease genes and Aβ" *Proceedings of the National Academy of Sciences USA* 98(11):6336-6341 (2001).

He, J., Cooper, HM., Reyes, A., Di Re, M., Kazak, L., Wood, SR., Mao, CC., Fearnley, IM., Walker, JE., Holt, IJ. "Human C4orf14 interacts with the mitochondrial nucleoid and is involved in the biogenesis of the small mitochondrial subunit" *Nucleic Acids Research* 40:6097-6108 (2012).

Heazlewood, JL., Tonti-Filippini, JS., Gout, AM., Day, DA., Whelan, J., Millar, AH. "Experimental analysis of the Arabidopsis mitochondrial proteome highlights signalling and regulatory components, provides assessment of targeting prediction programs, and indicates plant-specific mitochondrial proteins" *Plant Cell* 16(1):241-256 (2004).

Hirota, T., Kunitoku, N., Sasayama, T., Marumoto, T., Zhang, D., Nitta, M., Hatakeyama, K., Saya, H. "Aurora-A and an interacting activator, the LIM protein Ajuba, are required for mitotic commitment in human cells" *Cell* 114:585-598 (2003).

Hirst, J. "Mitochondrial complex I" *Annual Reviews in Biochemistry* 82:551-575 (2013).

Hori, O., Ichinoda, F., Tamatani, T., Yamaguchi, A., Sato, N., Ozawa, K., Kitao, Y., Miyazaki, M., Harding, HP., Ron, D., Tohyama, M., Stern, DM., Ogawa, S. "Transmission of cell stress from endoplasmic reticulum to mitochondria: enhanced expression of Lon protease" *Journal of Cell Biology* 157(7):1151-1160 (2002).

Hornig-Do, HT., Tatsuta, T., Buckermann, A., Bust, M., Kollberg, G., Rötig, A., Hellmich, M., Mijtmans, L., Wiesner, RJ. "Nonsense mutations in the COX1 subunit impair the stability of respiratory chain complexes rather than their assembly" *EMBO Journal* 31(5):1293-1307 (2012).

Hornig-Do, HT., Montanari, A., Rozanska, A., Tuppen, HA., Almaki, AA., Abg-Kamaludin, DP., Frontali, L., Francisci, S., Lightowlers, RN., Chrzanowska-Lightowlers, ZMA. "Human mitochondrial leucyl tRNA synthetase can suppress non cognate pathogenic mt-tRNA mutations" *EMBO Molecular Medicine* 6(2):183-193 (2014).

Iborra, FJ., Kimua, H., Cook, PR. "The functional organization of mitochondrial genomes in human cells" *BMC Biology* 2(1):9 (2004).

Ikeda, M., Ide, T., Fujino, T., Arai, S., Saky, K., Kakino, T., Tyynismaa, H., Yamasaki, T., Yamada, K-I., Kang, D., Suomalainen, A., Sunagawa, K. "Overexpression of TFAM or Twinkle increases mtDNA copy number and facilitates cardioprotection associated with limited mitochondrial oxidative stress" *PLOS One* 10(3):e0119687 (2015).

Innes, AM., Chudley, AE., Reed, MG., Shuckett, EP., Hildes-Ripstein, GE., Greenberg, CR. "Third case of cerebral, ocular, dental, auricular, skeletal abnormalities (CODAS) syndrome, further delineating a new malformation syndrome: first report of an affected male and a review of the literature" *American Journal of Medical Genetics* 102:42-47 (2001).

Inui, T., Anzai, M., Takezawa, Y., Endo, W., Kakisaka, Y., Kikuchi, A., Onuma, A., Kure, S., Nishino, I., Ohba, C., Saitsu, H., Matsumoto, N., Haginoya, K. "A novel mutation in the proteolytic domain of LONP1 causes atypical CODAS syndrome" *Journal of Human Genetics* 62(6):653-655 (2017).

Iwata, S., Lee, JW., Okada, K., Iwata, M., Rasmussen, B., Link, TA., Ramaswamy, S., Jap, BK. "Complete structure of the 11-subunit bovine mitochondrial cytochrome bc1 complex" *Science* 281(5373):64-71 (1998).

Jenkinson, EM., Rehman, AU., Walsh, T., Clayton-Smith, J., Lee, K., Morell, RJ., Drumond, MC., Khan, SN., Naeem, MA., Rauf, B., Billington, N., Schultz, JM., Urquhart, JE., Lee, MK., Berry, A., Hanley, NA., Mehta, S., Cilliers, D., Clayton, PE., Kingston, H., Smith, MJ., Warner, TT., University of Washington Center for Mendelian Genomics, Black, GC., Trump, D., Davis, JRE., Ahmad, W., Leal, SM., Riazuddin, S., King, M-C., Friedman, TB., Newman, WG. "Perrault syndrome is caused by recessive mutations in *CLPP*, encoding a mitochondrial ATP-dependent chambered protease" *American Journal of Human Genetics* 92(4):605-613 (2013).

Jourdain, AA., Koppen, M., Wydro, M., Rodley, CD., Lightowlers, RN., Chrzanowska-Lightowlers, ZMA. "GRSF1 regulates RNA processing in mitochondrial RNA granules" *Cell Metabolism* 17:399-410 (2013).

Jourdain, AA., Boehm, E., Maundrell, K., Martinou, J-C. "Mitochondrial RNA granules: compartmentalising mitochondrial gene expression" *Journal of Cell Biology* 212(6):611-614 (2016).

Käser, M., Langer, T. "Protein degradation in mitochondria" *Cell and Developmental Biology* 11:181-190 (2000).

Kashuba, E., Yurchenko, M., Yenamandra, SP., Snopok, B., Isaquliants, M., Szekely, L., Klein, G. "EBV-encoded EBNA-6 binds and targets MRPS18-2 to the nucleus, resulting in the disruption of pRb-EF21 complexes" *PNAS* 105(14):5489-5494 (2008).

Katayama, H., Sasai, K., Czerniak, BA., Carter, JL., Sen, S. "Aurora-A kinase phosphorylation of Aurora-A kinase interacting protein (AIP) and stabilisation of the enzyme-substrate complex" *Journal of Cellular Biochemistry* 102(5):1318-1331 (2007).

Kereïche, S., Kováĉik, L., Bednár, J., Pevala, V., Kunová, N., Ondroviĉová, G., Bauer, J., Ambro, L., Bellová, J., Kutejová, E., Raŝka, I. "The N-terminal domain plays a crucial role in the structure of a full-length human mitochondrial protease" *Scientific Reports* 6:33631 (2016).

Khatter, H., Masnikov, AG., Natchiar, SK., Klaholz, BP. "Structure of the 80S ribosome" *Nature* 520(7549):640-645 (2015).

Kiat, LS., Hui, KM., Gopalan, G. "Aurora-A kinase interacting protein (AIP), a novel regulator of human Aurora-A kinase" *Journal of Biological Chemistry* 277(47):45558-45565 (2002).

King, M., Attardi, G. "Human cells lacking mtDNA: repopulation with exogenous mitochondria by complementation" *Science* 246(4929):500-503 (1989).

Kirby, DM., Thorburn, DR., Turnbull, DM., Taylor, RW. "Biochemical assays of respiratory chain complex activity" *Methods in Cell Biology* 80:93-119 (2007).

Kissova, I., Diffieu, M., Manon, S., Camougrand, N. "Uth1p is involved in the autophagic degradation of mitochondria" *Journal of Biological Chemistry* 279:39068-39074 (2004).

Koc, EC., Spremulli, LL. "Identification of mammalian mitochondrial translational initiation factor 3 and examination of its role in initiation complex formation with natural mRNAs" *Journal of Biological Chemistry* 277:35541-35549 (2002).

Koc, EC., Cimen, H., Kumcuoglu, B., Abu, N., Akpinar, G., Hague, MD., Spremulli, LL., Koc, H. "Identification and characterization of CHCHD1, AURKAIP1 and CRIF1 as new members of the mammalian mitochondrial ribosome" *Frontiers in Physiology* 4:183 (2013).

Komaki, H., Fukazawa, T., Houzen, H., Yoshida, K., Nonaka, I., Goto, Y. "A novel D10G mutation in the adenine nucleotide transporter 1 gene in autosomal dominant progressive external ophthalmoplegia patients with mitochondrial DNA with multiple deletions" *Annals of Neurology* 51:645-648 (2002).

Koppen, M., Metodiev, MD., Casari, G., Rugarli, EI., Langer, T. "Variable and tissue-specific subunit composition of mitochondrial *m*-AAA protease complexes linked to hereditary spastic paraplegia" *Molecular and Cellular Biology* 27:758-767 (2007).

Kotani, T., Akabane, S., Takeyasu., Ueda, T., Takeuchi, N. "Human G-proteins, OgbH1 and Mtg1, associate with the large mitochondrial ribosome subunit and are involved in translation and assembly of respiratory complexes" *Nucleic Acids Research* 41:3713-3722 (2013).

Kühl, I., Miranda, M., Posse, V., Milenkovic, D., Mourier, A., Siira, SJ., Bonekamp, NA., Neumann, U., Filipovska, A., Polosa, PL., Gustafsson, CM., Larsson, NG. "POLRMT regulates the switch between replication primer formation and gene expression of mammalian mtDNA" *Science Advances* 2(8):e1600963 (2016).

Kukat, C., Wurm, CA., Spåhr, H., Falkenberg, M., Larsson, N-G., Jakobs, S. "Super-resolution microscopy reveals that mammalian mitochondrial nucleoids have a uniform size and frequently contain a single copy of mtDNA" *Proceedings of the National Academy of Sciences USA* 108(33):13534-13539 (2011).

Kukat, C., Davies, KM., Wurm, CA., Spåhr, H., Bonekamp, NA., Kühl, I., Joos, F., Polosa, PL., Park, CB., Posse, V., Falkenberg, M., Jakobs, S., Kühlbrandt, W., Larsson, N-G. "Cross-strand binding of TFAM to a single mtDNA molecule forms the mitochondrial nucleoid" *PNAS USA* 112(36):11288-11293 (2015).

Kulawiak, B., Höpker, J., Gebert, M., Guiard, B., Wiedemann, N., Gebert, N. "The mitochondrial protein import machinery has multiple connections to the respiratory chain" *Biochimica et Biophysica Acta – Bioenergetics* 1827(5):612-626 (2013).

Lamperti, C., Fang, M., Invernizzi, F., Liu, X., Wang, H., Zhang, W., Carrara, F., Moroni, I., Zeviani, M., Zhang, J., Ghezzi, D. "A novel homozygous mutation in *SUCLA2* gene identified by exome sequencing" *Molecular Genetics and Metabolism* 107(3):403-408 (2012).

Lee, KW., Bogenhagen, DF. "Assignment of 2'-O-methyltransferases to modification sites on the mammalian mitochondrial large subunit 16S rRNA" *Journal of Biological Chemistry* 289:24936-24942 (2014).

Levshenkova, EV., Ukraintsev, KE., Orlova, VV., Alibaeva, RA., Kovriga, IE., Zhugdernamzhilyn, O. *et al.* "The structure and specific features of the cDNA expression of the human gene *MRPL37*" *Bioorganic Chemistry* 30:499-506 (2004).

Liao, HX., Spremulli, LL. "Identification and initial characterization of translational initiation factor 2 from bovine mitochondria" *Journal of Biological Chemistry* 265:13618-13622 (1990).

Lieber, DS., Calvo, SE., Shanahan, K., Slate, NG., Liu, S., Hershman, SG., Gold, NB., Chapman, BA., Thorburn, DR., Berry, GT., Schmahmann, JD., Borowsky, ML., Mueller, DM., Sims, KB., Mootha, VK. "Targeted exome sequencing of suspected mitochondrial disorders" *Neurology* 80(19):1762-1770 (2013).

Lightfoot, DA. "Magnesium-dependence of *in vitro* translation programmed by gene-specific mRNAs" *Nucleic Acids Research* 16(9):4164 (1988).

Lightowlers, RN., Chrzanowska-Lightowlers, ZMA. "Terminating human mitochondrial protein synthesis: a shift in our thinking" *RNA Biology* 7:282-286 (2010).

Lightowlers, RN., Taylor, RW., Turnbull, DM. "Mutations causing mitochondrial disease: what is new and what challenges remain?" *Science* 349:1494-1499 (2015).

Lim, SK., Gopalan, G. "Antizyme1 mediates AURKAIP1-dependent degradation of Aurora-A" *Oncogene* 26(46):6593-6603 (2007).

Lind, C., Sund, J., Aqvist, J. "Codon-reading specificities of mitochondrial release factors and translation termination at non-standard stop codons" *Nature Communications* 4:2940 (2013).

Liu, T., Lu, B., Lee, I., Ondrovičova, G., Kutejová, E., Suzuki, CK. "DNA and RNA binding by the mitochondrial Lon protease is regulated by nucleotide and protein substrate" *Journal of Biological Chemistry* 279(14):13902-13910 (2004).

Liu, X., Weaver, D., Shirihai, O., Hajnóczky, G. "Mitochondrial 'kiss-and-run': interplay between mitochondrial motility and fusion-fission dynamics" *EMBO Journal* 28:3074-3089 (2009).

Lodeiro, MFF., Uchida, A., Bestwick, M., Moustafa, IM., Arnold, JJ., Shadel, GS., Cameron, CE. "Transcription from the second heavy-strand promoter of human mtDNA is repressed by transcription factor A *in vitro*" *PNAS* 109:6513-6518 (2012).

Lott, MT., Leipzig, JN., Derbeneva, O., Xie, HM., Chalkia, D., Sarmady, M., Procaccio, V., Wallace, DC. "mtDNA variation and analysis using Mitomap and Mitomaster" *Current Protocols in Bioinformatics* 44(1.23):1-26 (2013).

Lu, B., Yadav, S., Shah, PG., Liu, T., Tian, B., Pukszta, S., Villaluna, N., Kutejova, E., Newlon, CS., Santos, JH., Suzuki, CK. "Roles for the human ATP-dependent Lon protease in mitochondrial DNA maintenance" *Journal of Biological Chemistry* 282:17363-17374 (2007).

Mai, N. "*The role of MRPL45 and OXA1L in human mitochondrial protein synthesis"*. PhD thesis, Newcastle University (2016).

Mai, N., Chrzanowska-Lightowlers, ZMA., Lightowlers, RN. "The process of mammalian mitochondrial protein synthesis" *Cell and Tissue Research* 367(1):5-20 (2017).

Mancuso, M., Salviati, L., Sacconi, S., Otaegui, D., Camaño, P., Marina, A., Bacman, S., Moraes, CT., Carlo, JR., Garcia, M., Garcia-Alvarez, M., Monzon, L., Naini, AB., Hirano, M., Bonilla, E., Taratuto, AL., DiMauro, S., Vu, TH. "Mitochondrial DNA depletion. Mutations in thymidine kinase gene with myopathy and SMA" *Neurology* 59(8):1197-1202 (2002).

Mancuso, M., Filosto, M., Bonilla, E., Hirano, M., Shanske, S., Vu, TH., DiMauro, S. "Mitochondrial myopathy of childhood associated with mitochondrial DNA depletion and a homozygous (T77M) in the TK2 gene" *Archives of Neurology* 60(7):1007-1009 (2003).

Margulis, L. "Origin of eukaryotic cells" Yale University Press, New Haven, CT. (1970).

Marko-Varga, G., Omenn, GS., Paik, YK., Hancock, WS. "The first step toward completion of a genome-wide characterisation of the human proteome" *Journal of Proteomics Research* 12(1):1-5 (2013).

Martin, A., Baker, TA., Sauer, RT. "Pore loops of the AAA+ ClpX machine grip substrates to drive translocation and unfolding" *Nature Structural and Molecular Biology* 15(11):1147-1151 (2008).

Martin, WF. "The Origin of Mitochondria" *Nature Education* 3(9):58 (2010).

Matsushima, Y., Goto, Y., Kaguni, LS. "Mitochondrial Lon protease regulates mitochondrial DNA copy number and transcription by selective degradation of mitochondrial transcription factor A (TFAM)" *PNAS* 107(43):18410-18415 (2010).

Matulis, D., Kranz, JK., Salemme, FR., Todd, MJ. "Thermodynamic stability of carbonic anhydrase: measurements of binding affinity and stoichiometry using ThermoFluor" *Biochemistry* 44(13):5258-5266 (2005).

Meisinger, C., Sickmann, A., Pfanner, N. "The mitochondrial proteome: from inventory to function" *Cell* 134(1):22-24 (2008).

Menz, RI., Walker, JE., Leslie, AGW. "Structure of bovine mitochondrial F_1-ATPase with nucleotide bound to all three catalytic sites: implications for the mechanism of rotary catalysis" *Cell* 106:331-341 (2001).

Meraldi, P., Honda, R., Nigg, EA. "Aurora kinase link chromosome segregation and cell division to cancer susceptibility" *Current Opinion in Genetics & Development* 14:29-36 (2004).

Metodiev, MD., Lesko, N., Park, CB., Cámara, Y., Shi, Y., Wibom, R., Hultenby, K., Gustaffson, CM., Larsson, NG. "Methylation of 12S rRNA is necessary for *in vivo* stability of the small subunit of the mammalian mitochondrial ribosome" *Cell Metabolism* 9:386-397 (2009).

Metodiev, MD., Spåhr, H., Loguercio Polosa, P., Meharg, C., Becker, C., Altmueller, J., Habermann, B., Larsson, NG., Ruzzenente, B. "NSUN4 is a dual function mitochondrial protein required for both methylation of 12S rRNA and coordination of mitoribosomal assembly" *PLoS Genetics* 10(2):e1004110 (2014).

Meyer-Ficca, ML., Meyer, RG., Kaiser, H., Brack, AR., Kandolf, R., Küpper, JH. "Comparative analysis of inducible expression systems in transient transfection studies" *Analytical Biochemistry* 334:9-19 (2001).

Mitchell, P. "Coupling of phosphorylation to electron and hydrogen transfer by a chemi-osmotic type of mechanism" *Nature* 191:144-148 (1961).

Mitchell, P. "Possible molecular mechanism of the protonmotive function of cytochrome systems" *Journal of Theoretical Biology* 62:327-367 (1976).

Montoya, J., Gaines, GL., Attardi, G. "The pattern of transcription of the human mitochondrial rRNA genes reveals two overlapping transcription units" *Cell* 34(1):151-159 (1983).

Moreno-Lastres, D., Fontanesi, F., García-Consuegra, I., Martin, MA., Arenas, J., Barrientos, A., Ugalde, C. "Mitochondrial complex I plays an essential role in human respirasome assembly" *Cell Metabolism* 15(3):324-335 (2012).

Morino, H., Pierce, SB., Matsuda, Y., Walsh, T., Ohsawa, R., Newby, M., Hiraki-Kamon, K., Kuramochi, M., Lee, MK., Klevit, RE., Martin, A., Maruyama, H., King, M-C., Kawakami, H. "Mutations in Twinkle primase-helicase cause Perrault syndrome with neurologic features" *Neurology* 83(22):2054-2061 (2014).

Müller, M., Mentel, M., van Hellemond, JJ., Henze, K., Woehle, C., Gould, SB., Yu, R-Y., van der Giezen, M., Tielens, AGM., Martin, WF. "Biochemistry and evolution of anaerobic energy metabolism in eukaryotes" *Microbiology and Molecular Biology Reviews* 76(2):444-495 (2012).

Naora, H., Takai, I., Adachi, M., Naora, H. "Altered cellular responses by varying expression of a ribosomal protein gene: sequential coordination of enhancement and suppression of ribosomal protein S3a gene expression induces apoptosis" *Journal of Cell Biology* 141(3):741-753 (1998).

Napoli, L., Bordoni, A., Zeviani, M., Hadjigeorgiou, GM., Sciacco, M., Tiranti, V., Terentiou, M., Moggio, M., Papadimitriou, A., Scarlato, G., Comi, GP. "A novel missense adenine nucleotide translocator-1 gene mutation in a Greek adPEO family" *Neurology* 57:2295-2298 (2001).

Ngo, HB., Kaiser, JT., Chan, DC. "Tfam, a mitochondrial transcription and packaging factor, imposes a U-turn on mitochondrial DNA" *Nature Structural and Molecular Biology* 18(11):1290-1296 (2011).

Nicholls, DG., Budd, SL. "Mitochondria and neuronal survival" *Physiological Reviews* 80:315-360 (2000).

Nierhaus, KH. "Mg^{2+}, K^{+} and the ribosome" *Journal of Bacteriology* 196(22):3817-3819 (2014).

Nimmo, G., Pandey, A., Marshall, C., Venkatesh, S., Hazrati, L., Ahmed, S., Cameron, J., Pay, R., Suzuki, C., Yoon, G. "Profound hypotonia, muscle weakness, global development delays with stepwise regression, and cerebellar atrophy: expansion of the *LONP1*-related disease phenotype" *Neuromuscular Disorders* 27(Supp.2):S118 (2017)

Noji, H., Yasuda, R., Yoshida, M., Kinosita, K. "Direct observation of the rotation of F1-ATPase" *Nature* 386:299-302 (1997).

O'Brien, TW. "Properties of mitochondrial ribosomes" *International Union of Biochemistry and Molecular Biology Life* 55(9):505-513 (2003).

Ofengand, J., Bakin, A. "Mapping to nucleotide resolution of pseudouridine residues in large subunit ribosomal RNAs from representative eukaryotes, prokaryotes, archaebacterial, mitochondria and chloroplasts" *Journal of Molecular Biology* 266:246-268 (1997).

Ojala, D., Montoya, J., Attardi, G. "tRNA punctuation model of RNA processing in human mitochondria" *Nature* 290:470-474 (1981).

Old, SL., Johnson, MA. "Methods of microphotometric assay of succinate dehydrogenase and cytochrome *c* oxidase activities for use on human skeletal muscle" *The Histochemical Journal* 21(9-10):545-555 (1989).

Olivo, PD., Van de Walle, MJ., Laipis, PJ., Hauswirth, WW. "Nucleotide sequence evidence for rapid genotypic shifts in the bovine mitochondrial DNA D-loop" *Nature* 306:400-402 (1983).

Osman, C., Haag, M., Wieland, FT., Brügger, B., Langer, T. "A mitochondrial phosphatase required for cardiolipin biosynthesis: the PGP phosphatase Gep4" *EMBO Journal* 29(12):1976-1987 (2010).

Ostergaard, E., Christensen, E., Kristensen, E., Mogensen, B., Duno, M., Shoubridge, EA., Wibrand, F. "Deficiency of the α subunit of succinate-coenzyme A ligase causes fatal infantile lactic acidosis with mitochondrial DNA depletion" *American Journal of Human Genetics* 81(2):383-387 (2007).

Otera, H., Wang, C., Cleland, MM., Setoguchi, K., Yokota, S., Youle, RJ., Mihara, K. "Mff is an essential factor for mitochondrial recruitment of Drp1 during mitochondrial fission in mammalian cells" *Journal of Cell Biology* 191:1141-1159 (2010).

Ow, Y-LP., Green, DR., Hao, Z., Mak, TW. "Cytochrome c: functions beyond respiration" *Nature Reviews Molecular Cell Biology* 9:532-542 (2008).

Pagliarini, DJ. Calvo, SE., Chang, B., Sheth, SA., Vafai, SB., Ong, S-E., Walford, GA., Sugiana, C., Boneh, A., Chen, WK., Hill, DE., Vidal, M., Evans, JG., Thorburn, DR., Carr, SA., Mootha, VK. "A mitochondrial protein compendium elucidates complex I disease biology" *Cell* 143(1):112-123 (2008).

Patterson-Ward, J., Huang, J., Lee, I. "Detection and characterisation of two ATP-dependent conformational changes in proteolytically inactive *Escherichia coli* Lon mutants by stopped flow kinetic techniques" *Biochemistry* 46(47):13593-13605 (2007).

Perkins, GA., Renken, C., Martone, ME., Young, SJ., Ellisman, M., Frey, TG. "Electron tomography of neuronal mitochondria: three-dimensional structure and organisation of cristae and membrane contacts" *Journal of Structural Biology* 119:260-272 (1997).

Pfeffer, G., Gorman, GS., Griffin, H., Kurzawa-Akanbi, M., Blakely, EL., Wilson, I., Sitarz, K., Moore, D., Murphy, JL., Alston, CL., Pyle, A., Coxhead, J., Payne, B., Gorrie, GH., Longman, C., Hadjivassiliou, M., McConville, J., Dick, D., Imam, I., Hilton, D., Norwood, F., Baker, MR., Jaiser, SR., Yu-Wai-Man, P., Farrell, M., McCarthy, A., Lynch, T., McFarland, R., Schaefer, AM., Turnbull, DM., Horvath, R., Taylor, RW., Chinnery, PF. "Mutations in the *SPG7* gene cause chronic progressive external ophthalmoplegia through disordered mitochondrial DNA maintenance" *Brain* 137(Pt5):1323-1326 (2014).

Pierce, SB., Chisholm, KM., Lynch, ED., Lee, MK., Walsh, T., Opitz, JM., Li, W., Klevit, RE., King, M-C. "Mutations in mitochondrial histidyl tRNA synthetase *HARS2* cause ovarian dysgenesis and sensorineural hearing loss of Perrault syndrome" *PNAS* 108(16):6543-6548 (2011).

Pierce, SB., Gersak, K, Michaelson-Cohen, R., Walsh, T., Lee, MK., Malach, D., Klevit, RE., King, M-C., Levy-Lehad, E. "Mutations in *LARS2*, encoding mitochondrial leucyl-tRNA synthetase, lead to premature ovarian failure and hearing loss in Perrault syndrome" *American Journal of Human Genetics* 92(4):614-620 (2013).

Pierson, TM., Adams, D., Bonn, F., Martinelli, P., Cherukuri, PF., Teer, JK., Hansen, NF., Cruz, P., Mullikin, JC., Blakesley, RW., Golas, G., Kwan, J., Sandler, A., Fajardo, KF., Markello, T., Tifft, C., Blackstone, C., Rugarli, EI., Langer, T., Gahl, WA., Toro, C. "Whole-exome sequencing idenfies homozygous *AFG3L2* mutations in a spastic ataxia-neuropathy syndrome linked to mitochondrial m-AAA proteases" *PLOS Genetics* 7(10):e1002325

Pinti, M., Gibellini, L., De Biasi, S., Nasi, M., Roat, E., O'Connor, JE., Cossarizza, A. "Functional characterization of the promoter of the human Lon protease gene" *Mitochondrion* 11(1):200-206 (2011).

Pitceathly, RD., Rahman, S., Wedatilake, Y., Polke, JM., Cirak, S., Foley, AR., Sailer, A., Hurles, ME., Stalker, J., Hargreaves, I., Woodward, CE., Sweeney, MG., Muntoni, F., Houlden, H., Taanman, JW., Hannah, MG. "NDUFA4 mutations underlie dysfunction of a cytochrome *c* oxidase subunit linked to human neurological disease" *Cell Reports* 3(6):1795-805 (2013).

Ponten, J., Saksela, E. "Two established *in vitro* cell lines from human mesenchymal tumours" *International Journal of Cancer* 2:434-447 (1967).

Posse, V., Shahzad, S., Falkenberg, M., Hällberg, BM., Gustafsson, CM. "TEFM is a potent stimulator of mitochondrial transcription elongation *in vitro*" *Nucleic Acids Research* 43(5):2615-2624 (2015).

Potting, C., Wilmes, C., Engmann, T., Osman, C., Langer, T. "Regulation of mitochondrial phospholipids and Ups1/PRELI-like proteins depends on proteolysis and Mdm35" *EMBO Journal* 29(17):2888-2898 (2010).

Potting, C., Tatsuta, T., König, T., Haag, M., Wai, T., Aaltonen, MJ., Langer, T. "TRIAP1/PRELI complexes prevent apoptosis by mediating intramitochondrial transport of phosphatidic acid" *Cell Metabolism* 18(2):287-295 (2013).

Rainbolt, TK., Saunders, JM., Wiseman, RL. "YME1L degradation reduces mitochondrial proteolytic capacity during oxidative stress" *EMBO Reports* 16:97-106 (2015).

Rasmussen, FW., Bendifallah, N., Zachar, V., Shiraishi, T., Fink, T., Ebbesen, P., Nielsen, PE., Koppelhus, U. "Evaluation of transfection protocols for unmodified and modified peptide nucleic acid (PNA) oligomers" *Oligonucleotides* 16(1):43-57 (2006).

Reinders, J., Zahedi, RP., Pfanner, N., Meisinger, C., Sickmann, A. "Toward the complete yeast mitochondrial proteome: Multidimensional separation techniques for mitochondrial proteomics" *Journal of Proteome Research* 5(7):1543-1554 (2006).

Rep, M., van Dijl, JM., Suda, K., Schatz, G., Grivell, LA., Suzuki, CK. "Requirement for the yeast gene LON in intramitochondrial proteolysis and maintenance of respiration" *Science* 274:103-106 (1996).

Reyes, A., Kazak, L., Wood, SR., Yasukawa, T., Jacobs, HT., Holt, IJ. "Mitochondrial DNA replications proceeds via a 'bootlace' mechanism involving the incorporation of processed transcripts" *Nucleic Acids Research* 41(11):5837-5850 (2013).

Richter, R., Rorbach, J., Pajak, A., Smith, PM., Wessels, HJ., Huynen, MA., Smeitink, JA., Lightowlers, RN., Chrzanwoska-Lightowlers, ZMA. "A functional peptidyl-tRNA hydrolase, ICT1, has been recruited into the human mitochondrial ribosome" *EMBO Journal* 29:1116-1125 (2010).

Rivera, H., Merinero, B., Martinez-Pardo, M., Arroyo, I., Ruiz-Sala, P., Bornstein, B., Serra-Suhe, C., Gallardo, E., Marti, R., Moran, MJ., Ugalde, C., Perez-Jurado, LA., Andreu, AL., Garesse, R., Ugarte, M., Arenas, J., Martin, MA. "Marked mitochondrial DNA depletion associated with a novel *SUCLG1* mutation resulting in lethal neonatal acidosis multi-organ failure, and interrupted aortic arch" *Mitochondrion* 10(4):362-368 (2010).

Robertson, DE., Ding, H., Chelminski, PR., Slaughter, C., Hsu, J., Moomaw, CM., Tokito, M., Daldal, F., Dutton, PL. "Hydroubiquinone-cytochrome c_2 oxidoreductase from *Rhodobacter capsulatus*: definition of a minimal, functional isolated preparation" *Biochemistry* 32:1310-1317 (1993).

Rocha, MC., Grady, JP., Grünewald, A., Vincent, A., Dobson, PF., Taylor, RW., Turnbull, DM., Rygiel, KA. "A novel immunofluorescent assay to investigate oxidative phosphorylation deficiency in mitochondrial myopathy: understanding mechanisms and improving diagnosis" *Scientific Reports* 5: 15037 (2015).

Rodenburg, RJT. "Biochemical diagnosis of mitochondrial disorders" *Journal of Inherited Metabolic Disease* 34(2):283-292 (2011).

Rodríguez-Ezpeleta, N. and Embley, TM. "The SAR11 group of alpha-proteobacteria is not related to the origin of mitochondria" *PLoS One* 7(1): e30520 (2012).

Rorbach, J. *"Ribosome recycling in human mitochondria"* PhD Thesis, Newcastle University (2008).

Rorbach, J., Richter, R., Wessels, HJ., Wydro, M., Pekalski, M., Farhoud, M., Kühl, I., Gaisne, M., Bonnefoy, N., Smeitink, JA., Lightowlers, RN., Chrzanowska-Lightowlers, ZMA. "The human mitochondrial ribosome recycling factor is essential for cell viability" *Nucleic Acids Research* 36:5787-5799 (2008).

Rorbach, J., Minczuk, M. "The post-transcriptional life of mammalian mitochondrial RNA" *Journal of Biochemistry* 444:357-373 (2012).

Rorbach, J., Gammage, P., Minczuk, M. "C7orf30 is necessary for biogenesis of the large subunit of the mitochondrial ribosome" *Nucleic Acids Research* 40:4097-4109 (2012).

Rorbach, J., Gao, F., Powell, CA., D/Souza, A., Lightowlers, RN., Minczuk, M., Chrzanowska-Lightowlers, ZMA. "Human mitochondrial ribosomes can switch their structural RNA composition" *Proceedings of the National Academy of Sciences* 113(43):12198-12201 (2016).

Ross, JM. "Visualization of mitochondrial respiratory function using cytochrome *c* oxidase/succinate dehydrogenase (COX/SDH) double-labeling histochemistry" *Journal of Visualised Experiments* 57:3266 (2011).

Rossmanith, W. "Processing of human mitochondrial $tRNA^{Ser(AGY)}$: a novel pathway in tRNA biosynthesis" *Journal of Molecular Biology* 265:365-371 (1997).

Rossmanith, W., Karwan, RM. "Characterization of human mitochondrial RNaseP: novel aspects in tRNA processing" *Biochemical and Biophysical Research Communications* 247(2):234-241 (1998).

Rouzier, C., Le Guédard-Méreuze, S., Fragaki, K., Serre, V., Miro, J., Tuffery-Giraud, S., Chaussenot, A., Bannwarth, S., Caruba, C., Ostergaard, E., Pellisier, J-F., Richelme, C., Espil, C., Chabrol, B., Paquis-Flucklinger, V. "The severity of phenotype linked to *SUCLG1* mutations could be correlated with residual amount of SUCLG1 protein" *Journal of Medical Genetics* 47:670-676 (2010).

Rozanska, A., Richter-Dennerlein, R., Rorbach, J., Gao, F., Lewis, RJ., Chrzanowska-Lightowlers, ZMA., Lightowlers, RN. "The human RNA-binding protein RBFA promotes the maturation of the mitochondrial ribosome" *Biochemical Journal* AHEAD OF PRINT

Rutter, J., Winge, DR., Schiffman, JD. "Succinate dehydrogenase – assembly, regulation and role in human disease" *Mitochondrion* 10(4):393-401 (2010).

Sacco, T., Boda, E., Hoxha, E., Pizzo, R., Cagnoli, C., Brusco, A., Tempia, F. "Mouse brain expression patterns of *Spg7, Afg3l1* and *Afg3l2* transcripts, encoding for the mitochondrial *m*-AAA protease" *BMC Neuroscience* 11:55 (2010).

Saveliev, S., Bratz, M., Zubarev, R., Szapacs, M., Budamgunta, H., Urh, M. "Trypsin/Lys-C protease mix for enhanced protein mass spectrometry analysis" *Nature Methods* 10(11) (2013).

Scaduto, RC Jr., Grotyohann, LW. "Measurement of mitochondrial membrane potential using fluorescent rhodamine derivatives" *Biophysical Journal* 76:469-477 (1999).

Schuwirth, BS., Borovinskaya, MA., Hau, CW., Zhang, W., Vila-Sanjurjo, A., Holton, JM., Doudna Cate, JH. "Structures of the Bacterial Ribosome at 3.5Å Resolution" *Science* 310(5749):827-834 (2005).

Scorrano, L., Ashiya, M., Buttle, K., Weiler, S., Oakes, SA., Mannella, CA., Korsmeyer, SJ. "A distinct pathway remodels mitochondrial cristae and mobilises cytochrome *c* during apoptosis" *Developmental Cell* 2:55-67 (2002).

Schägger, H., Pfeiffer, K. "Supercomplexes in the respiratory chain of yeast and mammamlian mitochondria" *EMBO Journal* 19:1777-1783 (2000).

Schmidt, B., Neupert, W. "Processing of precursors of mitochondrial proteins" *Biochemical Society Transactions* 12(6):920-921 (1984).

Schwartzbach, CJ. And Spremulli, LL. "Interaction of animal mitochondrial EF-Tu·Ts with aminoacyl-tRNA, guanine nucleotides and ribosomes" *Journal of Biological Chemistry* 266(25):16324-16330 (1991).

Serero, A., Giglione, C., Sardini, A., Martinez-Sanz, J., Meinnel, T. "An unusual peptide deformylase features in the human mitochondrial N-terminal methionine excision pathway" *Journal of Biological Chemistry* 278(52):52953-52963 (2003).

Shebib, SM., Reed, MH., Shuckett, EP., Cross, HG., Perry, JB., Chudley, AE. "Newly recognised syndrome of cerebral, ocular, dental, auricular, skeletal anomalies: CODAS syndrome – a case report" *American Journal of Medical Genetics* 40:88-93 (1991).

Sherratt, HS. "Mitochondria: structure and function" *Nature Reviews Neurology (Paris)* 147(6-7):417-430 (1991).

Shi, Y., Dierckx, A., Wanrooij, PH., Wanrooij, S., Larsson, NG., Wihelmsson, LM., Falkenberg, M., Gustafsson, CM. "Mammalian transcription factor A is a core component of the mitochondrial transcription machinery" *Proceedings of the National Academy of Sciences USA* 109(41):16510-16515 (2012).

Shutt, TE., Gray, MW. "Bacteriophage origins of mitochondrial replication and transcription proteins" *Trends in Biochemical Sciences* 22(2):90-95 (2006).

Siciliano, G., Tessa, A., Petrini, S., Mancuso, M., Bruno, C., Grieco, GS., Malandrini, A., DeFlorio, L., Martini, B., Federico, A., Nappi, G., Santorelli, FM., Murri, L. "Autosomal dominant external ophthalmoplegia and bipolar affective disorder associated with a mutation in the *ANT1* gene" *Neuromuscular Disorders* 13(2):162-1655 (2003).

Siddiqui, SM., Sauer, RT., Baker, TA. "Role of the processing pore of the ClpX AAA+ ATPase in the recognition and engagement of specific protein substrates" *Genes & Development* 18(4):369-374 (2004).

Siepen, JA., Keevil, E-J., Knight, D., Hubbard, SJ. "Prediction of missed cleavage sites in tryptic peptides aids protein identification in proteomics" *Journal of Proteome Research* 6(1):399-408 (2007).

Sirrenberg, C., Bauer, MF., Guiard, B., Neupert, W., Brunner, M. "Import of carrier proteins into the mitochondrial inner membrane mediated by Tim22" *Nature* 384:582-585 (1996).

Smirnova, E., Griparic, L., Shurland, DL., van der Bliek, AM. "Dynamin-related protein Drp1 is required for mitochondrial division in mammalian cells" *Molecular Biology of the Cell* 12:2245-2256 (2001).

Smith, DGS., Gawryluk, RMR., Spencer, DF., Pearlman, RE., Siu, KWM., Gray, MW. "Exploring the mitochondrial proteome of the ciliate protozoon *Tetrahymena thermophile*: Direct analysis by tandem mass spectrometry" *Journal of Molecular Biology* 374(3):837-863 (2007).

Soleimanpour-Lichaei, HR., Kühl, I., Gaisne, M., Passos, JF., Wydro, M., Rorbach, J., Temperley, R., Bonnefoy, N., Tate, W., Lightowlers, RN., Chrzanowska-Lightowlers, ZMA. "MtRF1 is a human mitochondrial trnalsation release factor decoding the major termination codons UAA and UAG" *Molecular Cell* 27:745-757 (2007).

Spinazzola, A., VIscomi, C., Fernandez-Vizzara, E., Carrara, F., D'Adamo, P., Calvo, S., Marsano, RM., Donnini, C., Weiher, H., Strisciuglio, P., Parini, R., Sarzi, E., Chan, A., DiMauro, S., Rötig, A., Gasparini, P., Ferrero, I., Mootha, VK., Tiranti, V., Zeviani, M. "*MPV17* encodes an inner mitochondrial membrane protein and is mutated in infantile hepatic mitochondrial DNA depletion" *Nature Genetics* 38:570-575 (2006).

Stewart, JB., Chinnery, PF. "The dynamics of mitochondrial DNA heteroplasmy: implications for human health and disease" *Nature Reviews Genetics* 16:530-542 (2015).

Stiburek, L., Cesnekova, J., Kostkova, O., Fornuskova, D., Vinsova, K., Wenchich, L., Houstek, J., Zeman, J. "YME1L controls accumulation of respiratory chain subunits and is required for apoptotic resistance, cristae morphogenesis and cell proliferation" *Molecular Biology of the Cell* 23(6):1010-1023 (2012).

Strauss, KA., Jinks, RN., Puffenberger, EG., Venkatesh, S., Singh, K., Cheng, I., Mikita, N., Thilagavathi, J., Lee, J., Sarafianos, S., Benkert, A., Koehler, A., Zhu, A., Trovillion, V., McGlincy, M., Morlet, T., Deardorff, M., Innes, AM., Prasad, C., Chudley, AE., Lee, INW., Suzuki, CK. "CODAS syndrome is associated with mutations of *LONP1* encoding mitochondrial AAA+ Lon protease" *American Journal of Human Genetics* 96:121-135 (2015).

Sun, F., Huo, X., Zhai, Y., Wang, A., Xu, J., Su, D., Bartlam, M., Rao, Z. "Crystal structure of mitochondrial respiratory membrane protein complex II" *Cell* 121(7):1043-1057 (2005).

Suzuki, CK., Suda, K., Wang, N., Schatz, G. "Requirement for the yeast gene LON in intramitochondrial proteolysis and maintenance of respiration" *Science* 264(5156):273-276 (1994).

Szczepanowska, K., Maiti, P., Kukat, A., Hofsetz., E., Nolte, H., Senft, K., Becker, C., Ruzzenente, B., Hornig-Do, H-T., Wibom, R., Wiesner, RJ., Krüger, M., Trifunovic, A. "CLPP coordinates mitoribosomal assembly through the regulation of ERAL1 levels" *EMBO Journal* 35:2566-2583 (2016).

Szklarczyk, R., Wanschers, BFJ., Cuypers, TD., Esseling, JJ., Riemersma, M., van der Brand, MAM., Gloerich, J., Lasonder, E., van den Heuvel, LP., Nijtmans, LG., Huynen, MA. "Iterative orthology prediction uncovers new mitochondrial proteins and identifies C12orf62 as the human ortholog of COX14, a protein involved in the assembly of cytochrome *c* oxidase" *Genome Biology* 13(2):R12 (2012).

Takahashi, M., Takaku, H., Nashimoto, M. "Regulation of the human tRNase ZS gene expression" *FEBS Letters* 582(17):2532-2536 (2008).

Temperley, RJ., Wydro, M., Lightowlers, RN., Chrzanowksa-Lightowlers, ZMA. "Human mitochondrial mRNAs – like members of all families, similar but different" *Biochimica et Biophysica Acta* 1797(6-7):1081-1085 (2010a).

Temperley, RJ., Richter, R., Dennerlein, S., Lightowlers, RN., Chrzanowska-Lightowlers, ZMA. "Hungry codons promote frameshifting in human mitochondrial ribosomes" *Science* 327(5963):301 (2010b).

Thompson, K. "*Investigating the role of AURKAIP1 in mitochondrial gene expression"*. PhD thesis, Newcastle University (2014).

Thompson, K., Majd, H., Dallabona, C., Reinson, K., King, MS., Alston, CL., He, L., Lodi, T., Jones, SA., Fattal-Valevski, A., Fraenkel, ND., Sada, A., Haham, A., Isohanni, P., Vara, R., Barbosa, IA., Simpson, MA., Deshpande, C., Puusepp, S., Bonnen, PE., Rodenburg, RJ., Suomalainen, A., Õunao, K., Elpeleg, O., Ferrero, I., McFarland, R., Kunji, ES., Taylor, RW. "Recurrent *de novo* dominant mutations in *SLC25A4* cause severe early-onset mitochondrial disease and loss of mitochondrial DNA copy number" *American Journal of Human Genetics* 99(4):860-876 (2016).

Thrash, JC., Boyd, A., Huggett, MJ., Grote, J., Carini, P., Yoder, RJ., Robbertse, N., Spatafora, JW., Rappé, MS., Giovannoni, SJ. "Phylogenomic evidence for a common ancestor of mitochondria and the SAR11 clade" *Nature Scientific Reports* 1(13):1-9 (2011).

Tielens, AGM., Rotte, C., van Hellemon, JJ., Martin, W. "Mitochondria as we don't know them" *Trends in Biochemical Sciences* 27(11):564-572 (2002).

Tovar, J., Fischer, A., Clark, CG. "The mitosomes, a novel organelle related to mitochondria in the amitochondrial parasite *Entamoebia histolytica*" *Molecular Microbiology* 32(5):1013-1021 (1999).

Trumpower, BL., "The protonmotive Q cycle: Energy transduction by coupling of proteon translocation to electron transfer by the cytochrome bc_1 complex" *Journal of Biological Chemistry* 265(20):11409-11412 (1990).

Truscott, KN., Voos, W., Frazier, AE., Lind, M., Li, Y., Geissler, A., Dudek, J., Müller, H., Sickmann, A., Meyer, HE., Meisinger, C., Guiard, B., Rehling, P., Pfanner, N. "A J-protein is an essential subunit of the presequence translocase-associated protein import motor of mitochondria" *Journal of Cell Biology* 163(4):707-713 (2003).

Tsuboi, M., Morita, H., Nozaki, Y., Akama, K., Ueda, T., Ito, K., Nierhaus, K. "EF-G2mt is an exclusive recycling factor in mammalian mitochondrial protein synthesis" *Molecular Cell* 35:502-510 (2009).

Tsukihara, T., Aoyama, H., Yamashita, E., Tomizaki, T., Yamaguchi, H., Shinzawa-Itoh, K., Nakashima, R., Yaono, R., Yoshikawa, S. "The whole structure of the 13-subunit oxidised cytochrome *c* oxidase at 2.8Å" *Science* 272(5265):1136-1144 (1996).

Tu, YT., Barrientos, A. "The human mitochondrial DEAD-box protein DDX28 resides in RNA granules and functions in mitoribosome assembly" *Cell Reports* 10:854-864 (2015).

Tuppen, HA., Blakely, EL., Turnbull, DM., Taylor, RW. "Mitochondrial DNA mutations and human disease" *Biochimica et Biophysica Acta* 1797:113-128 (2009).

Uhlen, A., Oksvold, P., Fagerberg, L., Lundberg, E., Jonasson, K., Forsberg, M., Zwahlen, M., Kampf, C., Wester, K., Hober, S., Wernerus, H., Björling, K., Ponten, F. "Towards a knowledge-based Human Protein Atlas" *Nature Biotechnology* 28:1248-1250 (2010).

Urbani, A., De Canio, M., Palmieri, F., Sechi, S., Bini, L., Castagnola, M., Fasano, M., Modesti, A., Roncada, P., Timperio, AM., Bonizzi, L, Brunori, M., Cutruzzola, F., De Pinto, V., De ilio, C., Deferici, G., Folli, F., Foti, S., Gelfi, C., Lauro, D., Lucacchini, A., Magni, F., Messana, I., Pandolfi, PP., Papa, S., Pucci, P., Sacchetta, P., Italian mt-HPP Study Group-Italian Proteomics Association (www.itpa.it) "The mitochondrial Italian Human Proteome Project initiative (mt-HPP)" *Molecular BioSystems* 9:1984-1992 (2013).

Valgardsdottir, R., Brede, G., Eide, LG., Frengen, E., Prydz, H. "Cloning and characterization of MDDX28, a putative dead-box helicase with mitochondrial and nuclear localization" *Journal of Biological Chemistry* 276:32056-32063 (2001).

Vande Walle, L., Lamkanfi, M., Vandenabeele, P. "The mitochondrial serine protease HtrA2/Omi: an overview" *Cell Death and Differentiation* 15(3):453-460 (2008).

Van den Heuvel, LP., Smeitink, JA., Rodenburg, RJ. "Biochemical examination of fibroblasts in the diagnosis and research of oxidative phosphorylation (OXPHOS) defects" *Mitochondrion* 4(56):395-401 (2004).

Venkatesh, S., Lee, J., Singh, K., Lee, I., Suzuki, CK. "Multitasking in the mitochondrion by the ATP-dependent Lon protease" *Biochimica et Biophysica Acta* 1823(1):56-66 (2012).

Vinothkumar, KR., Zhu, J., Hirst, J. "Architecture of mammalian respiratory complex I" *Nature* 515(7525):80-84 (2014).

Vögtle, FN., Prinz, C., Kellermann, J., Lottspeich, F., Pfanner, N., Meisinger, C. "Mitochondrial protein turnover: role of the precursor intermediate peptidase Oct1 in protein stabilization" *Molecular Biology of the Cell* 22(13):2135-2143 (2011).

Walker, JE., Saraste, M., Runswick, MJ., Gay, NJ. "Distantly related sequences in the α- and β-subunits of ATP synthase, myosin, kinases and other ATP-requiring enzymes and a common nucleotide binding fold" *EMBO Journal* 1(8):945-951 (1982).

Wang, L., Limongelli, A., Vila, MR., Carrara, F., Zeviani, M., Eriksson, S. "Molecular insight into mitochondrial DNA depletion syndrome in two patients with novel mutations in the deoxyguanosine kinase and thymidine kinase 2 genes" *Molecular Genetics and Metabolism* 84(1):75-82 (2005).

Ward, B., Anderson, R., Bendich, A. "The size of the mitochondrial genome is large and variable in a family of plants (Cucurbitaceae)" *Cell* 25:793-803 (1981).

Wesolowska, MT., Richter-Dennerlein, R., Lightowlers, RN., Chrzanowska-Lightowlers, ZMA. "Overcoming stalled translation in human mitochondria" *Frontiers in Microbiology* 5:374 (2014)

Wiedemann, N., Truscott, KN., Pfannschmidt, S., Guiard, B., Meisinger, C., Pfanner, N. "Biogenesis of the protein import channel Tom40 of the mitochondrial outer membrane: intermembrane space components are involved in an early stage of the assembly pathway" *Journal of Biological Chemistry* 279:18188-18194 (2004).

Wohlever, ML, Baker, TA., Sauer, RT. "Roles of the N domain of the AAA+ Lon protease in substrate recognition, allosteric regulation and chaperone activity" *Molecular Microbiology* 91:66-78 (2014).

Wong, L-JC., Brunetti-Pierri, N., Zhang, Q., Yazigi, N., Bove, KE., Dahms, BB., Puchowicz, MA., Gonzalez-Gomez, I., Schmitt, ESS., Truong, CK., Hoppel, CL., Chou, P-C., Wang, J., Baldwin, EE., Adams, D., Leslie, N., Boles, RG., Kerr, DS., Craigen, WJ. "Mutations in the *MPV17* gene are responsible for rapidly progressive liver failure in infancy" *Hepatology* 46(4):1218-1227 (2007).

Xu, F., Ackerley, C., Maj, MC., Addis, JBL., Levandovskiy, V., Lee, J., MacKay, N., Cameron, JM., Robinson, BH. "Disruption of a mitochondrial RNA-binding protein gene results in decreased cytochrome b expression and a marked reduction in ubiquinol-cytochrome c reductase activity in mouse heart mitochondria" *Biochemical Journal* 416(1):15-26 (2008).

Yamaguchi, R., Lartigue, L., Perkins, G., Scott, RT., Dixit, A., Kushnareva, Y., Kuwana, T., Ellisman, MH., Newmeyer, DD. "Opa1-mediated cristae opening is Bax.Bak and BH3 dependent, required for apoptosis, and independent of Bak oligomerization" *Molecular Cell* 31:557-569 (2008).

Yang, MY., Bowmaker, M., Reyes, A., Vergani, L., Angeli, P., Gringeri, E., Jacobs, HT., Holt, IJ. "Biased incorporation of ribonucleotides on the mitochondrial L-strand accounts for apparent strand-asymmetric DNA replication" *Cell* 111:495-505 (2002).

Yasukawa, T., Reyes, A., Cluett, TJ., Yang, MY., Bowmaker, M., Jacobs, HT., Holt, IJ. "Replication of vertebrate mitochondrial DNA entails transient ribonucleotide incorporation throughout the lagging strand" *EMBO Journal* 25:5358-5371 (2006).

Yoo, YA., Kim, MJ., Park, JK., Chung, Ym., Lee, JH., Chi, SG *et al.* "Mitochondrial ribosomal protein L41 suppresses cell growth in association with p53 and p27Kip1" *Molecular Cell Biology* 25:6603:6616 (2005).

Yoon, Y., Krueger, EW., Oswald, BJ., McNiven, MA. "The mitochondrial protein hFis1 regulates mitochondrial fission in mammalian cells through an interaction with the dynamin-like protein DLP1" *Molecular Biology of the Cell* 23:5409-5420 (2003).

Zeng, X., Neupert, W., Tzagoloff, A. "The metalloprotease encoded by ATP23 has a dual function in processing and assembly of subunit 6 of mitochondrial ATPase" *Molecular Biology of the Cell* 18(2):617-626 (2007).

Zhang, Z. and Falk, MJ. "Integrated transcriptome analysis across mitochondrial disease etiologies and tissues improves understanding of common cellular adaptations to respiratory chain dysfunction" *International Journal of Biochemistry & Cell Biology* 50:106-111 (2014).

Zhao, Z., Su, W., Yuan, S., Huang, Y. "Functional conservation of tRNaseZL among *Saccharomyces cerevisiae*, *Schizosaccharomyces pombe* and humans" *The Biochemical Journal* 422(3):483-492 (2009).

Zick, M., Rabl, R., Reichert, AS. "Cristae formation – linking ultrastructure and function in mitochondria" *Biochimica et Biophysica Acta* 1793(1):5-19 (2009).

PUBLICATION ARISING

Bradley, P. and Waddington CL., Sommerville, EW., Hopton, S., Pyle, A., Champion, M., Ohlson, M., Siibak, T., Chrzanowska-Lightowlers, ZMA., Taylor, RW., Falkenberg, M., Lightowlers, RN. "Defective mitochondrial protease LonP1 can cause classical mitochondrial disease" *Human Molecular Genetics* 27(10):1743-1753 (2018).

APPENDICES

Appendix A: Vector Maps

A - Vector pcDNA5/FRT/TO™ was used for the cloning of AURKAIP1, AURKAIP1-FLAG and LONP1 exons 10-15. **B** - pET-20b+ was used for the cloning of LONP1-WT-His, LONP1-Y565H-His and LONP1-E733K-His, by Miss Monica Olsson. **C** - pGEM-4 was used for the cloning of SU9-DHFR, from Professor Roland Lill.

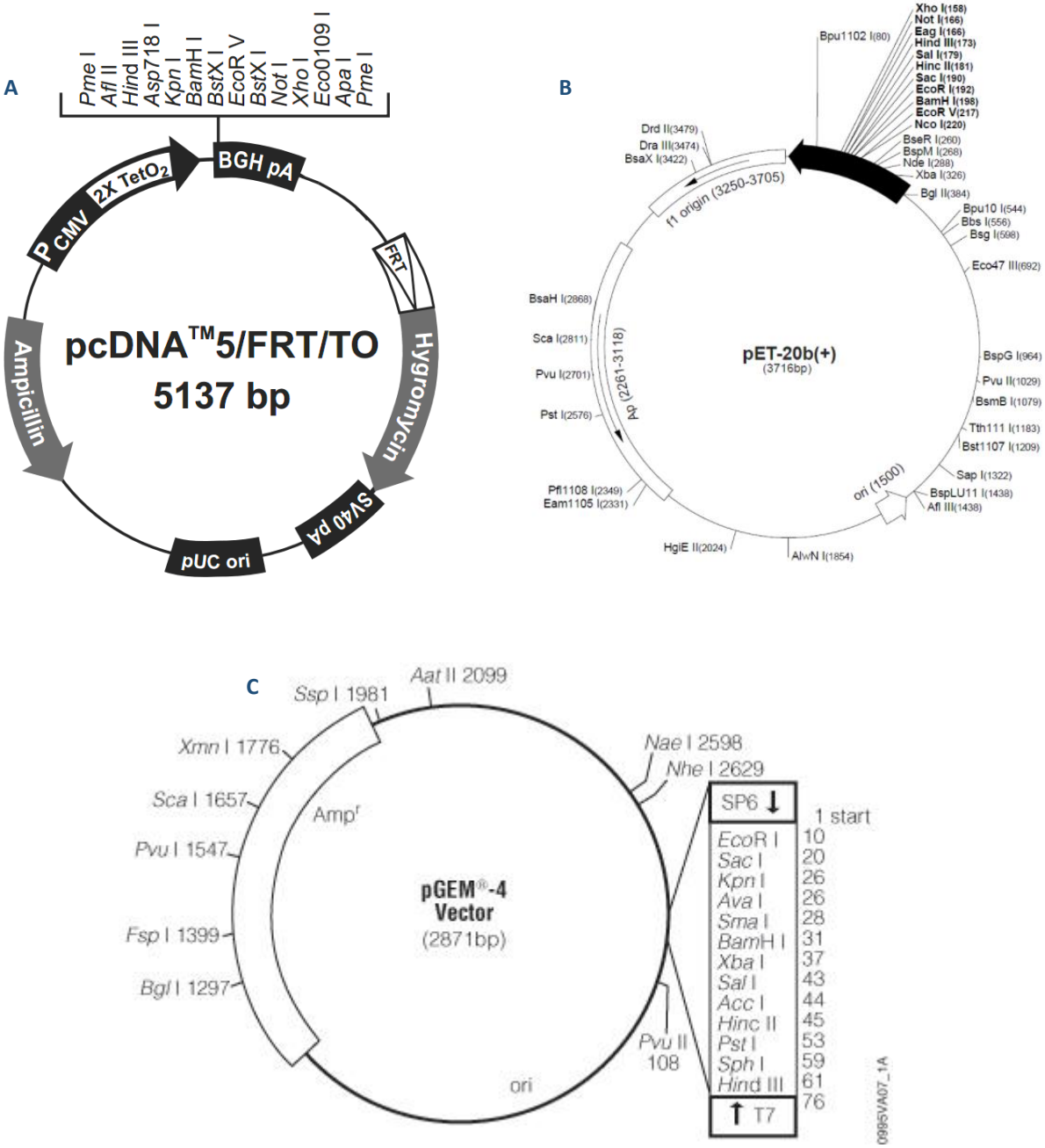

Appendix B: siRNA Duplexes

siRNA	Sense/antisense	Sequence (5'-3', with 3'-dTdT overhangs)	Stock conc'n	Final conc'n
Hs_AFG3L2_1 (AFG3L2 siRNA)	Sense	GGC-ACC-AAU-CGA-CCA-GAU-A	20µm	33nM
	Antisense	UUU-CUG-GUC-GAU-UGG-UGC-CGG		
Hs_CLPP_1 (CLPP siRNA)	Sense	CGA-UGC-AGU-ACA-UCC-UCA-A	20µm	33nM
	Antisense	UUG-AGG-AUG-UAC-UGC-AUC-GTG		
Hs_CLPX_3 (CLPX siRNA)	Sense	GAU-UGG-CAC-UAG-AAC-GAA-A	20µm	33nM
	Antisense	UUU-CGU-UCU-AGU-GCC-AAU-CTG		
Hs_PRSS15_1 (LONP1 siRNA)	Sense	CGC-GCU-UUA-UCA-AGA-UUA-U	20µm	33nM
	Antisense	AUA-AUC-UUG-AUA-AAG-CGC-GGG		
AUR1_siRNA1	Sense	GAU-GAA-CCA-CCA-CAA-GUA-C	20µm	33nM
	Antisense	GUA-CUU-GUG-GUG-GUU-CAU-C		
AUR1_siRNA2	Sense	GUA-CCG-GAA-GCU-GGU-GAA-G	20µm	33nM
	Antisense	CUU-CAC-CAG-CUU-CCG-GUA-C		
Non-Targeting	Sense+antisense	OR-0030-NEG05 (Eurogentec)	20µm	33nM

Appendix C: PCR Primers

Red lettering – nucleotides that were changed in the DNA template to change leucine to methionine. Bold lettering – binds to the reference sequence.

Primer	For/ Rev	Sequence (5'-3')	T_m	Ref. Seq	Nts
AURKForSP6	For	ATT-TAG-GTG-ACA-CTA-TAG-ACC-ACA-GAC-**CAT-GCT-CCT-G**	58°C	NM_017900.2	320-328
SP6TransSyn	For	ATT-TAG-GTG-ACA-CTA-TAG-ACC-ACA-GAC-**CAT-G**GT-TCT-GG	56°C	NM_017900.2	320-329
AURKRev	Rev	ATA-CTA-CTC-GAG-**CGG-ATC-ACA-GCA-GCA-ACG**	58°C	NM_017900.2	959-942
AURKRevFLAG	Rev	ATA-CTA-CTC-GAG-CTA-CTT-ATC-GTC-GTC-ATC-CTT-GTA-ATC-G**CC-CGC-AGG-TAG-ATC-TTG-G**	58°C	NM_017900.2	921-893
MtVal_For	For	**CAG-AGT-GTA-GCT-TAA-CAC-AAA-G**	52°C	**NC_012920**	1602-1623
MtVal_Rev	Rev	**CAC-TTA-GGA-GAT-TTC-AAC-TTA-A**	52°C	**NC_012920**	1656-1635
MtPhe_Ex_F	For	**ACC-GCT-GCT-AAC-CCC-ATA**	52°C	**NC_012920**	523-540
MtPhe_Ex_R	Rev	**GCT-AAT-AGA-AAG-GCT-AGG-A**	52°C	**NC_012920**	677-659
MtLeu1_For	For	**TAT-ACC-CAC-ACC-CAC-CCA-AG**	52°C	**NC_012920**	3200-3219
MtLeu1_Rev	Rev	**GCG-ATT-AGA-ATG-GGT-ACA-AT**	52°C	**NC_012920**	3353-3334
LON_ex10_F	For	TAC-TAT-AAG-CTT-**CTG-AAC-CGA-GAG-TAC-TTC-C**	58°C	NM_004793.3	1744-1762
LON_ex15_R	Rev	ATA-CTA-CTC-GAG-**AAG-TCC-TCC-TGC-AGG-TTC-TCG**	58°C	NM_004793.3	2343-2360

Appendix D: qPCR Primers

qPCR Primer	For/Rev	Gene	Sequence (5'-3')	T_m
18S_qPCR_For	For	*18S rRNA*	GTA-ACC-CGT-TGA-ACC-CCA-TT	59°C
18S_qPCR_Rev	Rev	*18S rRNA*	CCA-TCC-AAT-CGG-TAG-TAG-CG	59°C
hRNaseMRP_For	For	*RMRP*	CGT-GCT-GAA-GGC-CTG-TAT-CC	62°C
hRNaseMRP_Rev	Rev	*RMRP*	ACT-TTC-CCC-TAG-GCG-GAA-AG	56°C
APP_qPCR_For	For	*APP*	TTT-TTG-TGT-GCT-CTC-CCA-GGT-CT	64°C
APP_qPCR_Rev	Rev	*APP*	TGG-TCA-CTG-GTT-GGT-TGG-C	58°C
AUR1_qPCR_For	For	*AURKAIP1*	GCT-GCT-TCC-TGC-CCA-GAC	58°C
AUR1_qPCR_Rev	Rev	*AURKAIP1*	CGC-CTT-CAT-CCC-CCT-GCT	58°C
16S_qPCR_For	For	*MTRNR2*	CCA-ATT-AAG-AAA-GCG-TTC-AAG	58°C
16S_qPCR_Rev	Rev	*MTRNR2*	CAT-GCC-TGT-GTT-GGG-TTG-ACA	64°C
12S_qPCR_For	For	*MTRNR1*	ACA-CTA-CGA-GCC-ACA-G	50°C
12S_qPCR_Rev	Rev	*MTRNR1*	ACC-TTG-ACC-TAA-CGT-CT	50°C
Val16SFor	For	*MT-TV, MTRNR2*	CAA-CTT-AAC-TTG-ACC-GCT-C	56°C
Val16SRev	Rev	*MT-TV, MTRNR2*	AGG-TTT-CAA-TTT-CTA-TCG-CC	56°C
MTCOII_qPCR_For	For	*MT-COII*	CGT-CTG-AAC-TAT-CCT-GCC-CG	64°C
MTCOII_qPCR_Rev	Rev	*MT-COII*	TGG-TAA-GGG-AGG-GAT-CGT-TG	62°C

Appendix E: Primers used for Sanger Sequencing

Sequencing Primer	For/Rev	Sequence (5'-3')	T_m
CMV Forward	For	CGC-AAA-TGG-GCG-GTA-GGC-GTG	50°C
BGH Reverse	Rev	TAG-AAG-GCA-CAG-TCG-AGG	50°C

Appendix F: Oligonucleotide Sequences for EMSA

Oligonucleotide	Location on mtDNA (NC_012920)	Sequence (5'-3')
Oligo 262	m.12021-12100	ACC-ACA-TTA-ACA-ACA-TAA-AAC-CCT-CAT-TCA-CAC-GAG-AAA-ACA-CCC-TCA-TGT-TCA-TAC-ACC-TAT-CCC-CCA-TTC-TCC-TCC-TA
Oligo 263	m.12100-12021	TAG-GAG-GAG-AAT-GGG-GGA-TAG-GTG-TAT-GAA-CAT-GAG-GGT-GTT-TTC-TCG-TGT-GAA-TGA-GGG-TTT-TAT-GTT-GTT-AAT-GTG-GT
HSP_sense	m.500-550	CCC-ATC-CTA-CCC-AGC-ACA-CAC-ACA-CCG-CTG-CTA-ACC-CCA-TAC-CCC-GAA-CC
HSP_antisense	m.550-500	GGT-TCG-GGG-TAT-GGG-GTT-AGC-AGC-GGT-GTG-TGT-GTG-CTG-GGT-AGG-ATG-GG
LSP_sense	m.400-450	TTA-TCT-TTT-GGC-GGT-ATG-CAC-TTT-TAA-CAG-TCA-CCC-CCC-AAC-TAA-CAC-AT
LSP_antisense	m.450-400	ATG-TGT-TAG-TTG-GGG-GGT-GAC-TGT-TAA-AAG-TGC-ATA-CCG-GGA-AAA-GAT-AA

Appendix G: Restriction Enzymes

Restriction Enzyme	Recognition Sequence	Temperature	Digestion Time	Manufacturer
*Hind*III	A^AGCTT	37°C	3hrs	Promega
*Xho*I	C^TCGAG	37°C	3hrs	Roche
*Pvu*II	CAG^CTG	37°C	5hrs	Promega
*Bgl*II	A^GATCT	37°C	1.5hrs	NEB
*EcoR*I-HF	G^AATTC	37°C	1hr	NEB

Appendix H: Sanger Sequencing of HEK-AURKAIP1 clones 1 and 2

HEK-AURKAIP1 clone 1

AURKAIP1 sequenced is indicated by […] below.

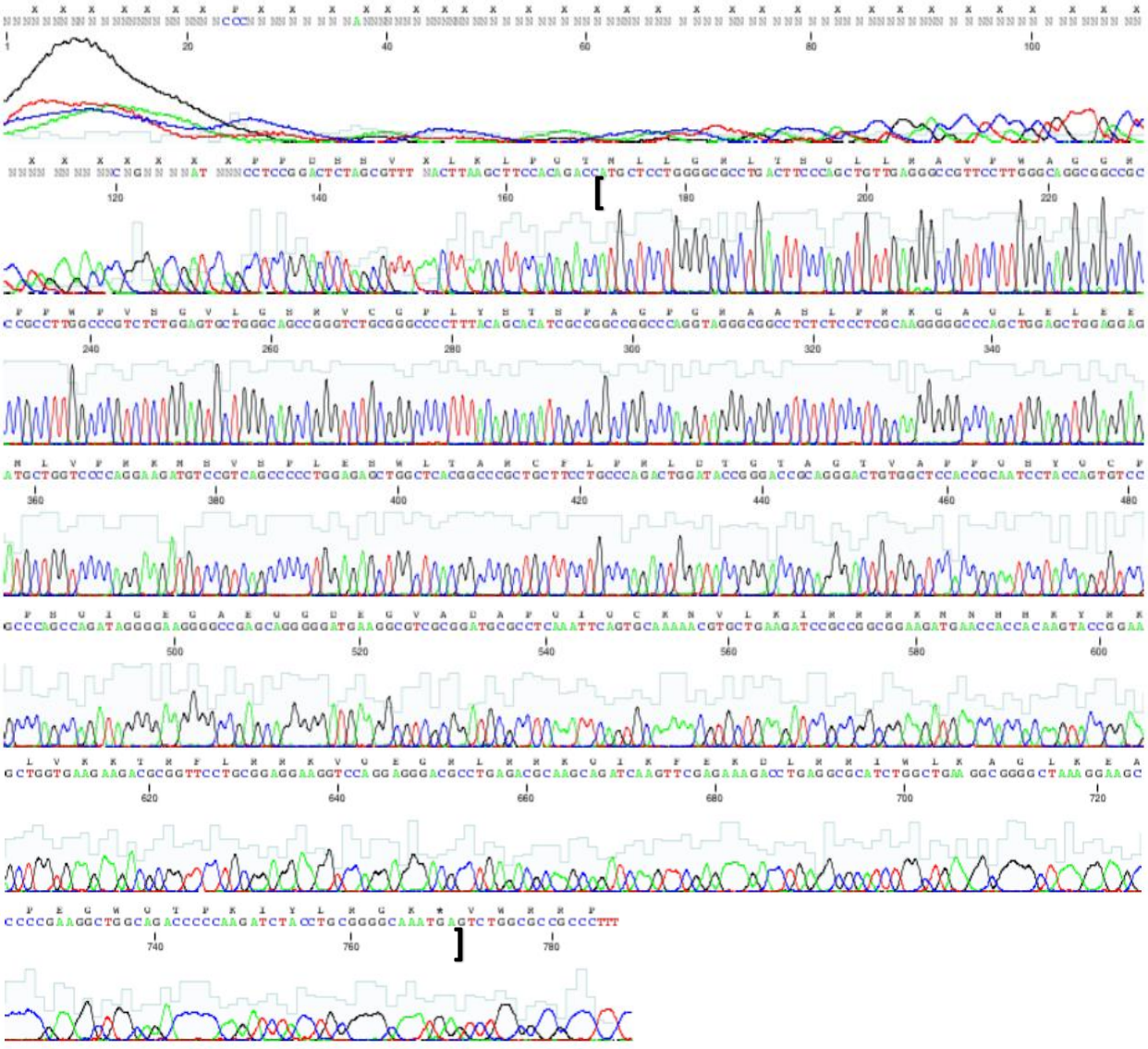

HEK-AURKAIP1 clone 2

AURKAIP1 sequenced is indicated by […] below.

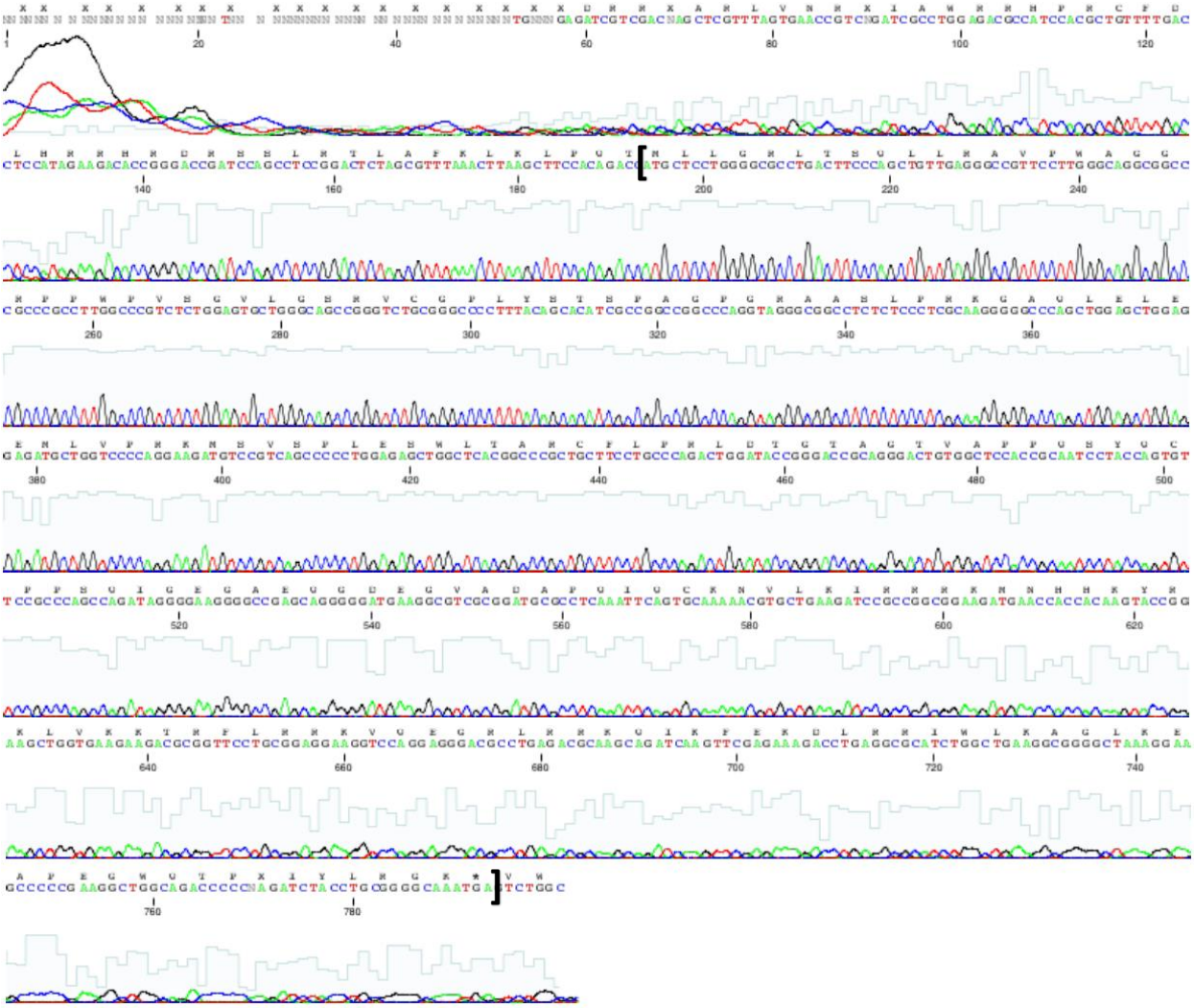

Appendix I: Sanger Sequencing of LONP1 exons 10-15 in patient

Clones containing the p.Tyr565His (c.1693T>C) mutation only

LONP1_cl1_Forward

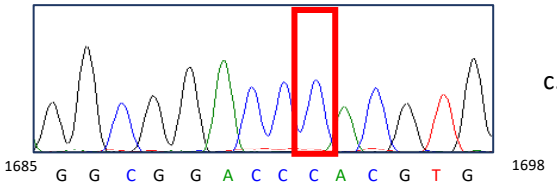

c.1693T>C (p.Tyr565His) is present

LONP1_cl1_Reverse

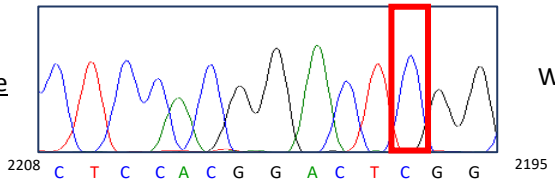

WT

LONP1_cl7_Forward

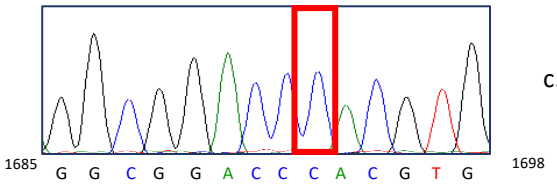

c.1693T>C (p.Tyr565His) is present

LONP1_cl7_Reverse

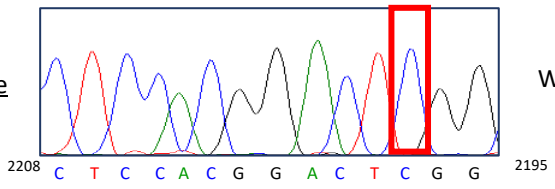

WT

LONP1_cl8_Forward

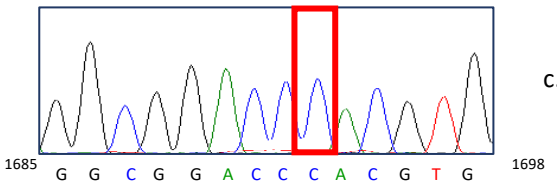

c.1693T>C (p.Tyr565His) is present

LONP1_cl8_Reverse

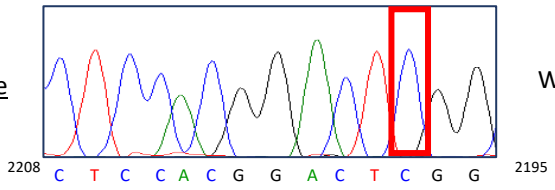

WT

LONP1_cl9_Forward

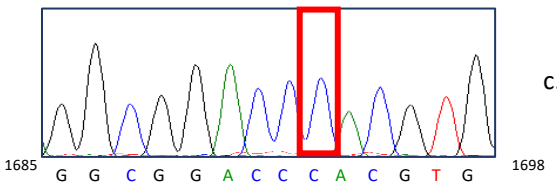

c.1693T>C (p.Tyr565His) is present

LONP1_cl9_Reverse

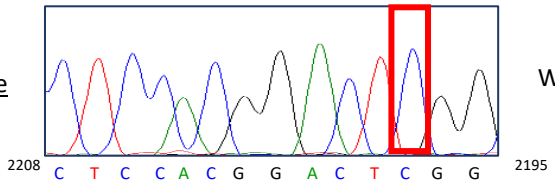

WT

LONP1_cl10_Forward

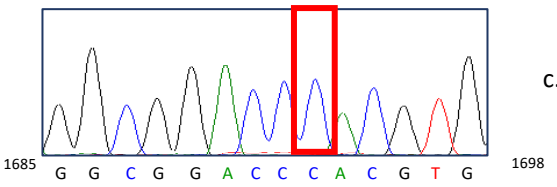

c.1693T>C (p.Tyr565His) is present

LONP1_cl10_Reverse

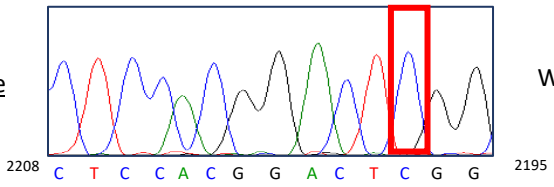

WT

LONP1_cl12_Forward

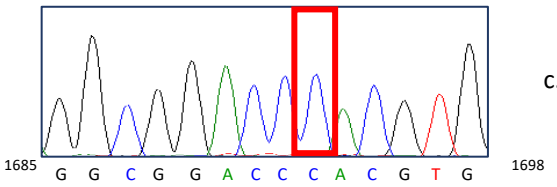

c.1693T>C (p.Tyr565His) is present

LONP1_cl12_Reverse

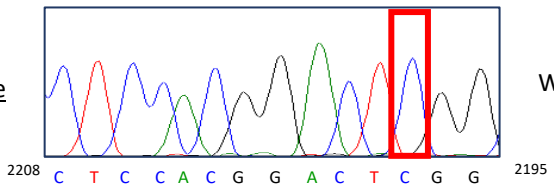

WT

LONP1_cl15_Forward

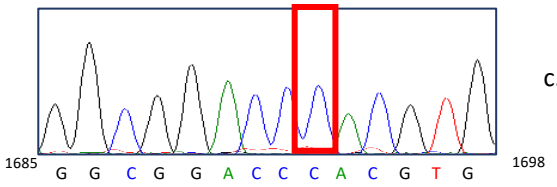

c.1693T>C (p.Tyr565His) is present

LONP1_cl15_Reverse

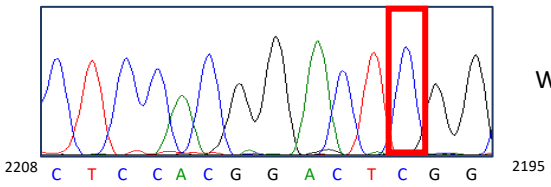

WT

LONP1_cl18_Forward

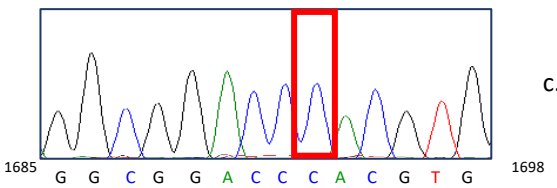

c.1693T>C (p.Tyr565His) is present

LONP1_cl18_Reverse

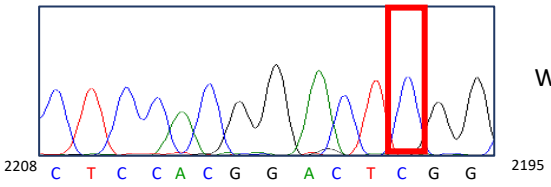

WT

LONP1_cl18_Forward

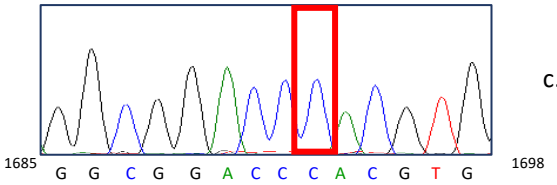

c.1693T>C (p.Tyr565His) is present

LONP1_cl18_Reverse

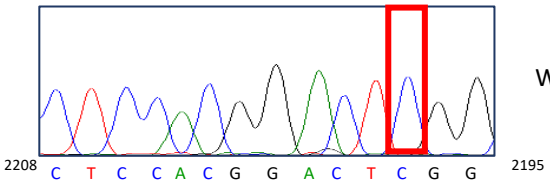

WT

LONP1_cl26_Forward

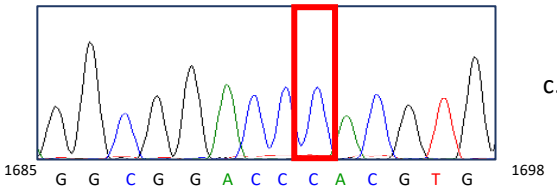

c.1693T>C (p.Tyr565His) is present

LONP1_cl26_Reverse

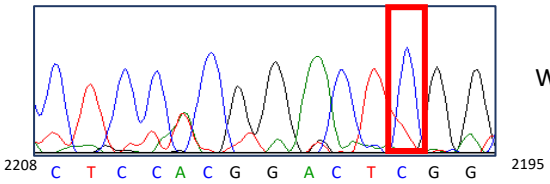

WT

Clones containing the p.Glu733Lys (c.2197G>A) mutation only

LONP1_cl3_Forward

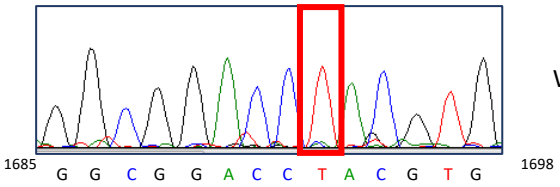

WT

LONP1_cl3_Reverse

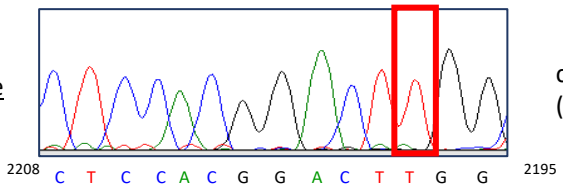

c.2197G>A
(p.Glu733Lys) is present

LONP1_cl5_Forward

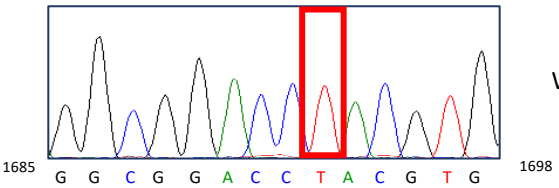

WT

LONP1_cl5_Reverse

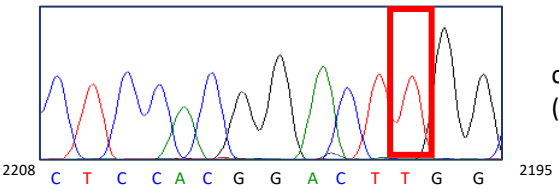

c.2197G>A
(p.Glu733Lys) is present

LONP1_cl11_Forward

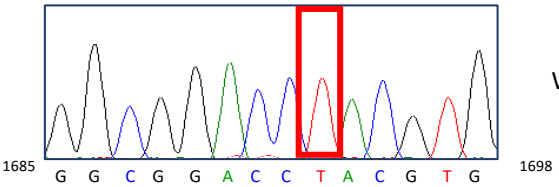

WT

LONP1_cl11_Reverse

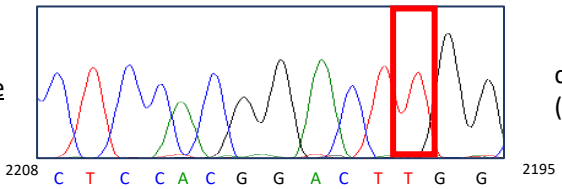

c.2197G>A
(p.Glu733Lys) is present

LONP1_cl21_Forward

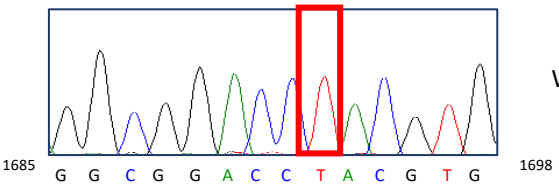

WT

LONP1_cl21_Reverse

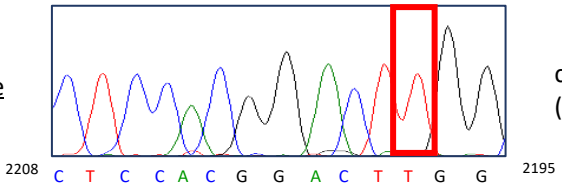

c.2197G>A
(p.Glu733Lys) is present

LONP1_cl22_Forward

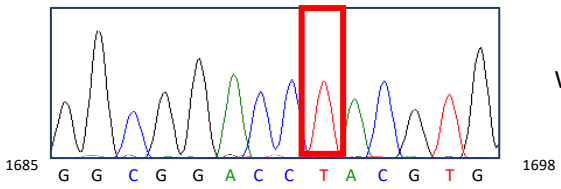

WT

LONP1_cl22_Reverse

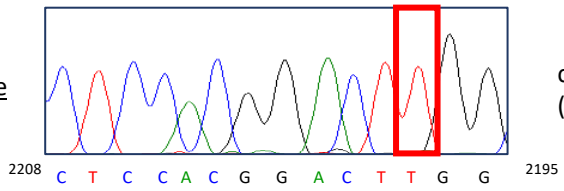

c.2197G>A
(p.Glu733Lys) is present

LONP1_cl36_Forward

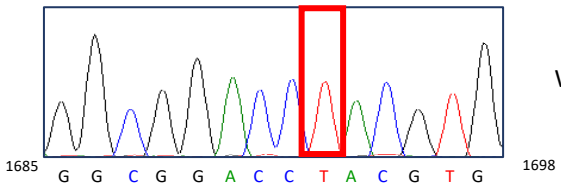

WT

LONP1_cl36_Reverse

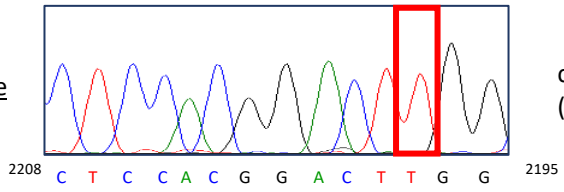

c.2197G>A
(p.Glu733Lys) is present

LONP1_cl37_Forward

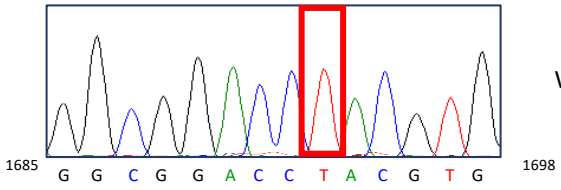

WT

LONP1_cl37_Reverse

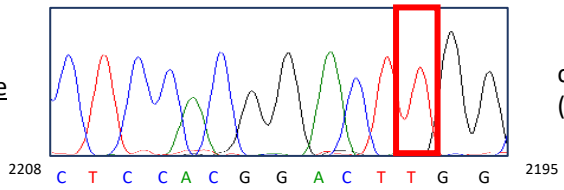

c.2197G>A
(p.Glu733Lys) is present

LONP1_cl16_Reverse

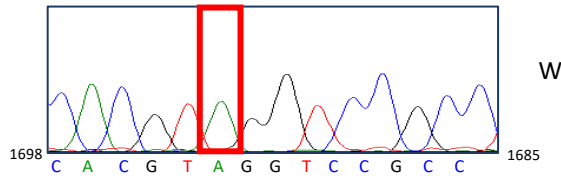

WT

LONP1_cl16_Reverse

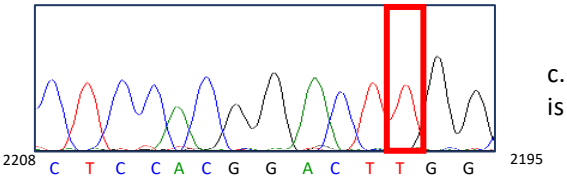

c.2197G>A (p.Glu733Lys)
is present

Due to the use of 40 cycles for PCR of LONP1 exons 10-15, PCR jumping may have occurred which resulted in one wild-type clone, and one double mutant clone. Unfortunately, there was not enough time for me to repeat the cloning, but this is currently ongoing in the lab.

Clone containing the p.Tyr565His (c.1693T>C) and p.Glu733Lys (c.2197G>A)

LONP1_cl42_Forward

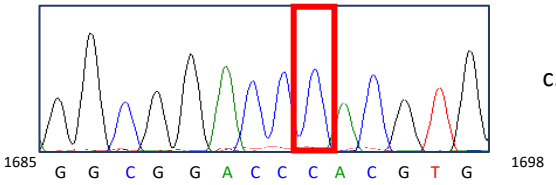

c.1693T>C (p.Tyr565His) is present

LONP1_cl42_Reverse

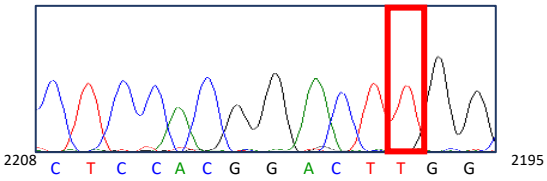

c.2197G>A (p.Glu733Lys) is present

Clone containing no mutations

LONP1_cl17_Forward

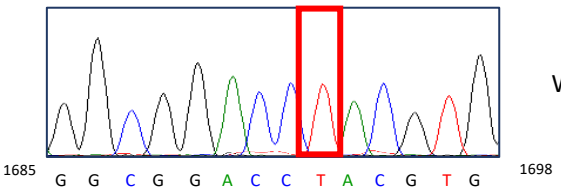

WT

LONP1_cl17_Reverse

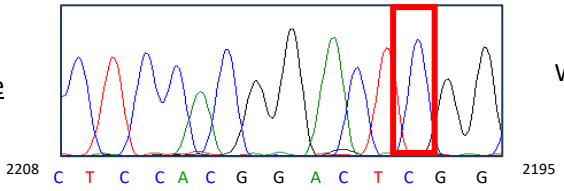

WT

Appendix J: Antibodies Used for Western Blotting

Antibody	Protein Size	Secondary	Dilution	Manufacturer
PRIMARY				
Anti-AFG3L2	88kDa	Rabbit polyclonal	1:1000	Proteintech (14631-1-AP)
Anti-ATP5A	53kDa	Mouse monoclonal	1:1000	Life Technologies (7F9BG1)
Anti-ATP6	18kDa	Rabbit polyclonal	1:600	Proteintech (55313-1-AP)
Anti-AURKAIP1	15kDa/25kDa	Rabbit polyclonal	1:1000	Eurogentec (custom)
Anti-β-actin	42kDa	Mouse monoclonal	1:10000	Sigma (A1978)
Anti-CLPP	30kDa	Rabbit monoclonal	1:1000	Abcam (ab124822)
Anti-CLPX	69kDa	Rabbit monoclonal	1:1000	Abcam (ab168338)
Anti-CORE2	45kDa	Mouse monoclonal	1:1000	Invitrogen (A11143)
Anti-COXI	39kDa	Mouse monoclonal	1:1000	Abcam (ab14705)
Anti-COXII	25kDa	Mouse monoclonal	1:1000	Abcam (ab110258)
Anti-FLAG	-	Mouse monoclonal	1:2000	Sigma Aldrich (F1804)
Anti-ICT1	20kDa	Rabbit polyclonal	1:800	Proteintech (10403-1-AP)
Anti-LONP1	106kDa	Rabbit polyclonal	1:1000	Sigma Aldrich (HPA002192)
Anti-uL3m	38kDa	Goat polyclonal	1:1000	Abcam (ab39268)
Anti-uL11m	21kDa	Rabbit monoclonal	1:1000	Cell Signalling Tech (D68F2)
Anti-bL12m	19kDa	Rabbit polyclonal	1:1000	Eurogentec (custom)
Anti-mL45	36kDa	Rabbit polyclonal	1:1000	Proteintech (15682-1-AP)
Anti-uS17m	14kDa	Rabbit polyclonal	1:1000	Proteintech (18881-1-AP_
Anti-mS22	39kDa	Rabbit polyclonal	1:1000	Proteintech (10984-4-AP)
Anti-mS26	24kDa	Rabbit polyclonal	1:1000	Proteintech (15989-1-AP)
Anti-mS27	47kDa	Rabbit polyclonal	1:1000	Proteintech (17280-1-AP)
Anti-mS29	45kDa	Mouse monoclonal	1:1000	Abcam (ab11928)
Anti-mS40	29kDa	Rabbit polyclonal	1:2000	Proteintech (16139-1-AP)
Anti-NDUFB8	20kDa	Mouse monoclonal	1:1000	Abcam (ab110242)
Anti-SDHA	72kDa	Mouse monoclonal	1:2000	Abcam (ab14715)
Anti-TFAM	28kDa	Mouse monoclonal	1:1000	Abcam (ab119684)
Anti-TOMM20	20kDa	Rabbit polyclonal	1:1000	Santa Cruz Biotech (Sc-17764)
Anti-VDAC1	39kDa	Mouse monoclonal	1:10000	Abcam (ab14734)
SECONDARY (IgG, HRP-Conjugated)				
Anti-rabbit	-	-	1:3000	Dako Cytomation (P0260)
Anti-mouse	-	-	1:2000	Dako Cytomation (P0339)
Anti-goat	-	-	1:2000	Dako Cytomation (P0449)

Appendix K: New Nomenclature for Ribosomal Proteins

Modified from Amunts *et al.* 2014.

Small Subunit (mtSSU)		
NEW	OLD	UNIPROT ID
bS1m	MRPS28	Q9Y2Q9
uS2m	MRPS2	Q9Y399
uS3m	MRPS24	Q96EL2
uS5m	MRPS5	P82675
bS6m	MRPS6	P82932
uS7m	MRPS7	Q9Y2R9
uS9m	MRPS9	P82933
uS10m	MRPS10	P82664
uS11m	MRPS11	P82912
uS12m	MRPS12	O15235
uS14m	MRPS14	O60783
uS15m	MRPS15	P82914
bS16m	MRPS16	Q9Y3D3
uS17m	MRPS17	Q9Y2R5
bS18b (mS40)	MRPS18b	Q9Y676
bS18c (bS18m)	MRPS18c	Q9Y3D5
bS21m	MRPS21	P82921
mS22	MRPS22	P82650
mS23	MRPS23	Q9Y3D9
mS25	MRPS25	P82663
mS26	MRPS26	Q9BYN8
mS27	MRPS27	Q92552
mS29	MRPS29 (DAP3)	P51398
mS31	MRPS31	Q92665
mS33	MRPS33	Q9Y291
mS34	MRPS34	P82930
mS35	MRPS35	P82673
mS37	MRPS37 (CHCHD1)	Q96BP2
mS38	MRPS38 (AURKAIP1)	Q9NWT8
mS39	MRPS39 (PTCD3)	Q96EY7

Large Subunit (mtLSU)					
NEW	OLD	UNIPROT ID	NEW	OLD	UNIPROT ID
uL1m	MRPL1	Q9BYD6	bL35m	MRPL35	Q9NZE8
uL2m	MRPL2	Q5T653	bL36m	MRPL36	Q9P0J6
uL3m	MRPL3	P09001	mL37	MRPL37	Q9BZE1
uL4m	MRPL4	Q9BYD3	mL38	MRPL38	Q96DV4
bL12m	MRPL7	P52815	mL39	MRPL39	Q9NYK5
bL9m	MRPL9	Q9BYD2	mL40	MRPL40	Q9NQ50
uL10m	MRPL10	Q7Z7H8	mL41	MRPL41	Q8IXM3
uL11m	MRPL11	Q9Y3B7	mL42	MRPL42	Q9Y6G3
uL13m	MRPL13	Q9BYD1	mL43	MRPL43	Q8N983
uL14m	MRPL14	Q6P1L8	mL44	MRPL44	Q9H9J2
uL15m	MRPL15	Q9P015	mL45	MRPL45	Q9BRJ2
uL16m	MRPL16	Q9NX20	mL46	MRPL46	Q9H2W6
bL17m	MRPL17	Q9NRX2	mL48	MRPL48	Q96GC5
uL18m	MRPL18	Q9H0U6	mL49	MRPL49	Q13405
bL19m	MRPL19	P49406	mL50	MRPL50	Q8N5N7
bL20m	MRPL20	Q9BYC9	mL51	MRPL51	Q4U2R6
bL21m	MRPL21	Q7Z2W9	mL52	MRPL52	Q86TS9
uL22m	MRPL22	Q9NWU5	mL53	MRPL53	Q96EL3
uL23m	MRPL23	Q16540	mL54	MRPL54	Q6P161
uL24m	MRPL24	Q96A35	mL55	MRPL55	Q7Z7F7
bL27m	MRPL27	Q9P0M9	mL56	MRPL56	P83111
bL28m	MRPL28	Q13084	mL63	MRPL63	Q9BQC6
uL29m	MRPL47	Q9HD33	ICT1	ICT1	Q14197
uL30m	MRPL30	Q8TCC3	CRIF1	CRIF1	Q8TAE8
bL32m	MRPL32	Q9BYC8	bS18a	MRPS18a	Q9NVS2
bL33m	MRPL33	O75394	mS30	MRPS30	Q9NP92
bL34m	MRPL34	Q9BQ48			

Appendix L: Summary of the CLIP Data Using AURKAIP1-FLAG

Data was taken from sequencing file: "IonXpress_033_R_2014_09_09_18_56_36_user_SN1-19-Agata_Auto_user_SN1-19-Agata_090914_13S". Nucleotide number and number of sequenced transcripts (hits) for each gene were determined using Microsoft Excel. Data has been filtered to remove outliers. This experiment was repeated twice and data shown here is representative of both samples. *MT-RNR1* = 16S rRNA, *MT-RNR2* = 12S rRNA.

Gene	mtDNA nucleotide (peak maximum)	No. of Hits
Conserved sequence Block 2	271	531
MT-RNR1 [m.648-1601]	874	1002
	910	954
	1150	992
	1348	305
	1574	668
MT-TV [m.1602-1669]	1638	1058
MT-RNR2 [m.1670-3227]	3060	550
	3115	1177
MT-TM	4444	1390

Appendix M: FLAG Immunoprecipitation of mS27-FLAG

A list of peptides identified using nanoLC-MS/MS, using eluate from an immunoprecipitation of mS27-FLAG with anti-FLAG resin beads. Performed in the laboratory of Professor Christine Carapito (University of Strasborg, France). The peptides listed below were successfully labelled at the N-terminus and sequenced.

Sequence	Accession	Description	Start	End
STHSLVGDK	Q8IYQ7|THNS1_HUMAN	Threonine synthase-like 1	48	56
VNDGDMR	Q08380|LG3BP_HUMAN	Galectin-3-binding protein	19	25
LHTDGDK	Q07021|C1QBP_HUMAN	Complement component 1 Q subcomponent-binding protein, mitochondrial	74	80
AHESVVK	P13073|COX41_HUMAN	Cytochrome c oxidase subunit 4 isoform 1, mitochondrial	23	29
LHTAANAAATATETTCQDVAATPVAR	Q9NP92|RT30_HUMAN	28S ribosomal protein S30, mitochondrial	18	43
VTGEGTSFR	Q8NBZ9|NEAS1_HUMAN	Putative uncharacterized protein NEXN-AS1	191	199
STSSSCHAPAVTQHAPYFK	P30048|PRDX3_HUMAN	Thioredoxin-dependent peroxide reductase, mitochondrial	55	73
APAVTQHAPYFK	P30048|PRDX3_HUMAN	Thioredoxin-dependent peroxide reductase, mitochondrial	62	73
LHSEPGLEER	Q96EH3|MASU1_HUMAN	Mitochondrial assembly of ribosomal large subunit protein 1	61	70
LAGAPLDNAPK	P52815|RM12_HUMAN	39S ribosomal protein L12, mitochondrial	48	58
GTNSVICSK	Q92665|RT31_HUMAN	28S ribosomal protein S31, mitochondrial	61	69
FGTNSVICSK	Q92665|RT31_HUMAN	28S ribosomal protein S31, mitochondrial	60	69
GTDAGVAVR	Q5JPH6|SYEM_HUMAN	Probable glutamate-tRNA ligase, mitochondrial	30	38
FSSVLASCPK	Q00059|TFAM_HUMAN	Transcription factor A, mitochondrial	42	51
SSVLASCPK	Q00059|TFAM_HUMAN	Transcription factor A, mitochondrial	43	51
SDMPPLTLEGIQDR	O14561|ACPM_HUMAN	Acyl carrier protein, mitochondrial	69	82
SSSGVIPNEK	Q96RP9|EFGM_HUMAN	Elongation factor G, mitochondrial	36	45
AALVPGVTQVDNK	Q9H7H0|MET17_HUMAN	Methyltransferase-like protein 17, mitochondrial	28	40
ASSFPVPPPGAQGVAELLR	Q8IVS2|FABD_HUMAN	Malonyl-CoA-acyl carrier protein transacylase, mitochondrial	22	40
SSFPVPPPGAQGVAELLR	Q8IVS2|FABD_HUMAN	Malonyl-CoA-acyl carrier protein transacylase, mitochondrial	23	40
ASASSTNLK	O75390|CISY_HUMAN	Citrate synthase, mitochondrial	26	34
RHTAFVIPK	P82933|RT09_HUMAN	28S ribosomal protein S9, mitochondrial	50	58
LGMLEAGILP	Q9NRC6|SPTN5_HUMAN	Spectrin beta chain, non-erythrocytic 5	469	478
STAEDTQNEGK	Q9H2K0|IF3M_HUMAN	Translation initiation factor IF-3, mitochondrial	56	66
LQDAAAK	P82912|RT11_HUMAN	28S ribosomal protein S11, mitochondrial	40	46
SNLHVDVPK	P82664|RT10_HUMAN	28S ribosomal protein S10, mitochondrial	48	56
SDVLELTDDNFESR	P30101|PDIA3_HUMAN	Protein disulfide-isomerase A3	25	38
MVPPVQVSPLIK	P56385|ATP5I_HUMAN	ATP synthase subunit e, mitochondrial	1	12
VPPVQVSPLIK	P56385|ATP5I_HUMAN	ATP synthase subunit e, mitochondrial	2	12
AQTAAATAPR	P21912|SDHB_HUMAN	Succinate dehydrogenase [ubiquinone] iron-sulfur subunit, mitochondrial	29	38

SEITFELPDNAK	Q9Y3B3|TMED7_HUMAN	Transmembrane emp24 domain-containing protein 7	35	46
LNTPSDK	Q9BUB7|TMM70_HUMAN	Transmembrane protein 70, mitochondrial	82	88
SSGGAYPNIPLSSPLPGVPKPVFATVDGQEK	Q10713|MPPA_HUMAN	Mitochondrial-processing peptidase subunit alpha	34	64
SCPGTVAK	Q9NVV4|PAPD1_HUMAN	Poly(A) RNA polymerase, mitochondrial	31	38
AAPAVQTK	P55084|ECHB_HUMAN	Trifunctional enzyme subunit beta, mitochondrial	34	41
AAQTSPSPK	P06576|ATPB_HUMAN	ATP synthase subunit beta, mitochondrial	47	55
ADQPIDADVTVIGSGPGGYVAAIK	P09622|DLDH_HUMAN	Dihydrolipoyl dehydrogenase, mitochondrial	36	59
LMARYGR	Q9UL40|ZN346_HUMAN	Zinc finger protein 346	218	224
FANDATFEIK	P08559|ODPA_HUMAN	Pyruvate dehydrogenase E1 component subunit alpha, somatic form, mitochondrial	30	39
FANDATFEIKK	P08559|ODPA_HUMAN	Pyruvate dehydrogenase E1 component subunit alpha, somatic form, mitochondrial	30	40
SHGSQETDEEFDAR	P20674|COX5A_HUMAN	Cytochrome c oxidase subunit 5A, mitochondrial	42	55
SSEAPPLINEDVKR	P04843|RPN1_HUMAN	Dolichyl-diphosphooligosaccharide--protein glycosyltransferase subunit 1	25	38
STGPSEPGAFQPPPKPVIVDK	P49406|RM19_HUMAN	39S ribosomal protein L19, mitochondrial	45	65
AGPLQGGGAR	Q9P015|RM15_HUMAN	39S ribosomal protein L15, mitochondrial	2	11
AAATLTSK	Q9UDW1|QCR9_HUMAN	Cytochrome b-c1 complex subunit 9	2	9
ANFVSWK	Q5T653|RM02_HUMAN	39S ribosomal protein L2, mitochondrial	61	67
LTPTHYLTK	P04844|RPN2_HUMAN	Dolichyl-diphosphooligosaccharide--protein glycosyltransferase subunit 2	23	31
SSSGGGDSAAAGASR	P23378|GCSP_HUMAN	Glycine dehydrogenase (decarboxylating), mitochondrial	37	51
SATPVPTPSLPER	P82673|RT35_HUMAN	28S ribosomal protein S35, mitochondrial	28	40
VYSATPVPTPSLPER	P82673|RT35_HUMAN	28S ribosomal protein S35, mitochondrial	26	40
SSSASPQEQDQDR	O00411|RPOM_HUMAN	DNA-directed RNA polymerase, mitochondrial	41	53
LSQTQGPPDYPR	Q13405|RM49_HUMAN	39S ribosomal protein L49, mitochondrial	26	37
SQTQGPPDYPR	Q13405|RM49_HUMAN	39S ribosomal protein L49, mitochondrial	27	37
QSHLAIK	Q04724|TLE1_HUMAN	Transducin-like enhancer protein 1	174	180
VLESVAR	Q8N5K1|CISD2_HUMAN	CDGSH iron-sulfur domain-containing protein 2	2	8
SSEAAESGSPETK	P82650|RT22_HUMAN	28S ribosomal protein S22, mitochondrial	54	66
STSSEPAAKPEVDPVENEAVAPEFTNR	Q9H0U6|RM18_HUMAN	39S ribosomal protein L18, mitochondrial	25	51
NSQSTSYLPGYVPK	Q7Z2W9|RM21_HUMAN	39S ribosomal protein L21, mitochondrial	40	53
SQSTSYLPGYVPK	Q7Z2W9|RM21_HUMAN	39S ribosomal protein L21, mitochondrial	41	53
SSSSSQLPLGQER	O75127|PTCD1_HUMAN	Pentatricopeptide repeat-containing protein 1, mitochondrial	47	59
SSGGGGGGGGGR	Q6UB35|C1TM_HUMAN	Monofunctional C1-tetrahydrofolate synthase, mitochondrial	32	43
SSLAEEAAR	Q9BYD3|RM04_HUMAN	39S ribosomal protein L4, mitochondrial	22	30
PVPPLPEYGGK	P24539|AT5F1_HUMAN	ATP synthase F(0) complex subunit B1, mitochondrial	43	53
AHLDNQVPVESPR	P51398|RT29_HUMAN	28S ribosomal protein S29, mitochondrial	34	46
IAAHLDNQVPVESPR	P51398|RT29_HUMAN	28S ribosomal protein S29, mitochondrial	32	46
SIAAHLDNQVPVESPR	P51398|RT29_HUMAN	28S ribosomal protein S29, mitochondrial	31	46

SSAAALPSPILNPDIPYNQLFINNEWQDAVSK	sp|P30837|AL1B1_HUMAN	Aldehyde dehydrogenase X, mitochondrial	20	51
TKPTHGIGK	Q96GC5|RM48_HUMAN	39S ribosomal protein L48, mitochondrial	50	58
LVEQLDIEETEQSK	Q92552|RT27_HUMAN	28S ribosomal protein S27, mitochondrial	313	326
VAASPEDIK	Q92552|RT27_HUMAN	28S ribosomal protein S27, mitochondrial	266	274
ALTSADGASEEQSQNDEDNQGSEK	Q92552|RT27_HUMAN	28S ribosomal protein S27, mitochondrial	289	312
IESEGLLSLTTQLVK	Q92552|RT27_HUMAN	28S ribosomal protein S27, mitochondrial	347	361
SSAYVDSHK	Q92552|RT27_HUMAN	28S ribosomal protein S27, mitochondrial	31	39
LLSSAYVDSHK	Q92552|RT27_HUMAN	28S ribosomal protein S27, mitochondrial	29	39
LLSSAYVDSHKWEAR	Q92552|RT27_HUMAN	28S ribosomal protein S27, mitochondrial	29	43
PSATSHSGSGSK	Q14444|CAPR1_HUMAN	Caprin-1	2	13
ASGGGVPTDEEQATGLER	P10606|COX5B_HUMAN	Cytochrome c oxidase subunit 5B, mitochondrial	32	49
IIEPSLR	P62987|RL40_HUMAN	Ubiquitin-60S ribosomal protein L40	77	83
ATLNQMHR	O15235|RT12_HUMAN	28S ribosomal protein S12, mitochondrial	31	38
VGTESGSESGSSNAK	Q9Y2Q9|RT28_HUMAN	28S ribosomal protein S28, mitochondrial	29	43
VGTESGSESGSSNAKEPK	Q9Y2Q9|RT28_HUMAN	28S ribosomal protein S28, mitochondrial	29	46
QTMQNLN	Q2M2I5|K1C24_HUMAN	Keratin, type I cytoskeletal 24	142	148
STQAATQVVLNVPETR	O75439|MPPB_HUMAN	Mitochondrial-processing peptidase subunit beta	44	59
DDLVTVK	P36957|ODO2_HUMAN	Dihydrolipoyllysine-residue succinyltransferase component of 2-oxoglutarate dehydrogenase complex, mitochondrial	68	74
LHVDVPK	P82664|RT10_HUMAN	28S ribosomal protein S10, mitochondrial	50	56
SGSATLSK	Q96EY7|PTCD3_HUMAN	Pentatricopeptide repeat domain-containing protein 3, mitochondrial	38	45
AEGQAAARR	Q9H1R3|MYLK2_HUMAN	Myosin light chain kinase 2, skeletal/cardiac muscle	133	141
LHAGSGADTGDTVNIGDVSYK	A3KMH1|VWA8_HUMAN	von Willebrand factor A domain-containing protein 8	46	66
ASSFQHSSSLGR	Q8NC60|NOA1_HUMAN	Nitric oxide-associated protein 1	39	50

Appendix N: Mass Spectrometry of *Mycoplasma* positive AURKAIP1-FLAG

The LC MS/MS was carried out by Dr Hans Wessels (UNMC, Nijmegen, Netherlands). Sample A = HEK-AUR1-FLAG, Sample B = HEK wild-type. SC% = percentage sequence coverage. Proteins shown here are unique to the HEK-AUR1-FLAG sample. Contaminants such as keratin have been removed. MYCMO = *Mycoplasma mobile* (strain ATCC 43663 / 163K / NCTC 11711), MYCFP = *Mycoplasma fermentans* (strain ATCC 19989 / NBRC 14854 / NCTC 10117 / PG18), MYCHR = *Mycoplasma hyorhinis*, MYCH2 = *Mycoplasma hyopneumoniae* (strain 232), MYCPU = *Mycoplasma pulmonis* (strain UAB CTIP), MYCH7 = *Mycoplasma hyopneumoniae* (strain 7448), MYCA5 = *Mycoplasma arthritidis* (strain 158L3-1), MYCS5 = *Mycoplasma synoviae* (strain 53), MYCAP = *Mycoplasma agalactiae* (strain PG2). The top 60 peptides are shown, listed from high (green) to low (red) number of peptides identified per protein.

Accession	Protein	Meta Score (A)	Meta Score (B)	Peptides (A)	Peptides (B)	SC% (A)	SC% (B)
FRIH_HUMAN	Ferritin heavy chain	199.8	0	9	0		0
SSRB_HUMAN	Translocon-assoc. protein subunit β	80.4	0	8	0		0
P29_MYCHR	Probable ABC transporter ATP-binding protein p29	121.9	0	7	0		0
SCO1_HUMAN	Protein SCO1 homolog, mitochondrial	171.4	0	6	0		0
RHOA_HUMAN	Transforming protein RhoA	203.5	0	6	0		0
CYB5B_HUMAN	Cytochrome b5 type B	133.6	0	5	0		0
ROA2_HUMAN	Heterogeneous nuclear ribonucleoproteins A2/B1	136.8	0	5	0		0
MAAI_HUMAN	Maleylacetoacetate isomerase	175.1	0	5	0		0
RM02_HUMAN	39S ribosomal protein L2, mitochondrial	314.3	0	4	0		0
RAB1B_HUMAN	Ras-related protein Rab-1B	224.1	0	4	0		0
RAC3_HUMAN	Ras-related C3 botulinum toxin substrate 3	72.7	0	4	0		0
HDHD3_HUMAN	Haloacid dehalogenase-like hydrolase domain-containing protein 3	59.4	0	4	0		0
GGH_HUMAN	Gamma-glutamyl hydrolase	100.8	0	3	0		0
KCRB_HUMAN	Creatine kinase B-type	79.9	0	3	0		0
RS3_MYCMO	30S ribosomal protein S3	20.9	0	3	0		0
PRLD1_HUMAN	PRELI domain-containing protein 1, mitochondrial	95.7	0	3	0		0
APT_MYCFP	AP-2 complex subunit alpha-1	20.9	0	3	0		0
TPIS_MYCHR	Triosephosphate isomerase	87.2	0	3	0		0
RL21_HUMAN	60S ribosomal protein L21	91.7	0	3	0		0
AP2A1_HUMAN	AP-2 complex subunit alpha-1	135.9	0	3	0		0
PGRC2_HUMAN	Membrane-associated progesterone receptor component 2	172	0	3	0		0

UCHL1_HUMAN	Ubiquitin carboxyl-terminal hydrolase isozyme L1	76.9	0	3	0		0
RM40_HUMAN	39S ribosomal protein L40, mitochondrial	172.5	0	3	0		0
PI4KA_HUMAN	Phosphatidylinositol 4-kinase alpha	17.8	0	3	0		0
PFD3_HUMAN	Prefoldin subunit 3	148.9	0	3	0		0
GILT_HUMAN	Gamma-interferon-inducible lysosomal thiol reductase	91.6	0	3	0		0
RL3_MYCH2	50S ribosomal protein L3	37.9	0	3	0		0
KTHY_HUMAN	Thymidylate kinase	109.9	0	3	0		0
MASU1_HUMAN	Mitochondrial assembly of ribosomal large subunit protein 1	126.8	0	3	0		0
YBOX3_HUMAN	Y-box-binding protein 3	137.9	0	3	0		0
RAB14_HUMAN	Ras-related protein Rab-14	160.8	0	3	0		0
CSN8_HUMAN	COP9 signalosome complex subunit 8	52.1	0	2	0		0
EFTU_MYCPU	Elongation factor Tu	20.8	0	2	0		0
SCAM1_HUMAN	Secretory carrier-associated membrane protein 1	99	0	2	0		0
SAR1B_HUMAN	GTP-binding protein SAR1b	51.2	0	2	0		0
SPRE_HUMAN	Sepiapterin reductase	116.1	0	2	0		0
HEBP1_HUMAN	Heme-binding protein 1	29	0	2	0		0
HSC20_HUMAN	Iron-sulfur cluster co-chaperone protein HscB, mitochondrial	46.4	0	2	0		0
AATM_HUMAN	Aspartate aminotransferase, mitochondrial	68.6	0	2	0		0
ATP6_HUMAN	ATP synthase subunit a, mitochondrial	79.8	0	2	0		0
MR1L1_HUMAN	MORF4 family-associated protein 1-like 1	22.8	0	2	0		0
FBX17_HUMAN	F-box only protein 17	53.9	0	2	0		0
RM01_HUMAN	39S ribosomal protein L1, mitochondrial	47	0	2	0		0
RB39B_HUMAN	Ras-related protein Rab-39B	69.6	0	2	0		0
T126A_HUMAN	Transmembrane protein 126A	40.6	0	2	0		0
TM109_HUMAN	Transmembrane protein 109	48.8	0	2	0		0
CREG1_HUMAN	Protein CREG1	33.4	0	2	0		0
MTAP_HUMAN	S-methyl-5'-thioadenosine phosphorylase	29.4	0	2	0		0
RM13_HUMAN	39S ribosomal protein L13, mitochondrial	56	0	2	0		0
DNS2A_HUMAN	Deoxyribonuclease-2-alpha	64.4	0	2	0		0
ICT1_HUMAN	Peptidyl-tRNA hydrolase ICT1, mitochondrial	80.5	0	2	0		0
MDHM_HUMAN	Malate dehydrogenase, mitochondrial	75.4	0	2	0		0
RS5_MYCH7	30S ribosomal protein S5	32.9	0	1	0		0

DNPH1_HUMAN	2'-deoxynucleoside 5'-phosphate N-hydrolase 1	49.5	0	1	0		0
DEOC_MYCA5	Deoxyribose-phosphate aldolase	15.9	0	1	0		0
ESRP2_HUMAN	Epithelial splicing regulatory protein 2	19.2	0	1	0		0
EFTU_MYCS5	Elongation factor Tu	27.3	0	1	0		0
VLPC_MYCHR	Variant surface antigen	23.5	0	1	0		0
RL1_MYCH2	50S ribosomal protein L1	20.6	0	1	0		0
KTHY_MYCAP	Thymidylate kinase	16.9	0	1	0		0

Proteins shown here are enriched in the HEK-AUR1-FLAG sample (A) vs HEK293T wild-type sample (B). SC% = percentage sequence coverage. The top 60 peptides are shown, listed from high (green) to low (yellow) ratio of peptides in sample A vs sample B.

Accession	Protein	Meta Score (A)	Meta Score (B)	Ratio Pep.A/ Pep.B	SC% (A)	SC% (B)
PSB7_HUMAN	Proteasome subunit beta type-7	479.5	195.7	8	54.2	20.9
AR6P1_HUMAN	ADP-ribosylation factor-like protein 6-interacting protein 1	119.1	27.1	7	17.7	3.9
PSB4_HUMAN	Proteasome subunit beta type-4	591.4	157	6.5	37.1	11
PSB6_HUMAN	Proteasome subunit beta type-6	452.7	120	6.3333	38.9	13.8
PSB2_HUMAN	Proteasome subunit beta type-2	575.1	202.6	5	75.1	31.8
DCXR_HUMAN	L-xylulose reductase	744.4	566.3	4.8	72.1	41
PSA3_HUMAN	Proteasome subunit alpha type-3	260.6	209.1	4.5	27.8	12.2
PGAM1_HUMAN	Phosphoglycerate mutase 1	242.5	78	4	43.7	16.5
ERP29_HUMAN	Endoplasmic reticulum resident protein 29	230.6	90.2	4	26.1	10.3
ETHE1_HUMAN	Persulfide dioxygenase ETHE1, mitochondrial	257.6	92.7	4	36.2	11.4
TSN_HUMAN	Translin	228.1	92.6	4	51.8	9.6
NACA_HUMAN	Nascent polypeptide-associated complex subunit alpha	137.2	39.9	4	19.5	7
PSA2_HUMAN	Proteasome subunit alpha type-2	608.5	283.5	3.5	56.8	26.5
RL11_HUMAN	60S ribosomal protein L11	229.3	182.1	3.5	37.6	14.6
6PGL_HUMAN	6-phosphogluconolactonase	111.3	151	3.5	21.7	14.3
PSA6_HUMAN	Proteasome subunit alpha type-6	481.8	436.8	3.2	56.1	23.2
PSB5_HUMAN	Proteasome subunit beta type-5	745.8	398.5	3.1428	56.3	28.1
PSA1_HUMAN	Proteasome subunit alpha type-1	444.5	120.3	3	47.5	14.8
CPSF5_HUMAN	Cleavage and polyadenylation specificity factor subunit 5	204.6	136.7	3	37.9	14.5
RAB10_HUMAN	Ras-related protein Rab-10	154.8	127.4	3	24	11.5
SODM_HUMAN	Superoxide dismutase [Mn], mitochondrial	213.6	205.2	3	33.8	15.3
DCAKD_HUMAN	Dephospho-CoA kinase domain-containing protein	130.5	63.7	3	16	5.6
RL18A_HUMAN	60S ribosomal protein L18a	70.7	94.3	3	11.9	7.4
SAR1A_HUMAN	GTP-binding protein SAR1a	145.4	50.9	3	23.2	5.6
DOPP1_HUMAN	Dolichyldiphosphatase 1	113.1	16.4	3	20.6	5.5
RRAS2_HUMAN	Ras-related protein R-Ras2	104.9	57.9	3	11.8	7.8
PPIB_HUMAN	Peptidyl-prolyl cis-trans isomerase B	80.6	22.6	3	15.7	4.2
SPCS3_HUMAN	Signal peptidase complex subunit 3	41.6	58.5	3	11.1	5
RU2B_HUMAN	U2 small nuclear ribonucleoprotein B	70.9	14.9	3	19.1	5.8
YBOX1_HUMAN	Nuclease-sensitive element-binding protein 1	125.6	106.4	3	14.2	5.2
RAN_HUMAN	GTP-binding nuclear protein Ran	618.6	555.1	2.9090	79.6	49.5
RAB35_HUMAN	Ras-related protein Rab-35	274.2	272.8	2.75	53.2	22.9
GRPE1_HUMAN	GrpE protein homolog 1, mitochondrial	693.4	413	2.7142	59	37.3

NPS3A_HUMAN	Protein NipSnap homolog 3A	592.1	276.8	2.6666	59.1	30
DGUOK_HUMAN	Deoxyguanosine kinase, mitochondrial	180.2	218.3	2.6666	39.4	17
RM19_HUMAN	39S ribosomal protein L19, mitochondrial	182.6	72.4	2.6666	26.4	11.3
HEXB_HUMAN	Beta-hexosaminidase subunit beta	405.5	147.1	2.6	29.1	9.5
ACTB_HUMAN	Actin, cytoplasmic 1	228.1	81.3	2.5	20.3	7.7
CBR1_HUMAN	Carbonyl reductase [NADPH] 1	172.9	155.7	2.5	23.1	10.8
RT25_HUMAN	28S ribosomal protein S25, mitochondrial	167.6	134.2	2.5	37	16.8
1433G_HUMAN	14-3-3 protein gamma	585.5	360.9	2.4166	55.5	37.2
PSA5_HUMAN	Proteasome subunit alpha type-5	366	318.8	2.4	44	29
PGES2_HUMAN	Prostaglandin E synthase 2	500.5	484.2	2.4	34.2	16.2
PSA7_HUMAN	Proteasome subunit alpha type-7	651.2	573.9	2.3333	60.5	50.4
PSA4_HUMAN	Proteasome subunit alpha type-4	590.5	481.2	2.3333	59	34.9
TMEDA_HUMAN	Transmembrane emp24 domain-containing protein 10	256.1	94.4	2.3333	21.5	12.8
RAB8A_HUMAN	Ras-related protein Rab-8A	169.2	123.2	2.333333	25.1	14.5
CY1_HUMAN	Cytochrome c1, heme protein, mitochondrial	696.3	577.6	2.1333	54.8	51.1
ABHDB_HUMAN	Protein ABHD11	590.8	370.2	2	60	32.1
DIC_HUMAN	Mitochondrial dicarboxylate carrier	458.2	419	2	43.9	35.5
HCDH_HUMAN	Hydroxyacyl-coenzyme A dehydrogenase, mitochondrial	389.2	370.4	2	54.8	39.2
PSB1_HUMAN	Proteasome subunit beta type-1	478.4	382.2	2	42.7	29.5
RL6_HUMAN	60S ribosomal protein L6	207.5	206.8	2	21.5	14.6
RMD1_HUMAN	Regulator of microtubule dynamics protein 1	277.7	108.5	2	20.1	11.1
PSB3_HUMAN	Proteasome subunit beta type-3	202	224	2	24.9	32.2
D39U1_HUMAN	Epimerase family protein SDR39U1	178.1	126.7	2	22.9	5
SCOT1_HUMAN	Succinyl-CoA:3-ketoacid coenzyme A transferase 1, mitochondrial	167	98.4	2	10	6.3
MBLC2_HUMAN	Metallo-beta-lactamase domain-containing protein 2	183.7	181.3	2	24.4	13.6
VAMP7_HUMAN	Vesicle-associated membrane protein 7	151.5	43.5	2	19.5	5.5
OXND1_HUMAN	Oxidoreductase NAD-binding domain-containing protein 1	143.3	96.7	2	20.2	9.6

Appendix O: Mass spectrometry of AURKAIP1-FLAG, treated with siLONP1

			AutoMSn			Targeted AutoMSn		
Sample	Proteins	Peptides	AUR1_ Human	AUR1_ Human Score	AUR1_Human Seq. Cov (%AA)	AUR1_ Human	AUR1_ Human Score	AUR1_Human Seq. Cov (%AA)
Un, siLONP1	608	2595	NaN	NaN	NaN	NaN	NaN	NaN
Ind, siLONP1	268	1044	3	253	19.1	4	318	39.2

	NL summed area/protein		
Sample	PHB	ADT2	AURKAIP1
Uninduced, siLONP1 A	4727715.571	3314415.306	0
Uninduced, siLONP1 B	4201849	3788558	0
Induced, siLONP1 A	4371976.747	3635163.902	643204.5958
Induced, siLONP1 B	3905719.796	4055560.137	883582.3667

Appendix P: Histochemistry and Immunohistochemistry Methods

COX/SDH Staining

COX/SDH staining was performed by Mr Gavin Falkous (NHS Highly Specialised Mitochondrial Diagnostic Service, Newcastle-upon-Tyne). The technique is used to assess mitochondrial respiratory chain activity by measuring complex IV (COX, cytochrome *c* oxidase) and complex II (SDH, succinate dehydrogenase) activity in individual muscle fibres from 10µm transverse skeletal muscle sections. Serial skeletal muscle sections (10µm) on Polysine™ microscope slides (631-0107, VWR) were removed from the freezer and allowed to thaw at room temperature for 1hr. The sections were rehydrated in 1 x PBS, and incubated with 100µl COX solution (100µM cytochrome *c,* 4mM diaminobenzidine tetrahydrochloride, 20µg/ml catalase in 0.2M phosphate buffer, pH 7) for 45mins at 37^{o}C. The sections were washed in 1 x PBS for 3 x 5mins, and then incubated with 100µl SDH solution (130mM sodium succinate, 200µM phenazine methosulphate, 1mM sodium azide, 1.5mM nitroblue tetrazolium in 0.2M phosphate buffer, pH 7) for 40mins at 37^{o}C. The sections were washed in 1 x PBS, 70% ethanol, 95% ethanol, 2 x 100% ethanol and 2 x Histo-Clear (HS2001GLL, National Diagnostics). Sections were mounted in DPX medium (36029 4H, VWR) and covered with a coverslip prior to analysis.

Hematoxylin and Eosin (H&E) Staining

H&E staining was performed by Mr Gavin Falkous (NHS Highly Specialised Mitochondrial Diagnostic Service, Newcastle-upon-Tyne). The technique is used to shown general tissue architecture. Serial skeletal muscle sections (10µm) were prepared onto Polysine™ microscope slides (631-0107, VWR), left to air dry for 1hr and fixed in formol calcium solution for 10mins. The sections were washed in running tap water for 2mins and stained in Mayers Haemalum (LAMB/170-D, Raymond Lamb) for 2mins. The sections were washed in running tap water for 2mins until blue, and then stained in 1% aqueous eosin solution (LAMB/100-D, Raymond Lamb) for 4mins. The sections were washed rapidly running water three times to remove excess eosin, and then washed in 70% ethanol, 95% ethanol, 2 x 100% ethanol and 2 x Histo-Clear (HS2001GLL, National Diagnostics). Sections were mounted in DPX medium (36029 4H, VWR) and covered with a coverslip prior to analysis.

Quadruple Immunofluorescence Assay

The quadruple immunofluorescence assay (Rocha *et al.* 2016) was kindly performed by Miss Sila Hopton (NHS Highly Specialised Mitochondrial Diagnostic Service, Newcastle-upon-Tyne). Briefly, skeletal muscle sections (10µm) were fixed in 4% paraformaldehyde solution for 3mins and then permeabilised in a gradient of methanol solutions. The sections were washed in TBS-T, blocked in 5% normal goat serum for 30mins at room temperature and incubated with MTCO1, NDUFB8, porin and laminin α-1 primary antibodies (Table A1) at 4°C overnight in a humidified chamber. The sections were washed in TBS-T and then incubated with secondary antibodies (Appendix K) for 2hrs at room temperature in a humidified chamber. The sections were then incubated with streptavidin 647 (Table A2) for 1hr at room temperature, washed in TBS-T and mounted with Vectashield hard set mounting medium (Vector Laboratories, 101098-048).

Table A1: Primary antibodies for the quadruple immunofluorescence assay.

PRIMARY COCKTAIL				
Antibody	Ig type	Secondary	Dilution	Manufacturer
MTCO1	IgG2a	Mouse monoclonal	1:100	Abcam (ab14705)
NDUFB8	IgG1	Mouse monoclonal	1:100	Abcam (ab110242)
Porin	IgG2b	Mouse monoclonal	1:100	Abcam (ab14734)
Laminin α-1	IgG	Rabbit polyclonal	1:50	Sigma Aldrich (L9393)

Table A2: Secondary antibodies for the quadruple immunofluorescence assay.

SECONDARY		
Antibody	Dilution	Manufacturer
Anti-mouse IgG2a, biotin	1:200	Life Technologies (M32315)
Anti-mouse IgG1, Alexa fluor – 546nm	1:200	Life Technologies (A21123)
Anti-mouse IgG2b, Alexa fluor – 488nm	1:200	Life Technologies (A21143)
Anti-rabbit IgG, Alexa fluor – 405nm	1:50	Life Technologies (A31556)
Streptavidin – 647nm	1:100	Life Technologies (S31556)